OCULUS | Pentacam®
Pentacam® HR
Pentacam® AXL

INTERPRETATION GUIDE

3rd edition

OCULUS®

Foreword

We thank you for the trust you have put in us by purchasing this OCULUS instrument. In doing so you have chosen a modern, sophisticated product which was manufactured and tested according to strict quality standards.

Our company has been doing business for over 120 years. Today OCULUS is a medium-sized company focused entirely on developing and manufacturing advanced and innovative instruments for examinations and surgery on the eye to help ophthalmologists, optometrists and opticians in their routine work.

The Pentacam® is based on the Scheimpflug principle, which generates precise and sharp images of the anterior eye segment. This instrument takes extremely accurate measurements and is easy to use.

If you have questions or desire further informations on this product, please turn to your OCULUS representative or directly to OCULUS.

We will be glad to help you.

OCULUS Optikgeräte GmbH

Note

OCULUS Optikgeräte GmbH wishes to emphasize that the user bears full responsibility for the correctness of data measured, calculated or displayed using the Pentacam®. The manufacturer will not accept claims based on erroneous data or misinterpretation. This Interpretation Guide can no more than assist in the interpretation of examination data generated by the Pentacam®.

In making a diagnosis physicians should not neglect to consider other medical information which may be obtainable through other methods such as slit lamp examination or ultrasound biomicroscopy, judiciously weighing the significance of each.

This Interpretation Guide should be seen as a complement to the User Guide and Instruction Manual. The current version of these documents and the Interpretation Guide are on every Pentacam® Software USB drive and should be read by all users prior to use.

OCULUS has been certified according to DIN EN ISO 13485 and therefore sets high quality standards in the development, production, quality assurance and servicing of its entire product range.

Table of contents

1 Introduction

This guide is intended to assist Pentacam®/Pentacam® HR/ Pentacam® AXL (referred to here as Pentacam®) users in interpreting the results and screens of the Pentacam®. We may not have covered everything which might be of interest, and we therefore ask anyone using the Pentacam® for their help in improving this guide step by step. Please forward us any cases or observations of particular interest, and we will be happy to incorporate them in this guide.

This guide cannot, of course, replace the knowledge and experiences that only come from long years of medical studies and professional practice, but it will be of help in cases of doubt as well as to beginners. At the same time, since medical findings may also depend on the practitioner's personal experience and perceptions, the individual patient's history or the particular combination of instruments used, it is quite possible for results obtained by other means to differ from those shown in this guide yet be nonetheless valid.

2 Description of the unit and general remarks

The OCULUS Pentacam® is a rotating Scheimpflug camera. The rotational measuring procedure generates Scheimpflug images in three dimensions, with the dot matrix fine-meshed in the centre due to the rotation. It takes 2 seconds to generate a complete image of the anterior eye segment. Any eye movement is detected by a second camera and corrected for in the process. The Pentacam® calculates a 3D model of the anterior eye segment from as many as 25.000 (HR/AXL: 138.000) distinct elevation points.

The topography and pachymetry of the entire anterior and posterior surface of the cornea from limbus to limbus are calculated and depicted. The analysis of the anterior eye segment includes a calculation of the chamber angle, chamber volume and chamber height and a manual measuring function that can be applied to any location in the anterior chamber of the eye. Images of the anterior and posterior surface of the cornea, the iris and the anterior and posterior surface of the lens are generated in a moveable virtual eye. The densitometry of the lens and cornea is automatically quantified.

The Scheimpflug images taken during the examination are digitalized in the main unit, and all image data are transferred to the PC. When the examination is finished, the PC calculates a 3D virtual model of the anterior eye segment, from which all additional information is derived.

The Pentacm® AXL also measures the axial length of the human eye. This measurement is performed by partial coherence interferometry (PCI) before the rotating Scheimpflug measuring procedure. The axial length is measured from the anterior surface of the cornea to the retina. Based on this additional measurement the Pentacam® AXL is a two-in-one device which allows also IOL power calculation. For more detailed information please refer to the instruction manual or user guide for the Pentacam® AXL.

3 Differences between the various topography maps of Pentacam®

3.1 Calculation of corneal power

Corneal Placido topographers measure geometrical corneal slope values. These values are converted into curvature values e.g. values of axial (sagittal) curvature or instantaneous (tangential) curvature which are initially given in mm. The Pentacam® measures geometrical height (elevation) values, which are likewise converted into values of axial (sagittal) or instantaneous (tangential) curvature and given in mm. These geometrical radius (mm) values are commonly converted it into refractive power values, which are given in diopters (D). This is normally done according the simple formula of D = (1.3375-1)*(1000)/Rmm.

A. The refractive effect

A sphere (sph) has the same radius of curvature at every point of its surface; however, due to the phenomenon of spherical aberration (SA) its refractive power is not the same everywhere. If the effect of SA is not taken into account, a corneal sphere with a radius of, say, 7.5 mm may be considered to have the same refractive power of 45 D at every point of its surface (assuming the keratometer calibration index of 1.3375, see below). Due to SA, however, the refractive power in the periphery is actually higher. The Pentacam® refractive maps, as they are called, are calculated on the basis of "Snell's law" of refraction using precision ray tracing, thereby taking this effect into account.

B. Inclusion of anterior/posterior surface

By convention most keratometers use the refractive index of 1.3375 when calculating the dioptric power of the anterior radius; in doing so they assume the cornea to have a single refracting surface. However, it has been known for quite some time that this keratometric index is not the best approximation to the rather physiological power of the cornea. Due to the contribution of the posterior surface and the more rather refractive index of the cornea (n cornea = 1.376), the True Net Power of the cornea, calculated using thick lens models or high-precision ray tracing, is lower than the value reported by standard keratometry. The deviation between True Net Power and corneal power as determined by standard keratometry (Sim K's) becomes even greater when dealing with corneas after excimer laser ablation (LASIK, LASEK and PRK) of the anterior surface. After refractive corneal surgery it is no longer possible to calculate corneal refractive power based only on the anterior surface, as the ratio between the anterior and posterior radius of the cornea has changed considerably. When the calcultio of the total corneal astigmatism comes into focus the effect of the posterior corneal surface cannot be disregarded anymore. Depending to the orientation of the anterior and posterior corneal kertometry the total corneal astigmatism can be over or underestimated and the axis of the total corneal astigmatism is influenced [1].

C. The refractive index

For historical reasons, most Placido topographers and keratometers use the refractive index of 1.3375 for calculating corneal refractive power. However, this refractive index is actually incorrect even for the untreated eye (n ≈ 1.332). It assumes the ratio between the anterior and posterior curvature of the cornea to be constant. Many intraocular lens (IOL) power calculation formulas use the incorrect 'K-reading', necessitating empirical correction to obtain the correct IOL power even in normal cases. Care should also be taken when using 'K-readings' from post-LASIK corneas or based on True Net Power or ray tracing, as the resultant D readings will be out of range for the applied IOL calculation formulas unless they are corrected for or converted into equivalent keratometer readings (EKR). Some modern formulas are able to deal with the rather measured curvatures of the front and back surface of the cornea, however.

D. Location of the principal planes

Calculation of corneal power by ray tracing involves sending parallel light through the cornea. It must take into account that each light beam is refracted according to the refractive index (1.376/1.336), the slope of the surfaces, and the exact location of refraction. This is necessary because the principal planes of the anterior and posterior surface differ slightly from one another due tocorneal thickness. The Pentacam® is able to measure the anterior as well as the posterior surface of the cornea. This allows further corrections to be made. The Pentacam® provides a number of different maps for predicting corneal power.

3.2 Sagittal power map (also called axial power map)

This is the common Placido style map with corneal power calculated using a refractive index of 1.3375 and the simple formula D = (1.3375-1)*(1000)/Rmm. It shows power values (Figure 1) similar to those of other Placido topographers.

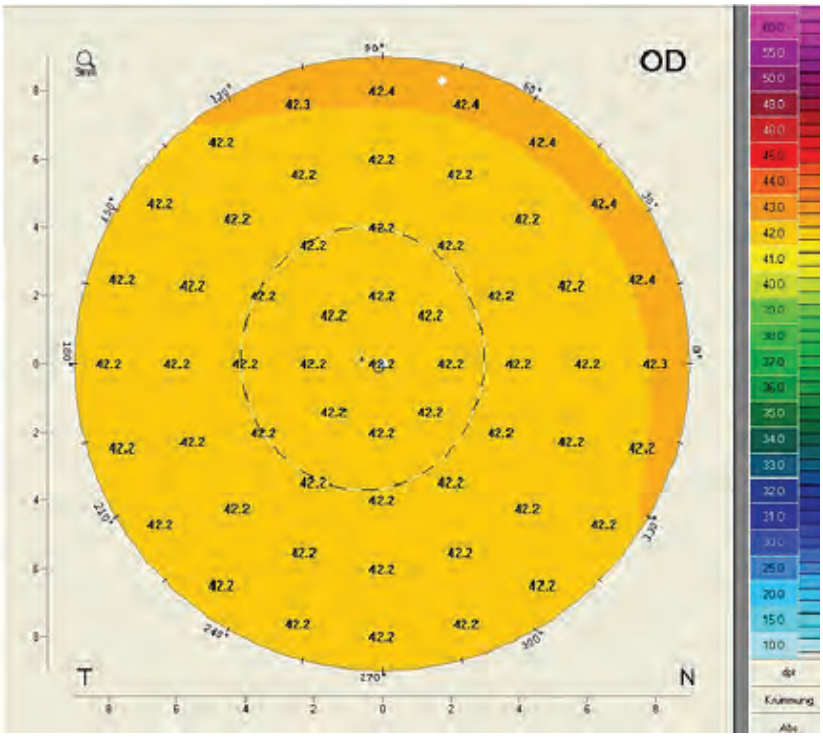

Figure 1: Sagittal power map of a sphere, r= 8 mm

3.3 Refractive power map

This map (Figure 3) uses only values from the anterior surface, but it also takes effect "A" (see above) into account. It calculates corneal power according to Snell's law of refraction assuming a refractive index of 1.3375 to convert curvature into refractive power (Figure 2). This is a map that other Placido topographers also may show because it only considers the anterior surface.

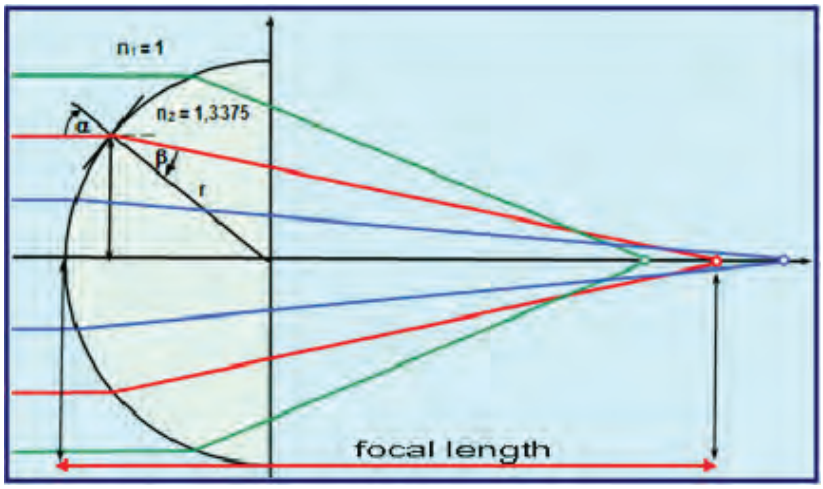

Figure 2: Snell´s law of refraction

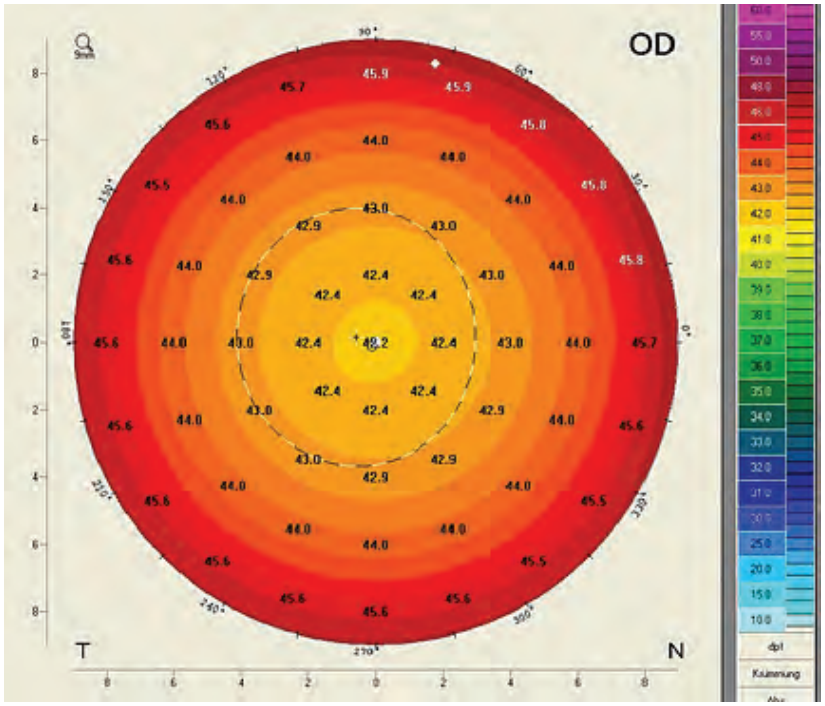

Figure 3: Refractive power map of a sphere, r = 8 mm

3.4 True Net Power

This map (Figure 4) shows the optical power of the cornea based on two different refractive indices, one for the anterior (corneal tissue: 1.376) and one for the posterior surface (aqueous humour: 1.336), as well as the sagittal curvature of each. These results are aggregated. The True Net Power map thus takes effects "A" and "B" into account. The underlying equation is:

$$TrueNet\ Power = \frac{1{,}376 - 1}{r_{ant\_surface}} * 1000 + \frac{1{,}336 - 1{,}376}{r_{post\_surface}} * 1000$$

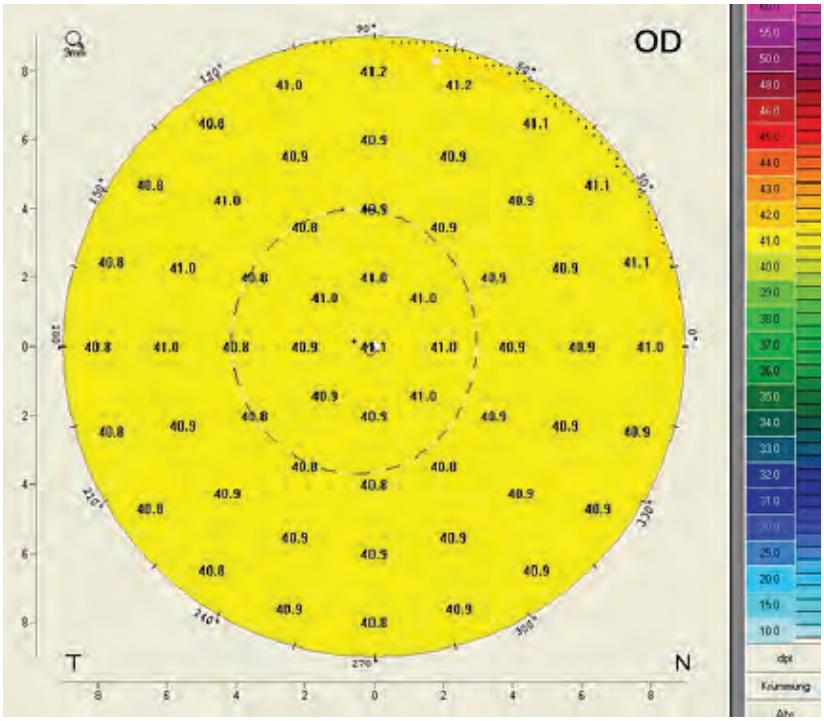

Figure 4: True Net Power map calculated by two spheric surfaces of anterior r = 8 mm and posterior r = 6.58 mm

3.5 Equivalent Keratometer Readings power map

This map (Figure 5) was designed to take into account the refractive effects of both the anterior and the posterior surface. Another requirement was that it should output power values which in normal cases (no Lasik) would be comparable with simulated K (SimK) values, which are usually derived from sagittal curvature map. Its output is therefore also referred to as Equivalent Keratometer Readings (EKR). It calculates power according to Snell's law using the refractive indices of corneal tissue and aqueous humour and aggregating the values for anterior and posterior power. Then the output is shifted such that for a normal eye (posterior corneal radius 82% of anterior corneal radius) its values (EKR) are identical to those of SimK readings from a sagittal map. In other words, the EKR map is corrected by adding the error that would be created by a refractive index of 1.3375 in a sagittal map. In this way it provides equivalent K-values (EKR) that can be used in IOL formulas that correct for n=1.3375. The EKR map thus takes into account effects "A", "B" and "C".

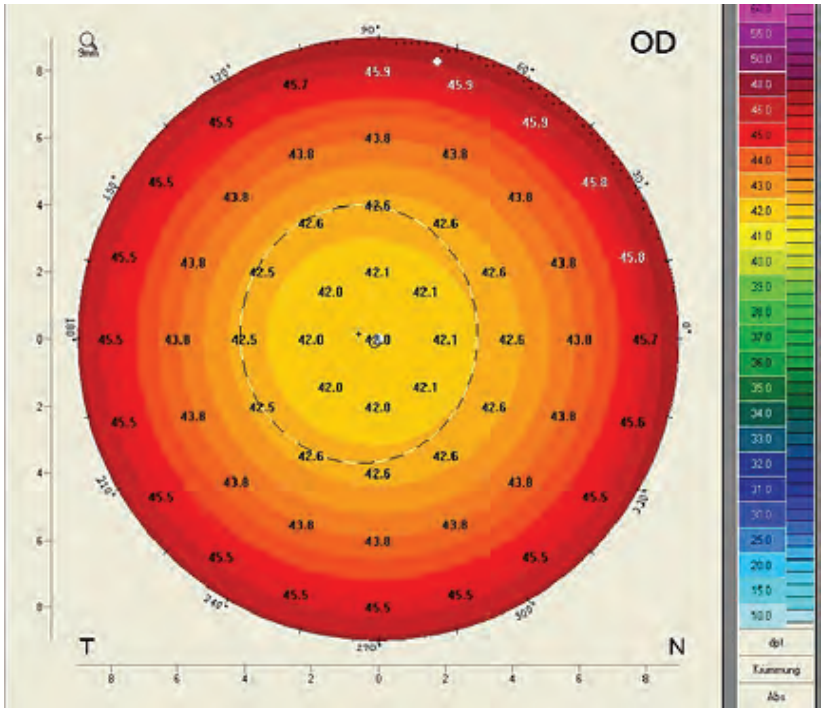

Figure 5: EKR power map calculated by twospheric surfaces of anterior r = 8 mm and posterior r = 6.58 mm

The study to validate the method was conducted using the Holladay 2 formula. Here it was determined that after LASIK the best correlation with the traditional method, with a mean prediction error of -0.06 D ± 0.56 D, is obtained using a mean zonal EKR for the 4.5 mm zone. For post-RK patients, the mean prediction error is –0.04 D ± 0.94 D [2].

3.6 Total Cornea Refractive Power map

This map (Figure 7) uses ray tracing to calculate the refractive power of the cornea. It takes into account how parallel light beams are refracted according to the relevant refractive indices (1.376 and 1.336), the exact location of refraction and the slope of the surfaces. The location of refraction is a determinant of surface slope, since the anterior and posterior surfaces have slightly differing principal planes due to corneal thickness. In this way the map takes effects "A", "B", "C" and "D" into account. Its results are more realistic than any other, but they will deviate from normal (sagittal) SimK values so they cannot be used in conventional IOL formulas.

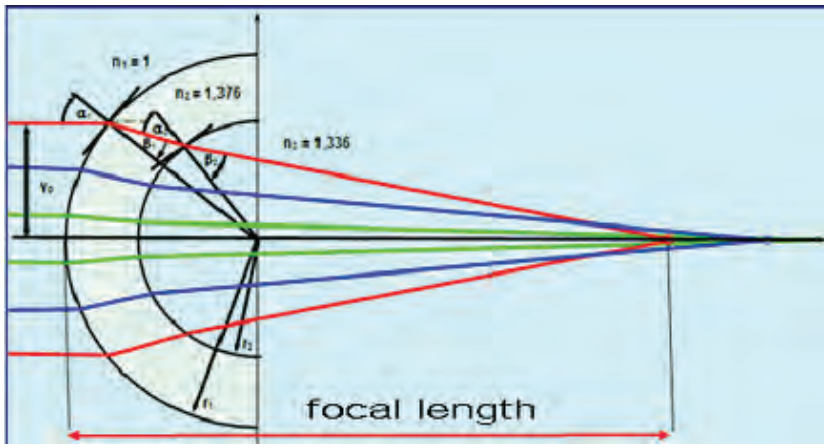

Figure 6: Calculation of power according to Snell´s law taking the different refractive indices and the different principal planes of the anterior and posterior corneal surfaces into account

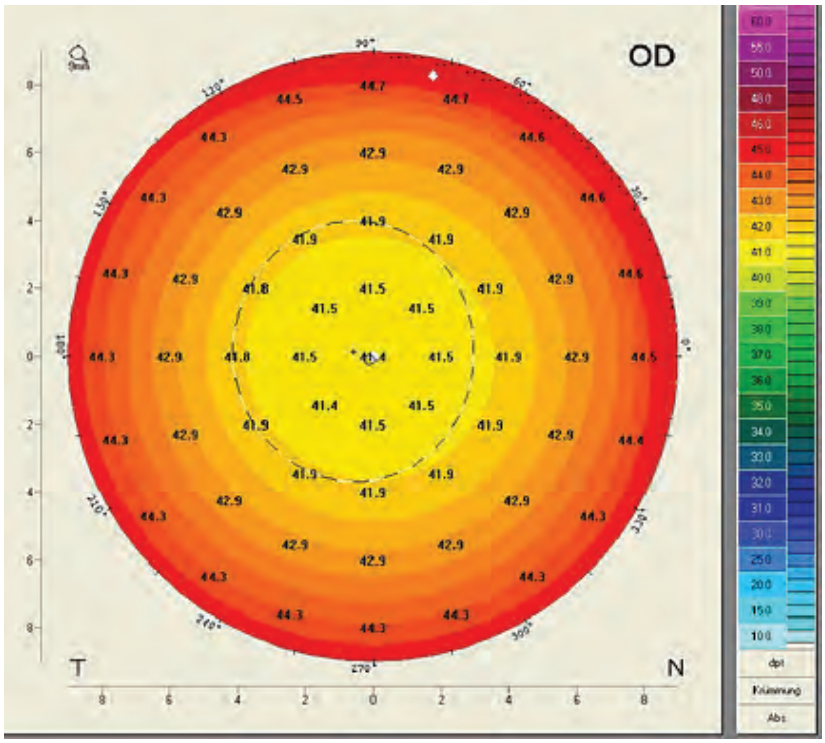

Figure 7: Total Corneal Refractive Power map calculated by two spheric surfaces of anterior r = 8 mm and posterior r = 6.58 mm and pachimetry

4 Recommended settings and color maps, displays and values

Physicians who are starting to work with the Pentacam® often turn to us with questions on settings such as step width on the color scale, or which maps and values to consider before doing LASIK, PRK, RK or phakic IOL (pIOL) implantation or in keratoconus examinations etc.

In the following chapter we present our recommendations on the more frequently addressed issues. Hopefully they will also cover most of your questions or even provide new insights as you work through them. They are no more than recommendations and not necessarily intended to discourage you from using other maps and settings that you may have found to work best for you.

4.1 Recommended settings

When working through the following chapters it is advisable to consistently use the same settings so as to be able to reproduce the values given.

- In the elevation maps, use a sphere fitted in float (BFS) and set the calculation diameter to manual and use 8 mm or 9 mm
- In the scan menu, select "25 images per scan" and "auto release"
- Keratometer presentation: R flat/R steep, unitdiopter (D)
- Corneal form factor asphericity Q:
  Q < 0: Untreated cornea, normal case
  Q > 1: Treated cornea LASIK/PRK/RK etc
- Color scale: American style
- Step width:
  Normal (10 µm) for pachymetry maps
  Normal (1 D) for topography maps
  Rel. (2.5 µm) Minimum for elevation maps
- Use the 9 mm loupe function to obtain maps comparable with those of Placido based topographers

4.2 Recommended color maps, displays and values

4.2.1 Screening for corneal refractive surgery

We recommend using the following maps and analysis displays:

- Fast Screening Report to check whether the displayed parameters are within normal limits
- 4 Maps Refractive to check the pachymetry, topography and elevation maps of both corneal surfaces
- Belin/Ambrósio Enhanced Ectasia Display to check whether there deviations from normal limits which can be a sign of early ectatic changesor keratoconus
- Zernike Analysis to see whether the LOA or HOA are withon normal limits
- Important values: R flat and R steep, asti and axis, Q-value, QS, pachymetry at thinnest spot and pupil centers, distance between the corneal apex and thinnest spot. In the elevation maps please use the parameters recommended in **chapter 10.1.2**

4.2.2 Pre-op screening for iris fixated phakic IOL implantation

We recommend using the following maps and analysis displays:

- The 3D pIOL Simulation Software and Aging Prediction prior to iris fixated pIOL implantation (available in the Pentacam® HR only). Calculate the required pIOL power using the implanted calculator. Use the database to find a pIOL that best matches the patient's subjective refraction. Its fit in the anterior chamber is simulated in 3D and the minimum clearances are displayed. The aging simulation allows a simulation of the pIOL position in up to 30 years. Double-check your calculations and evaluations with the manufacturer of the respective pIOL
- For all further pIOL e.g. Intraocular Contact Lens (ICL): Scheimpflug images to obtain information on the dimensions of the anterior chamber, the iris curve and the densitometry of the cornea and crystal lens. The view of the anterior chamber angle (ACA) shows whether there is an open or closed angle
- Evaluate the horizontal corneal diameter (HWTW). It is displayed automatically if the new iris camera optic is built in. If not it can be measured manually in the Scheimpflug image at the 180° position (horizontal)
- Important values: R flat and R steep, asti and axis, HWTW, Q-value, QS, anterior chamber depth (ACD) pachymetry in the thinnest spot and in the pupil center

4.2.3 Glaucoma screening

We recommend using the following maps and analysis displays:

- Fast Screening Report to check whether the displayed parameters are within normal limits
- General Overview display to view the chamber angle in the Scheimpflug images and corneal thickness. While clicking to the button "Enter IOP" the tonometrically measured IOP can be entered manually or the respective IOP change can be viewed. The displayed IOP is based on pre-programmed IOP corrections tables. For more details refer to the Pentacam® User Guide
- Important values: ACD, ACV, ACA, Q-value, QS, pachymetry, IOP-correction

4.2.4 Cataract surgery and IOL calculation for virgin and post refractive corneas

We recommend using the following maps and analysis displays

- Fast Screening Report to check whether the displayed parameters are within normal limits
- Cataract Pre-OP Display that offers a comprehensive overview. Prof. Maeda recommended the 4 following steps to select the IOL:
  1. Evaluation of corneal irregularities
  2. Corneal shape assessment
  3. Evaluations of corneal spherical aberrations
  4. Evaluations of the corneal astigmatism

  (An article was published in „The Highlights of Ophthalmology" *Assessment of Corneal Optical Quality for Premium IOLs with Pentacam®"* Highlights of Ophthalmology • Vol. 39, N° 4, 2011)
- Zernike Analysis to determine the amount HOA and LOA
- ACD, manual horizontal white-to-white (HWTW) for keratometry readings from virgin eyes
- Scheimpflug images to obtain information on the dimensions of the anterior chamber and the condition of the crystalline lens. Lens density can be quantified in a single location, a line, an area or a volume, as desired. The grading PNS can be used for optimizing Phaco settings (doi:10.1016/j.jcrs.2009.08.032) and for the effective phaco time (http://dx.doi.org/10.1016/j.ajo.2013.09.017)
- The Holladay Report and the Holladay EKR65 Detail Report for a comprehensive overview of the cornea. This includes the topographic as well as the pachymetry map and the anterior and posterior elevation maps. For more information refer to **chapter 17**
- The BESSt formula, developed from Edmondo Borrasio, MD. This requires Rm anterior, Rm posterior, CCT and ACD doi:10.1016/j.jcrs.2006.08.037
- Okulix or Phaco Optics, which are IOL power calculation software based on the ray tracing principle. More information can be found under: www.phacoptics.com; www.okulix.de
- Important values: Keratometry, asti and axis, Q-value, QS, ACD, pachymetry in the thinnest spot and in the pupil center

5 Differences between Placido and elevation-derived curvature maps by Prof. Michael W. Belin

5.1 Keratoconus in OD and OS?

The case shown below explains the difference between suspicious and significant elevation maps and numbers. The topographic map (Figure 8) shows the left and right eye but gives no unequivocal statement if it is a keratoconus or not.

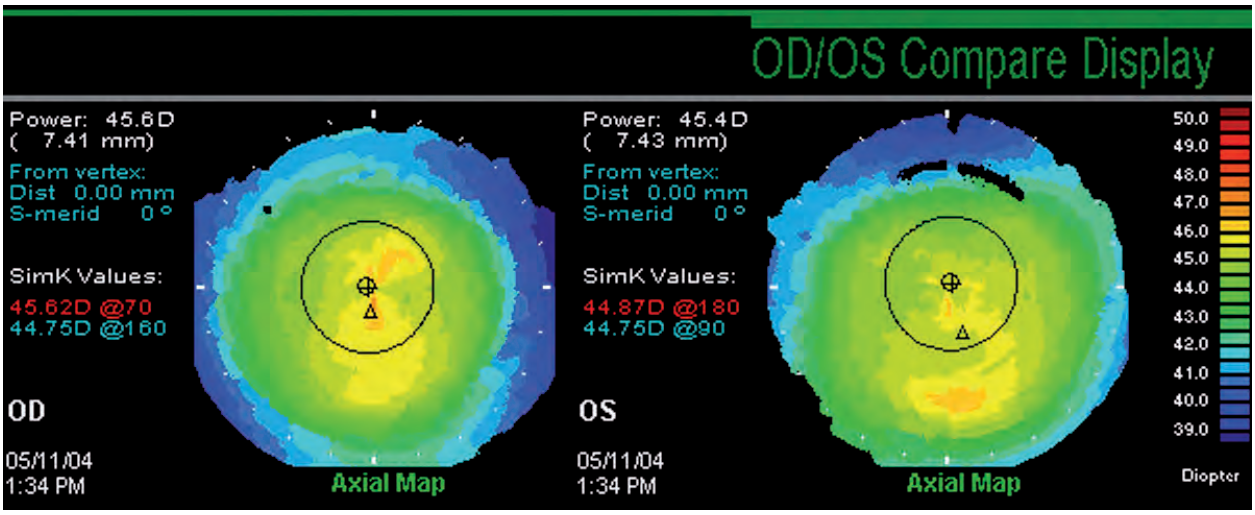

Figure 8: Placido based topography of OD and OS allowing no conclusion regarding keratoconus

The right eye seems to be fine. The left eye is a little steeper. The Pentacam® 4 Maps Selectable answers clearly the question.

The right eye (Figure 9) has a regular corneal thickness, but the elevation maps of the anterior and posterior surface indicates this cornea as a suspicious cornea. Both sides show an inferior position of the cone with suspicious elevations.

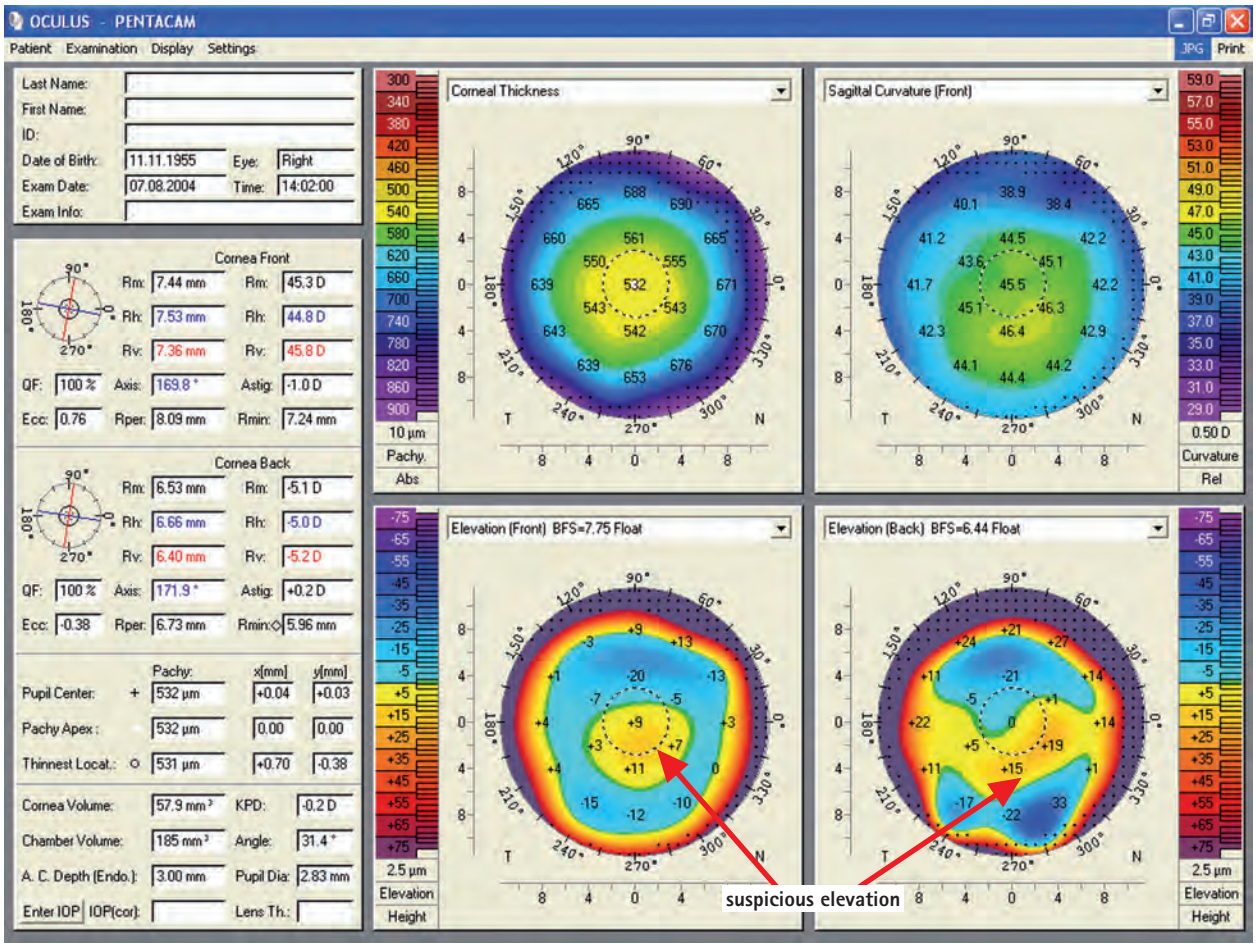

Figure 9: 4 Maps Selectable showing keratoconus-suspicious elevations in OD

The left eye (Figure 10) indicates an inferior steepening, but a smooth anterior elevation map. The reason for the thinning in the pachymetry map is the posterior elevation map, where there are significant elevations of more than 30 µm. Note that the position of the thinning in the pachymetry map and the highest spot on the elevation map are exactly at the same position.

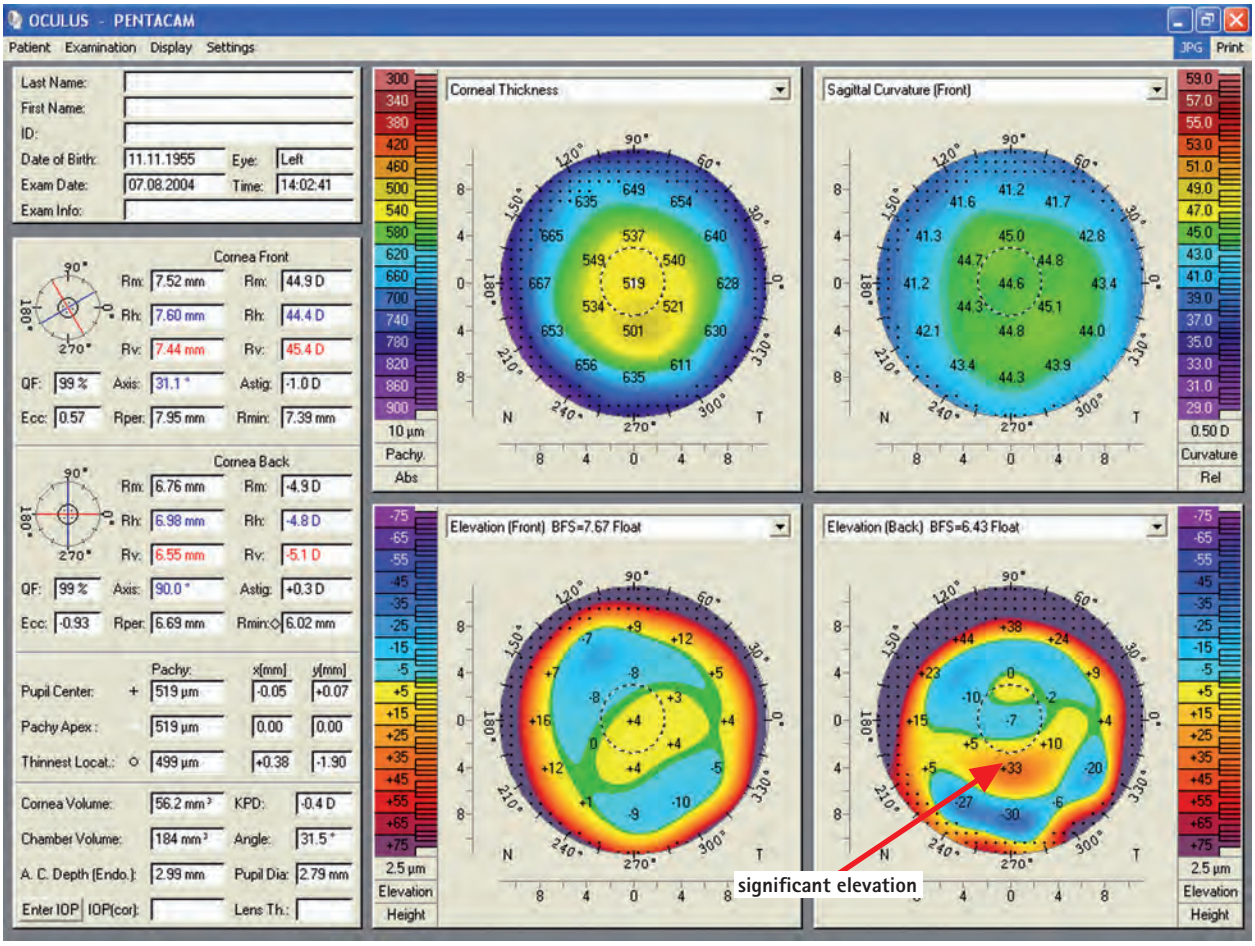

Figure 10: 4 Maps Selectable showing significant elevation in OS

This is an excellent example to document that topography or anterior elevation only does not indicate keratoconus.

5.2 Form fruste keratoconus?

A 47-year-old female presented for a second opinion. She had previously been told she was not a candidate for refractive surgery and that she had "form fruste" keratoconus.

Her exam had revealed a BSCVA 20/20+ OD, and the slit lamp and external examination findings had been WNL. However, Placido topography showed the following (Figure 11):

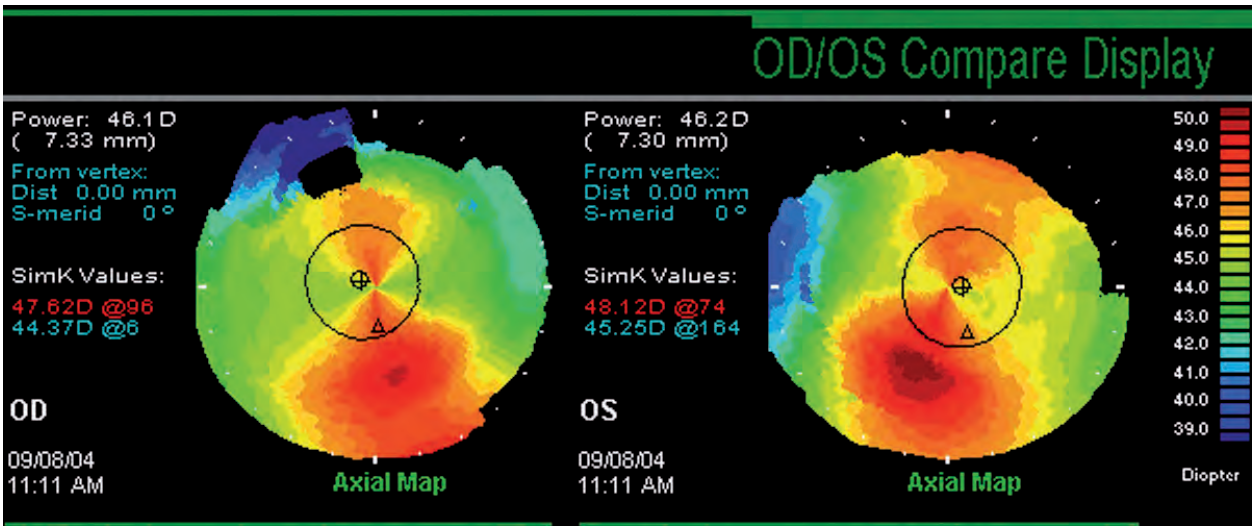

Figure 11: Placido based topography of OD and OS

Pentacam® anterior segment analysis revealed normal pachymetry (normal distribution & central thickness > 650 µm).

The anterior and posterior elevation revealed a slightly decentered apex. This had led to a "false positive" inferior steepening on the curvature map. Custom LASIK was performed without incident (Figure 12, Figure 13).

Note:

This case illustrates the limitations of curvature analysis in trying to analyze a shape abnormality. Curvature is a reference-based measurement and in this case, inaccurately reflects shape information. Elevation data are independent of axis or orientation and does not have the false positive rates as curvature maps commonly do.

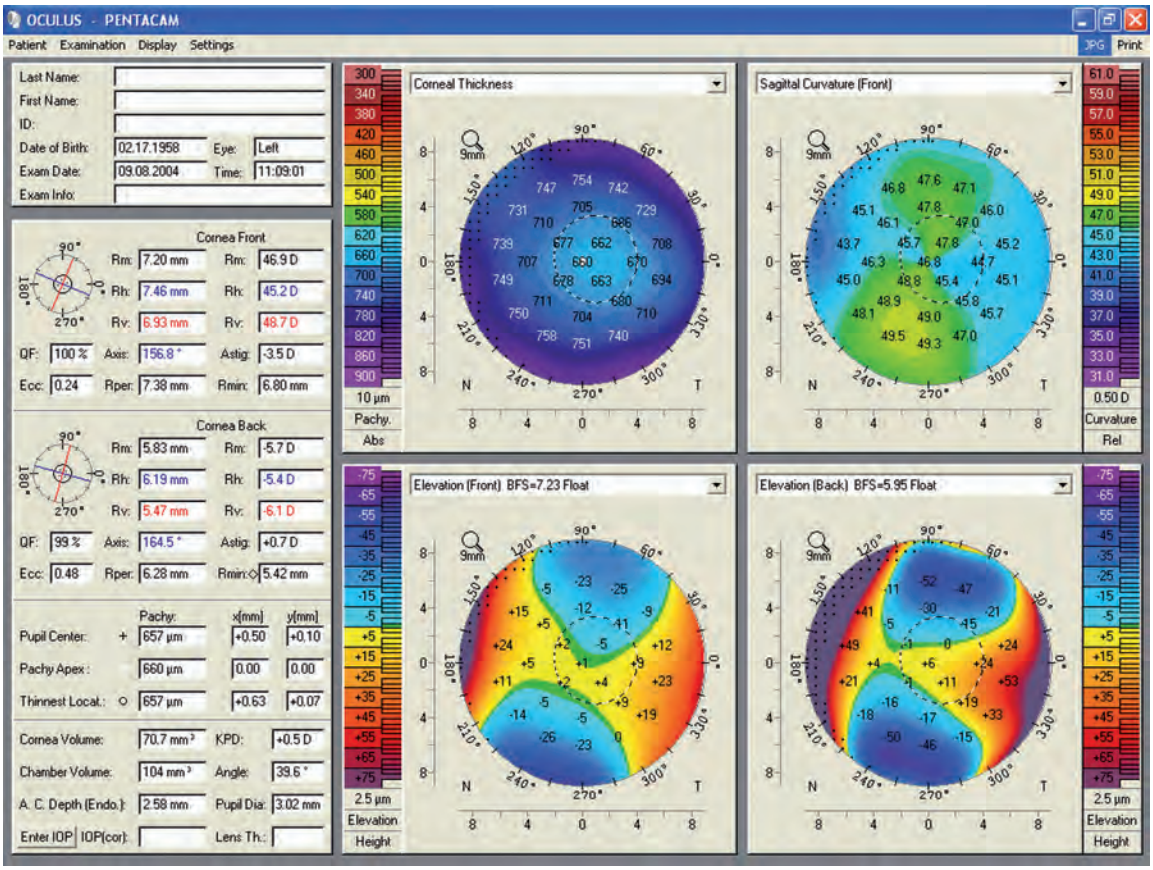

Figure 12: 4 Maps Selectable showing a form fruste keratoconus false-positive topography in OS

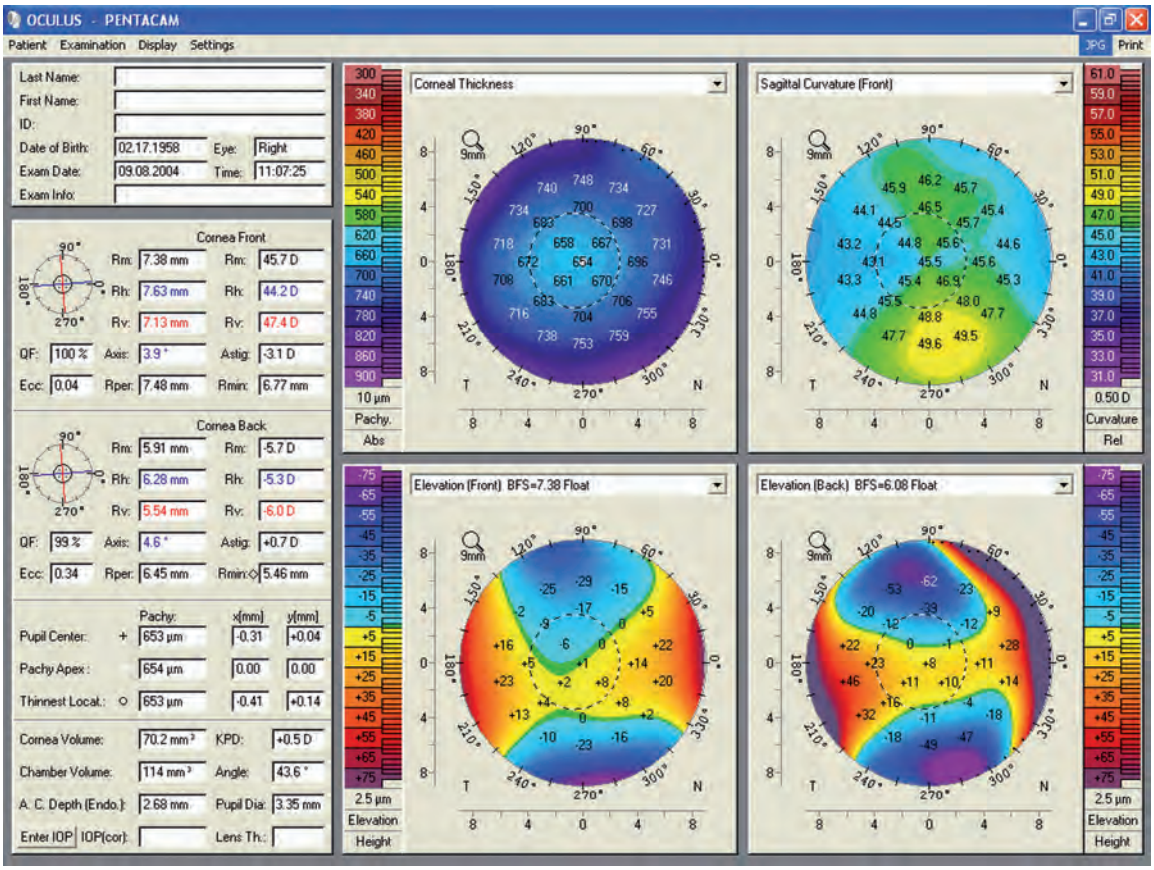

Figure 13: 4 Maps Selectable showing a form fruste keratoconus false-positive topography in OD

6 The Fast Screening Report as a first step in examining a patient and evaluating one's findings by Ina Conrad-Hengerer, MD

The Fast Screening Report is a very good way of gaining a quick overview when examining patients, especially when they are presenting for the first time. The Pentacam® analysis is a contactless examination routine which provides you with all relevant data in a mere two seconds. These are compared with normative data and converted to index (marker) values using suitable algorithms. These index values can give helpful indications of possible underlying pathology. How does the anterior chamber compare with that of a normal eye? Or how about the pachymetry or the elevation data of the front or back surface of the cornea? Might there be something remarkable about the patient's corneal densitometry? The black line always indicates the value of the current patient, and its position in the grey bar chart shows where it comes to lie in a standard normal distribution. In the red-and-green chart this normal distribution is shown in green so that it can be compared with that of the relevant pathological patient group, shown in red. The navigation bar at the top of the Fast Screening Report leads you to other maps. If a suspicious value has been detected, it will indicate the name of the map with which this can be explored further. Clicking on the name will take you directly to the relevant map. In the lower part of the Fast Screening Report you can see whether the corneal elevation data (BAD D) are within the normal range or not, whether there is keratoconus, and if so, of what degree (TKC), and if there is a cataract, the degree of nuclear opacity (PNS).

6.1 Case 1: Unilateral high astigmatism with suspicion of bilateral keratoconus

A male patient aged 45 years presented for the first time in 2010 to have his distance spectacles refitted. He reported having a long history of amblyopia of his left eye with a visual acuity of 20/100 – 20/67 at best and no known strabismus. Lang's stereotest I was positive. Correction with sph 0.00 cyl -5.00 A 14° gave him a visual acuity of 20/25 on his left eye, while sph -0.50 cyl -0.50 A 170° improved his visual acuity to 20/20 on the right.

Slit lamp microscopy showed clear, refracting media bilaterally with no corneal scarring or other abnormalities. Fundoscopy revealed 2 chorioatrophic foci in the left eye. All other examinations (without the Pentacam®) yielded unremarkable results.

It was not until 5 years later that the patient presented again, now suspecting that the refraction of his right eye had changed. The slit lamp microscopy findings were virtually unchanged.

- OD: sph -0.50 cyl -1.25 A 167° visual acuity (VA) 20/20
- OS: sph 0.00 cyl -4.75 A 14° visual acuity (VA) 20/25

The Pentacam® Fast Screening Report provides an immediate and clear picture of the unusual pachymetry and elevation profile of the anterior and posterior corneal surface (Figure 14), whereas the maps appear relatively normal. On following the navigation bar to the Belin/Ambrósio Enhanced Ectasia Display one finds unmistakable evidence of an advanced keratoconus of both eyes (Figure 16, Figure 17). Here the Pentacam® reveals a disease that the patient could have been made aware of many years earlier.

The patient was informed about this corneal pathology and its prognosis. To improve his visual acuity he had a rigid contact lens fitted for his left eye. He is coming for follow-up every six months to monitor how the disease progresses.

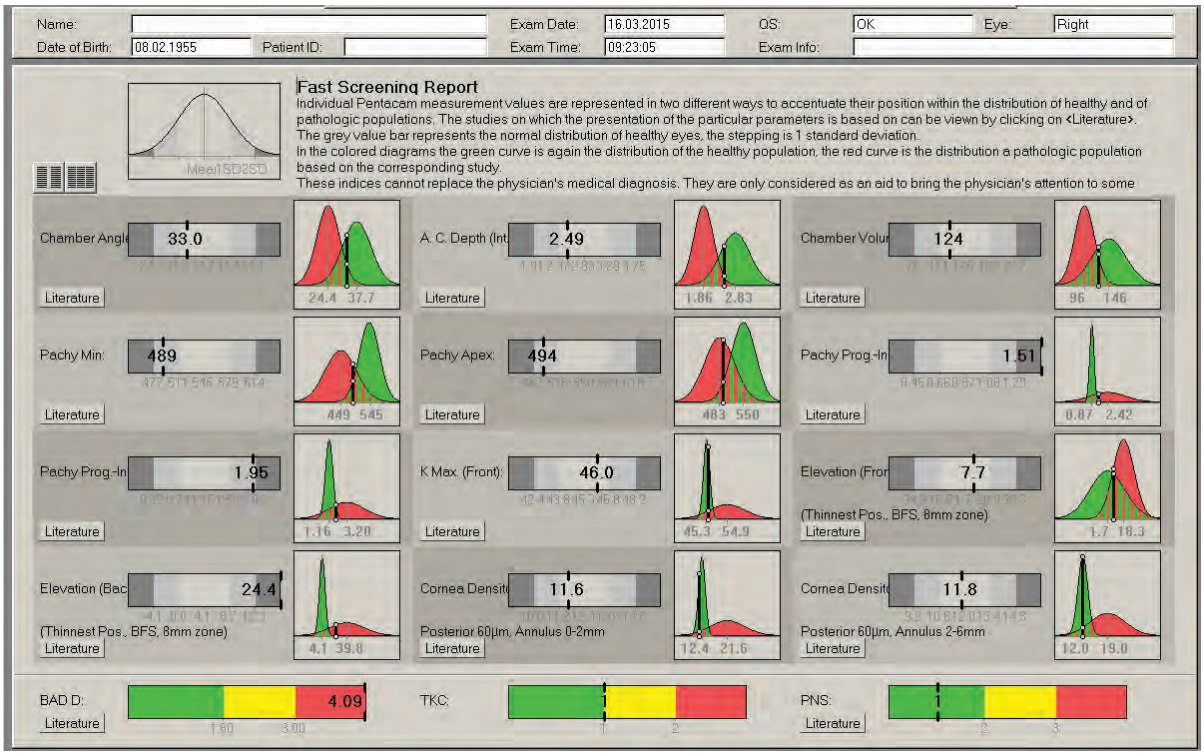

Figure 14: Fast Screening Report showing abnormal pachymetry and elevation data with unambiguous signs of keratoconus in OD

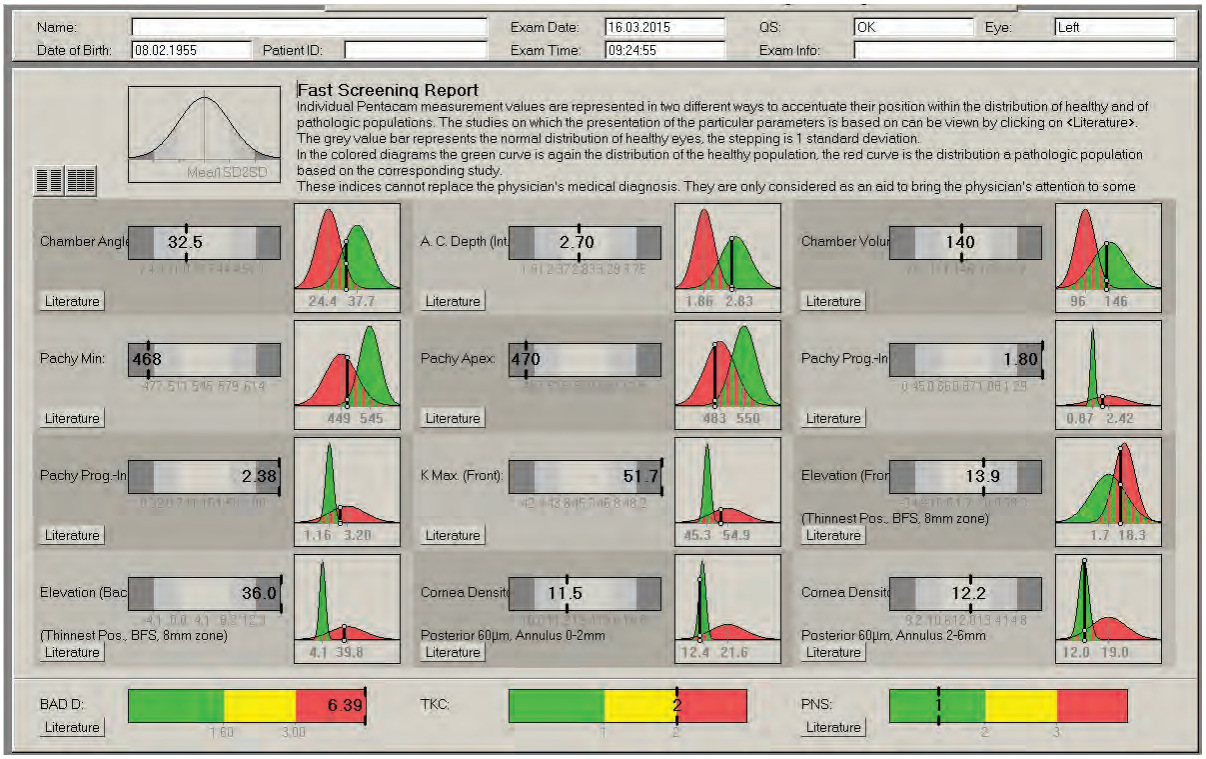

Figure 15: Fast Screening Report showing abnormal pachymetry and elevation data with unambiguous signs of keratoconus in OS

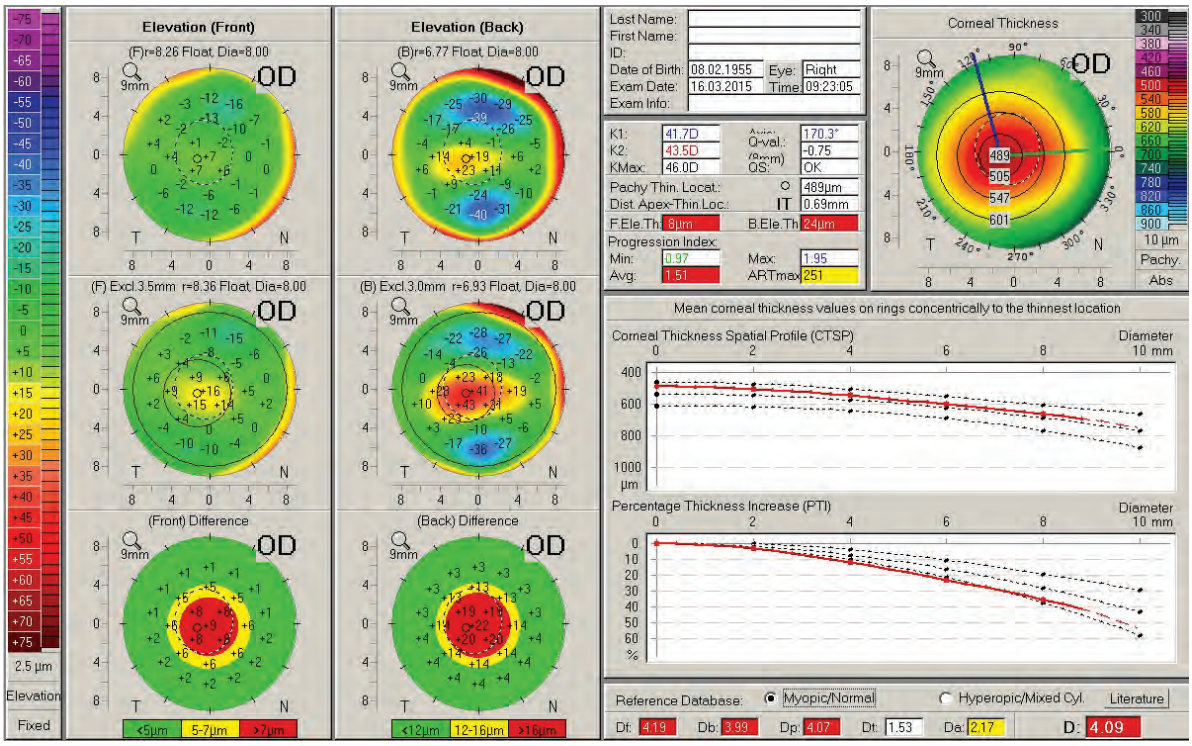

Figure 16: Belin/Ambrósio Enhanced Ectasia Display (version III) showing keratokonus in OD

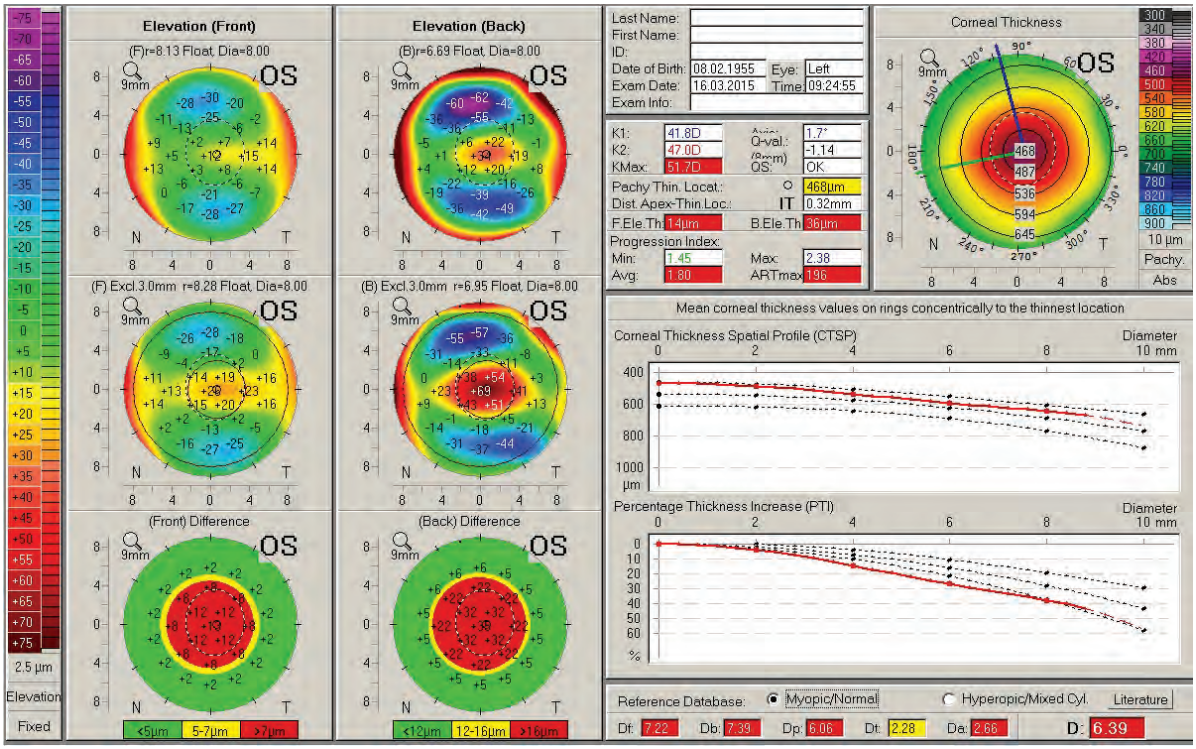

Figure 17: Belin/Ambrósio Enhanced Ectasia Display (version III) showing keratokonus in OS

6.2 Case 2: Fuchs' dystrophy with DMEK cataract surgery – progress evaluation

A 63-year-old female patient with bilateral cataract and Fuchs' dystrophy underwent combined cataract and DMEK surgery. This section reports on her progress, documenting the condition of her right eye prior to surgery with the Fast Screening Report (Figure 19) and the Corneal Optical Densitometry display (Figure 21). The symptoms of Fuchs' dystrophy are clearly to be seen in these displays. After the surgery it was possible to follow her course of healing, marked by gradual deturgescence of the corneal stroma. From follow-up measurements performed one month after the surgery (Figure 22) it was verified that the corneal graft lay flat against the host stroma, and transplant deturgenscence was functionally assessed on the basis of the Compare 4 Exams display (Figure 18). At one week postoperative central apical corneal thickness measured 670 µm. In the course of the following 8 days it increased to 704 µm and after another 9 days had dropped back to 630 µm. At one month postoperative it had reached a relatively normal value of 582 µm. Since the graft was obviously functioning well, there was no need to force further deturgenscence with hyperosmolar eye drops. At 4 weeks postoperative her right eye showed refraction values of sph +0.50 cyl -1.00 A 108° and a visual acuity of 20/25. Her combined cataract and DMEK surgery has turned out well, as is also confirmed by the Fast Screening Report (Figure 20). She currently comes regularly every 2 weeks for follow-up.

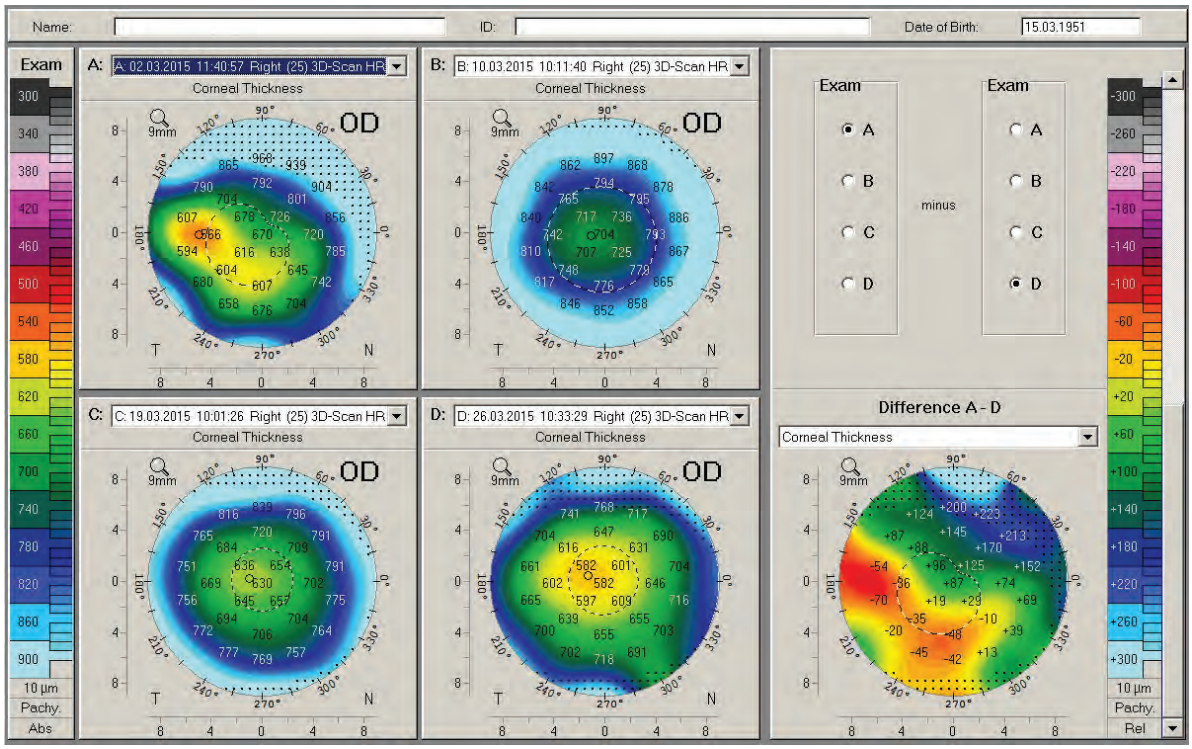

Figure 18: Compare 4 Exams for postoperative monitoring of corneal deturgescence over the course of one month

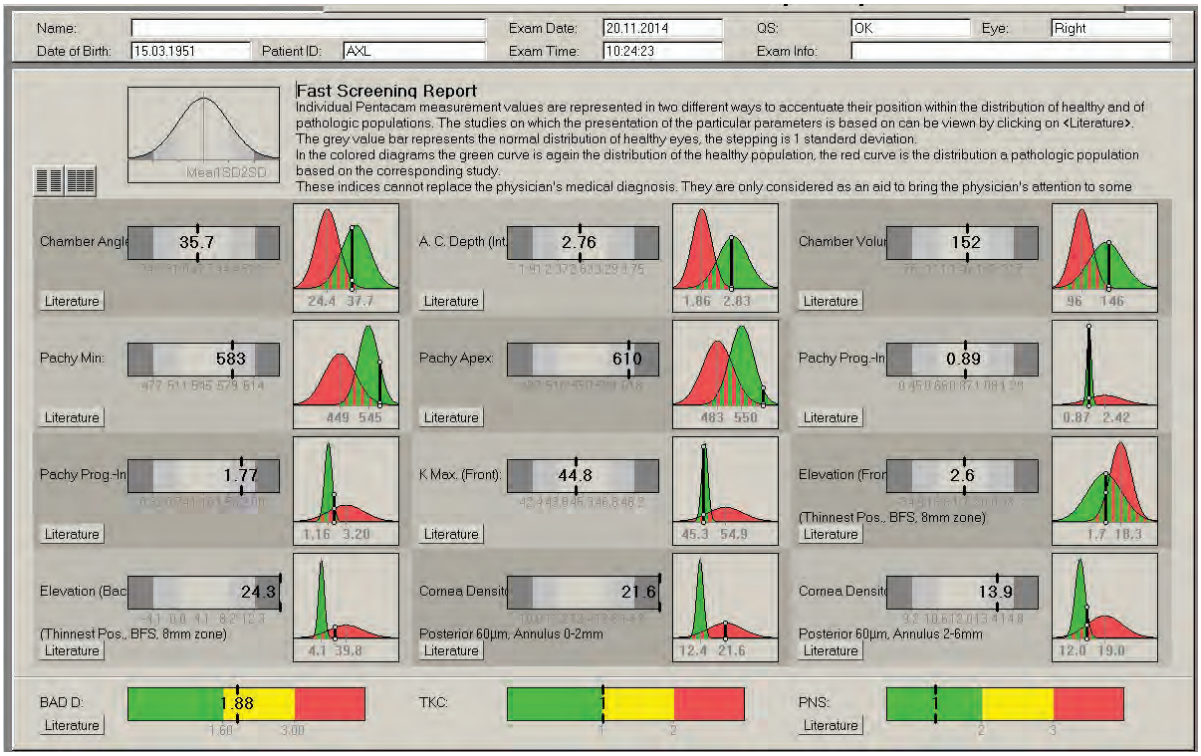

Figure 19: Fast Screening Report showing the presurgical condition in a case of Fuchs' dystrophy

Figure 20: Fast Screening Report at one month after DMEK surgery

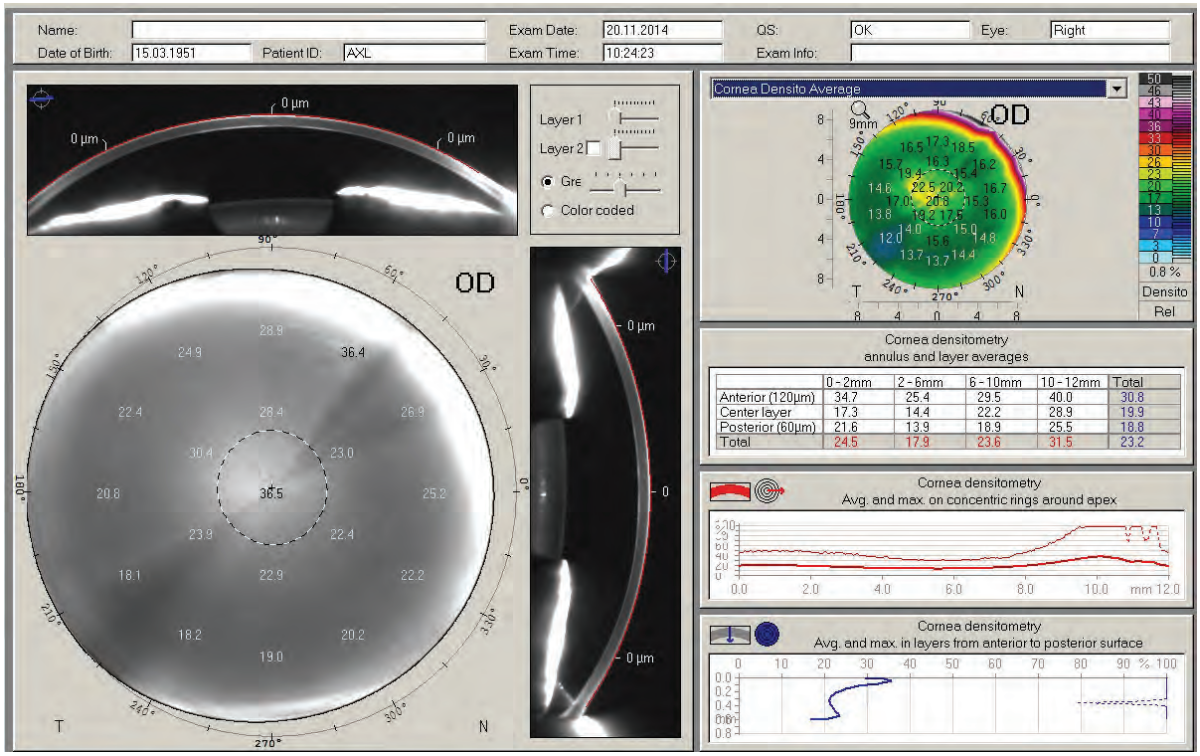

Figure 21: Corneal Optical Densitometry showing the presurgical condition in a case of Fuchs' dystrophy

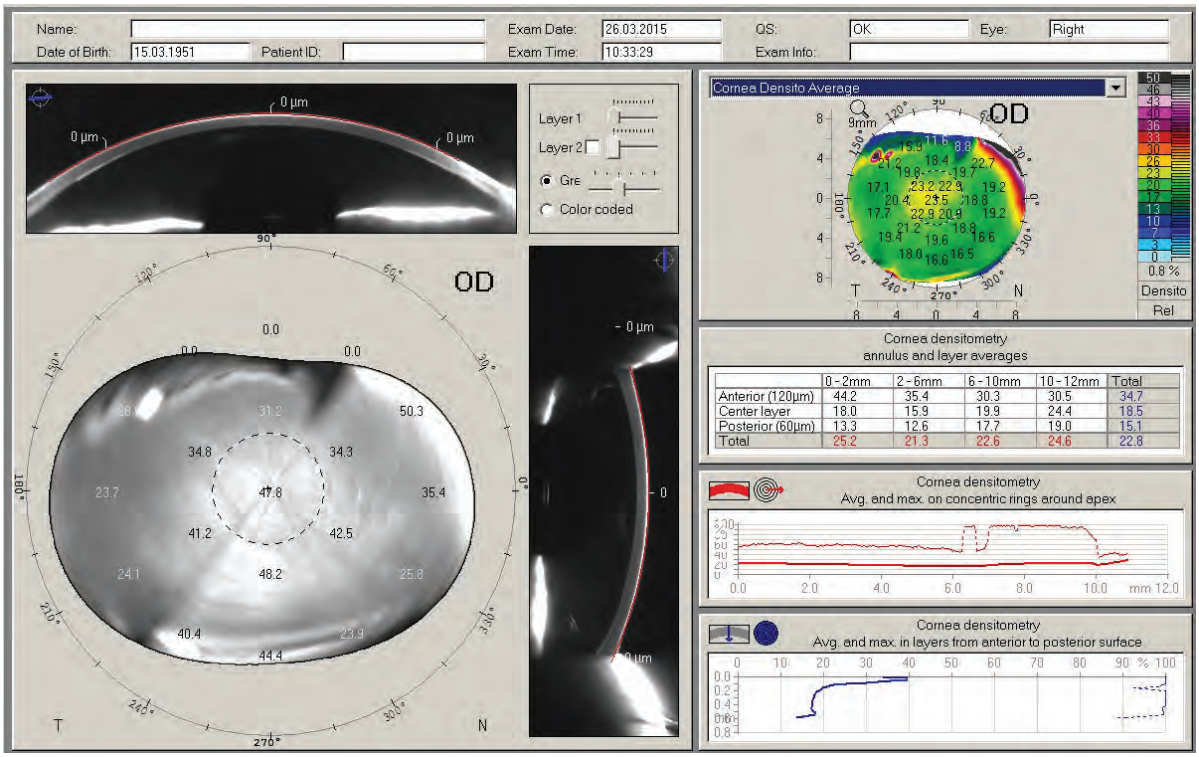

Figure 22: Corneal Optical Densitometry at one month after DMEK surgery

6.3 Case 3: Corneal injury sustained from an eye drop bottle after cataract surgery

A 54-year-old patient underwent cataract surgery on his highly myopic right eye. The surgery was performed without any complications, resulting in a postoperative visual acuity of 20/20 with refraction values of sph -1.75 cyl -0.75 A 25°. After 3 weeks the patient complained of deteriorated visual acuity without pain.

Slit lamp microscopy showed the cornea to be completely transparent, with a small irregularity paracentrally. His refraction had changed to sph -4.50 cyl -1.50 A 108° and his visual acuity had dropped to 20/25, and there was no intraocular irritation. The possibility of a macular oedema (Irvine-Glass syndrome) was reliably excluded by fundoscopy. The patient expressed dissatisfaction at this unexpected turn of events, but on inquiry remembered having knocked the eye drop bottle against his right eye.

Analysis based on the Pentacam® Fast Screening Report revealed an abnormal value for K Max (anterior surface) as well as posterior elevation (Figure 23). After calling up the 4 Maps Refractive color display via the navigation bar it was possible explain the changes to the patient. He was able to see for himself the abnormal distribution of refractive power and anterior elevation profile around the centre of his right pupil (Figure 24). A week later Pentacam® measurements showed that the disturbance had subsided, with refraction values of sph -2.00 cyl -0.25 A 0° and visual acuity back at 20/20. The patient was shown the Compare 2 Exams display, demonstrating the improvement that had occurred in only a week (Figure 25). It was decided to postpone refitting his spectacle lenses by 2 weeks, since the Pentacam® analysis indicated that his right-eye refraction had not yet reached its ultimate distribution.

Figure 23: Fast Screening Report showing suspicious values of K Max (anterior surface) and posterior elevation

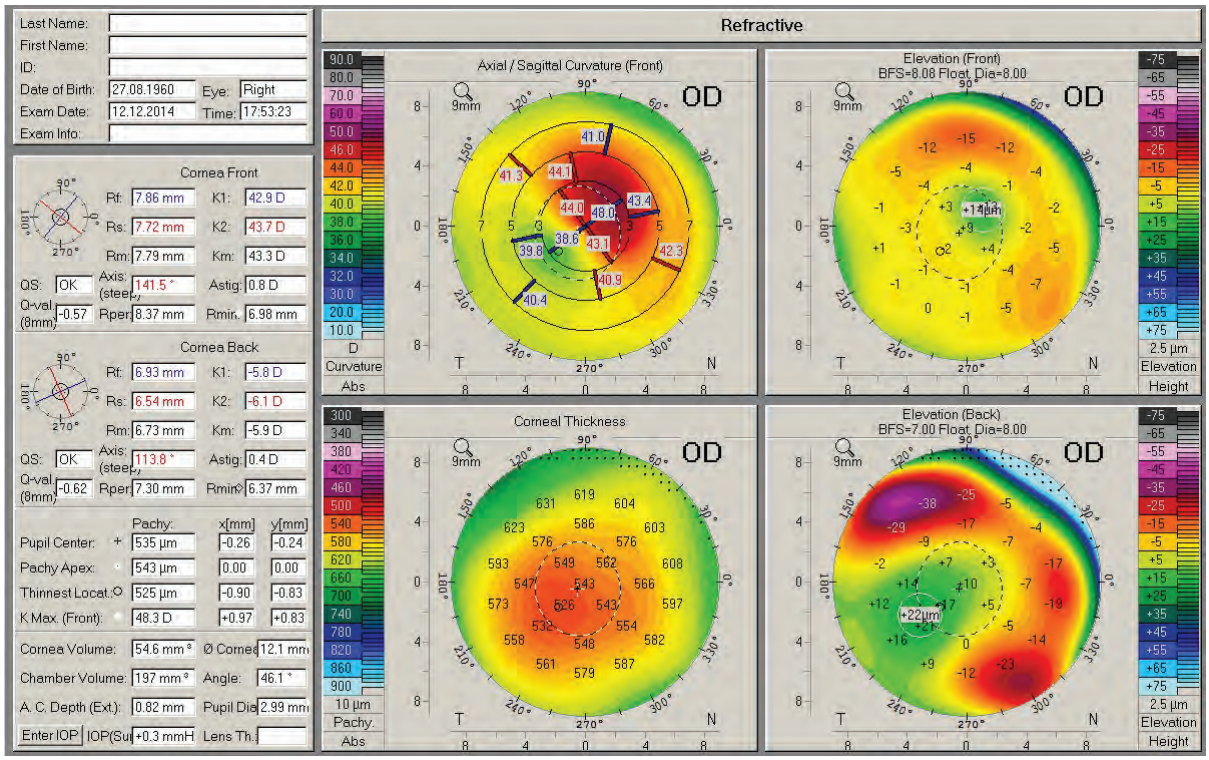

Figure 24: 4 Maps Refractive with suspicious curvature and elevation maps of the anterior surface

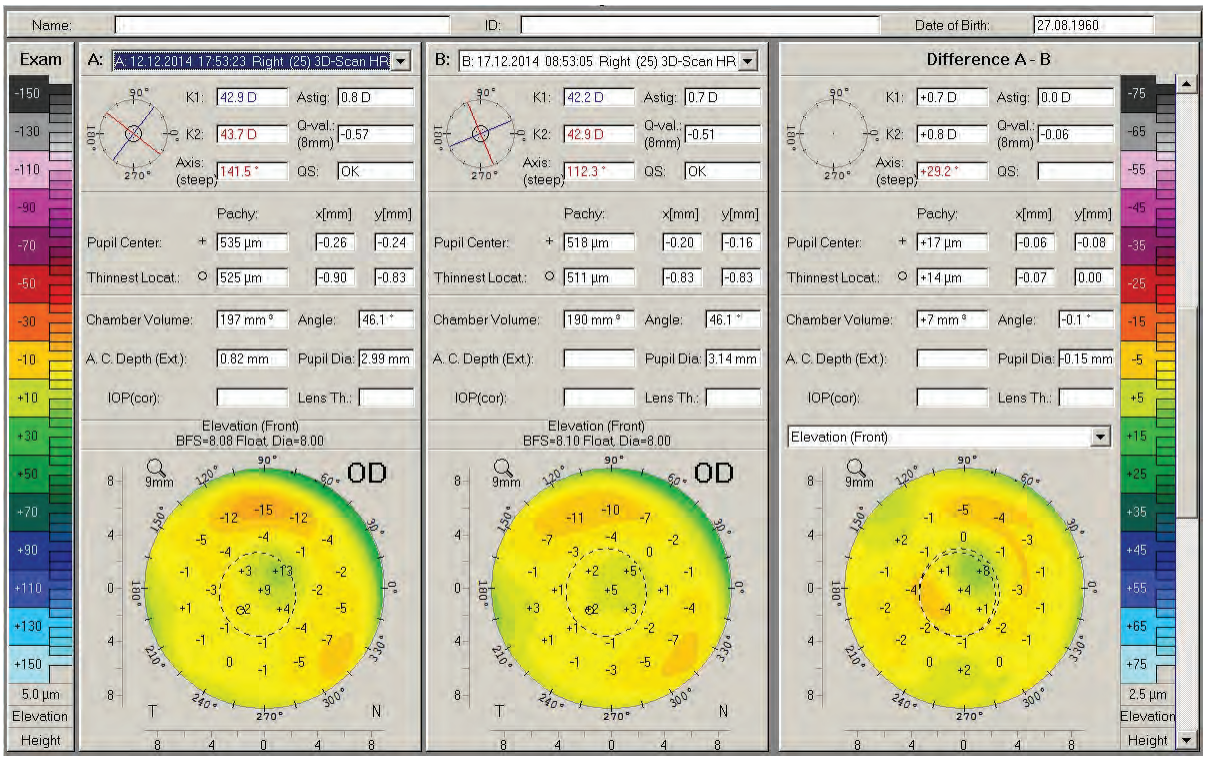

Figure 25: Compare 2 Exams showing changes in anterior surface elevation within a period of one week

7 Corneal Power Distribution display by Ina Conrad-Hengerer, MD

7.1 Visual acuity impairment during nighttime driving with distance spectacles – nocturnal myopia?

A driver had been wearing distance spectacles with the following refraction values for 2 years:

- OD: sph -0.25 cyl -0.50 A 170° VA 20/20
- OS: sph -1.00 cyl -0.25 A 27° VA 20/20

Slit lamp microscopy showed clear, refracting media bilaterally with no corneal scarring or other abnormalities. Fundoscopy was unremarkable. Mesopic pupil diameter was 3.00 – 3.50 mm. The possibility of keratoconus was excluded (Figure 26, Figure 27).

With the Corneal Power Distribution display covering a diameter zone from 1.0 to 8.0 mm the Pentacam® calculated right-eye total cornea refractive power (TCRP) as having an almost constant astigmatism at around 1.00 – 1.10 D from the centre up to 5.0 mm peripherally, which then rose from 1.30 D at 6.0 mm to 1.60 D at 7 mm and further to 2.10 D at 8 mm (Figure 28). For the left eye the Corneal Power Distribution display showed an astigmatism of 0.30 D from the center up to 2.0 mm which then rose towards the periphery, reaching 0.60 D at 3.0 mm, 0.90 D at 4.0 mm, 1.10 D at 5.0 mm, 1.20 D at 6.0 mm, 1.40 D at 7.0 mm and 1.70 D at 8.0 mm (Figure 29).

It was therefore decided to determine the correction needed for nighttime driving by subjective testing. A satifacory outcome was achieved by increasing left-eye astigmatic correction by 0.75 D (giving a refraction of sph -1.00 cyl -1.00 A 30°), and a pair of nighttime driving spectacles were fitted accordingly.

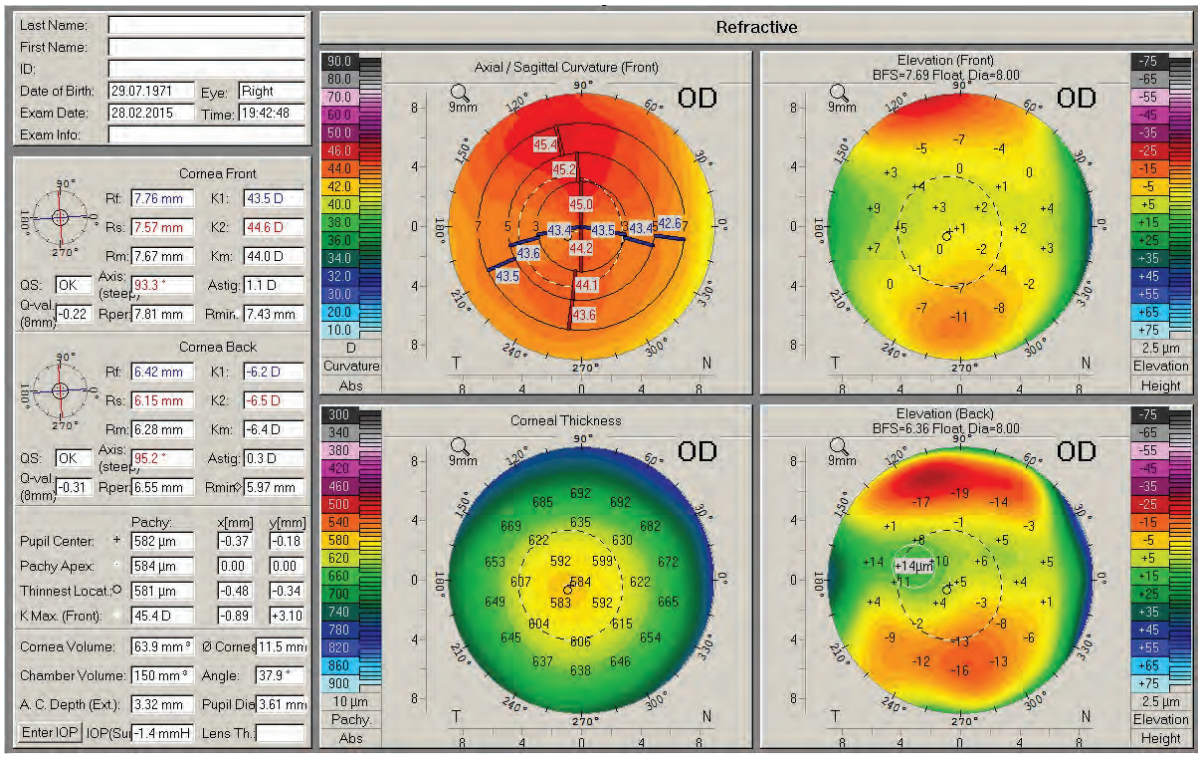

Figure 26: 4 Maps Refractive showing with unremarkable elevation maps and curvature map in OD

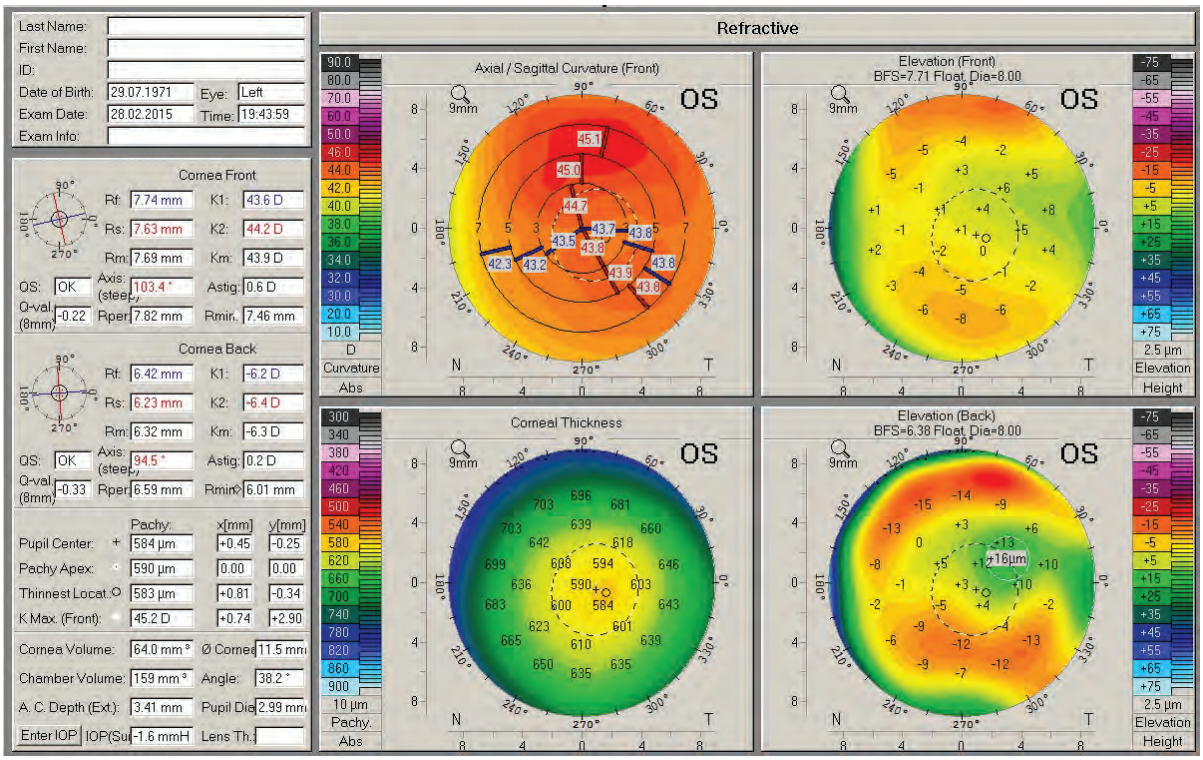

Figure 27: 4 Maps Refractive showing unremarkable elevation maps and curvature map in OS

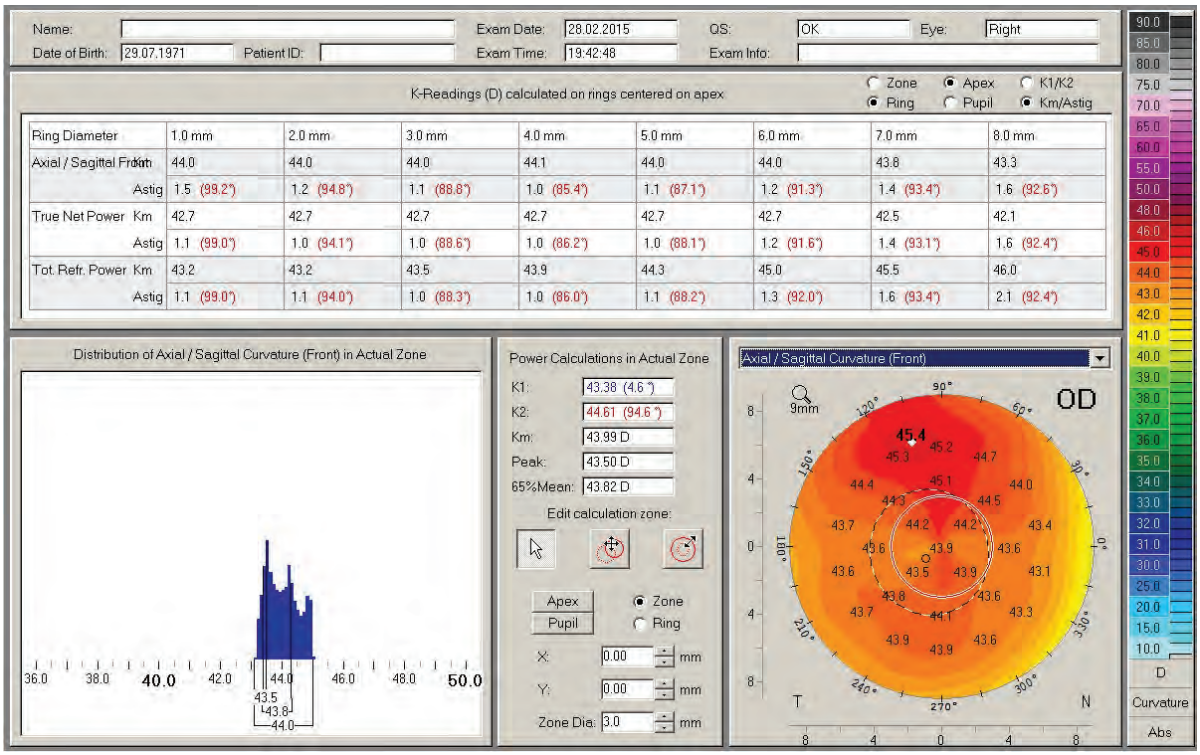

Figure 28: Corneal Power Distribution showing normal power distribution in OD

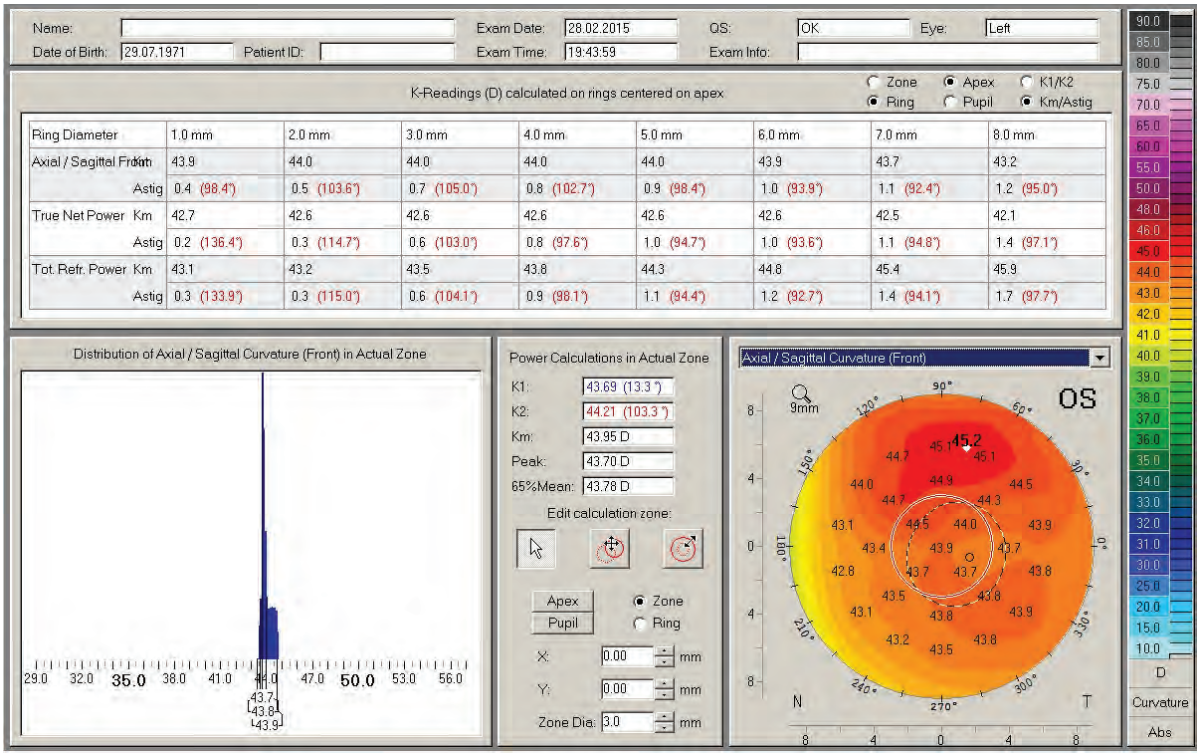

Figure 29: Corneal Power Distribution showing a markedly increased power from 2.0 to 3.0 mm in OS

8 Corneal ectasia

8.1 Case 1: Ectasia after radial keratotomy by Prof. Renato Ambrósio Jr

A 28-year-old male patient had RK (radial keratotomy) in 1995 for myopic astigmatism followed by RK enhancement three years later in OS. Corneal topography was not performed prior to surgery according to patient information. Uncorrected vision acuity was 20/30 in OD and 20/200 in OS. Patient refers severe glare and starburst all day, mainly at night.

- OD: sph -0.25 cyl -3.00 A 156° VA 20/20
- OS: sph -5.00 cyl -2.25 A 39° VA 20/30

The Pentacam® 4 Maps Refractive map (revealed corneal ectasia in both eyes, with a more advanced condition in OS (Figure 31). In OD (Figure 30) the central cornea showed less distortion, permitting relatively good uncorrected vision.

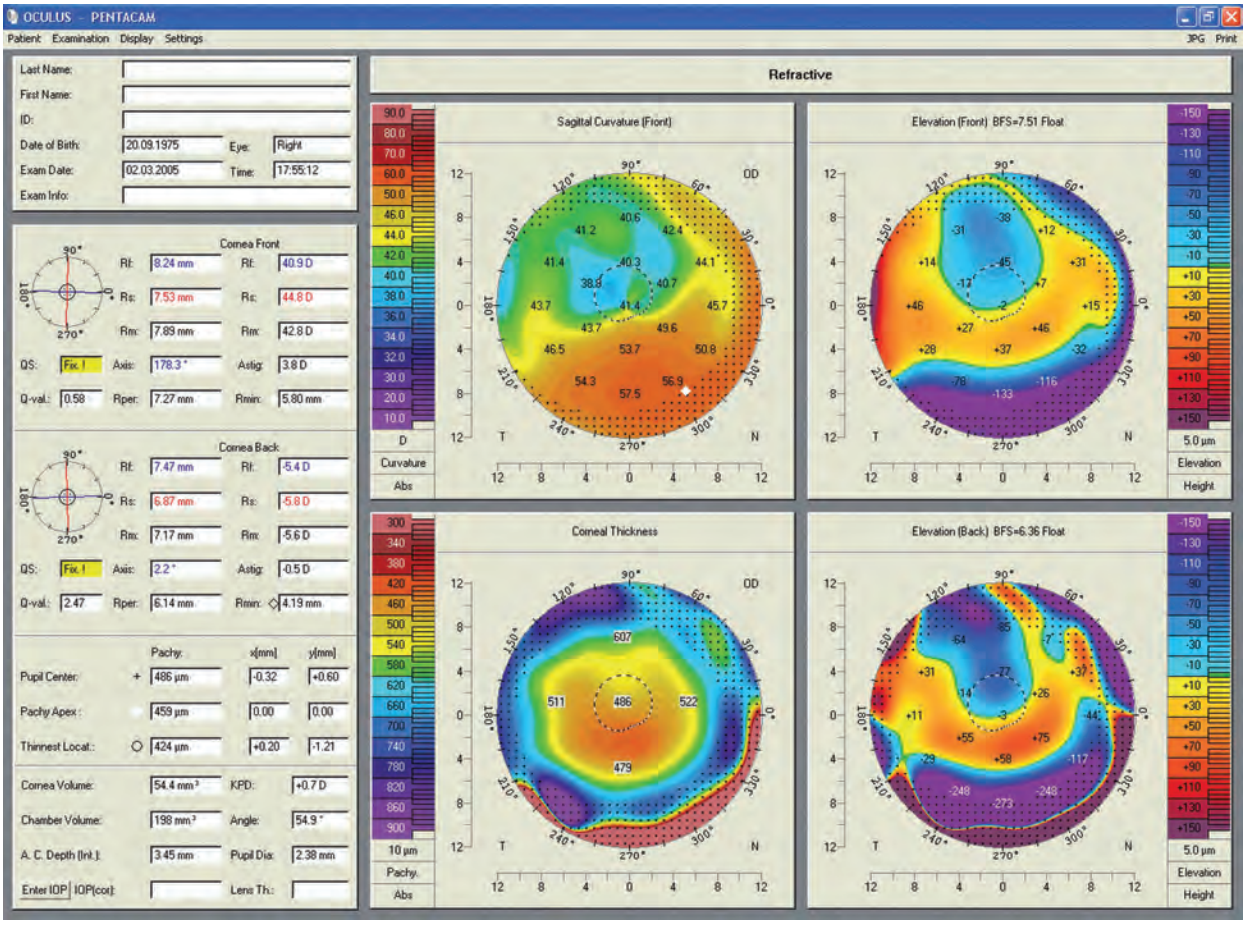

Figure 30: 4 Maps Refractive of OD showing post-LASIK ectasia

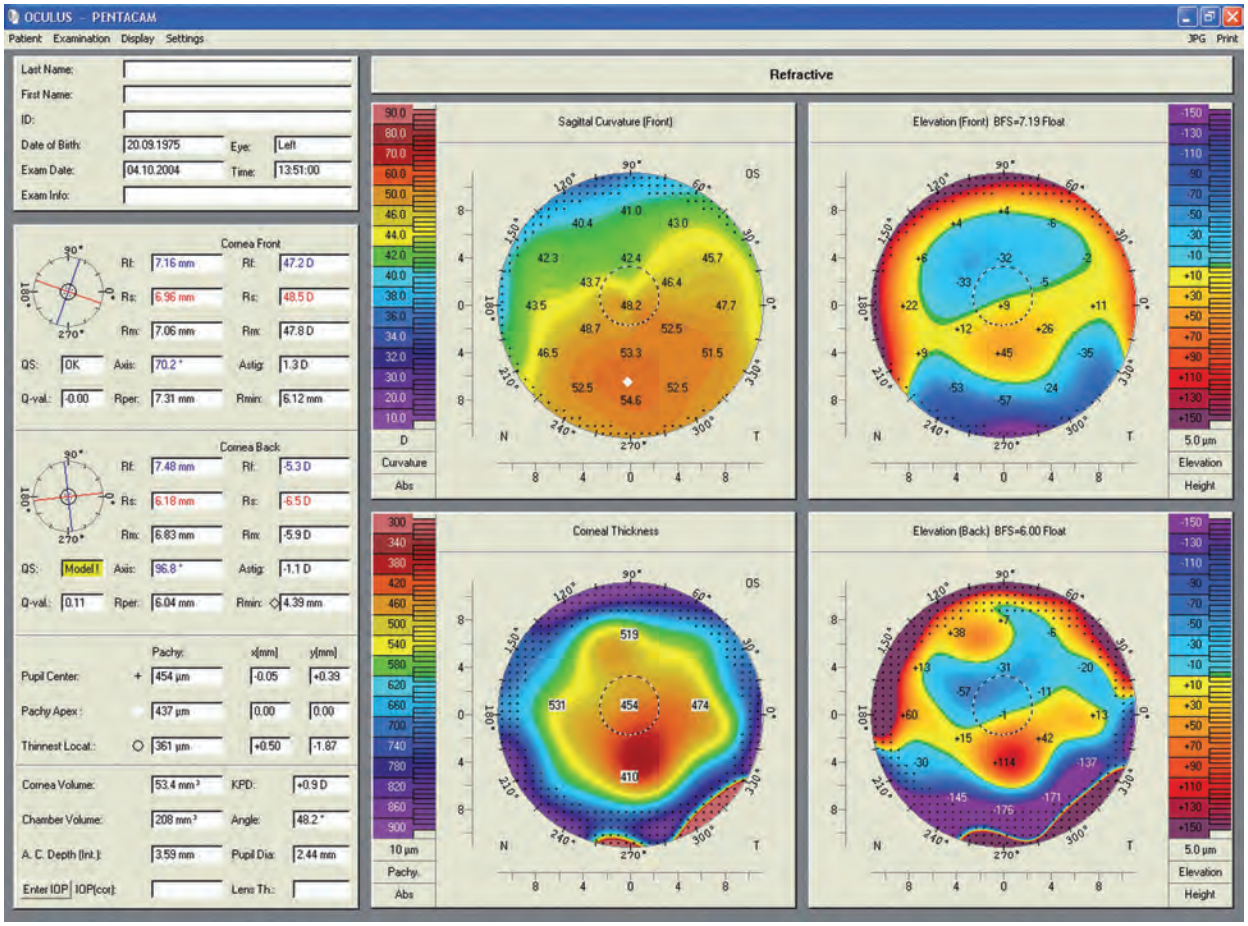

Figure 31: 4 Maps Refractive of OS showing post-LASIK ectasia

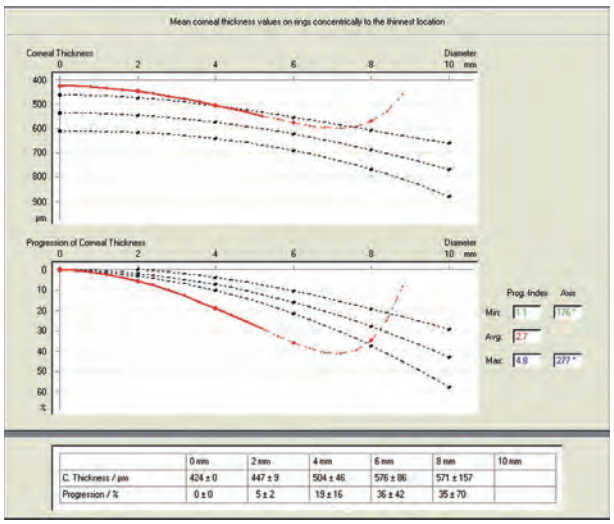

Figure 32: Pachymetry progression in OD

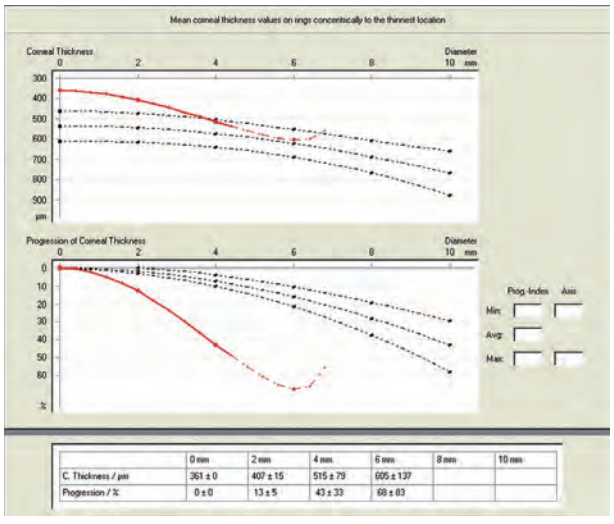

Figure: 33 Pachymetry progression in OS

The pachymetric progression is abrupt in both eyes, providing a significant indication of ectasia (Figure 32, Figure 33).

Probably mild ectasia could have been diagnosed prior to surgery if corneal topography and tomography would have performed and well interpreted. This case would have been considered as a bad candidate for RK.

8.2 Case 2: Ectasia after LASIK? by Prof. Michael W. Belin

A 46-year-old female had undergone LASIK 2 years prior. She was interested in further vision enhancement for her dominant right eye. Her best spectacle corrected visual acuity (BSCVA) was 20/20+ with sph -1.25 D.

The referring surgeon was concerned about post LASIK ectasia based on an Orbscan® topography showing significant posterior elevation (Figure 34).

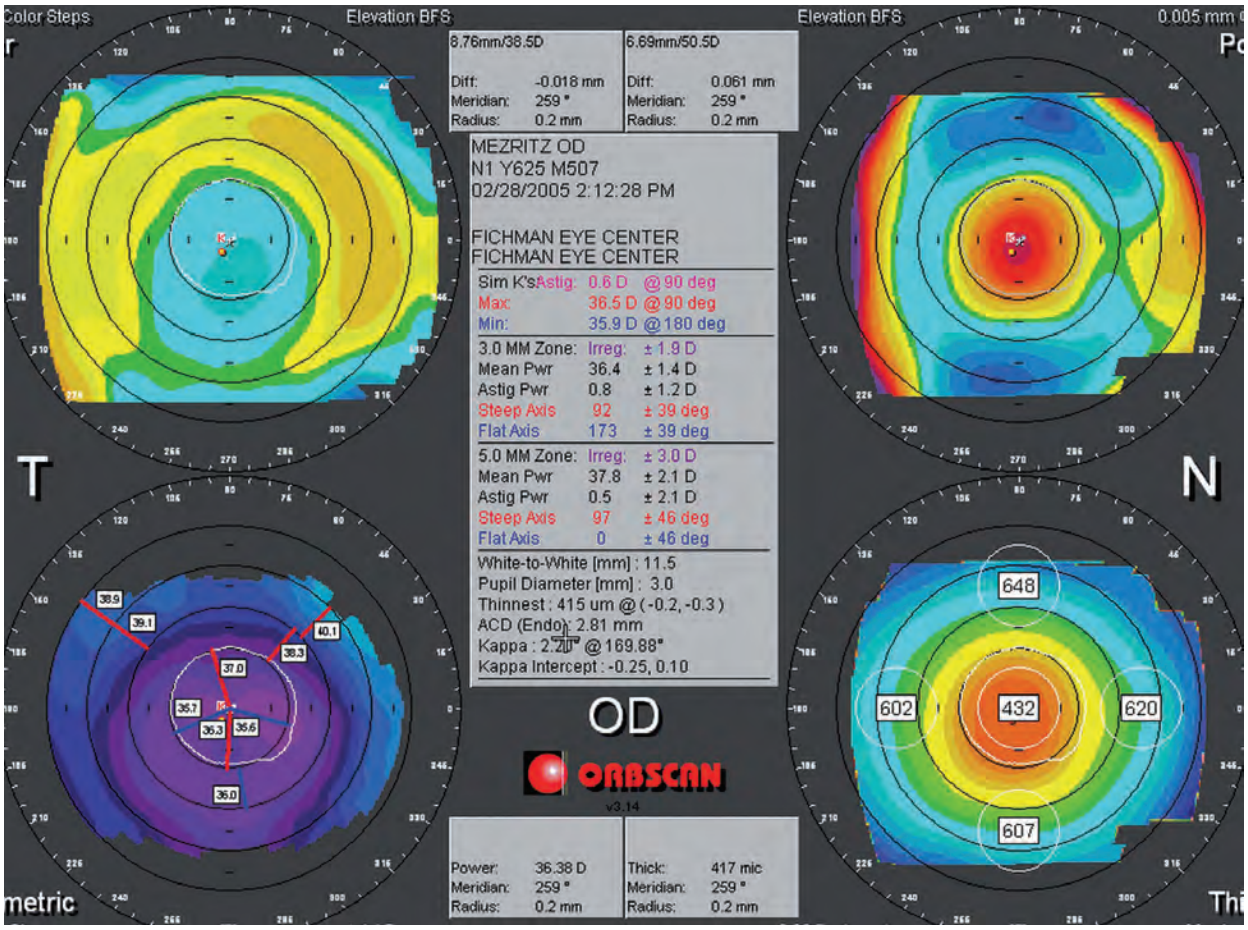

Figure 34: Orbscan® incorrencly suggests post-LASIK ectasia

Evaluation with the Pentacam® revealed no posterior elevation abnormality and no evidence of postoperative ectasia (Figure 35).

The patient underwent routine LASIK enhancement without incident.

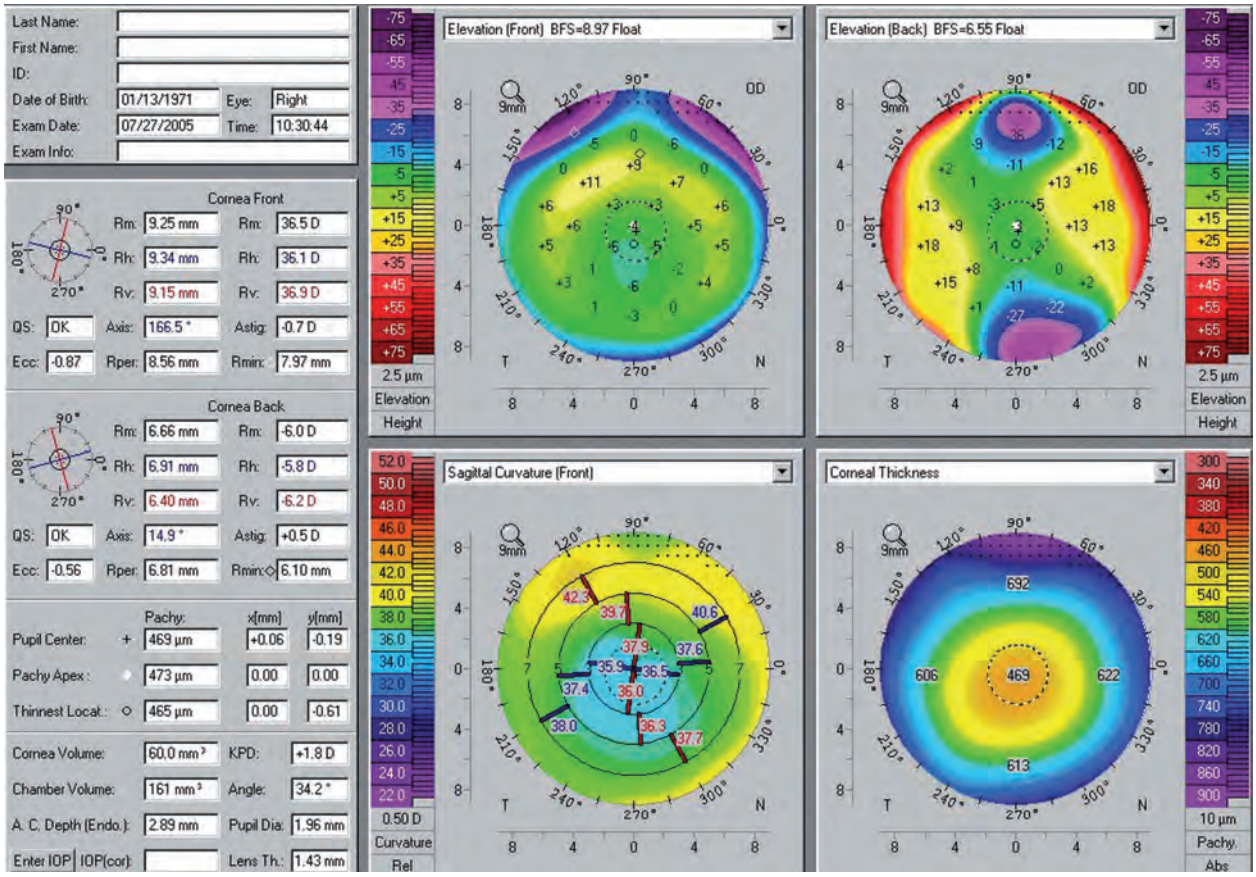

Figure 35: 4 Maps Selectable revealing there to be no post-LASIK ectasia

Note:

This case demonstrates one of the limitations with the current version of the Bausch & Lomb Orbscan®. This device routinely fails to correctly identify the posterior corneal surface in postoperative patients, leading to underestimates of residual bed thickness and frequent incorrect diagnosis of post-LASIK ectasia.

Here the Orbscan® incorrectly reads the corneal thickness 37 µm thinner than the Pentacam®, incorrectly suggesting ectasia (Figure 36). The Pentacam® shows a normal postoperative appearance (Figure 37).

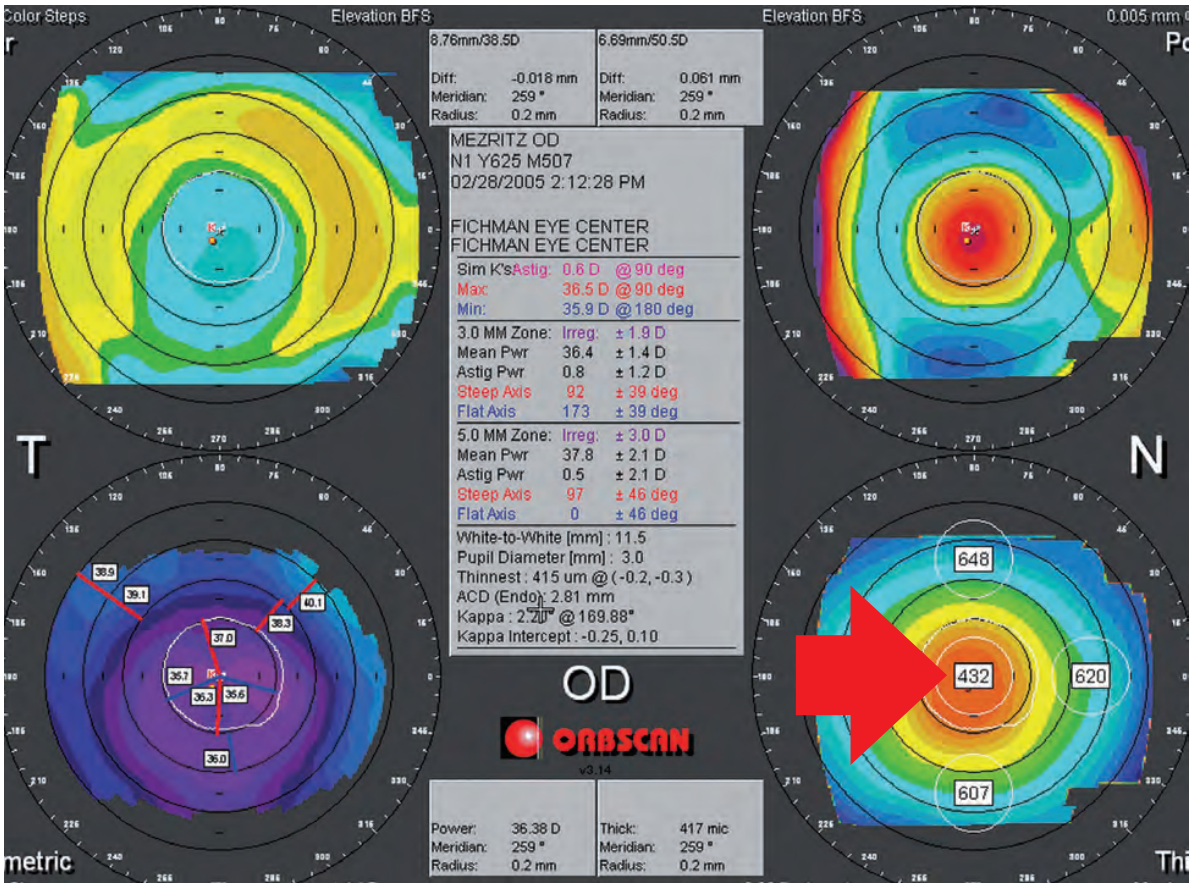

Figure 36: Orbscan® 4 maps incorrectly suggesting ectasia in OD

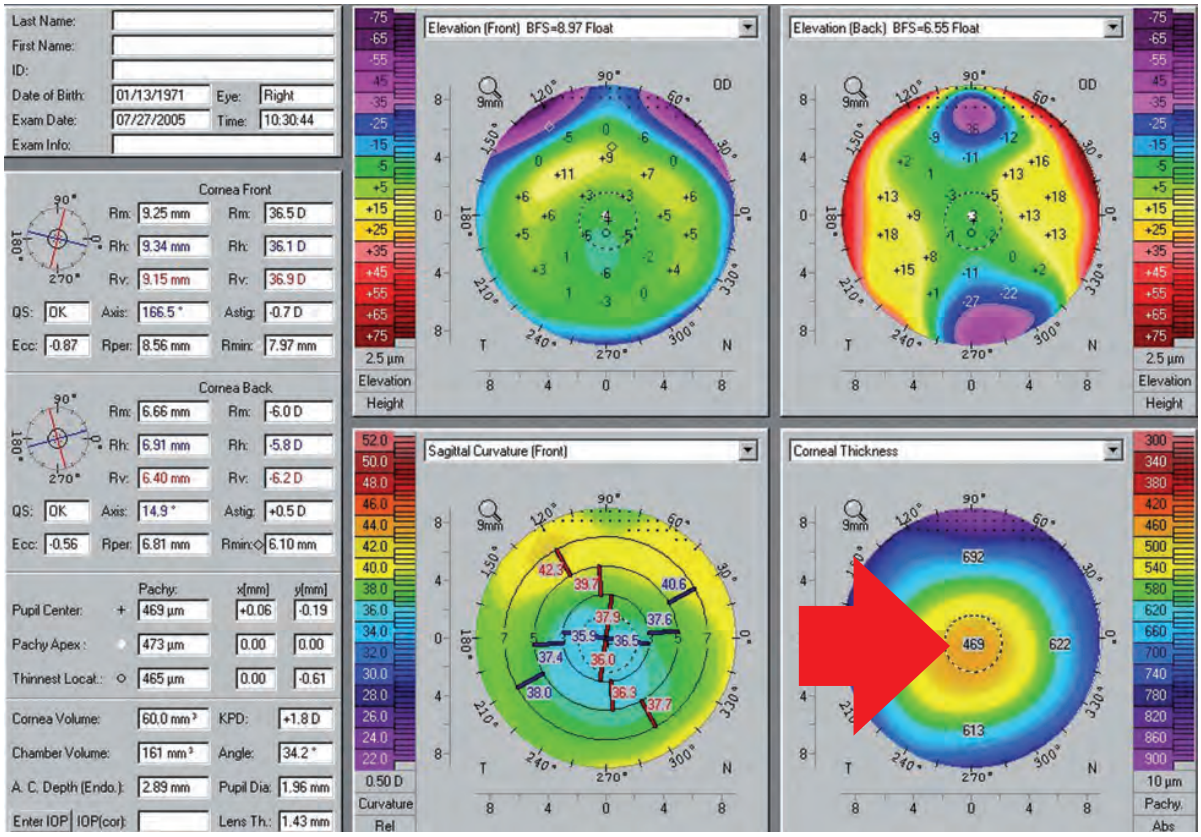

Figure 37, Pentacam® 4 Maps Selectable revealing there to be no post-LASIK ectasia

In this example Orbscan® measured the pachymetry 37 microns (µm) thinner than Pentacam®.

9 Glaucoma

9.1 Case 1: General screening by Tobias H. Neuhann, MD

A 48-year-old white male patient presented for a second opinion on his glaucoma treatment. His father and grandfather had had glaucoma. After ten years of glaucoma medical treatment his ophthalmologist was now recommending a second medication. We measured 24 mmHg with a Goldmann tonometer.

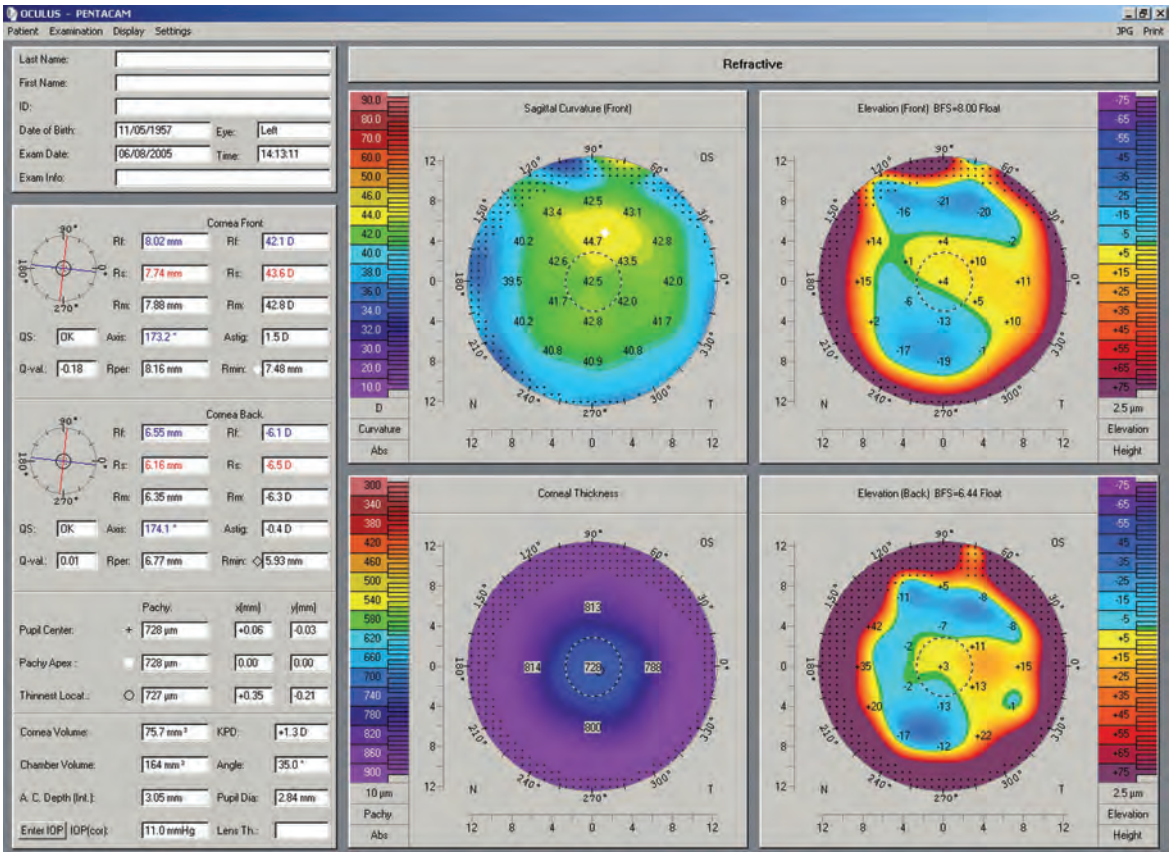

Figure 38: 4 Maps Refractive revealing a thick cornea

Examination with the Pentacam® 4 Maps Refractive display (Figure 38) yielded a corneal thickness of 728 µm, resulting in a corrected IOP of 11 mmHg according to the Dresdner scale. Further examination on the Heidelberg-Retina-Tomograph (HRT) revealed a healthy optic nerve, and we therefore advised the patient to stop his medication. His IOP today is between 19 and 22 mmHg during the daytime. We are still seeing him 4 times a year for an IOP and HRT checkup (Figure 39, Figure 40).

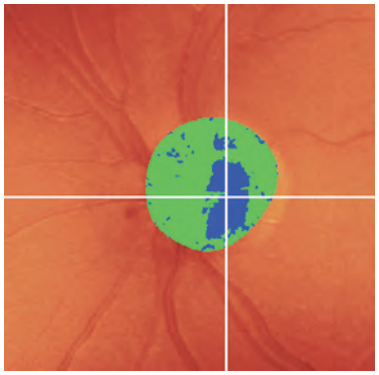

Figure 39: HRT Image

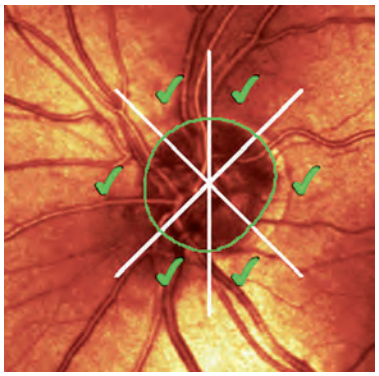

Figure 40: HRT Image

9.2 Case 2: YAG laser iridectomy by Eduardo Viteri, MD

This is a 64-year-old female patient who was complaining of episodes of blurred vision and tearing. Her IOP was 18 mmHg in both eyes. Her anterior chamber was shallow on slit lamp examination and her optic nerve had a cup/disc ratio of 0.6 in both eyes. The lens was clear, and gonioscopy examination revealed a narrow angle in both eyes (grade I-II).

The anterior segment exam with the Pentacam® (Figure 41) documented an ACA of 22.5 degrees with an ACD (epithelial) of 2.43 mm. The patient was reluctant to have YAG laser iridectomy until she was able to compare her anterior segment biometry with that of other normal patients.

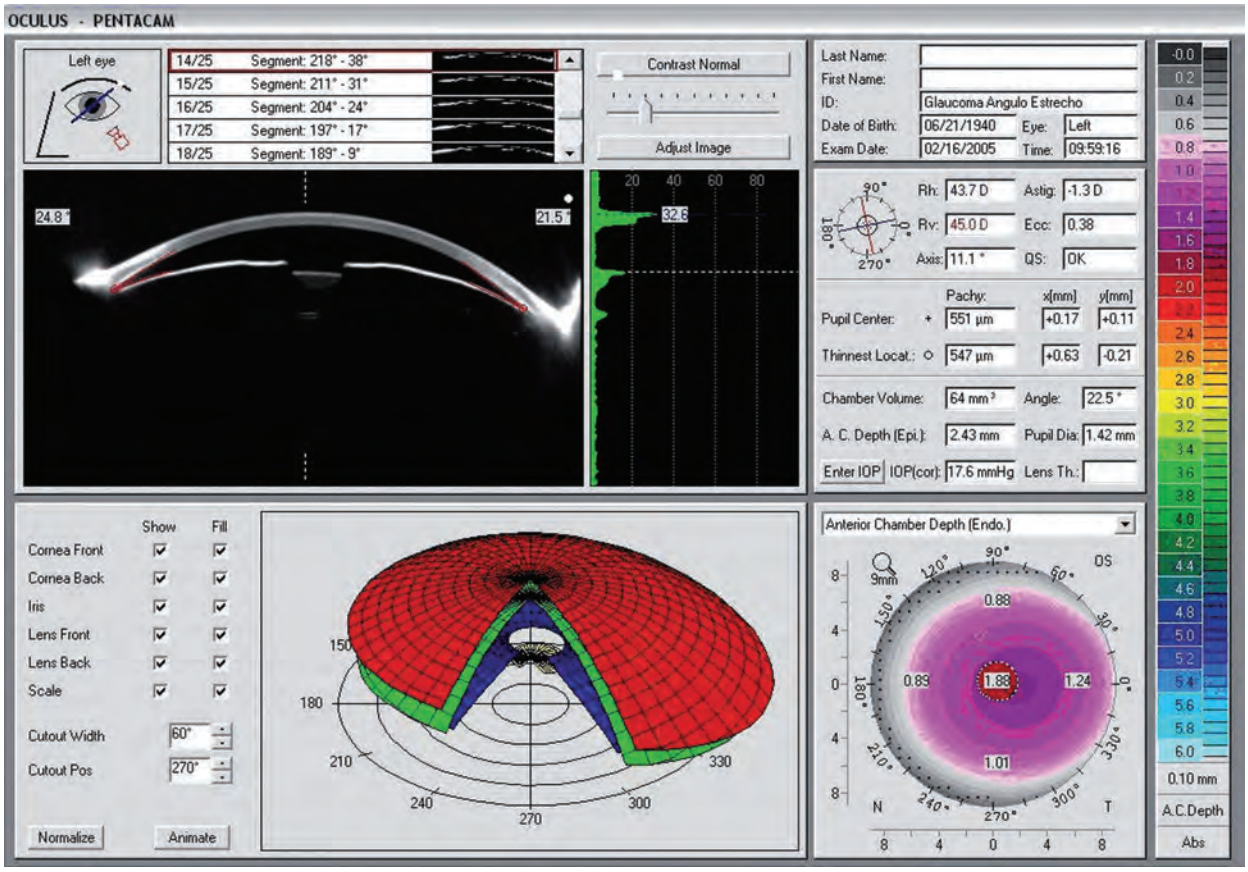

Figure 41: General Overview display showing status in OS prior to YAG laser iridectomy

After YAG laser iridectomy had been performed several of her anterior segment measurements changed (Figure 42). This is quite evident in the differential display (Figure 43).

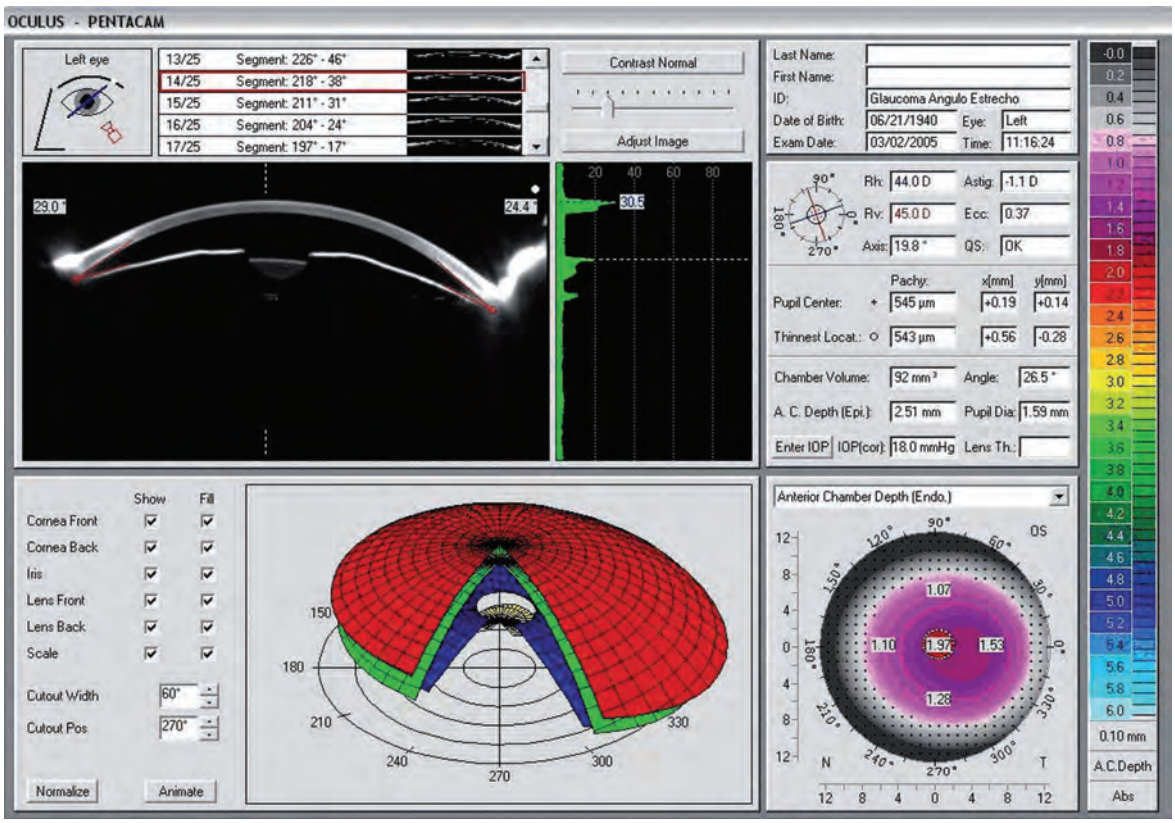

Figure 42: General Overview display 10 days after YAG laser iridectomy in OS showing improved ACA and ACD values

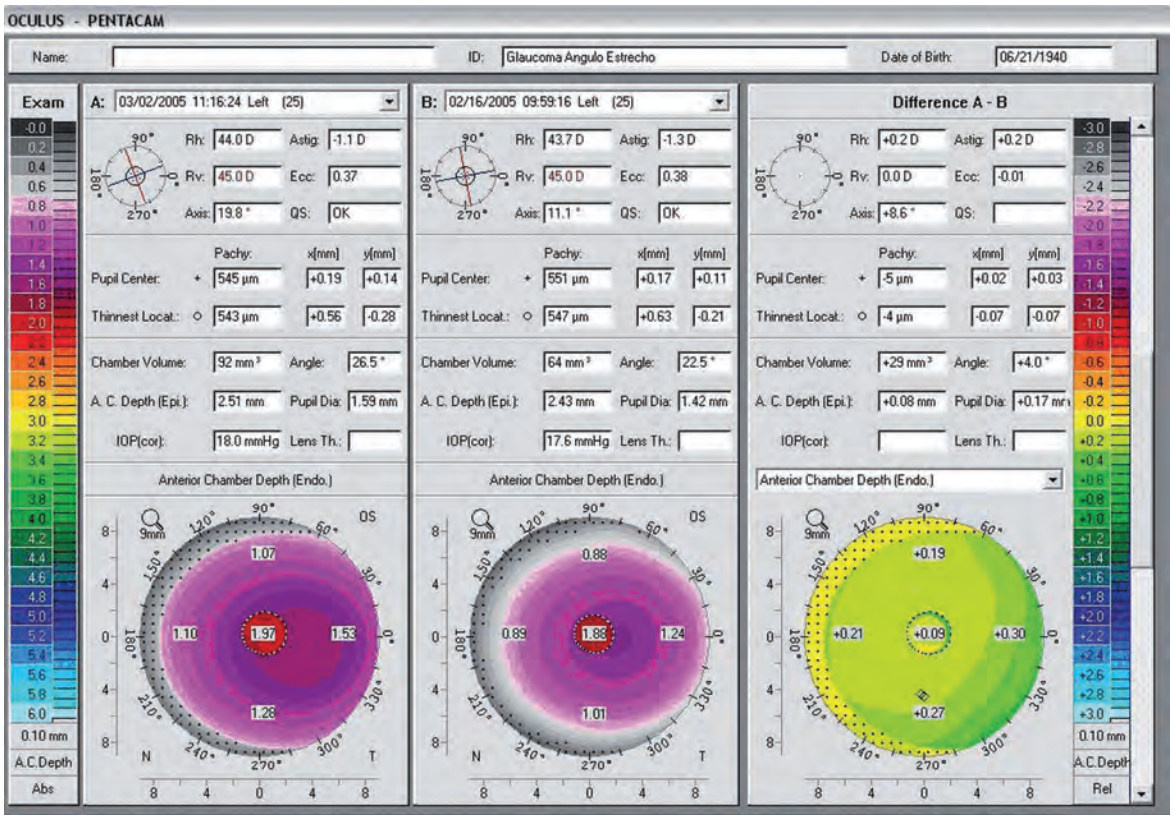

Figure 43: Compare 2 Exams showing changes from before to 10 days after YAG laser iridectomy in OS

The ACA is 4° wider, and, although the ACD only deepened 0.09 mm centrally, the main difference is evident in the periphery, where you can see changes ranging from 0.19 mm to 0.30 mm. This was enough to increase the ACV from 64 to 92 mm³.

Comments

The Pentacam® is quite useful for measuring the ACA in narrow angle glaucoma, although this may be difficult in 360° because of eyelid interference.

More consistent data can be obtained by measuring peripheral ACD and ACV.

The exam has been of great help also in educating the patient about this disease and making the effect of the treatment evident to her.

9.3 Screening for narrow angles by Dilraj S. Grewal, MD

9.3.1 Case 1

A 64-year-old Indian female patient presented for a routine eye exam. Her vision was 20/20 in both eyes. She was found to have a shallow anterior chamber on slit lamp biomicroscopy (Figure 44). Gonioscopy showed Shaffer's Grade 1 in all quadrants in both eyes. These findings were confirmed by Scheimpflug images showing a shallow ACD of 1.80 mm in OD and 1.83 mm in OS. The ACV was 64 mm³ in both eyes. The ACA was 20.6 degrees in OD and 19.7 degrees in OS. The ACD ratio was 0.5 in both eyes. Central corneal thickness was 557 µm in OD and 589 µm in OS (Figure 45, Figure 46).

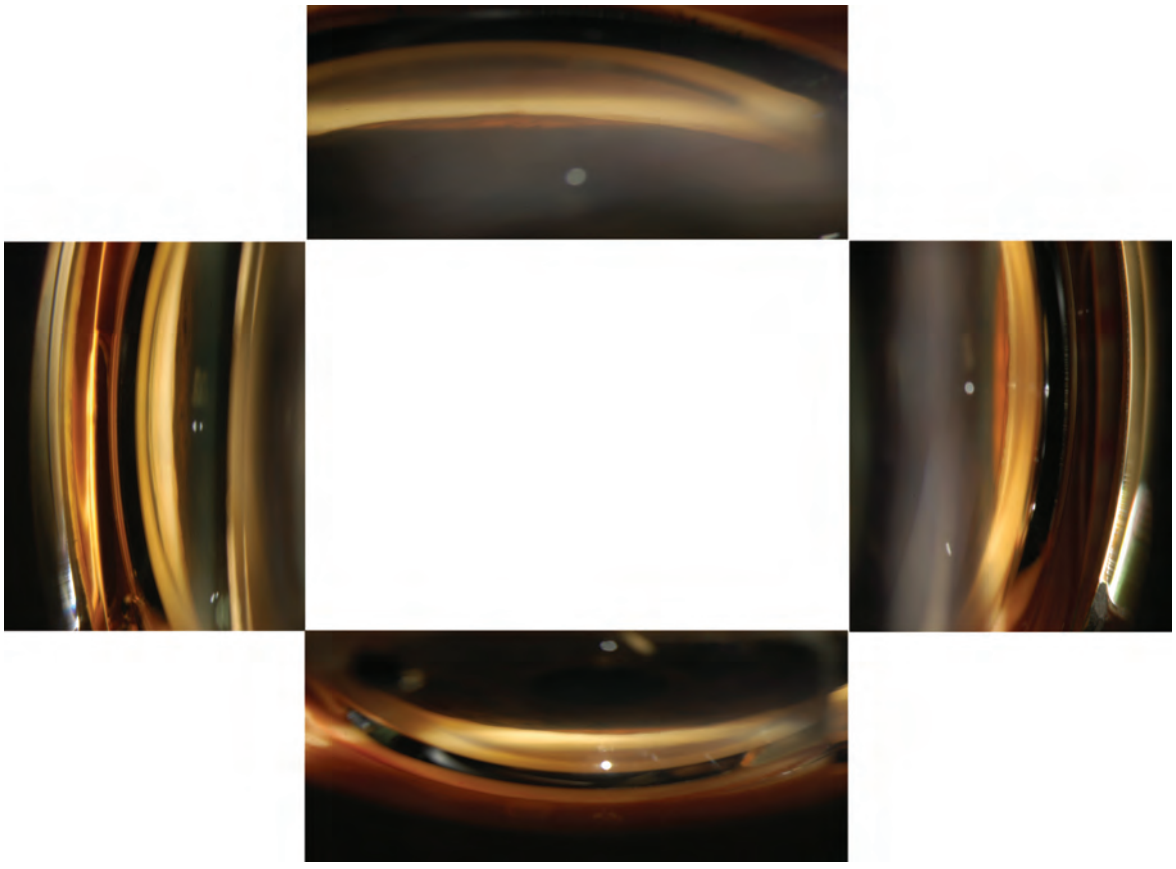

Figure 44: Slit lamp gonioscopy pictures showing a narrow angle in all four quadrants

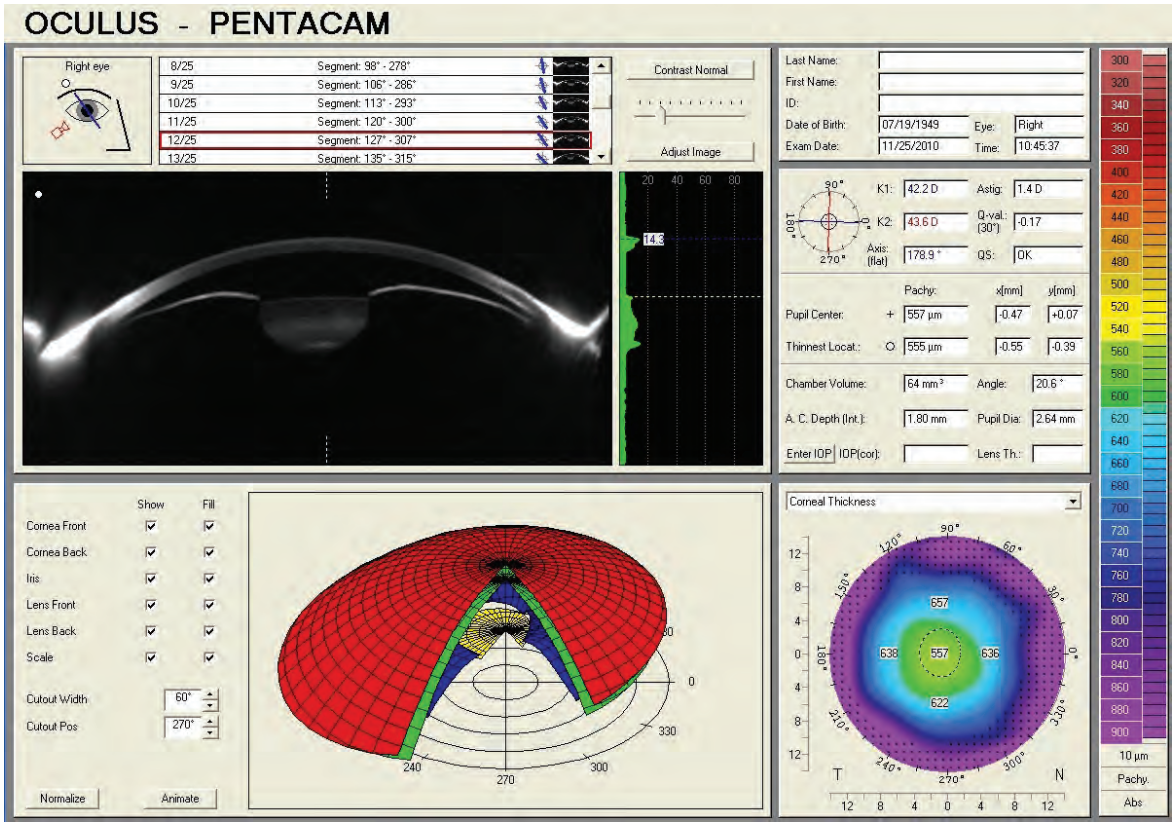

Figure 45: General Overview display showing a low ACV, shallow ACD and narrow angle in OD

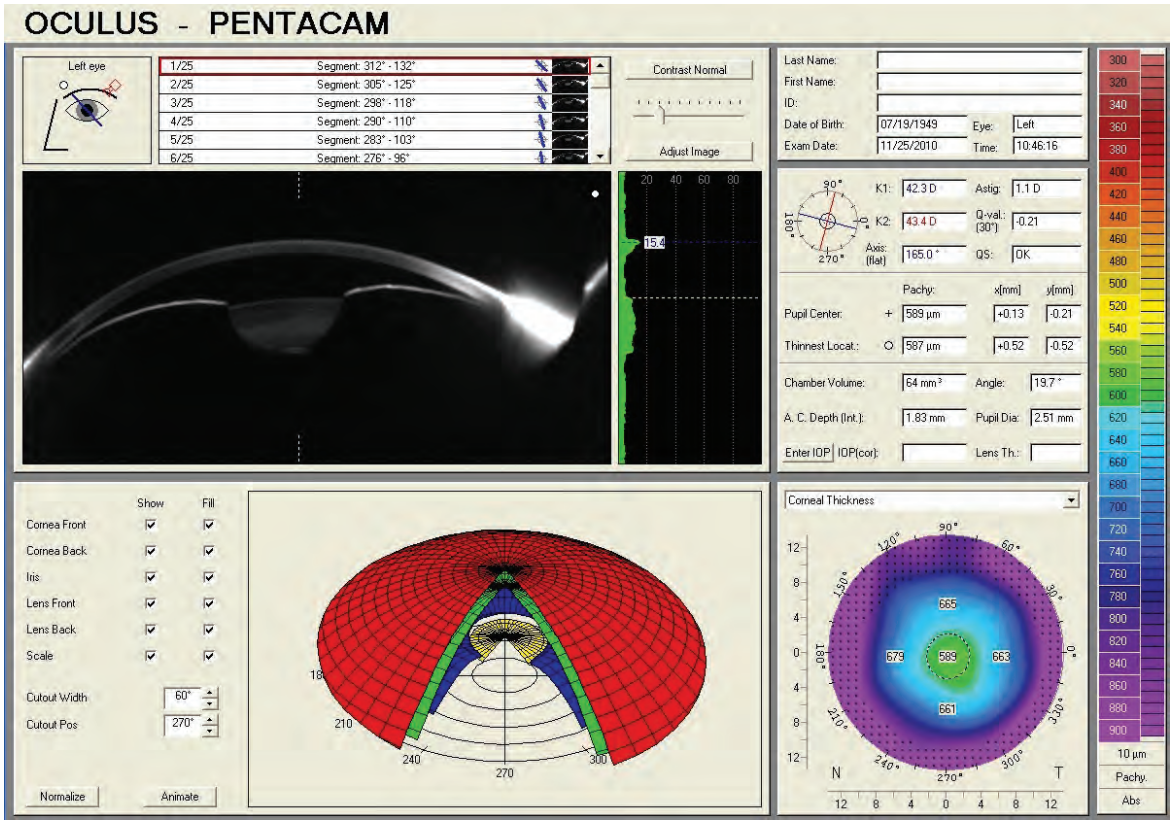

Figure 46: General Overview display showing a low ACV, shallow ACD and narrow angle in OS

Humphrey visual fields were full in both eyes (Figure 47, Figure 48), and optical coherence tomography (OCT) and retinal nerve fiber layer (RNFL) scans showed retinal thickness to be normal in both eyes (Figure 49).

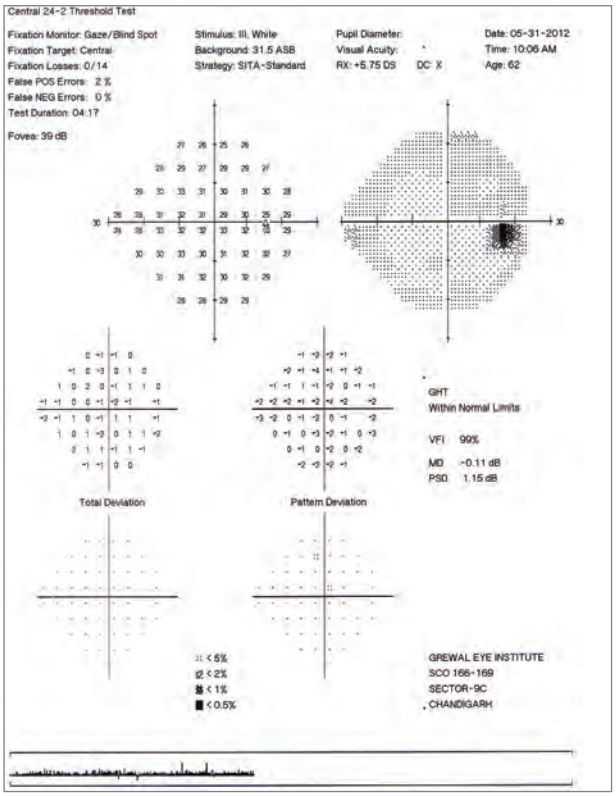

Figure 47: 24-2 Humphrey visual field: full visual field in OD

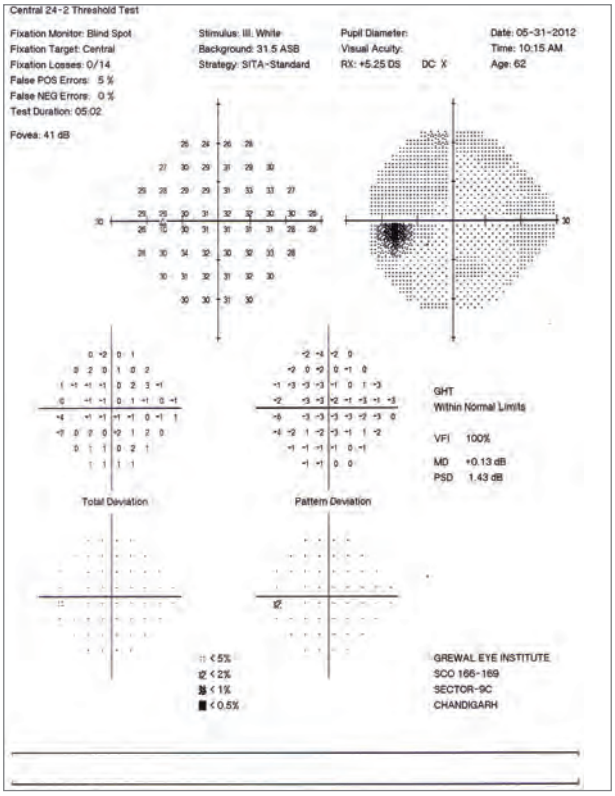

Figure 48: 24-2 Humphrey visual field: full visual field in OS

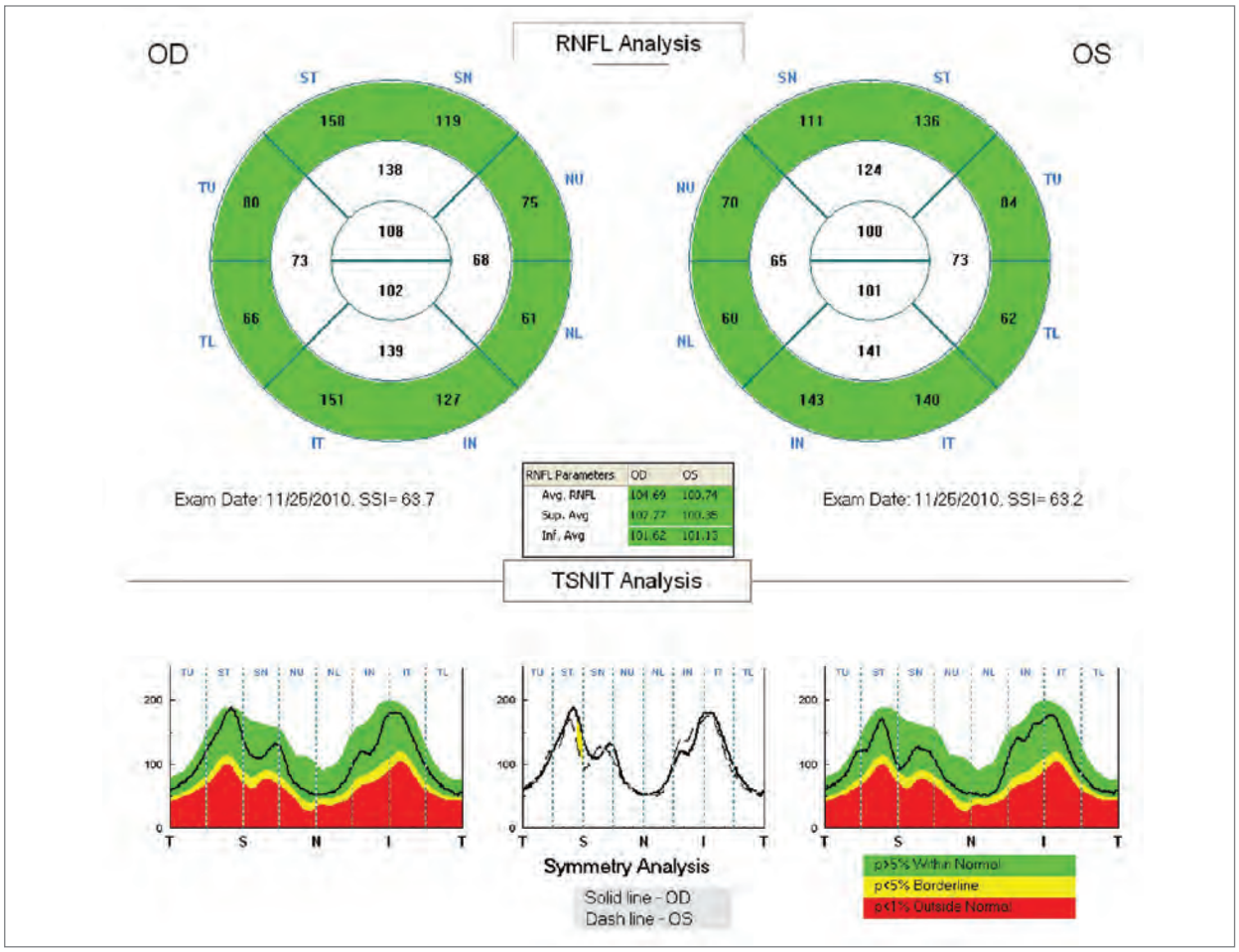

Figure 49: Spectral domain OCT showingnormal RNFL thickness in both eyes

She underwent a prophylactic laser peripheral iridectomy in both eyes, following which ACV increased from 64 to 94 µm, ACA widened from 19.7 to 26.4 degrees and ACD deepened from 1.83 to 2.08 mm.

We previously demonstrated that a cutoff value of 113 mm3 for ACV discriminates narrow angles with 90% sensitivity and 88% specificity [3,4]. The positive and negative likelihood ratios for ACV in that study were 8.63 (95% coincidence interval (CI) = 7.4-10.0) and 0.11 (95% CI = 0.03-0.4), respectively.

9.3.2 Case 2

A 50-year-old Indian female patient presented for a routine eye exam. Her vision was 20/20 in both eyes. She was found to have a shallow anterior chamber on slitlamp biomicroscopy. Gonioscopy showed Shaffer's Grade 1 in all quadrants in both eyes. These findings were confirmed by Scheimpflug images showing a shallow ACD of 2.03 mm in OD and 2.08 mm in OS. The ACV was 95 mm^3 in OD and 95 mm^3 in OS. The ACA was 20.7 degrees in OD and 26.4 degrees in OS. The ACD ratio was 0.5 in both eyes. Central corneal thickness was 540 µm in OD and 559 µm in OS. Her IOP was 19 mmHg in OD and 18 mmHg in OS (Figure 50, Figure 51).

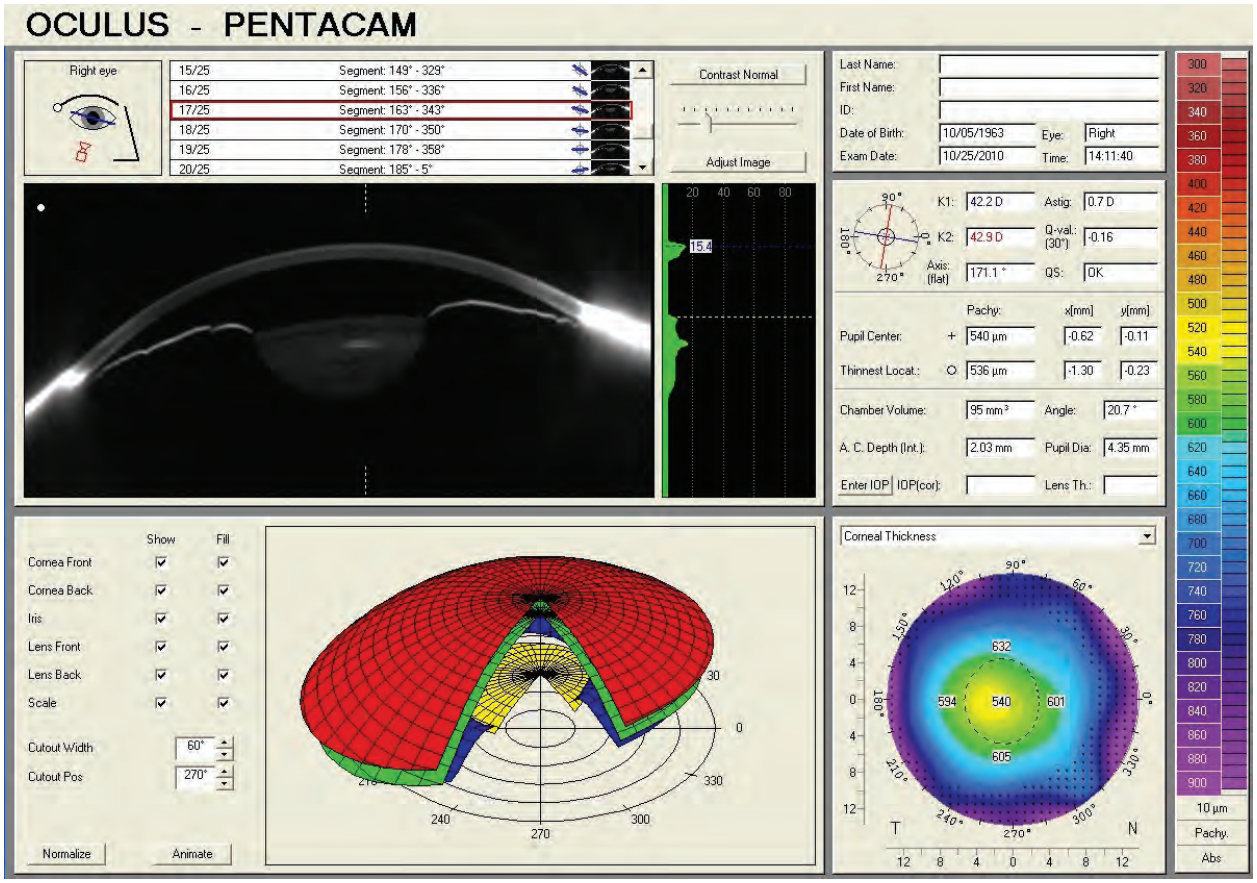

Figure 50: General Overview display showing a low ACV, shallow ACD and narrow angle in OD

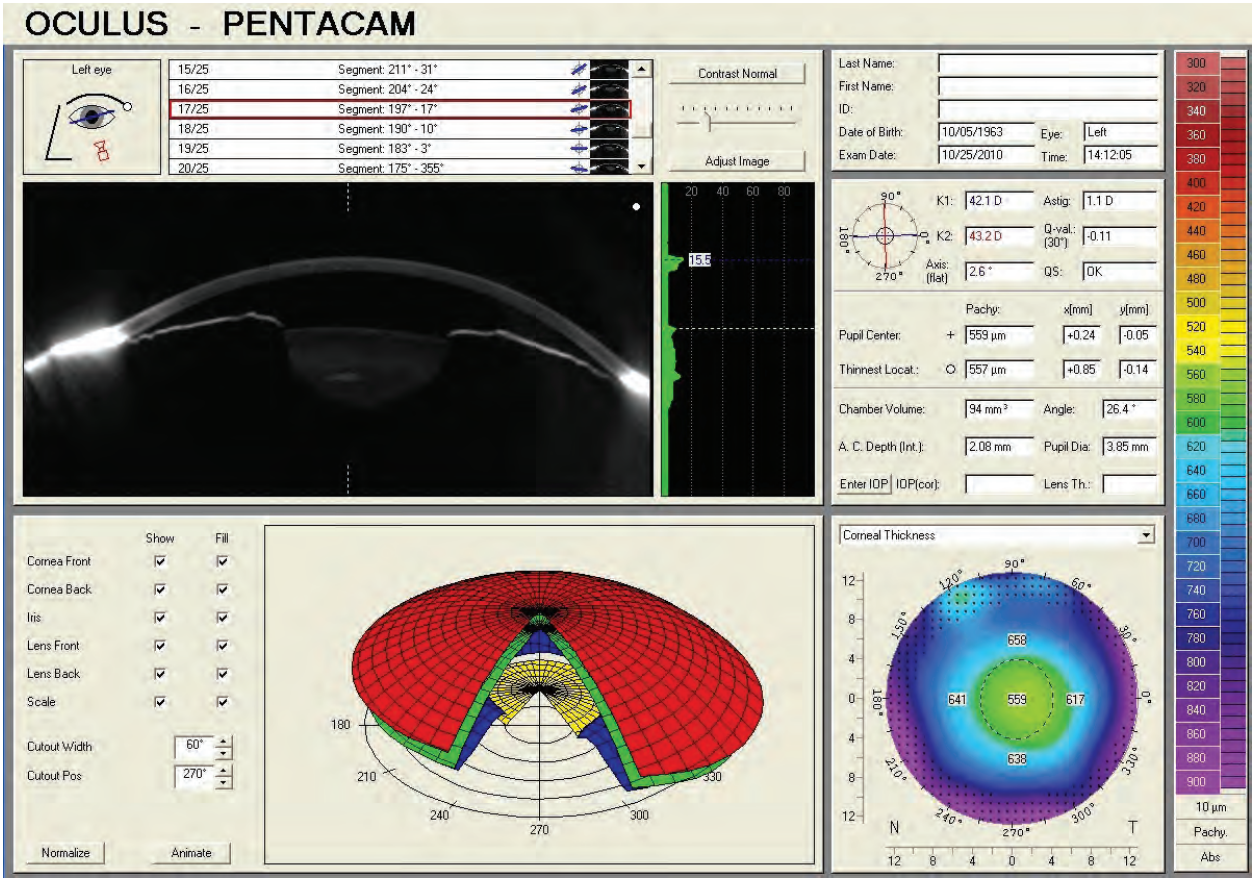

Figure 51, General Overview display showing a low ACV, shallow ACD and narrow angle in OS

Humphrey visual fields revealed early defects in both eyes (Figure 52, Figure 53), while the OCT RNFL scan showed an abnormally thin RNFL corresponding to the visual field defects in both eyes (Figure 54).

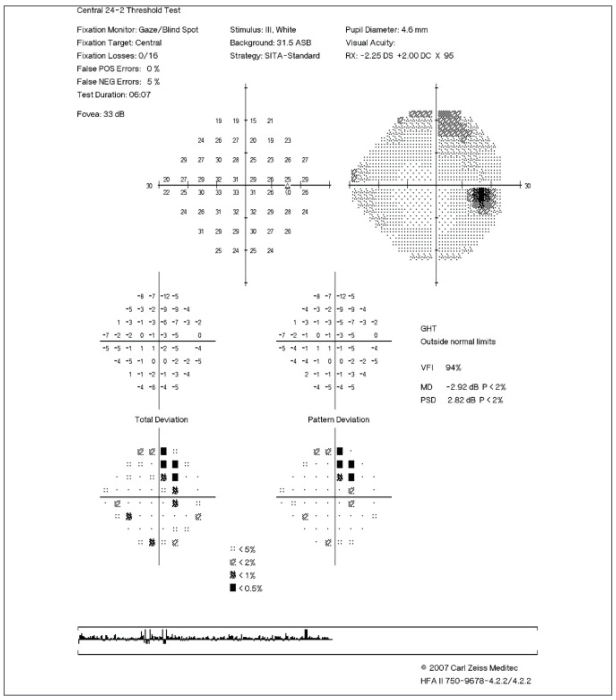

Figure 52: 24-2 Humphrey visual field showing an early superior arcuate defect in OD

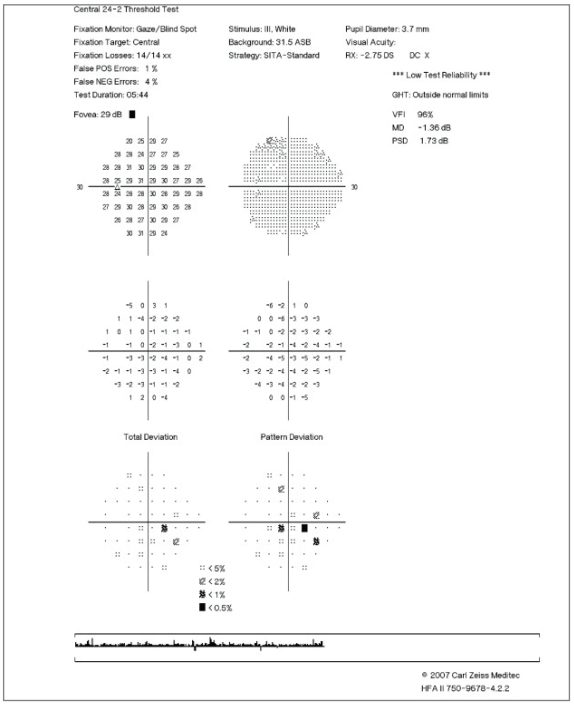

Figure 53: 24-2 Humphrey visual field showing an early inferior paracentral defect in OS

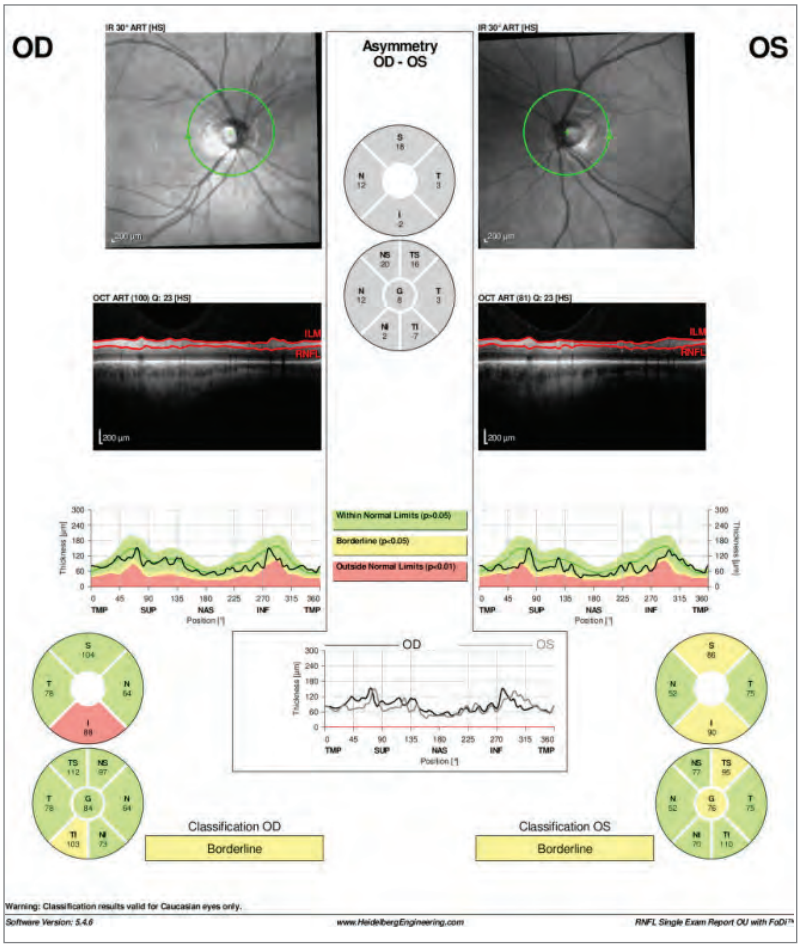

Figure 54:

Spectral domain OCT showing abnormal RNFL thickness inferiorly in OD, corresponding to the early superior arcuate defect in that eye (also look Figure 52)

9.4 Evaluating the anterior segment in phacomorphic glaucoma by Dilraj S. Grewal, MD

A 76-year-old caucasian female patient presented with acute pain and redness in her right eye. Her IOP was elevated to 58, she had microcystic edema and her pupil was minimally reactive with her vision at "count fingers" in her right eye and 20/40 in her left. She had undergone an uncomplicated aortic valve repair 4 days prior to presentation. Prior ocular history was significant for an episode with similar symptoms in her left eye 7 years prior, which had also occurred a few days following a major surgery. At that time she had undergone bilateral laser peripheral iridotomies, which were patent on examination. On slitlamp biomicroscopy she was found to have a very shallow anterior chamber but no irido-corneal touch.

Pentacam® Scheimpflug imaging (Figure 55) confirmed the diagnosis of phacomorphic glaucoma as evidenced by a shallow ACD of 1.75 mm, an ACV of 65 mm^3 and ACA of 17.5 degrees in the right eye. An anterior vaulting of the lens was visible on the Scheimpflug image.

Her IOP was emergently controlled with intravenous Diamox and IOP lowering drops. Once the corneal edema had cleared in 3 days she underwent an uneventful phacoemulsification and posterior chamber IOL implantation. Post-operative Scheimpflug (Figure 56) images demonstrated a significantly increased ACV and ACD and widening of the ACA. Her IOP was 17 mmHg and no more medication is postoperatively required and her vision improved to 20/40. In this case the Scheimpflug images helped us confirm the diagnosis of phacomorphic glaucoma in an eye with a very shallow chamber and elevated IOP in the presence of a patent PI and demonstrated a deepening of the anterior chamber following lens extraction.

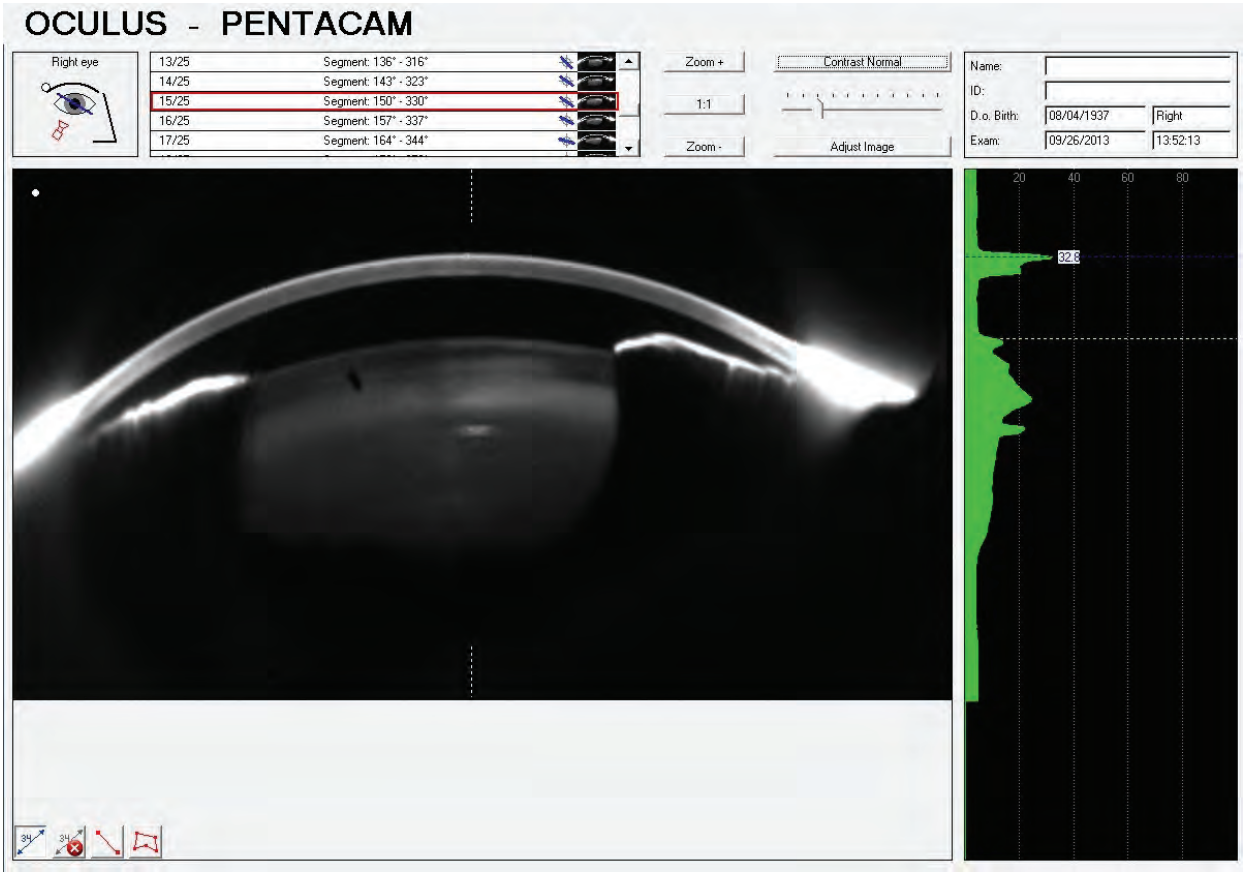

Figure 55: Scheimpflug Image showing very low ACV, shallow ACD, narrow ACA and anterior vaulting of the lens in OD

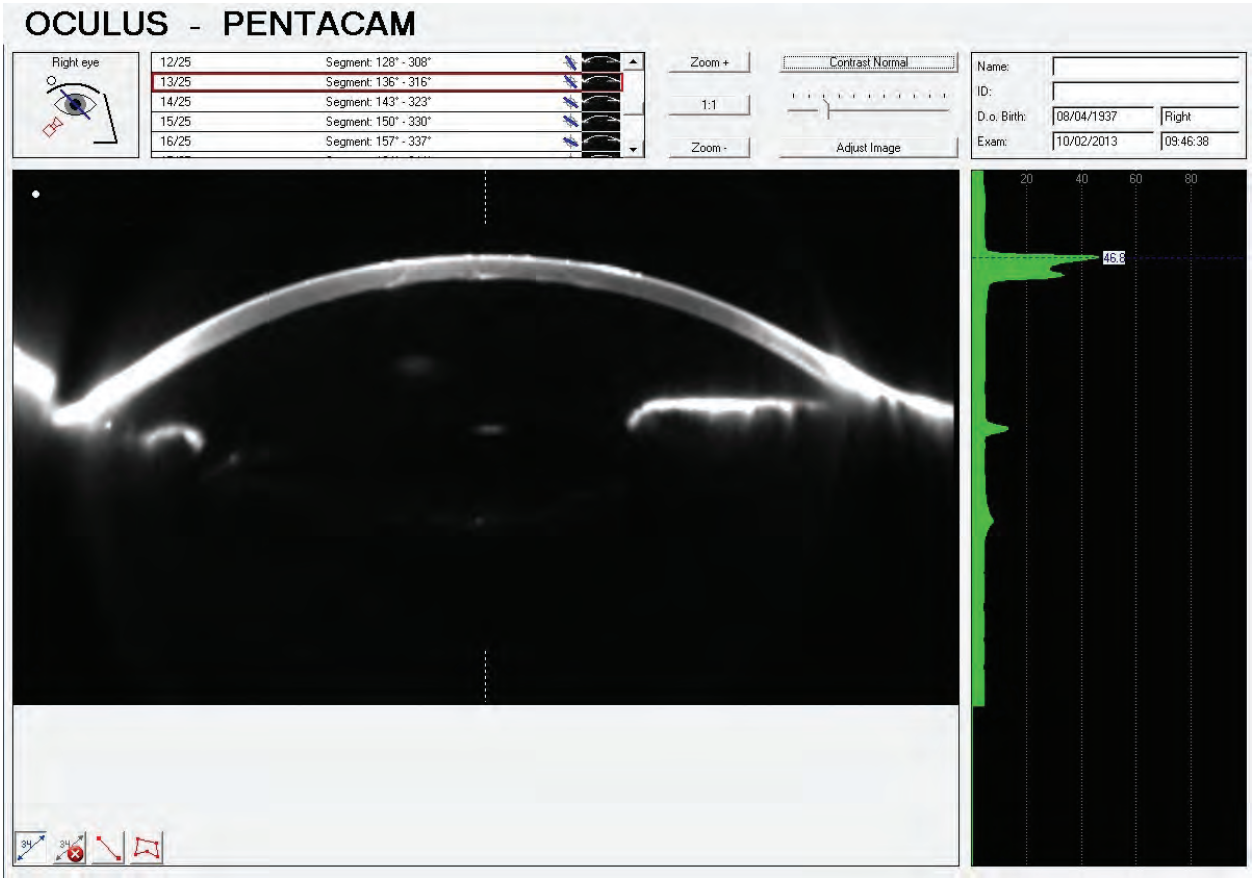

Figure 56: Scheimpflug Image showing increased ACV, deeper ACD and wider ACA following removal of the lens and posterior chamber IOL implantation

10 Screening for refractive surgery by Prof. Michael W. Belin

10.1 Screening parameters, 4 Maps Refractive Display

10.1.1 Suggested installation settings

The following are my guidelines for pre-operative refractive surgery screening for keratoconus:

- Use the 4 Maps Refractive Display showing anterior elevation, posterior elevation, pachymetry and anterior sagittal curvature. It is advisable to keep the display, scales and colors constant for refractive screening, as this will allow for a rapid visual inspection

Pachymetry

- Right-click on the scale and set Abs: normal, (300-900 µm)
- Right-click on the actual display to open the drop down menu. Turn on the following: Show Apex Position (1), Show Thinnest Location (2), Show Pupil Edge (6), Show Nasal/Temp (7), Show Max Diameter 9mm (12) and Show Numeric Values (14)

Anterior elevation & posterior elevation

- Right-click on the scale and set to
- "Belin intuitive" +/- 75 µm for refractive practice
- "Belin intuitive" +/- 150 µm for medical practice
- Best-fit-sphere (BFS), float, manual, BFS diameter set to 9.0 mm or 8.0 mm
- On the 9.0 mm display you should have no or minimal extrapolated data for the study to be valid
- Right-click on the display and turn on the following: Show Apex Position (1), Show Thinnest Location (2), Show Pupil Edge (8), Show Nasal/Temp (9), Schow Max Diameter 9mm (14) and Show Numeric Values (15)

Sagittal curvature

- Right-click on the scale and set to Abs: Normal, American Style and Diopter
- Right-click on the display and set to Show Min. Radius Pos. Front (3), Show Pupil Edge (6), Show Nasal/Temp (7), Schow Max Diameter 9 mm (12) and Show Numeric Values (13)

Note:

The different borderline numbers for the elevation maps depend on the BFS diameter you are using, i.e. 9 mm or 8 mm.

10.1.2 Proposed screening parameters

It is essential to check the settings for the fitting zone of the BFS in the settings of the Pentacam®, since this influences the borderline numbers (Figure 57).

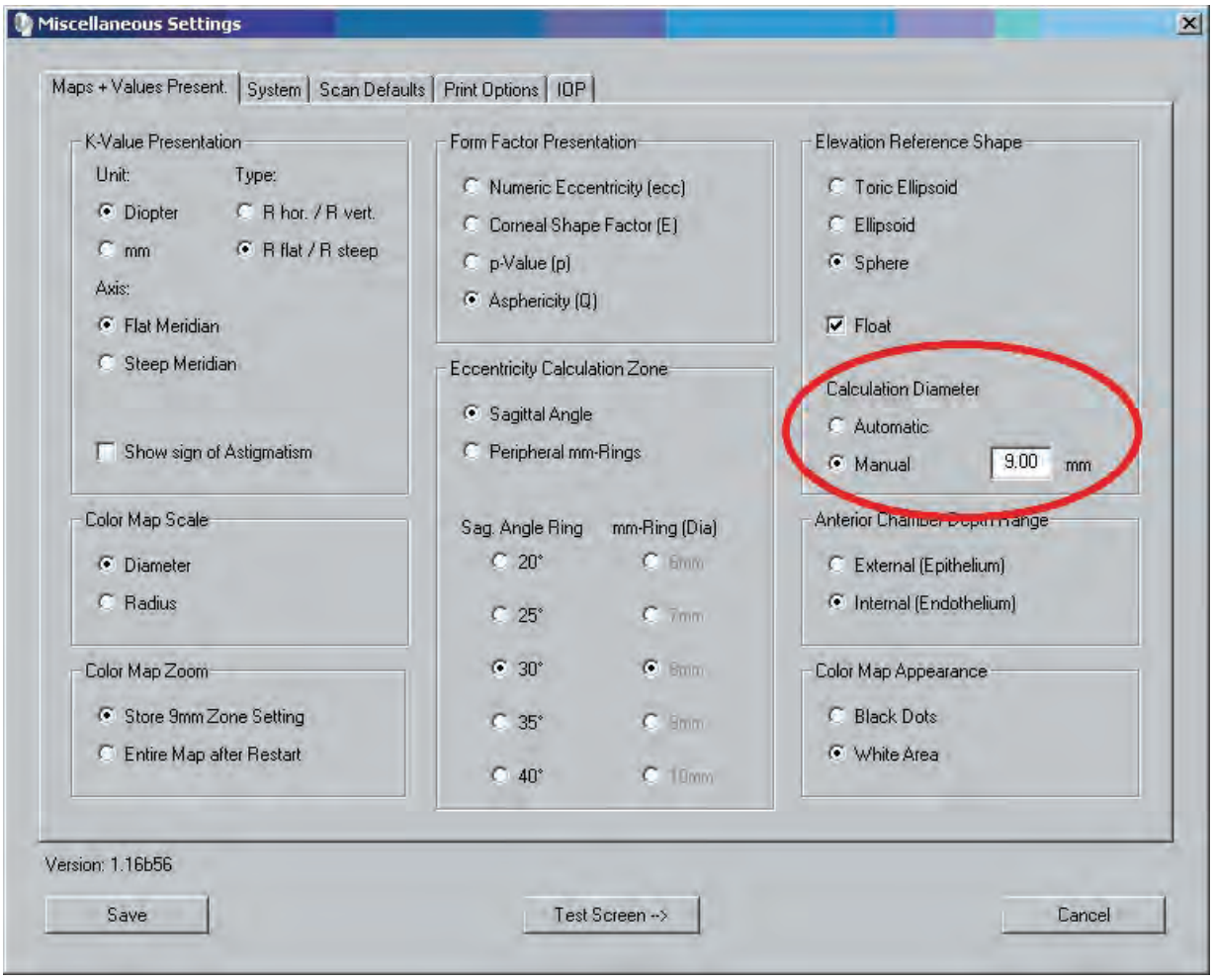

Figure 57: BFS fitting zone

- If you are using the manual (fixed) **9 mm** zone for fitting the BFS, the proposed screening parameters I use are:
  In the anterior elevation map differences between the BFS and the corneal contour less than +12 µm are considered normal, while differences between +12 µm and +15 µm are suspicious, and differences > 15 µm are typically indicative of keratoconus. Similar numbers about 5 µm higher apply to posterior elevation maps
- If you are using the manual (fixed) **8 mm** zone for fitting the BFS, the proposed screening parameters I use are:
  Anterior elevation differences less than 8 µm are considered in the normal range, while differences > 8 µm are typically indicative of keratoconus or other ectatic disorders (in the central zone). Posterior elevation differences < 11 µm are considered in the normal range, while differences >16 µm are suspicious

10.1.3 Strategy on how to go through the exams

The way I usually go through the exams is:

- ➔ Look at anterior elevation first
- ➔ Look at posterior elevation
- ➔ Look at the pachymetry and thickness distribution. Off-center distribution of corneal thickness is highly suspicious
- ➔ Look at the symmetry of both eyes. If one eye is abnormal, usually both eyes are abnormal
- ➔ Look at curvature last

Note:

The above relates to elevation island patterns, not astigmatism. These numbers pertain to elevation in the central and paracentral region in an island pattern.

10.2 Normal, astigmatic cornea

This 4 Maps Selectable display (Figure 58) shows a normal with-the-rule astigmatic cornea (both anterior and posterior surfaces). The sagittal curvature appears normal as it would be expected from the normal symmetric anterior elevation, and the pachymetry map reveals a normal thickness with a normal pachymetry distribution.

DIAGNOSIS – normal astigmatic cornea

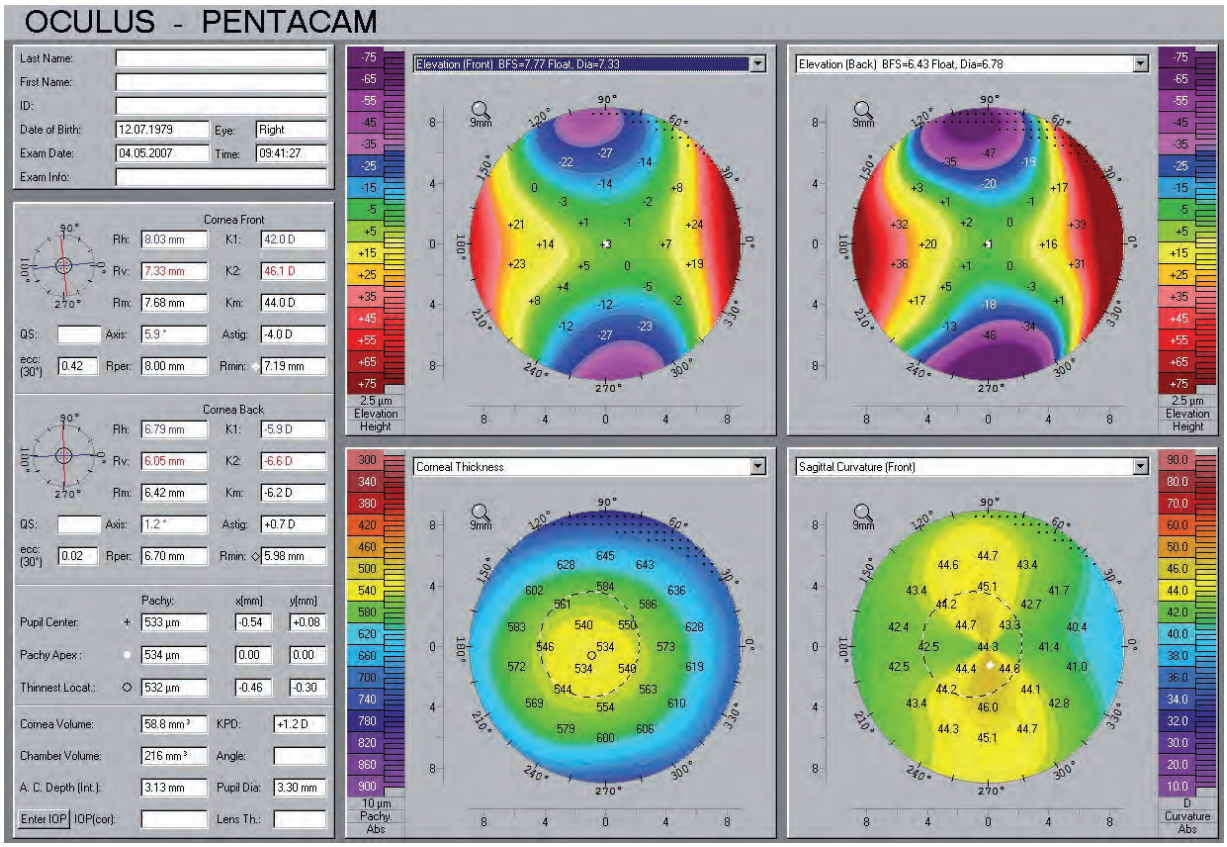

Figure 58: 4 Maps Selectable showing an astigmatic cornea

This 4 Maps Selectable display (Figure 59) shows a normal with-the-rule astigmatic cornea (astig. 2.6 D). Both the anterior and posterior elevations demonstrate a similar pattern, as does the anterior sagittal curvature. The curvature maps reveal a steep cornea (K1 = 47.6, K2 = 50.2), but the elevation maps do not reveal any suspicious areas. The pachymetry map is well centered with a thinnest reading of 546 µm. This is an astigmatic cornea with steep curvature, but otherwise normal.

DIAGNOSIS – normal astigmatic eye

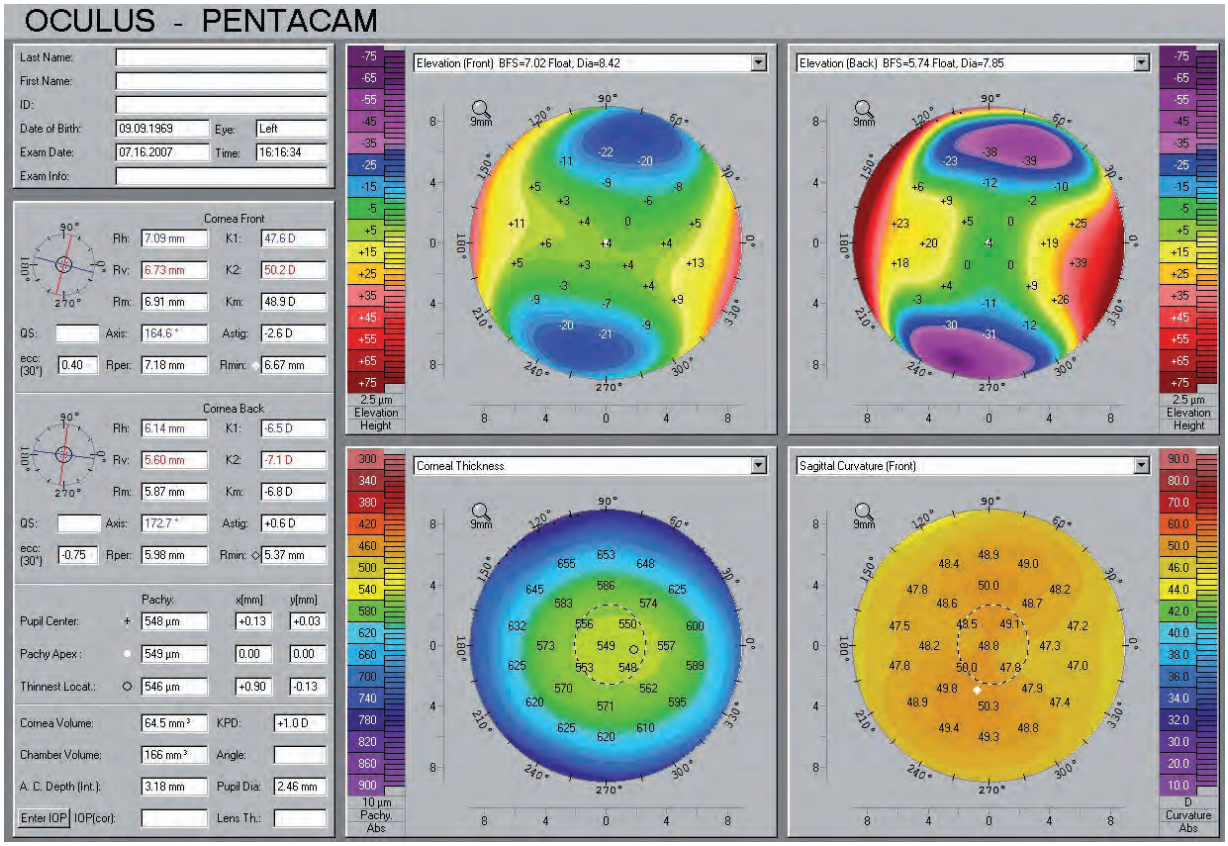

Figure 59: 4 Maps Selectable showing an astigmatic cornea

This 4 Maps Selectable display (Figure 60) shows a normal with-the-rule astigmatic cornea (astig. 4.1 D). Both the anterior and posterior elevations have a similar pattern, as does the anterior sagittal curvature. The anterior elevation map is symmetric, and the curvature shows a symmetric astigmatic pattern. The pachymetry map is well centered with a thinnest reading of 522 µm.

DIAGNOSIS – normal astigmatic eye

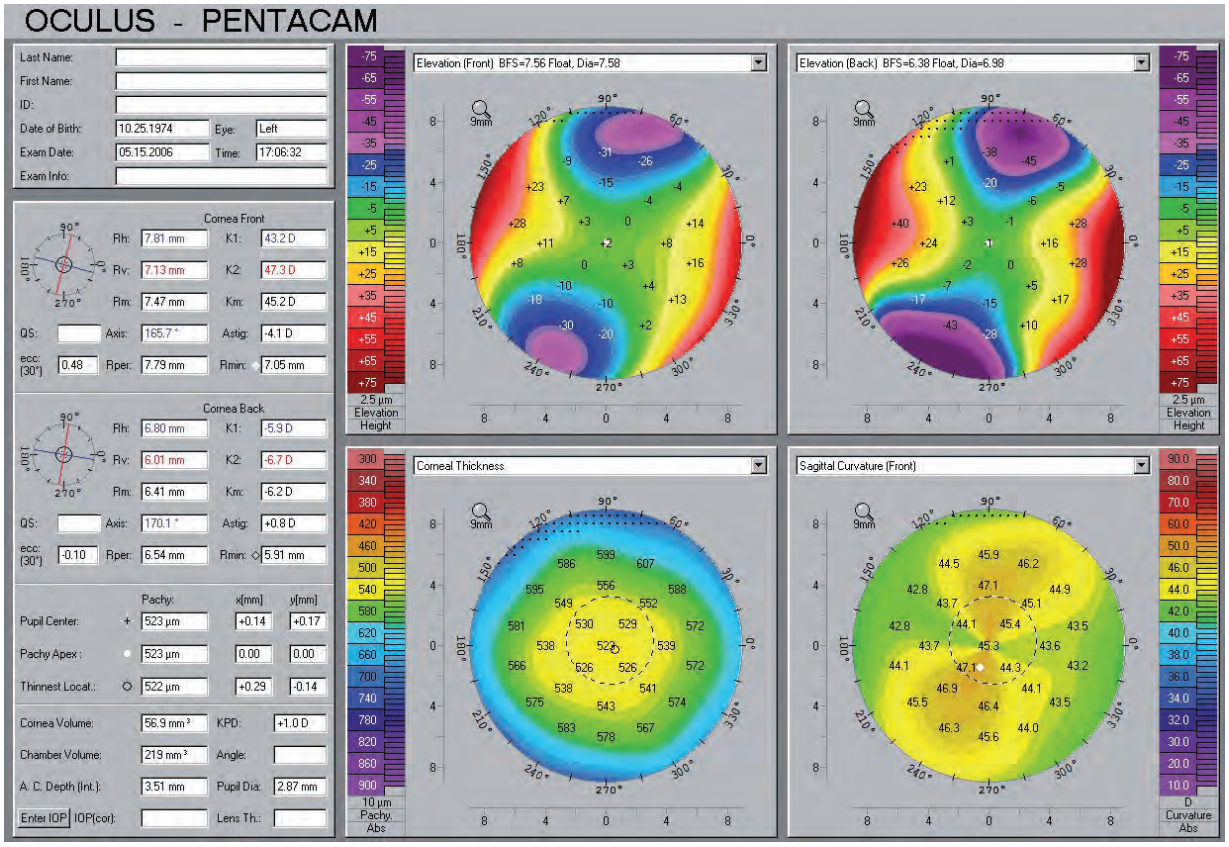

Figure 60: 4 Maps Selectable showing an astigmatic cornea

10.3 Astigmatism on the posterior cornea

This 4 Maps Selectable display (Figure 61) shows only a small amount of anterior (astig. 1.1 D) but a larger amount of posterior astigmatism (a more defined astigmatic pattern). However, because the posterior cornea contributes a much smaller amount to the overall refractive state of the eye, the posterior astigmatism reads only 0.4 D, in spite of a fairly well defined astigmatic pattern.

DIAGNOSIS – normal cornea with posterior astigmatism

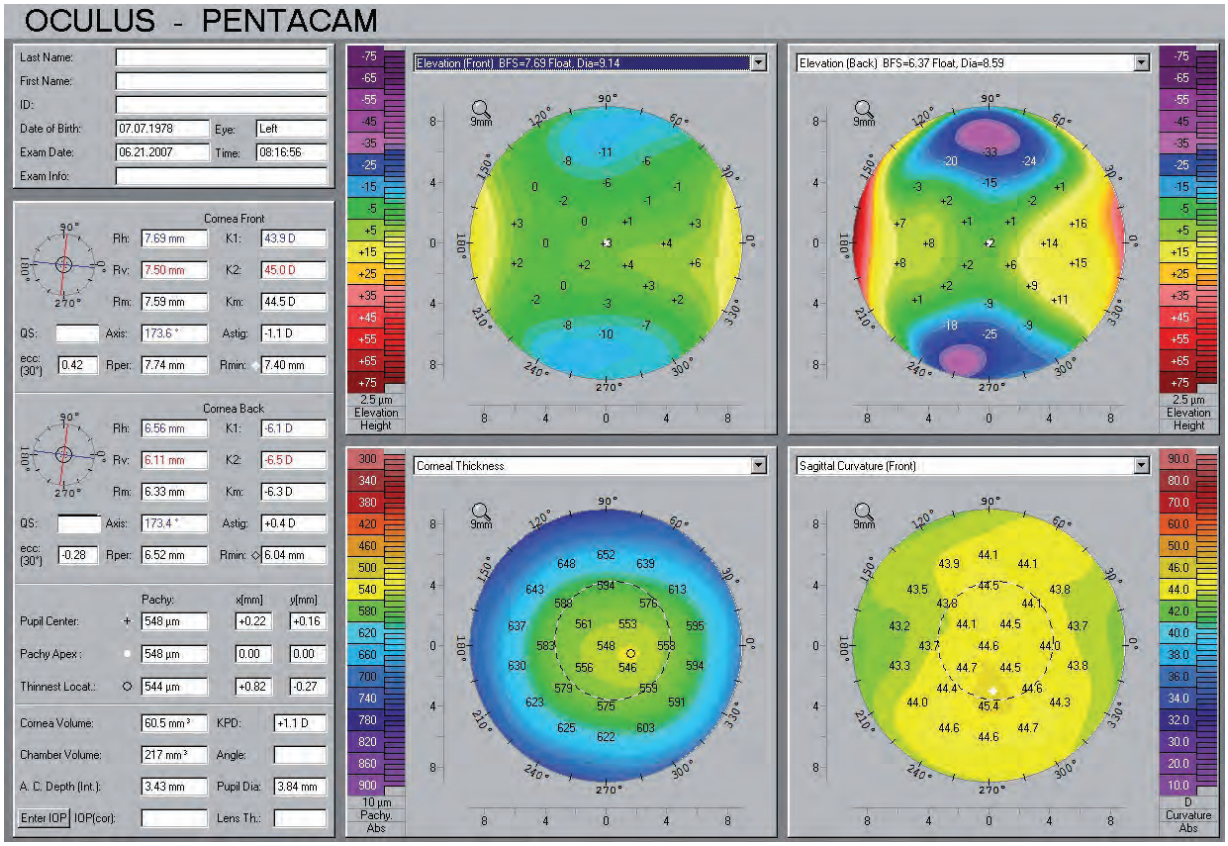

Figure 61: 4 Maps Selectable showing posterior astigmatism

10.4 Spherical cornea

This 4 Maps Selectable display (Figure 62) shows a normal, relatively spherical cornea (astig. 0.7 D). The anterior elevation shows no defined pattern, which is mirrored by the anterior sagittal curvature. The corneal thickness is slightly high (583 µm in the thinnest reading).

DIAGNOSIS – normal spherical cornea

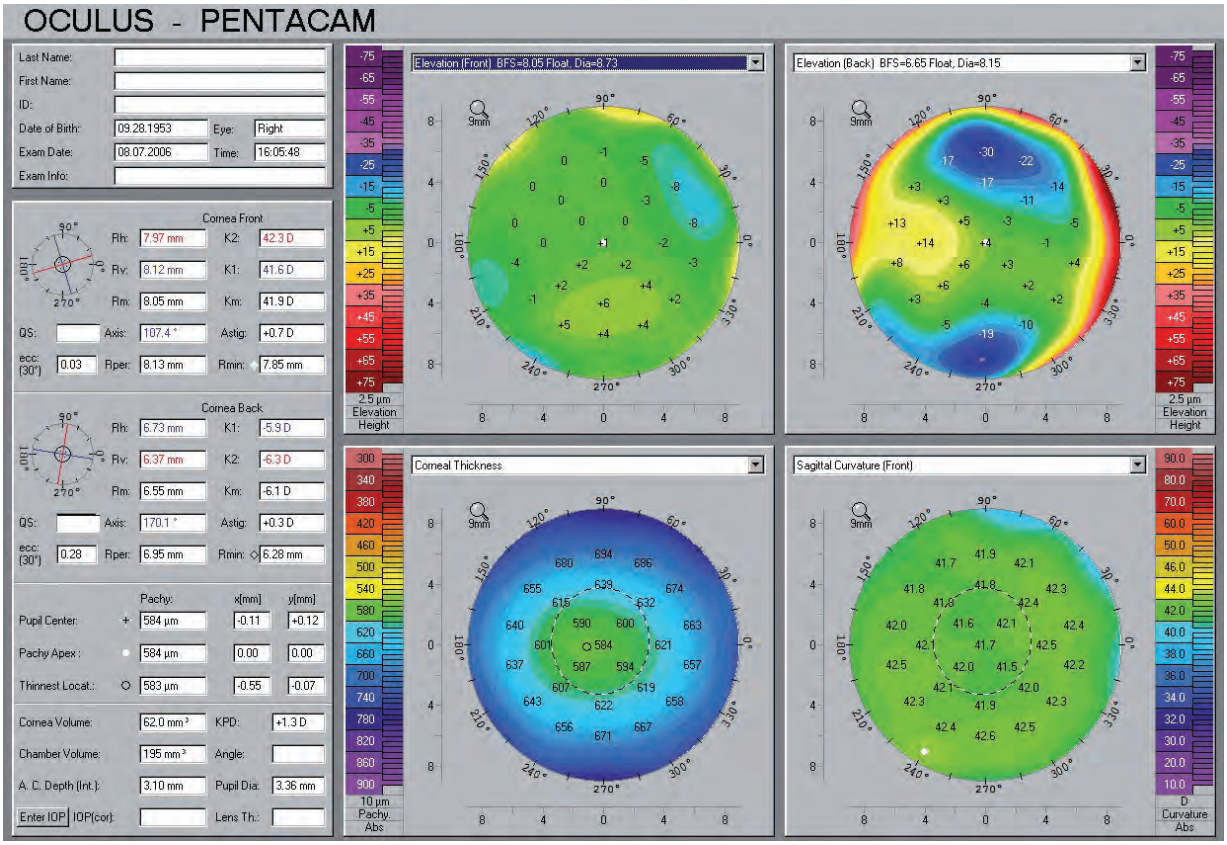

Figure 62: 4 Maps Selectable showing a spherical cornea

10.5 Thin spherical cornea

This 4 Maps Selectable display (Figure 63) shows a relatively spherical anterior cornea (both anterior elevation and anterior sagittal maps) and a more pronounced astigmatic pattern on the posterior corneal surface. Because the optical properties of the posterior cornea (no cornea/air interface) differ from those of the anterior surface, the refractive astigmatism of the posterior cornea is listed only as 0.3 D. The pachymetry map shows a thin cornea (thinnest reading 496 µm) with a slight inferior displacement of the thickness distribution.

DIAGNOSIS – normal thin spherical cornea with posterior astigmatism

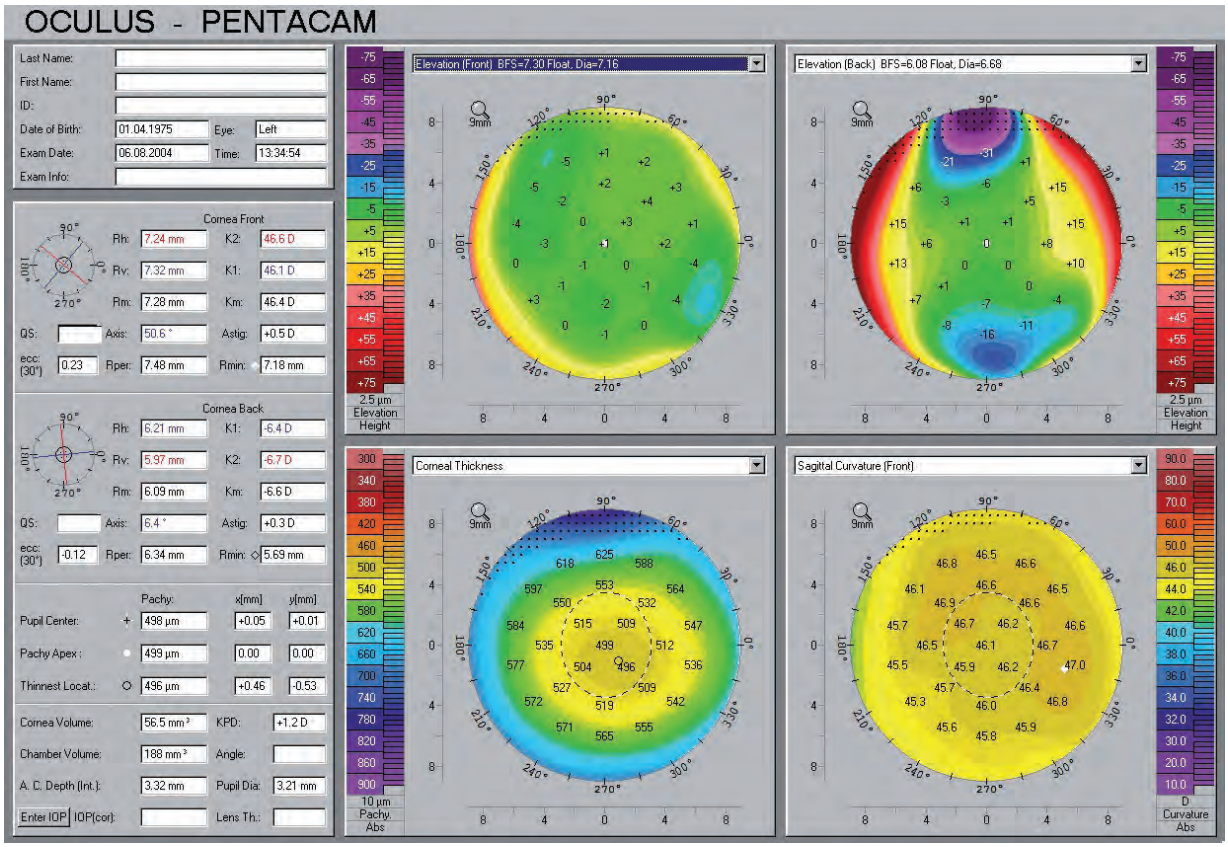

Figure 63: 4 Maps Selectable showing a thin spherical cornea

10.6 Thin cornea

This Show 2 Exams display (Figure 64) shows from OD and OS the posterior elevation and the pachymetry maps. The posterior elevation shows a normal astigmatic pattern, as does the anterior elevation (not shown). The pachymetry maps show the thinnest regions OD at 492 µm and OS at 483 µm. This is a normal eye topographically, but one that is on the thin side.

DIAGNOSIS – normal but thin cornea

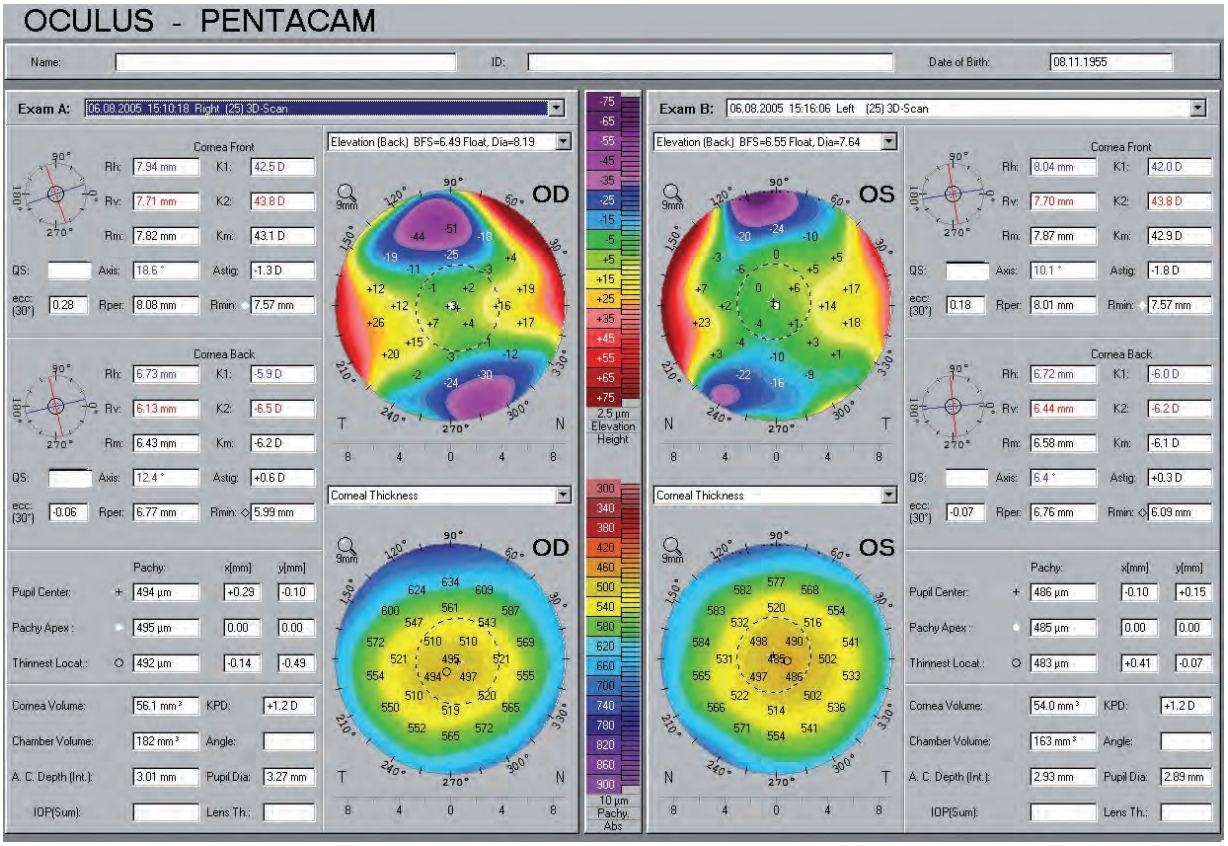

Figure 64: Show 2 Exams showing thin cornea in OD and OS

10.7 Borderline case of keratoconus

This 4 Maps Selectable display (Figure 65) shows a low-grade paracentral island (maximal elevation in island + 7 µm) in the anterior elevation map and a diffuse oval island on the posterior surface (maximal elevation in island + 13 µm). The anterior values are within the normal range, while the posterior numbers are nearly outside the normal range. The pachymetry map is normal, revealing a thick cornea (thinnest region 608 µm) with a normal pachymetry distribution. The completely normal pachymetry map suggests that the borderline elevation changes are probably acceptable.

DIAGNOSIS – borderline cornea map of keratoconus

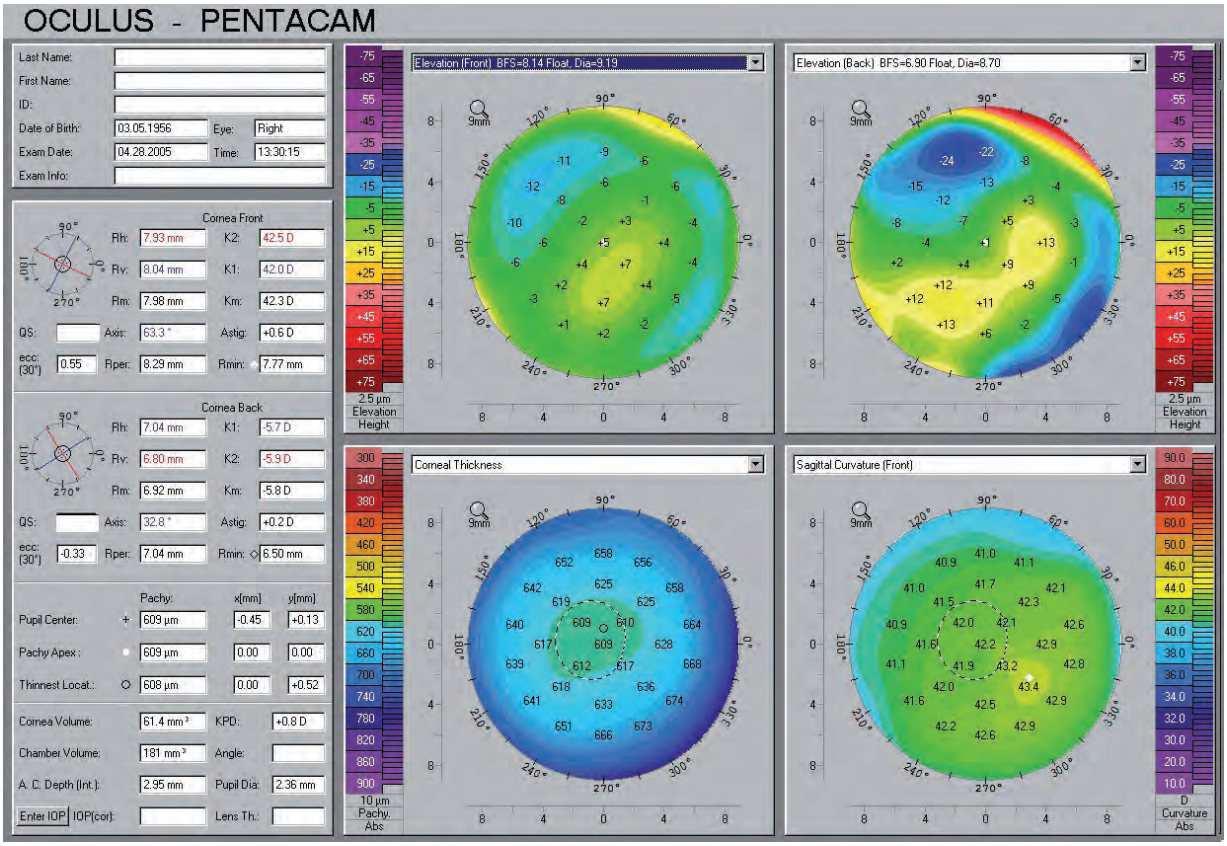

Figure 65: 4 Maps Selectable showing a borderline case of keratoconus

10.8 Displaced apex

This is a 4 Maps Selectable display of a normal astigmatic eye with a thick cornea (644 µm) (Figure 66). The anterior elevation map shows a "displaced apex" (displaced inferiorly). This causes the curvature map (anterior tangential curvature) to show an asymmetric pattern. Curvature is a reference-based measure. An asymmetric curvature pattern can occur with a completely normal astigmatic cornea when the apex, line of sight and measurement axis do not line up. This is a normal variant and in itself not indicative of pathology.

DIAGNOSIS – normal astigmatic eye with a false positive "asymmetric bowtie" on curvature

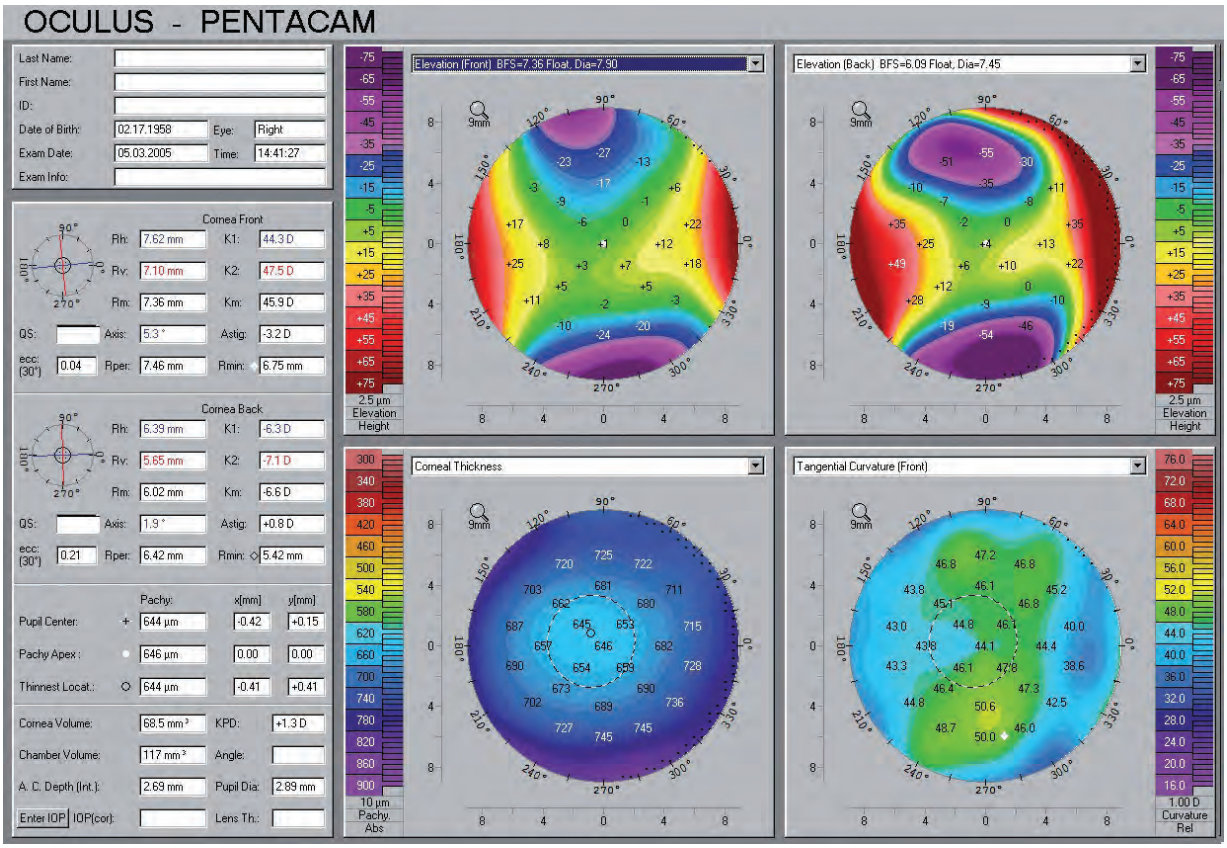

Figure 66: 4 Maps Selectable showing a displaced apex

10.9 Pellucid marginal degeneration

These are pictures of classic pellucid marginal degeneration (PMD). The pachymetry map (Figure 69) shows the band of thinning located 1 - 2 mm from the inferior limbus. This is an area that cannot be imaged on a Placido system, which is limited to imaging the central 9.0 mm.

The Scheimpflug images (Figure 67, Figure 89) show a relatively normal appearance when the cornea is viewed through a horizontal cut and the pathognomonic appearance when viewed through a vertical cross-section, revealing severe flattening over most of the cornea, an inferior band of thinning and a sharp change in corneal contour over the area of thinning. PMD is one of the most misdiagnosed conditions when the diagnosis is based on Placido imaging. A Placido system cannot reach to the area of the pathology. Descriptive curvature terms such as "lobster claw" pattern, etc. are fraught with problems and are associated with a very high false positive rate.

DIAGNOSIS - pellucid marginal degeneration

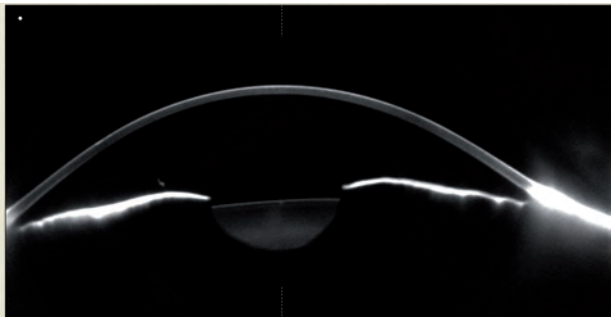

Figure 67: Scheimpflug image 180° showing PMD

Figure 68: Scheimpflug image 90° showing PMD

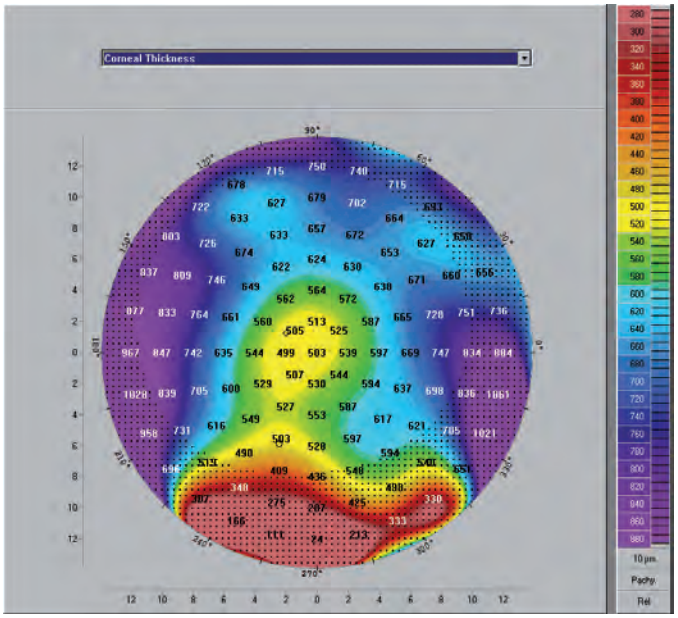

Figure 69: Corneal thickness in a case of PMD

10.10 Asymmetric keratoconus

This is a 4 Maps Selectable display (Figure 70) of a normal astigmatic eye (OD) with a thin cornea (thinnest reading 485 µm) and a noteworthy abnormality in the pachymetry distribution with a significant inferior-temporal displacement of the thinnest zone. At times the only indicator of potential pathology may be the magnitude and distribution of the corneal pachymetry.

DIAGNOSIS – normal astigmatic eye

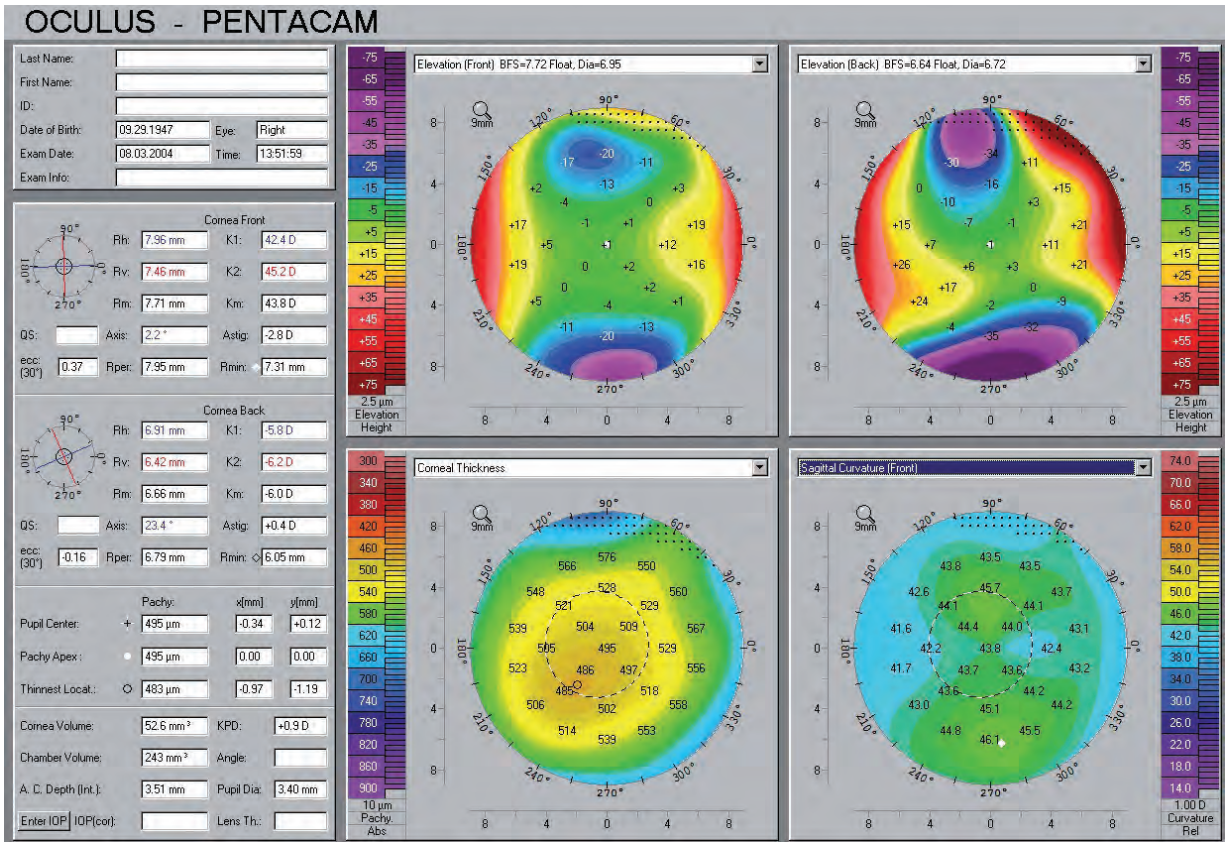

Figure 70: 4 Maps Selectable showing an asymmetric cornea of normal topography in OD

The left eye shows a major posterior ectasia (+ 79 µm) on inferior island, and marked inferior displacement of the pachymetry map (thinnest reading 426 µm) (Figure 71). The anterior elevation shows a somewhat irregular astigmatic pattern but without any obvious positive island. The tangential curvature incorrectly locates the cone much more inferiorly than the cone location shown by both the posterior elevation data and the pachymetry map.

DIAGNOSIS – asymmetric keratoconus greater in OS than OD

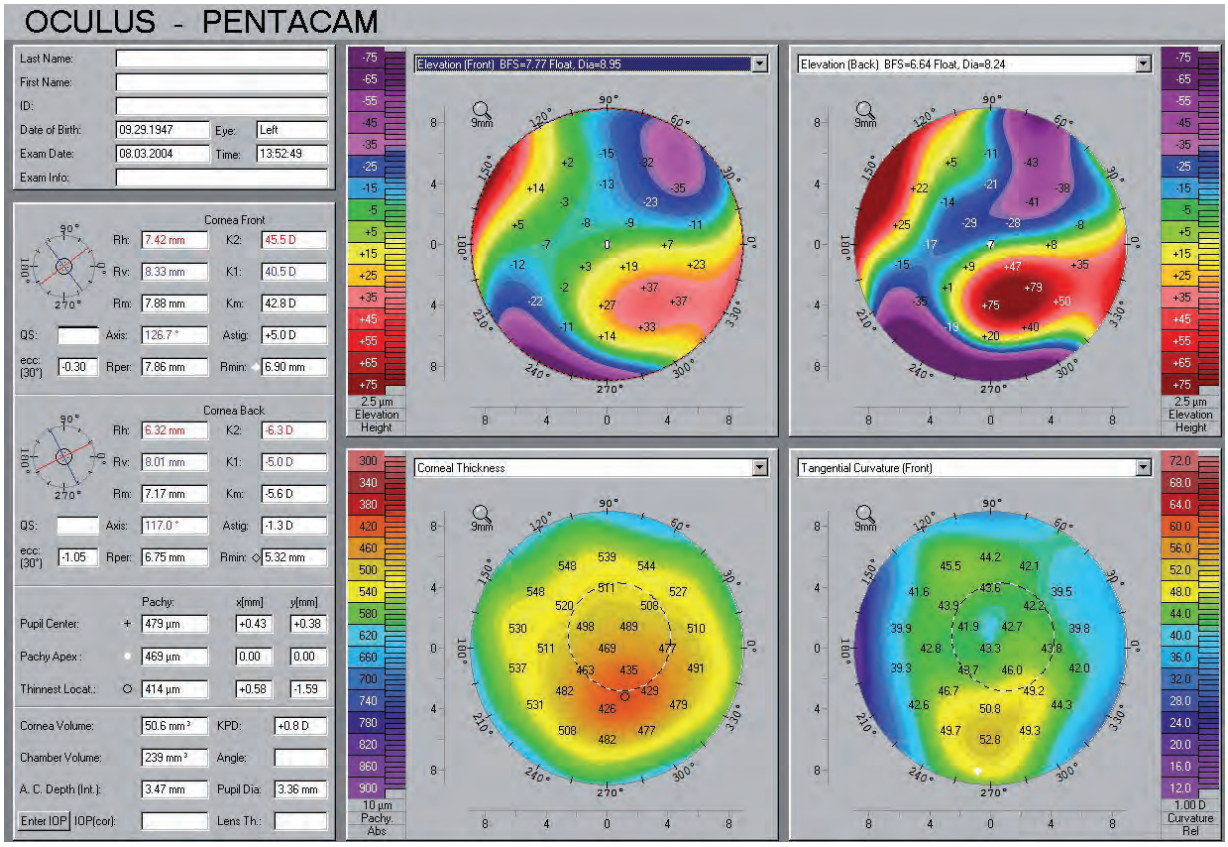

Figure 71: 4 Maps Selectable showing an asymmetric cornea with keratoconus in OS

10.11 Keratoconus with false negative findings on curvature map

This 4 Maps Selecable display (Figure 72) shows a classic keratoconus in OS. The anterior elevation map shows a minor island that is still within the normal range. The posterior elevation, however, shows a very significant area of inferior ectasia (positive island up to + 35 µm), and the pachymetry map is significantly displaced and thinned to 499 µm. If the surgeon had only relied on anterior curvature and central corneal thickness readings, this patient would have been classified as normal (normal anterior curvature and central corneal thickness of 520 µm). This demonstrates the importance of having accurate posterior elevation data in addition to anterior surface analysis.

DIAGNOSIS – form fruste or sub-clinical keratoconus, false negative on curvature

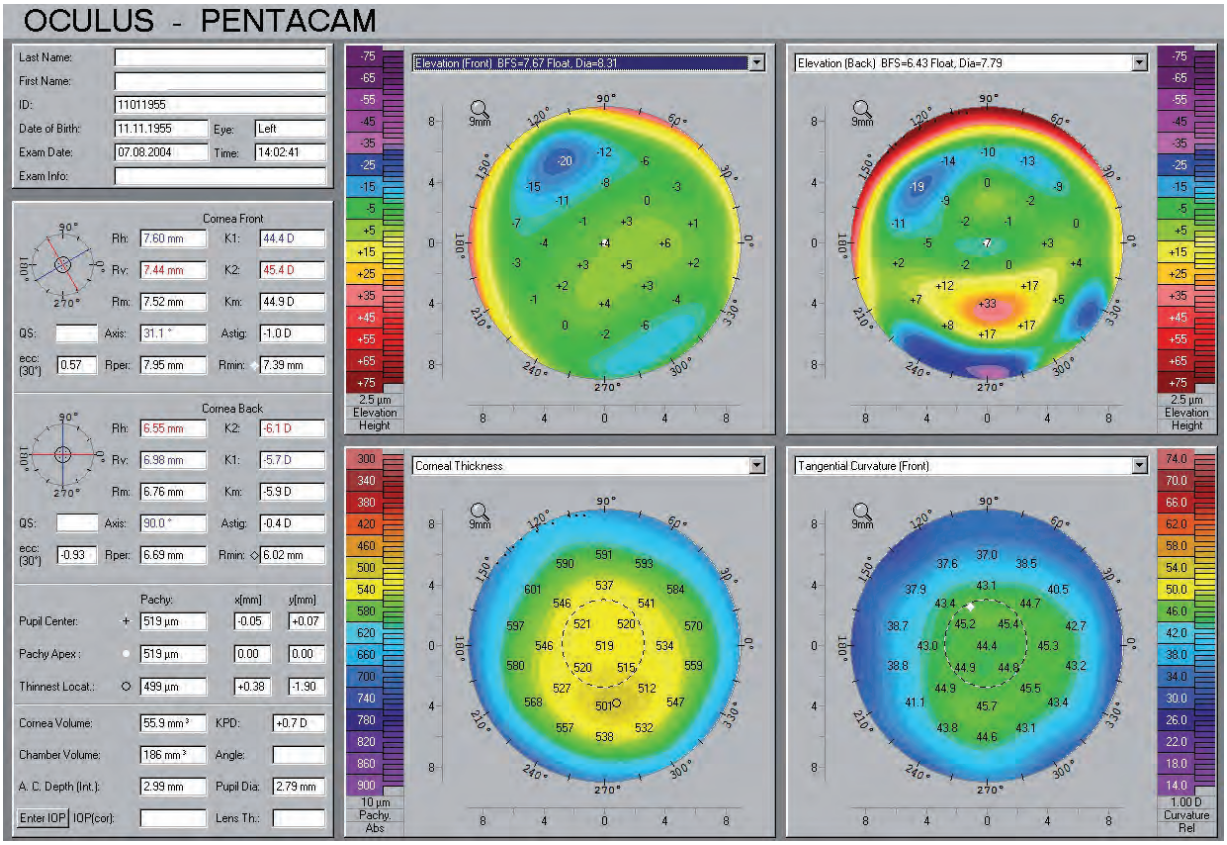

Figure 72: 4 Maps Selectable showing a form fruste keratoconus in OS with false negative topography in the anterior curvature map

10.12 Keratoconus greater in OD than OS

Look at the Show 2 Exams display of posterior elevation and pachymetry of OD and OS in this patient with keratoconus (Figure 73). The right eye shows a significant posterior island (ectatic area) associated with marked corneal thinning (430 µm) and significant inferior-temporal displacement of the thinnest area towards the area of the abnormal posterior elevation. The left eye shows a relatively normal posterior astigmatic pattern, but a distinctly abnormal pachymetry distribution with marked inferior-temporal displacement and a thinnest reading of 440 µm. This example shows the importance of looking at the pachymetry distribution, which may be the single abnormal finding.

DIAGNOSIS – keratoconus greater in OD than OS

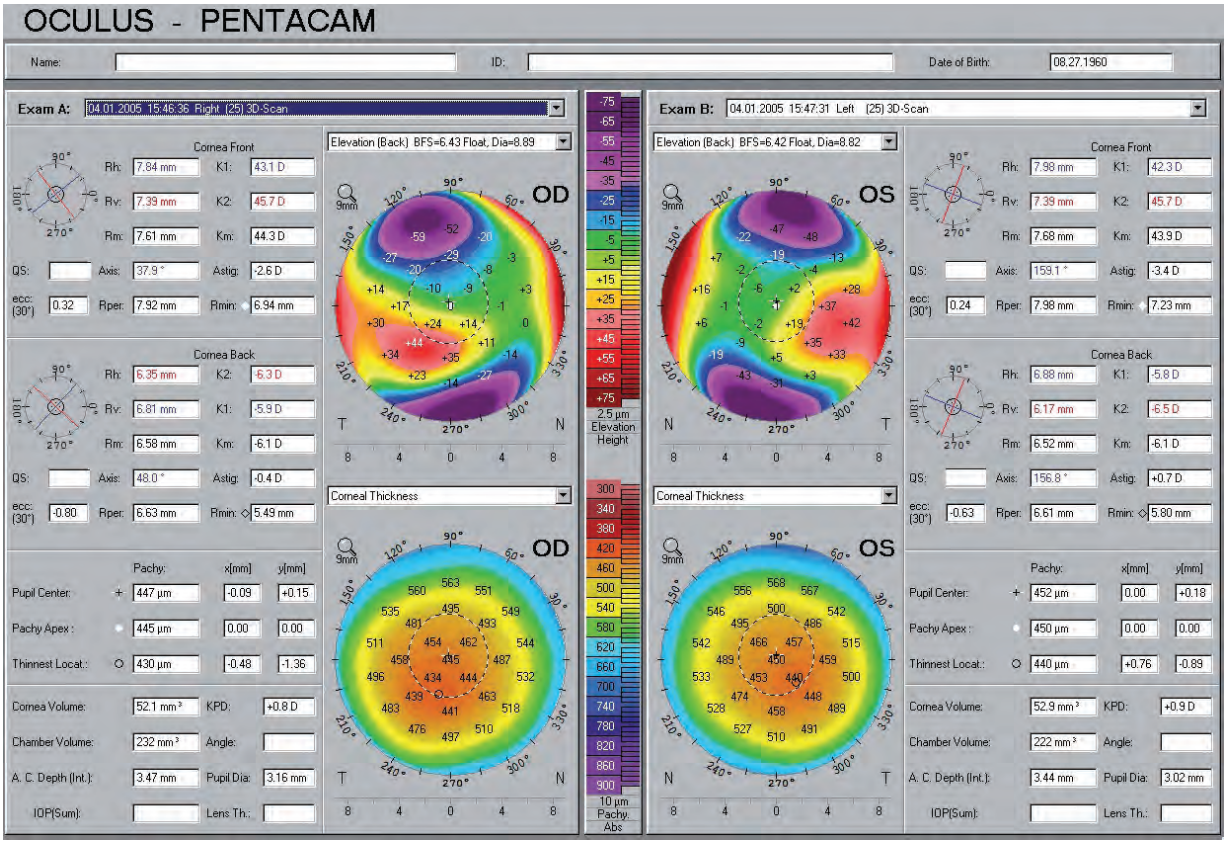

Figure 73: Show 2 Exams showing keratoconus greater in OD than OS

10.13 Classic keratoconus

This 4 Maps Selectable display shows a case of classic keratoconus in OD (Figure 74). Both anterior and posterior elevations show a prominent island of positive deviation (maximal at +33 µm anterior and +89 µm posterior) with an accompanying displacement of the pachymetry map (thinnest reading 485 µm). The tangential curvature map also shows inferior steepening, but again does not accurately locate the cone.

DIAGNOSIS – classic keratoconus

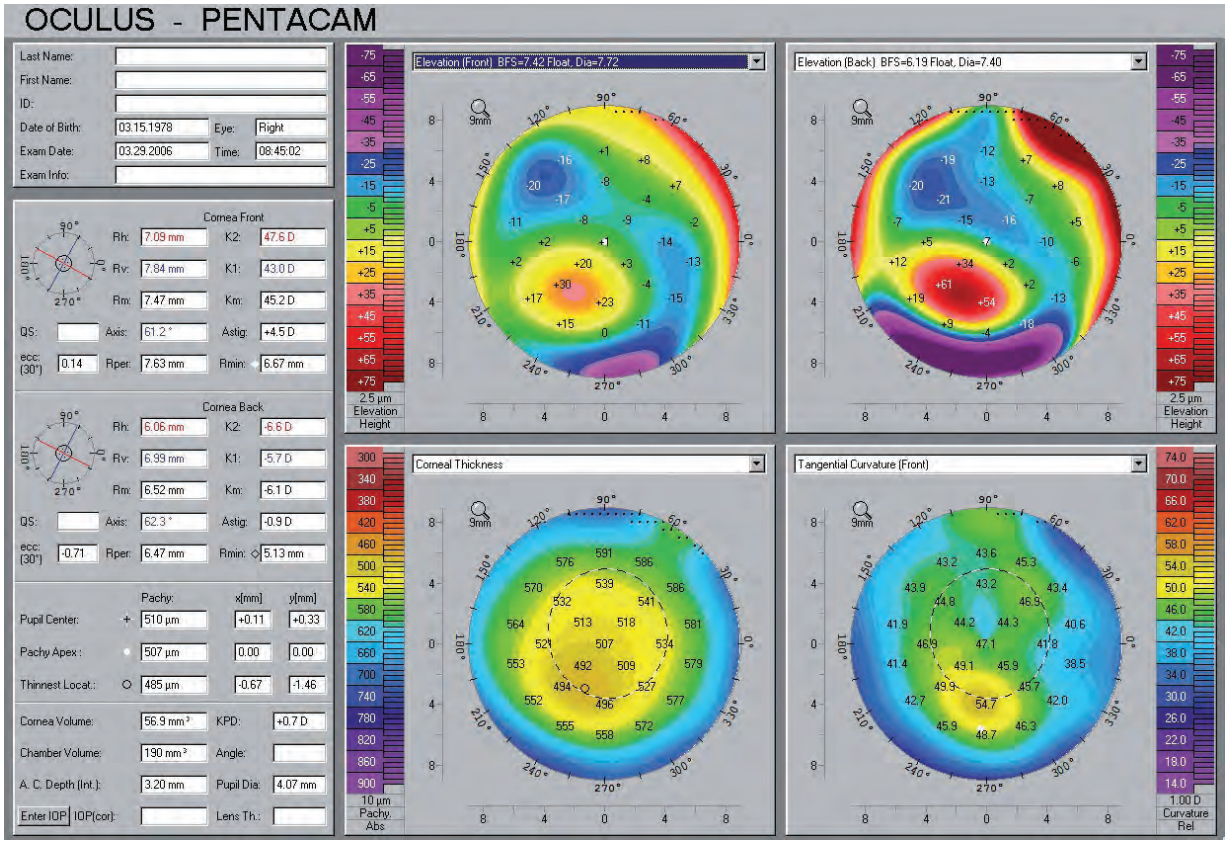

Figure 74: 4 Maps Selectable showing a case of classic keratoconus in OD

11 Corneal Thickness Spatial Profile by Prof. Renato Ambrósio Jr

The measurement of corneal thickness has become an important factor in a variety of clinical situations, including planning and evaluation of results of most types of corneal and anterior segment surgeries and evaluation of corneal endothelium dehydrating function as well as its consideration as a risk factor for glaucoma.

Ultrasonic central corneal thickness is usually referred to the measurements at the corneal geometric center or at the apex, which is not the corneal thinnest point (TP).

Regional US pachymetry can been used, but the need for the pachymetric map for determining the location and value of the cornea's TP becomes clear when we consider that the difference between central and TP thickness is greater than 10 µm in over 10% of normal corneas.

Corneal tomography provides a three-dimensional reconstruction of the cornea, thus permitting evaluation of the anterior and posterior corneal surfaces and thereby the creation of a pachymetric map.

We believe tomography to be a better term for such diagnostic approaches. It derives from the Greek word "tomos", which means "slice", and "graphia", which means "describing".

The aim of this section is to provide a comprehensive understanding of the current corneal thickness profile studies that have appeared since the introduction of the Pentacam® software, along with other approaches that could be developed in the future.

Corneal Thickness Spatial Profile (CTSP)

Corneal thickness values at the TP is determined and the averages of thickness values of the points within twenty-two imaginary circles centered on the TP with increased diameters at 0.4 mm steps are calculated to create the CTSP (Figure 75).

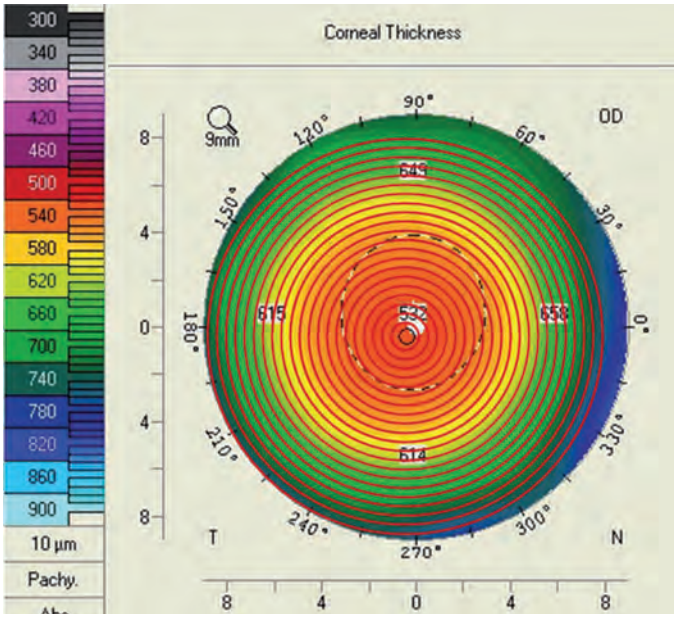

Figure 75: The Corneal Thickness Spatial Profile (CTSP)

Percentage of Increase in Thickness (PIT)

PIT can then be calculated for each position using the simple formula:

$$\text{PIT} = \frac{(\text{mean corneal thickness in the ring} - \text{thinnest corneal thickness})}{\text{thinnest corneal thickness}}$$

Clinical results

In a published study involving 46 eyes of 23 patients (13 females) diagnosed with mild to moderate keratoconus and 364 normal eyes from 196 patients (97 females), statistically significant differences were observed between the two groups ($P < 0.01$) for all positions of CTSP and PIT [5]. Keratoconic eyes had much lower (thinner) values than normals, with an estimated average difference of 27.3 µm. In keratoconic eyes mean TP was 428 µm, (standard deviation (SD) 72 µm, 95% confidence interval (CI95) 391-474 µm, range 245-563 µm), while in normal eyes the mean value was 537 µm (SD 36.7 µm, CI95 513-562 µm, range 439-630 µm). For example, in keratoconic eyes mean corneal thickness on the 4.8 mm diameter circle was 536.5 µm, (SD 48.3 µm, 95CI 516-566 µm, range 377-623 µm), while in normal eyes, mean thickness was 589 µm (SD 36.9, 95CI 564-614.8 µm, range 467-693 µm).

The statistical significance of differences in PIT between normal and keratoconic eyes over all locations considered was very high ($p < 0.0001$). Keratoconic corneas had a much higher thickness percentage increase than normal eyes on each of the 22 diameters.

In keratoconic eyes mean PIT on the 0.4 mm diameter was 0.27% (SD 0.29, CI95 0.19-0.26, range 0.0-1.6 µm), while in normal eyes, the mean value was 0.07% (SD 0.09%, CI95 0.0-0.18%, range 0.0-0.23%). On the 4.8 mm diameter circle mean PIT in keratoconic corneas 28.2% (SD 21.4%, 95CI 13.8-34.8%, range 6.1-129%), while in normal eyes the mean value was 9.9% (SD 1.9% (95CI 8.7-11.1%, range 3.3-17.9%).

This study demonstrated that modern corneal tomography provides us in CTSP and PIT with two powerful discriminators of keratoconus. We also found that keratoconic eyes have thinner corneas with less volume and a faster increase in thickness from the TP towards the periphery than do normal corneas. The Scheimpflug images below, one of a normal thin cornea and the other of a moderately keratoconic eye, clearly illustrate the differences in thickness profile between normal and ectatic eyes (Figure 76).

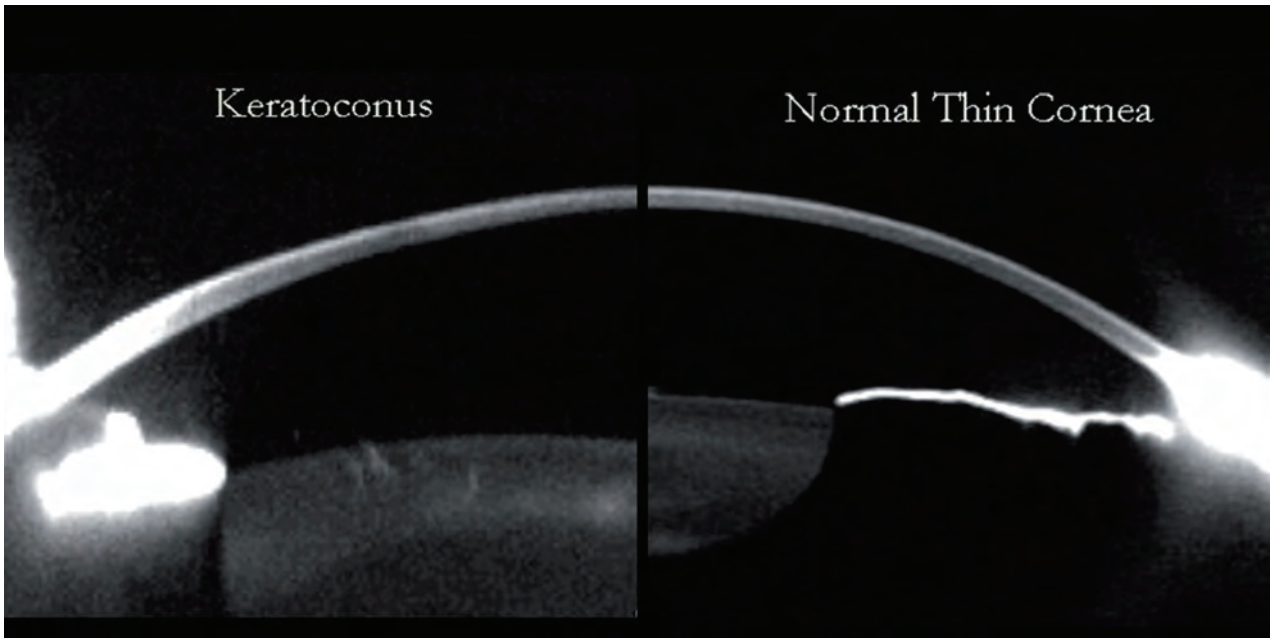

Figure 76: Thickness profile in an ectatic and a normal eye

It is worth noting that Mandell and Polse pioneered this field in a study using a modified Haag-Streit optical pachymeter with an electronic recording system to document the variation in thickness over the horizontal meridian measured at different angles [6]. However, this interesting approach to evaluating the cornea was not used clinically for decades.

In developing the Pentacam® software the results of our studies served as a basis for engineering new summaries and graphs that would help clinicians explore CTSP and PIT so as to be able to objectively evaluate thickness profiles and detect ectasia. The software displays the CTSP and PIT curves of the examined eye together with the CI95 limits of a normal population. Initially, these graphs were included in a "keratoconus page" along with other topographic indices derived from the 8 mm anterior corneal curvature which were similar to those used in Placido topography.

11.1 Screening for ectasia
by Prof. Renato Ambrósio Jr, Marcela Q. Salomão, MD

The new software combines the elevation criteria of Michael Belin, MD for screening for ectasia. This opens up new horizons in analysing corneal thickness for diagnosis and classification of corneal ectasia. The CTSP and PIT graphs are furthermore relevant in evaluating abnormal thick corneas in endothelial disease. They provide very relevant clinical data for differentiating between normal thin corneas (Figure 77, Figure 78) and ectatic corneas (Figure 79, Figure 80).

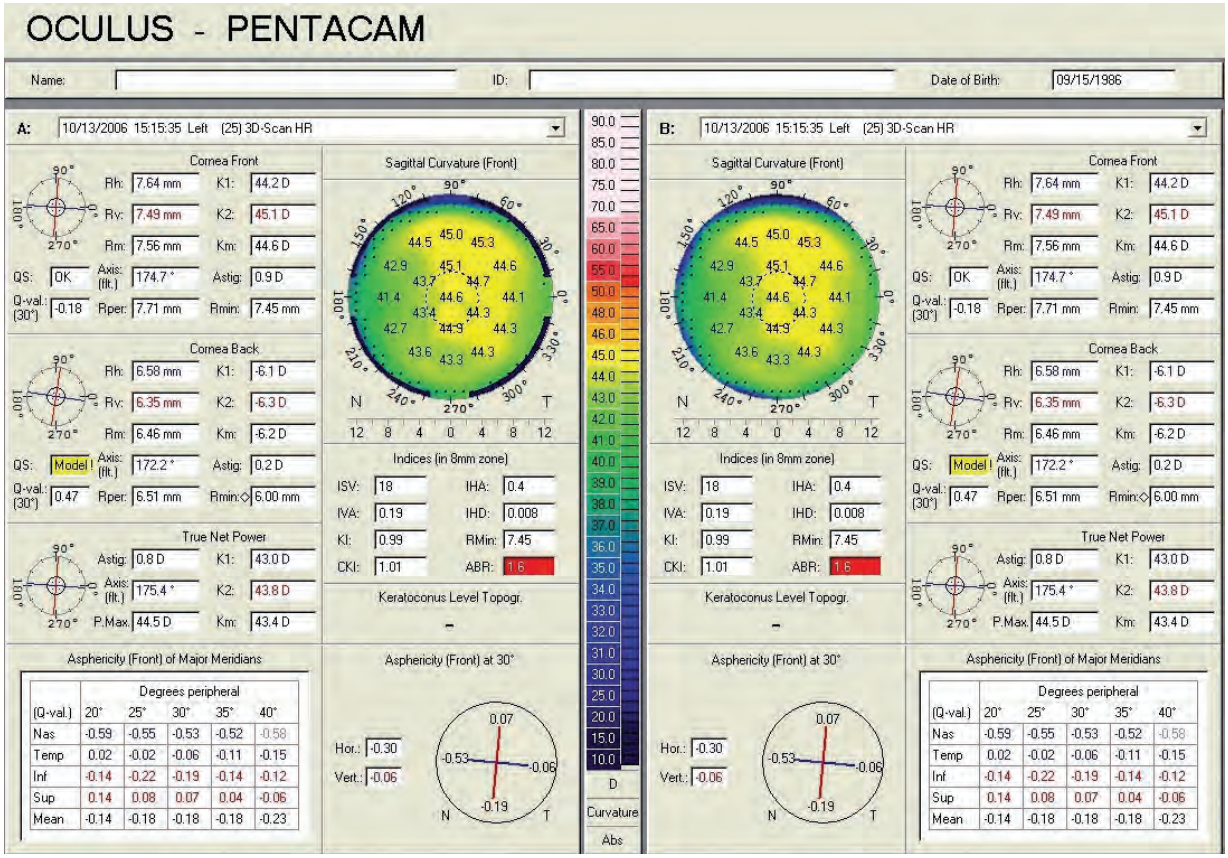

Figure 77: Show 2 Exams Topometric showing a normal thin cornea

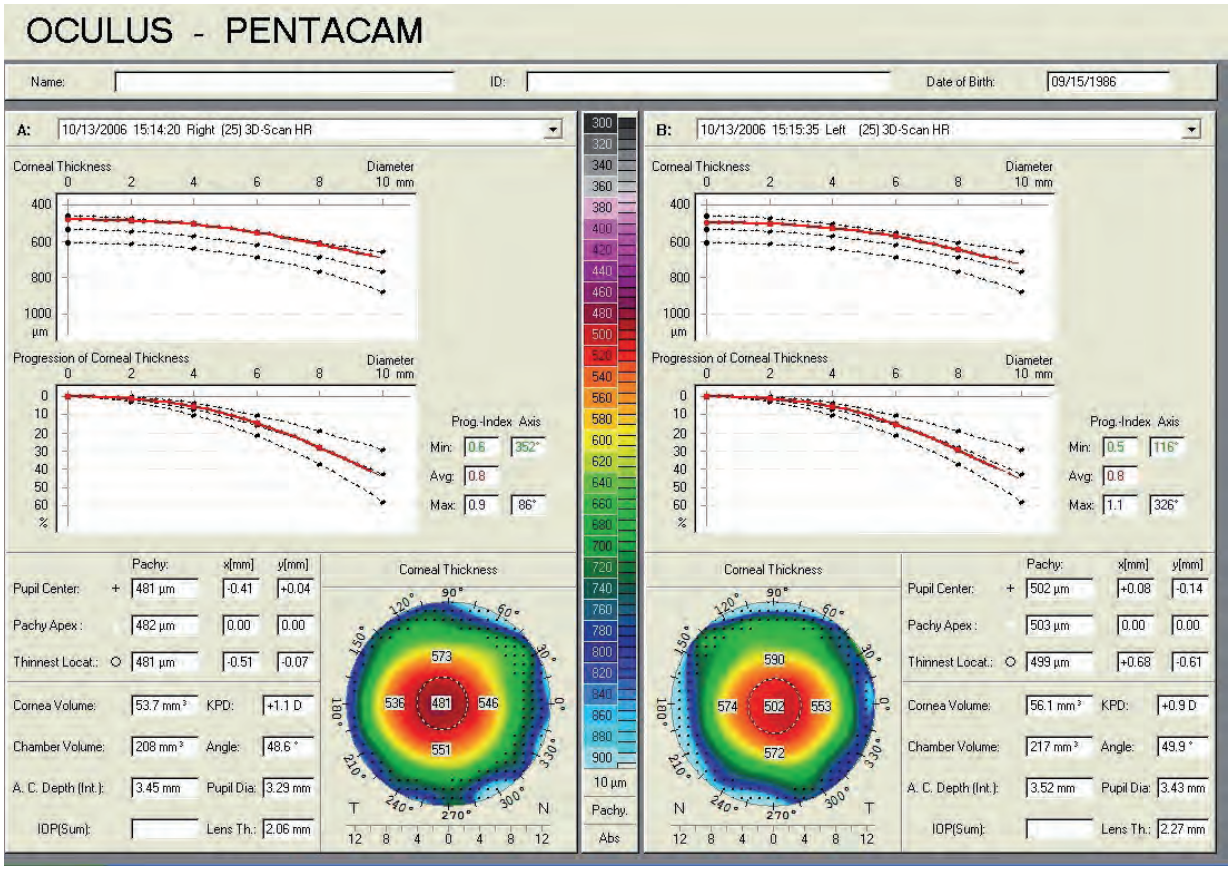

Figure 78: Show 2 Exams Pachymetric showing a normal thin cornea

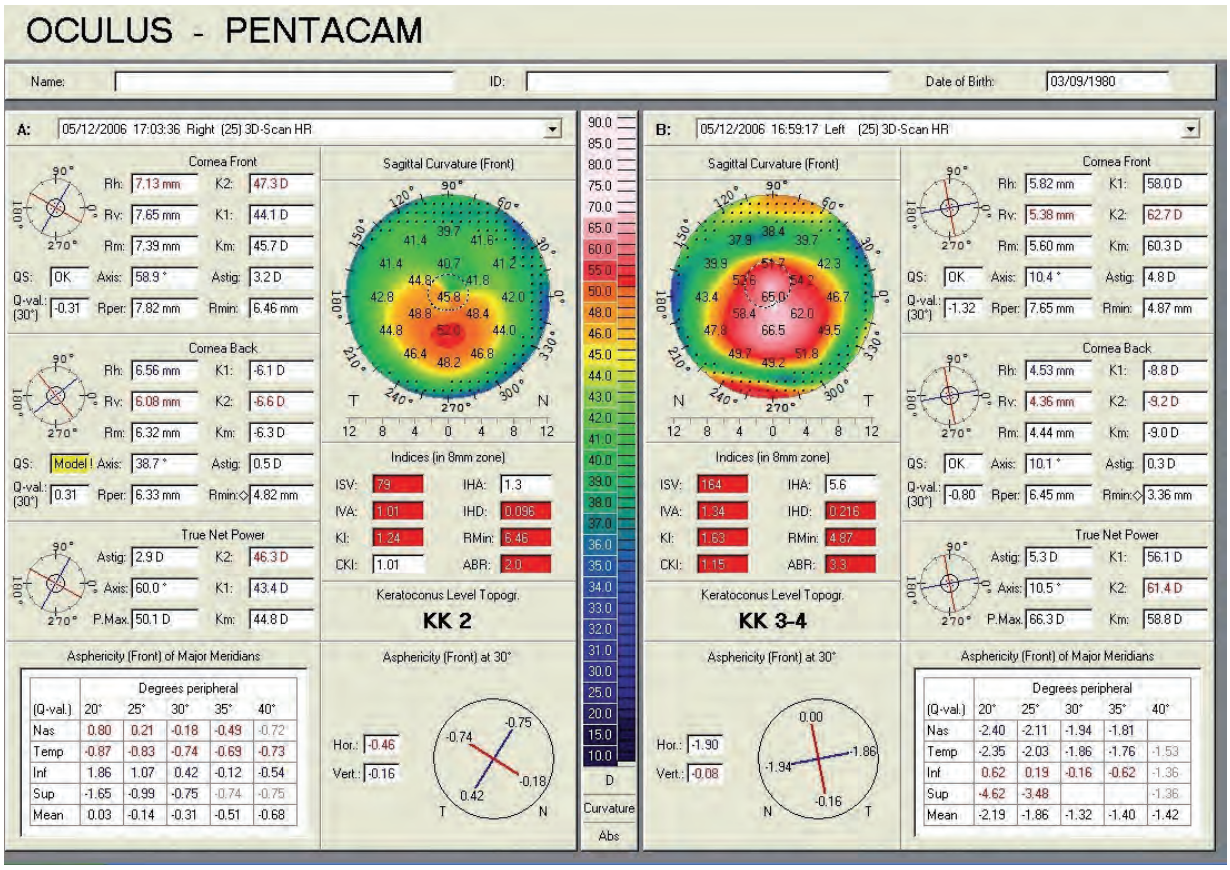

Figure 79: Show 2 Exams Topometric showing an ectatic cornea

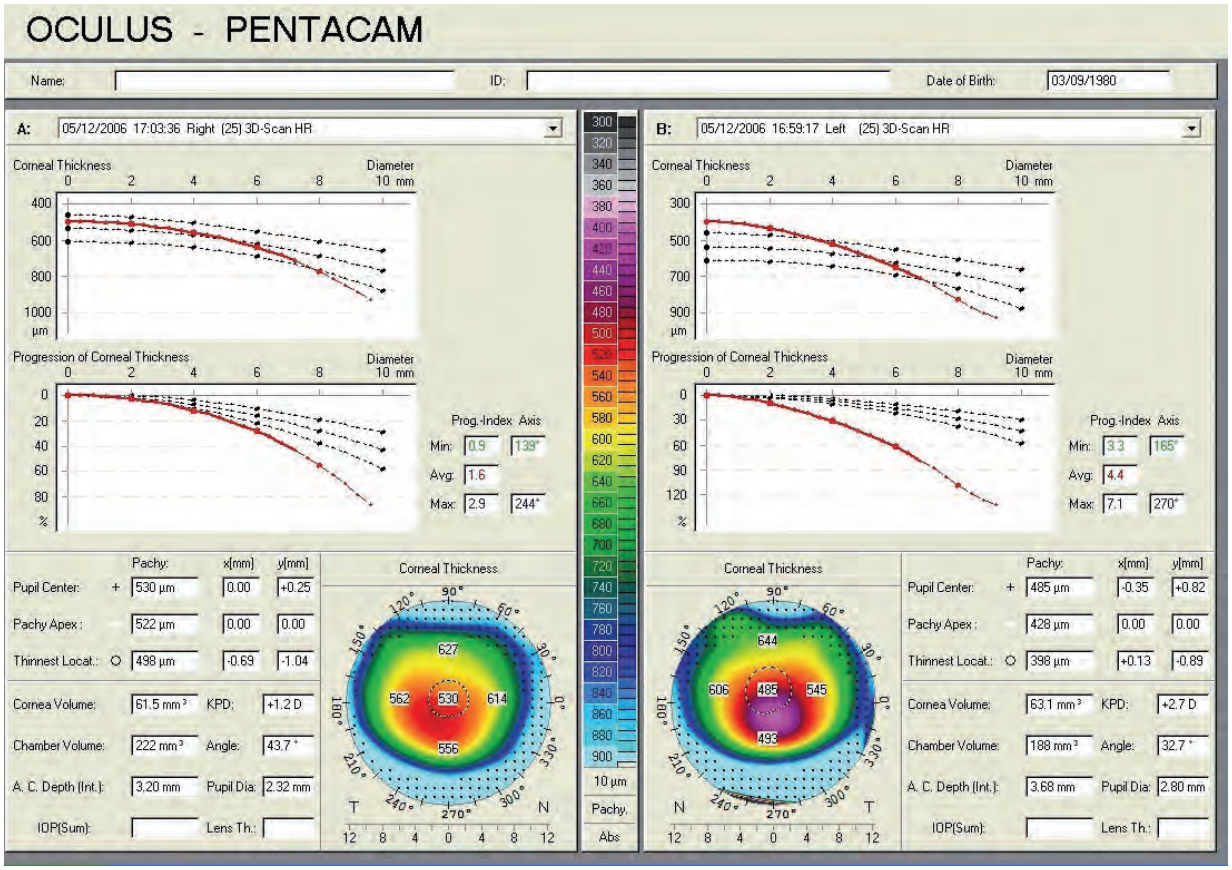

Figure 80: Show 2 Exams Pachymetric showing an ectatic cornea

Currently, most diagnostic and classification criteria for keratoconus are based on anterior corneal curvature data derived from corneal topography. We wish to emphasize that the thickness profile described here should be used in conjunction with the classic ones provided by corneal topography.

To test the hypothesis that the CTSP and PIT increase sensitivity for the detection of very early forms of keratoconus we studied patients with keratoconus in one eye and in the other a cornea of normal surface curvature as evidenced by Placido topography. Interestingly, the contra-lateral eyes also exhibited signs of abnormality on the CTSP and PIT graphs (Figure 81, Figure 82).

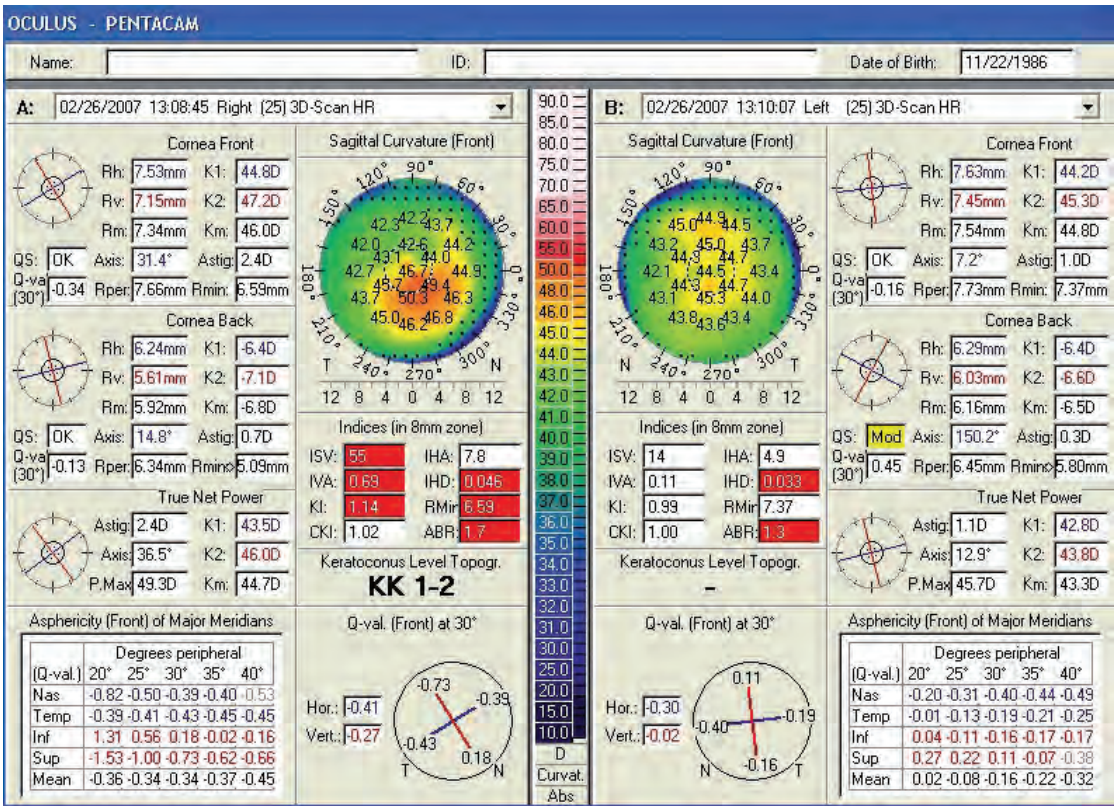

Figure 81: Show 2 Exams Topometric showing an asymmetric cornea

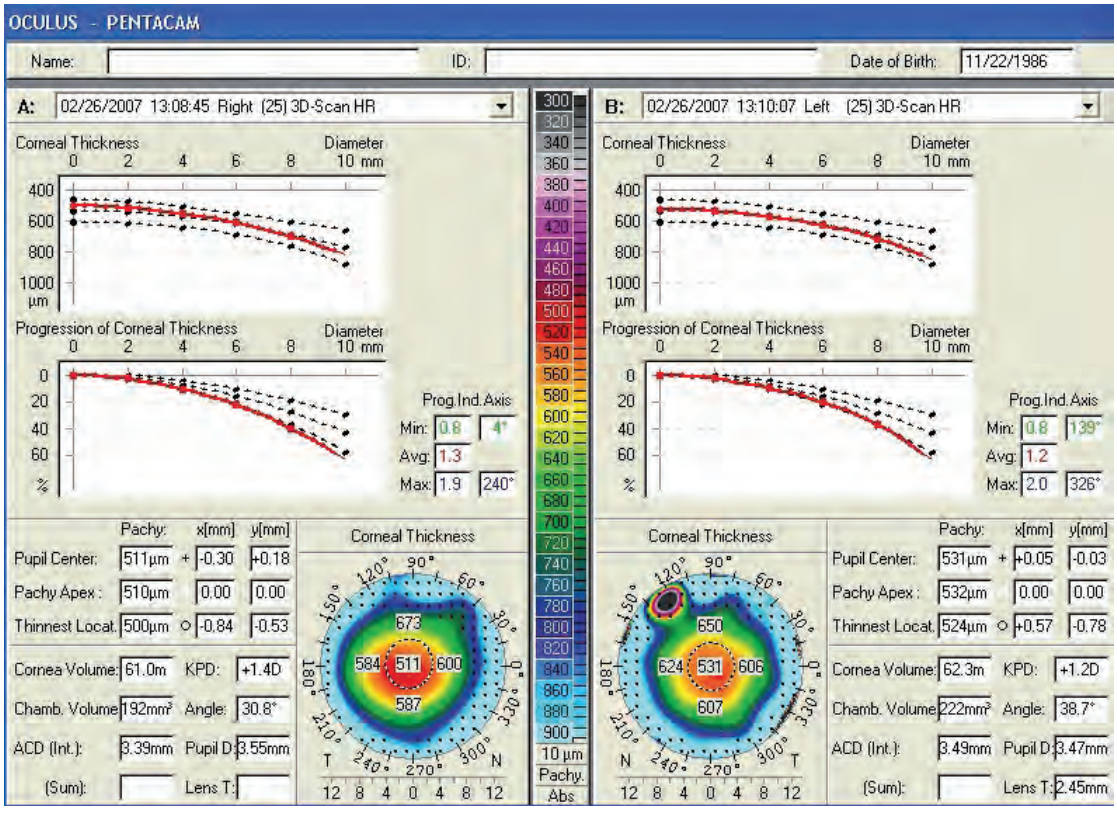

Figure 82: Show 2 Exams Pachymetric showing an asymmetric cornea

With regard to the specificity of the indices for the detection of ectasia, the topometric values show a high false positive rate, especially in cases with moderate keratometric asymmetry and inferior steepening (Figure 83, Figure 84).

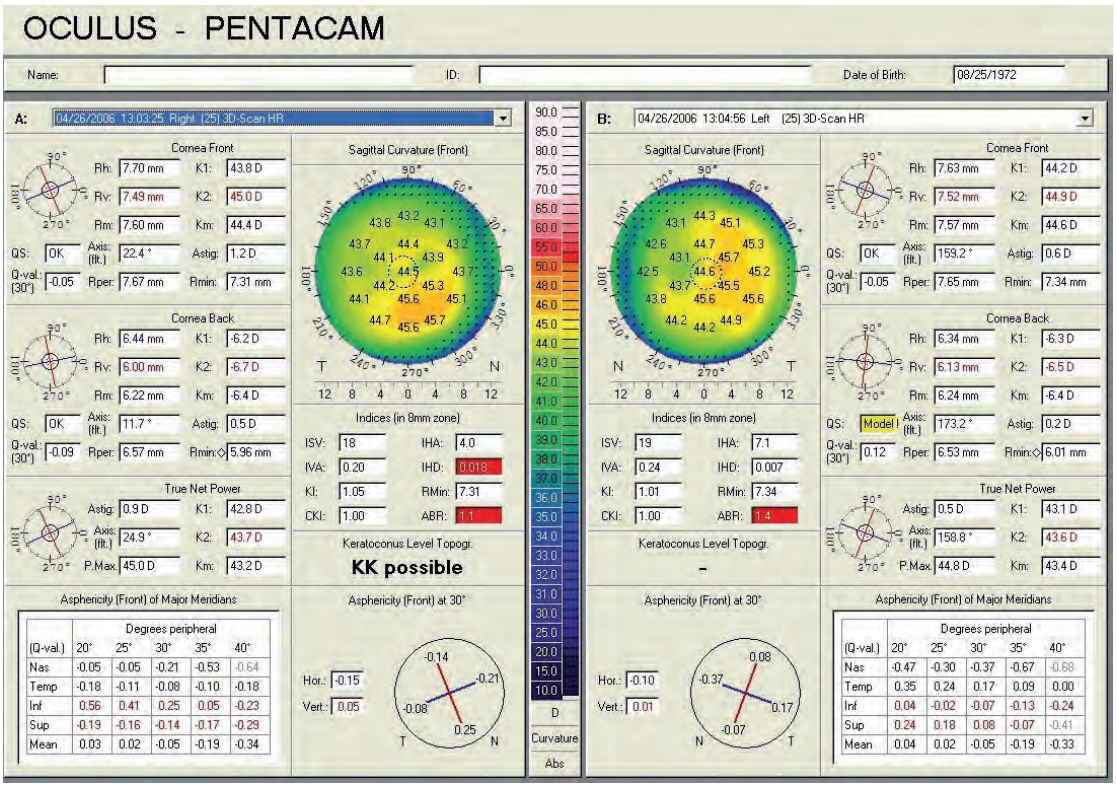

Figure 83: Show 2 Exams Topometric giving a false positive diagnosis of ectasia

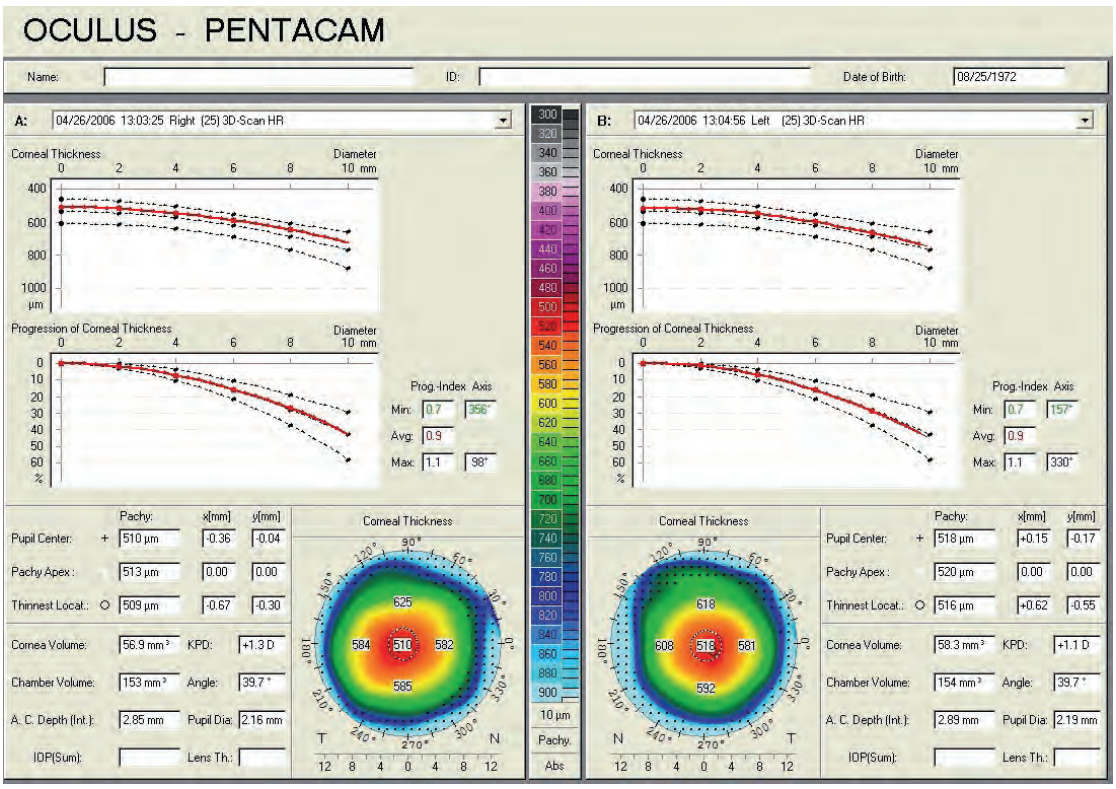

Figure 84: Show 2 Exams Pachymetric showing a normal cornea

11.2 Case 1: Fuchs' dystrophy by Prof. Renato Ambrósio Jr, Marcela Q. Salomão, MD

Contrary to ectasia, in which central thinning causes a more pronounced or abrupt increase in the thickness values from the center towards the periphery, corneal swelling makes the cornea homogeneously thick, decreasing the increase in thickness values towards the periphery.

We have found that the "flattening" of the CTSP and PIT curves occurs even in cases of very early increase in corneal thickness caused by Fuchs' dystrophy, when the cornea is still clear (Figure 85, Figure 86).

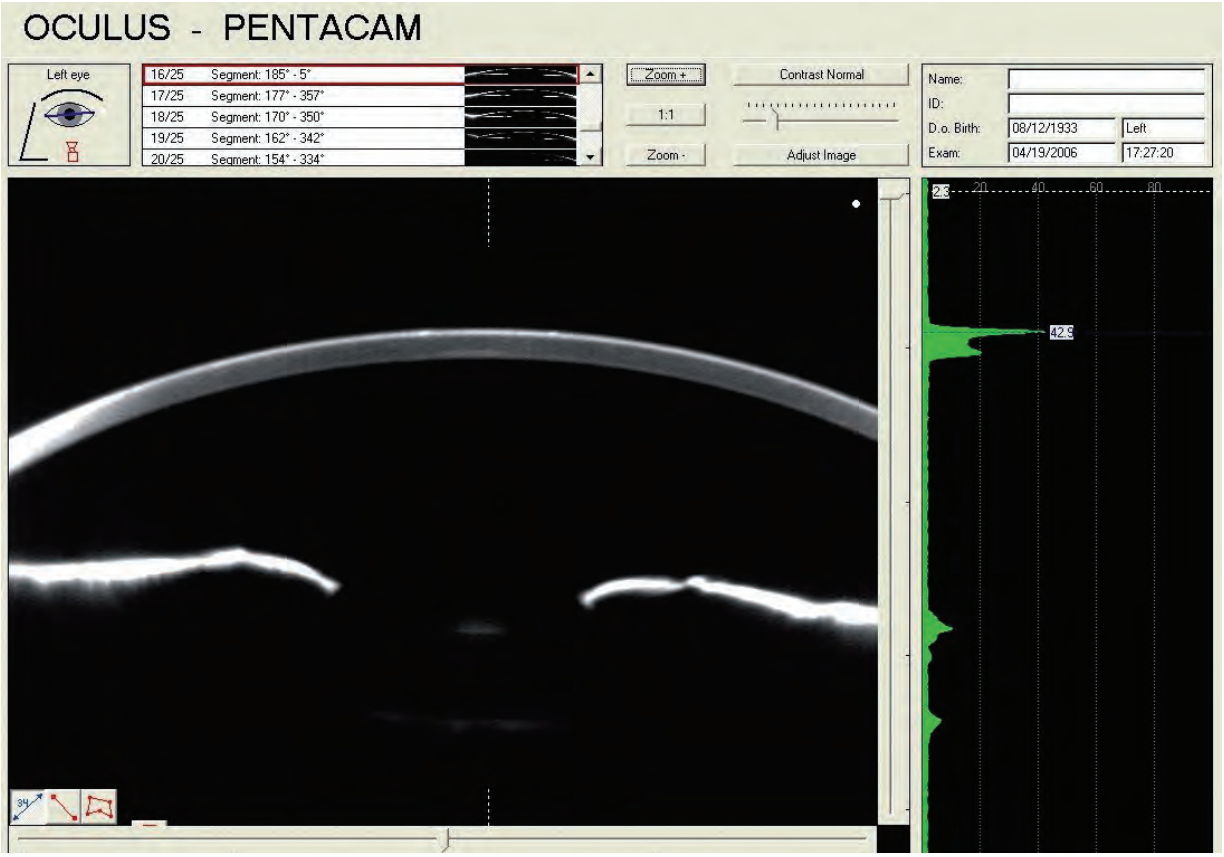

Figure 85: Scheimpflug Image showing a case of Fuchs' dystrophy in OS

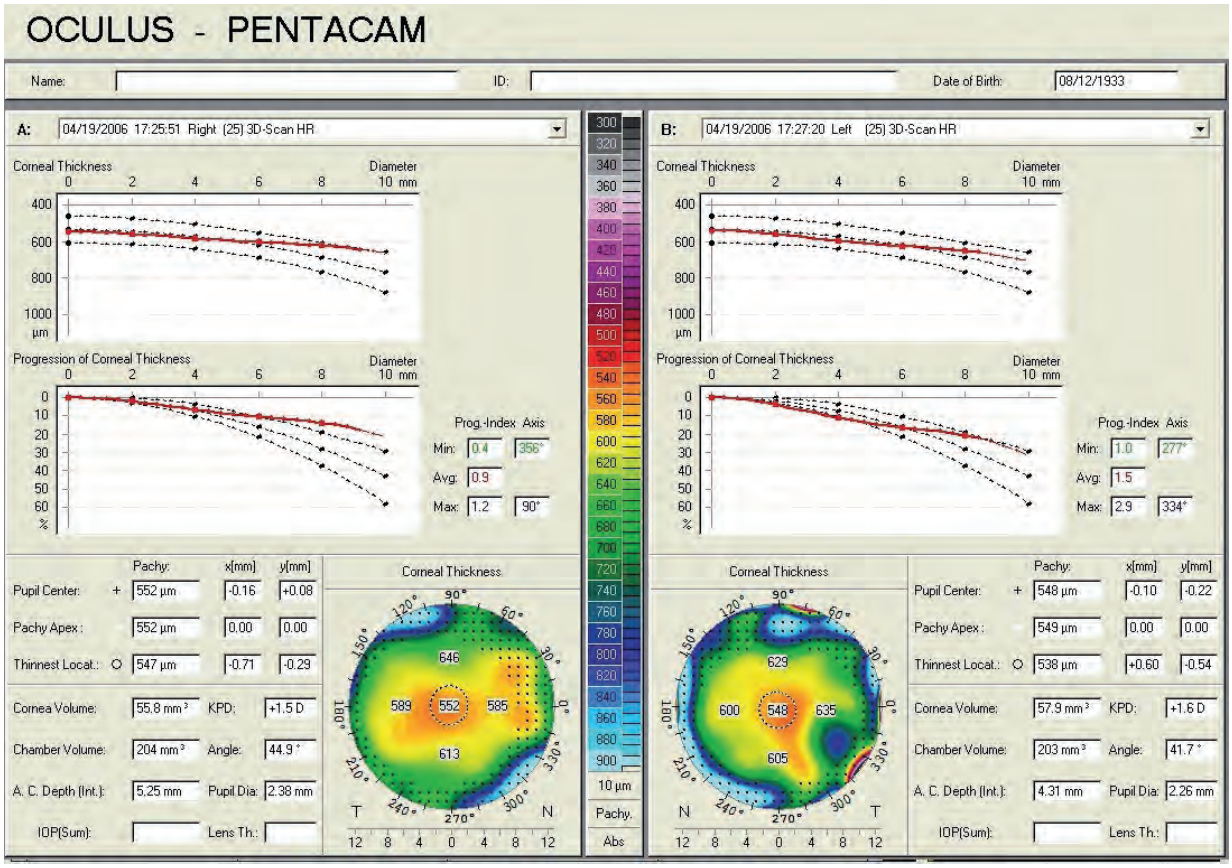

Figure 86: Show 2 Exams Pachymetric showing a case of Fuchs' dystrophy

11.3 Case 2: Ocular hypertension
by Prof. Renato Ambrósio Jr, Marcela Q. Salomão, MD

The case below shows a patient with ocular hypertension. Please note the clear appearance of the corneas in the Scheimpflug images (Figure 87, Figure 88) below as well as their thickness in the Show 2 Exams display (Figure 89).

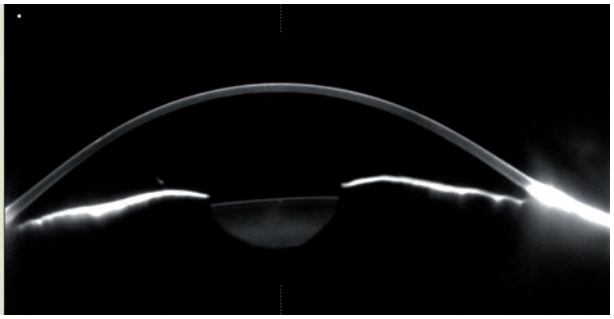

Figure 87: Scheimpflug image showing clear cornea in OD with no peak in the densitogram for the endothelium

Figure 88: Scheimpflug image showing clear cornea in OS with no peak in the densitogram for the endothelium

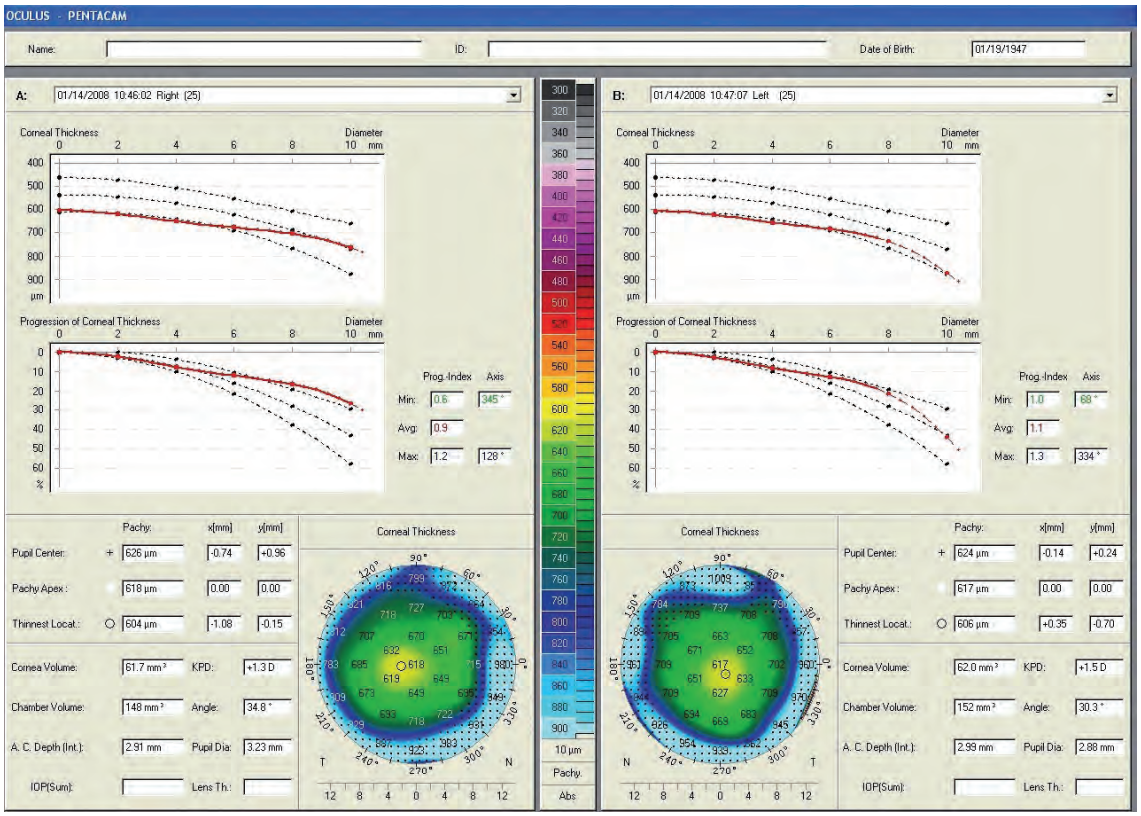

Figure 89: Show 2 Exams Pachymetric showing thick corneas with abnormal corneal thickness progression in OD and OS

It is shown (Figure 89) that moving peripherally from the 4 mm zone the thickness progression graph does not run parallel to the normative data. The progression index is 0.9 for OD and 1.1 for OS. When screening for ectasia we would consider 1.2 as the borderline. Here the profile curves should be analyzed in combination with the progression indices and Scheimpflug images for a more accurate clinical decision.

The IOP, measured with the Goldmann tonometer (2 p.m.), was 22 and 24 mmHg in OD and OS, respectively. Interestingly, the averages of two ocular response analyser measurements of Goldmann-correlated IOP, corneal compensated IOP and hysteresis were 20.4, 17.8 and 13.2 mmHg in OD and 25.1, 20.5 and 14.1 mmHg in OS.

A HRT examination showed both optic nerves to be within normal limits (Figure 90). Pascal Dynamic Contour Tonometer IOP measurements were 18.4 and 19.6 mmHg in OD and OS, respectively.

This is a case of normal thick corneas of correspondingly high stiffness, leading to ocular hypertension. There is no indication for topical medications to decrease the IOP.

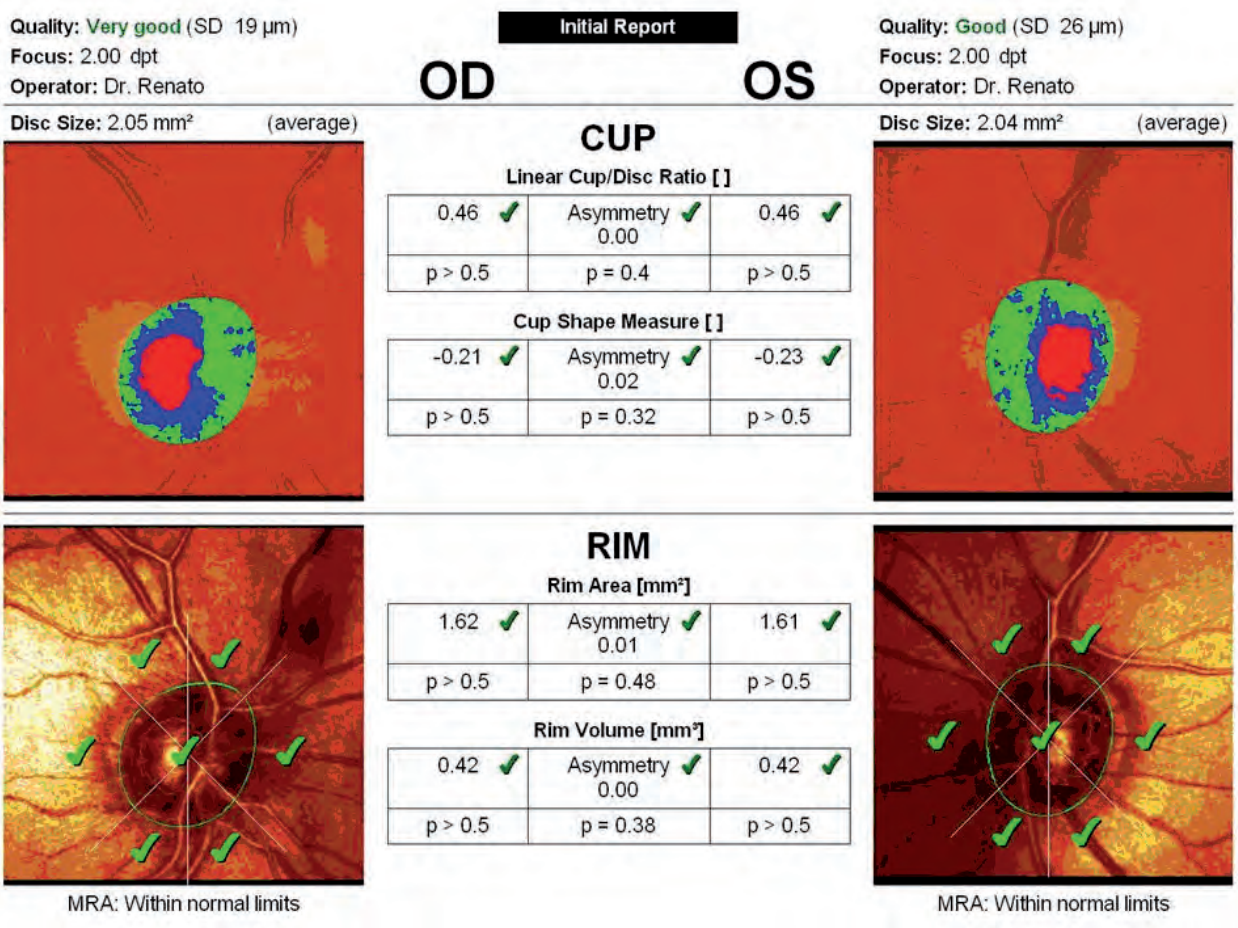

Figure 90: HRT single report with images of the optic nerve in OD and OS

11.4 Case 3: Early Fuchs' dystrophy with glaucoma by Prof. Renato Ambrósio Jr, Marcela Q. Salomão, MD

This 60-year-old patient was referred to us for a second opinion on his diagnosis of normal tension glaucoma, corneal disease and early cataract. The Scheimpflug images show higher scatter (less clarity) and a second peak at the level of Descemet's membrane and the endothelium (Camel's sign) in both eyes (Figure 91, Figure 92). This indicates a less transparent cornea. Both lenses can be seen to lack clarity, even with non-dilated pupils. In both eyes corneal thickness is slightly thicker than usual and the corneal thickness progression curve runs almost horizontally, indicating early oedema.

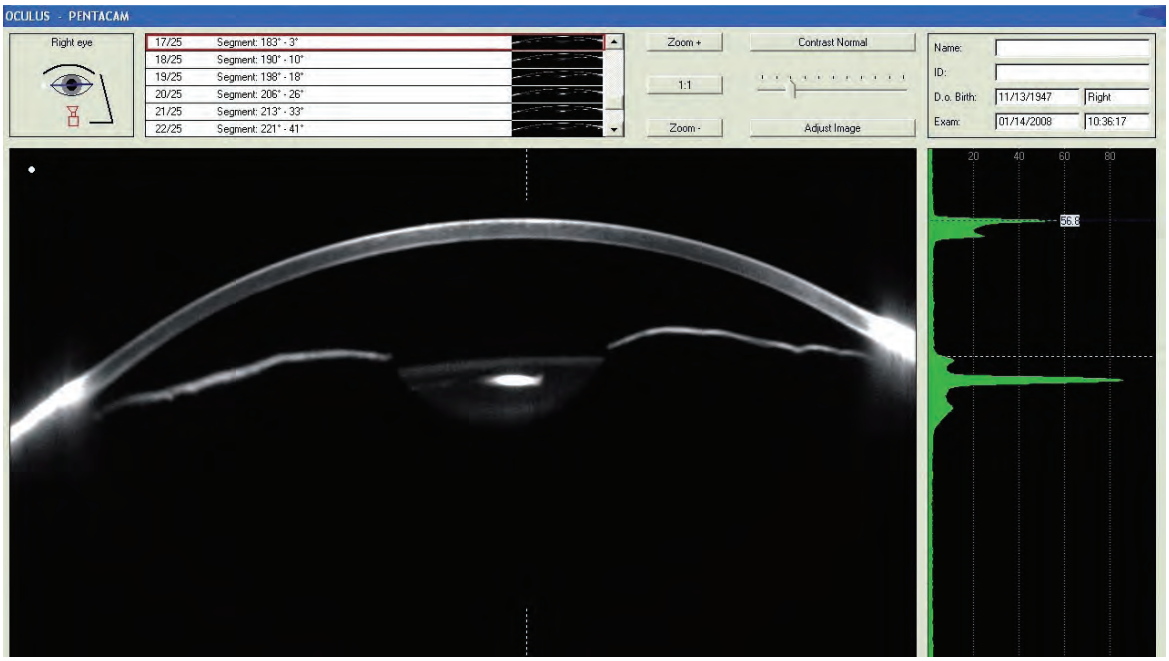

Figure 91: Scheimpflug Image showing a hazy cornea in OD

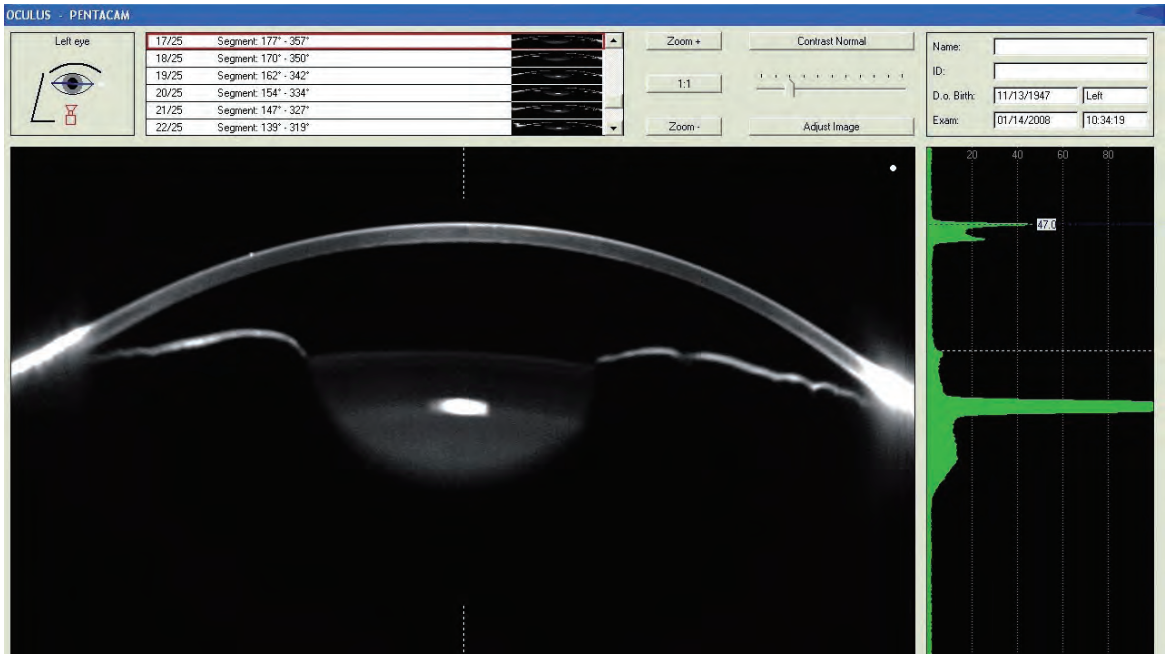

Figure 92: Scheimpflug Image showing a hazy cornea in OS

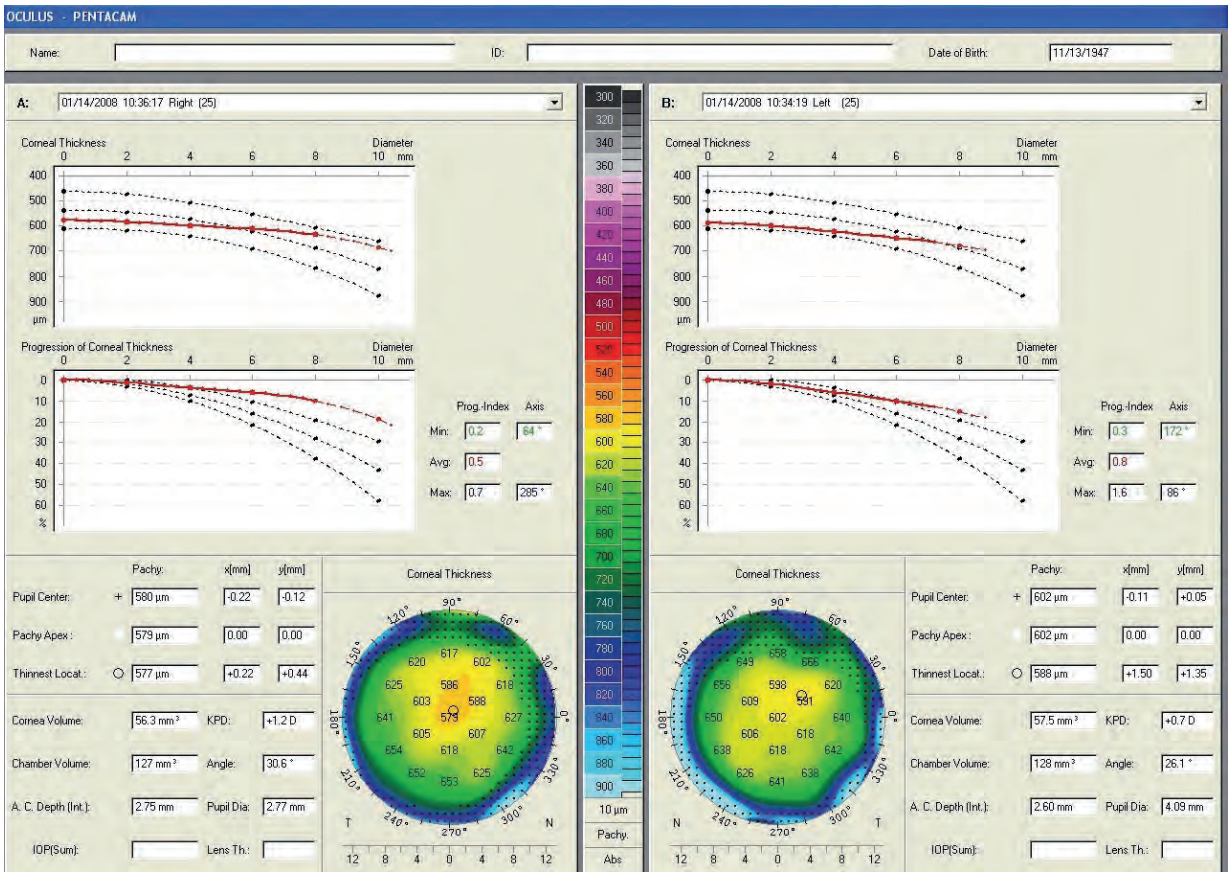

Figure 93: Show 2 Exams Pachymetric showing an abnormal cornea in OD and OS

The progression index was 0.5 in OD and 0.8 in OS, i.e. lower than normal in both eyes.

Goldmann IOP (10 a.m.) was 18 mmHg in both eyes. The averages of two ocular response analyzer measurements of Goldmann-correlated IOP, corneal compensated IOP and hysteresis were 19.6, 24.1 and 5.2 mmHg in OD and 16.7, 23.5 and 6.1 mmHg in OS. The optic nerve exam was difficult due to opacification of the ocular media (early cataract) in both eyes, but demonstrated cupping of 0.8 in both eyes.

HRT was not possible in OD due to impaired transparency of the ocular media (early cataract) and had a below average quality in OS (Figure 95).

Pascal Dynamic Contour Tonometer IOP measurements were not possible due to inadequate patient cooperation and irregular reflexes in both eyes. Computerized visual field tests were inconclusive, with diffuse vision loss in both eyes.

Examination with a specular microscope (BIO-OPTICS) demonstrated moderate guttae with loss of normal endothelial mosaic. Cell counts were less than 1.000 cells per mm² in both eyes. This is a case of moderate endothelial Fuchs' dystrophy and glaucoma with early cataract. These findings constitute a formal indication for topical glaucoma treatment.

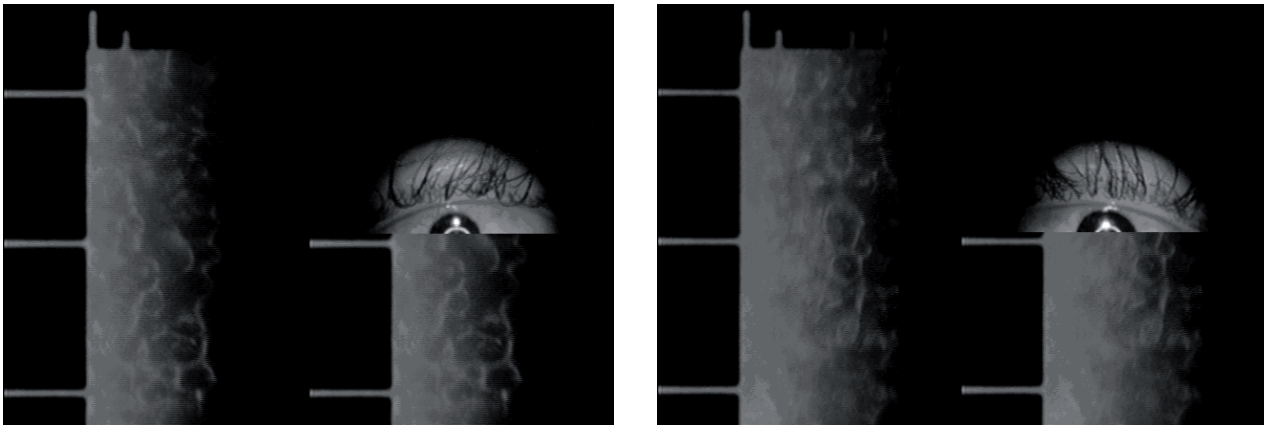

Figure 94: Specular microscopy in OD and OS

Completing the case report is the HRT examination displayed below. The optic nerve is damaged, and the rim configuration is abnormal both in the image and according to Moorefield's classification. This patient has glaucoma as well.

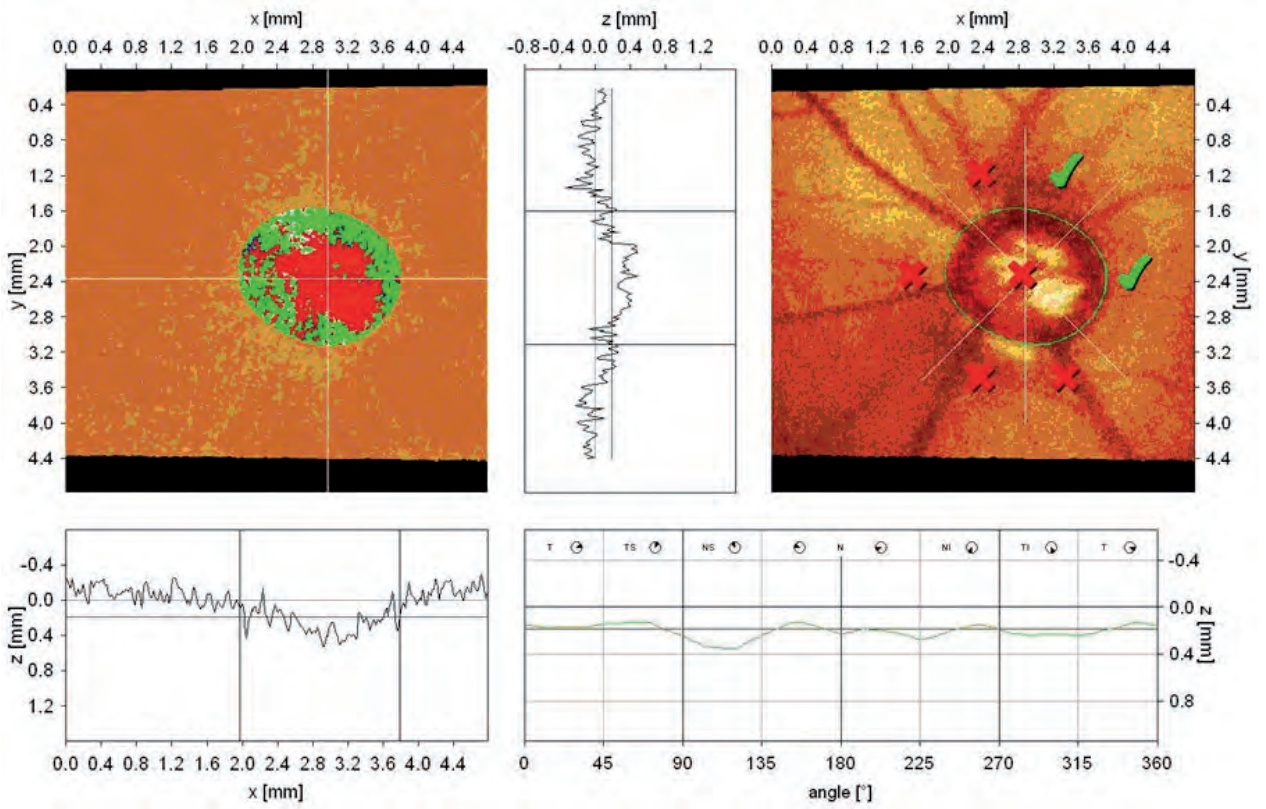

Figure 95: HRT single initial report showing a rim configuration out of normal limits that is indicative of a diagnosis of glaucoma

11.5 Screening parameters by Prof. Renato Ambrósio Jr

From my experience the following parameters can be used for screening corneal thickness profiles. It is very important to look out for blinking or significant fixation loss during the scan and repeat the exam whenever necessary. These parameters can be used as a guideline, but the clinician should also consider other clinical parameters of the Pentacam® and clinical diagnostics.

Average pachymetry progression index

- 0.5 < average pachymetry progression index < 0.8: Fuchs' dystrophy or oedema
- 0.8 < average pachymetry progression index < 1.2: normal or ocular hypertension
- average pachymetry progression index > 1.2: ectasia

The shapes of the curves of the thickness profile and percentage of thickness increase give additional information:

- flat curve: may be a normal cornea, but watch out for endothelial disease Fuchs´ dystrophy or guttae
- steep curve: ectasia or ectasia susceptibility
- flattening in the periphery only: ocular hypertension

In this way the course of the CTSP and PIT curves and the average pachymetry progression index all provide additional information for making clinical decisions.

12 Belin/Ambrósio Enhanced Ectasia Display

12.1 Why elevation is displayed by Prof. Michael W. Belin

Before we can talk about how we display elevation tomographic data, we should take a step back and understand why I am a proponent of elevation based tomography. To do that we need to have an understanding of how elevation and curvature differ.

Using curvature to describe the cornea dates back to the early 1600s when father Christopher Scheiner observed how glass spheres of different radii produced reflected images of different sizes. He produced spheres of different curvature, simulating corneal parameters, and measured the cornea by matching the size of the image reflected by the cornea with that of the calibrated sphere. Late in the following century (1796), Ramsden introduced a measuring device that included both a magnification and a doubling mechanism enabling the examiner to match the corneal reflection to itself. This technique was popularized by Helmholtz in 1854, who coined the original term "ophthalmometer". Javal and Schiotz further improved on its design in 1881 and that instrument (Javal/Schiotz Ophthalmometer, (Figure 96) has remained essentially unchanged for over 130 years and is marketed today as the Haag-Streit ophthalmometer.

Figure 96: Javal/Shiotz Ophthalmometer

A variation of the ophthalmometer in which the doubling device was internalized and the image size fixed was called a keratometer and was further improved upon by Bausch and Lomb in 1932 to allow simultaneous measurement of both principal meridians. The term keratometer is technically a trade name for this specific device (Figure 97), but is the term most commonly used for the generic technique of corneal measurement. Currently this is the most commonly used device for measuring simple corneal curvature.

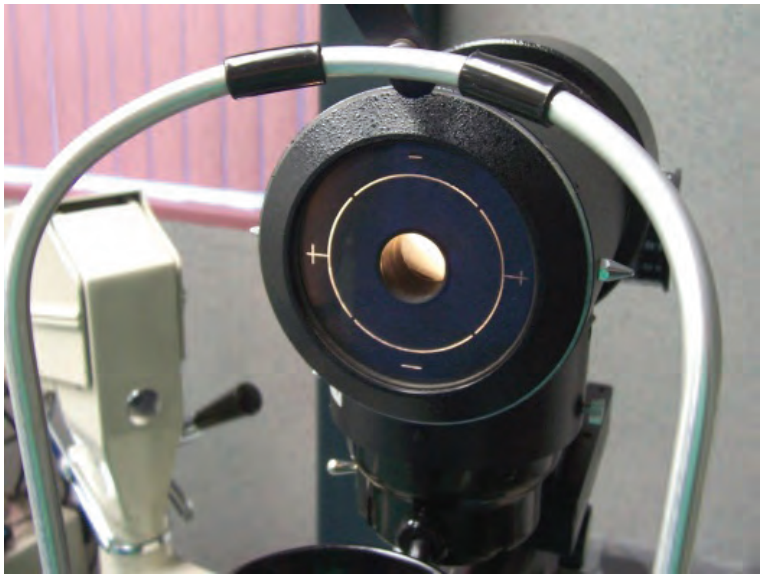

Figure 97: Keratometer

The modern keratometers in use today are very similar to those used over a century ago and similar inherent limitations apply. The accuracy of the keratometer is conditional on the uniformity of the central corneal curvature over the area measured. The formula used by the keratometer assumes that the cornea has a spherical or cylindrical surface with a single radius of curvature in each meridian and a major and minor axis that are orthogonal. Additionally, keratometry provides no information about areas central or peripheral to the points measured; it is based only on four localized data points within the central 3mm of the cornea. In most normal eyes the curvature over the visual axis is fairly uniform, and this simple measurement is sufficiently descriptive. This explains why most surgeons still utilize keratometry data for their standard IOL computation formulas.

The need to evaluate more of the corneal surface by reflection (keratoscopy) was first described in the 1820's by Cuignet, and the first keratoscope was presented by Goode in 1847. While keratometry was able to measure only a small portion of the cornea, keratoscopy was able to provide a qualitative picture of approximately 50% of the cornea. Antonio Placido, however, who is often credited with this technique, was the first to photograph these corneal reflections. Placido used a series of illuminated concentric black and white rings as a target in the 1880's. This device was unique because it had a viewing tube in the center that was used for alignment. Collimating keratoscopes, which used the Placido disk in a more "cone shaped" fashion, were used in an attempt to increase corneal coverage. Physical limitations (nose and brow) and optical limitations (inability to reflect light from the peripheral cornea back to the central camera) still limit the scope of these devices to approximately 60% corneal coverage.

While keratoscopy provided qualitative information, it was the union of rapid computer analysis and digital video image processing by Klyce in 1984 that transformed the gross examination of the cornea into a refined quantitative measurement. The first color coded map of corneal curvature was published in 1987 and led to multiple commercially available computerized videokeratoscopes. These are capable of digitizing information from a collimating keratoscope (Figure 98) to produce detailed color-coded maps depicting corneal curvature.

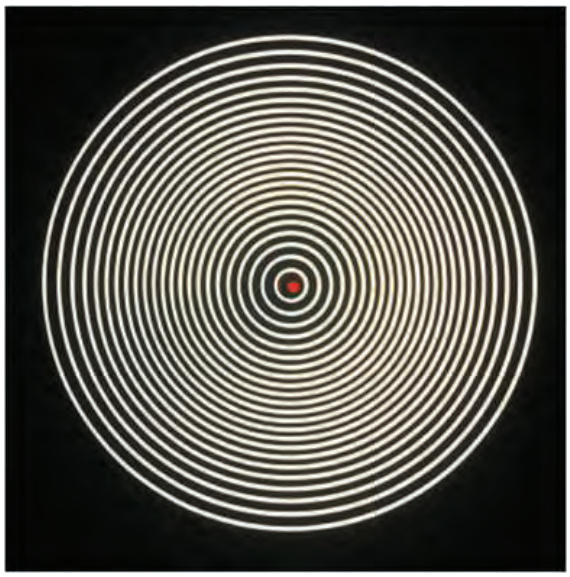

Figure 98: Keratoscope

Computerized videokeratoscopes provided a wealth of new information but still suffered from the same limitations of the century-old earlier techniques. Some of these limitations are related to the physical limits of reflective technology (permitting examination only of the anterior surface), and others are related to curvature measurements regardless of the technology used to produce them. These limitations were less important when most of our work was limited to normal spherical andcylindrical optics or gross corneal abnormalities (visually significant keratoconus). It was not until we began altering "normal eyes" (i.e. by refractive surgery) or needed to screen for pathology before visual loss occurred (e.g. ectatic disease) that the limitations of keratometry and curvature measurements became both apparent and significant. It is important that we understand how curvature and elevation measurement differ.

There is a common misunderstanding in the assumption that curvature maps reflect the shape of the cornea. Curvature, regardless of how it is generated, does not convey shape information. This is analogous to the difference between the power of a spectacle lens and its shape (curvature is very similar to power in the paraxial region). Asked to measure a spectacle lens, most ophthalmologists would place the lens in a lensometer and give you a power reading. The power of the lens may tell you how the lens will perform optically but conveys nothing about its rather shape, as multiple lenses of different shapes can have the same optical power (Figure 99).

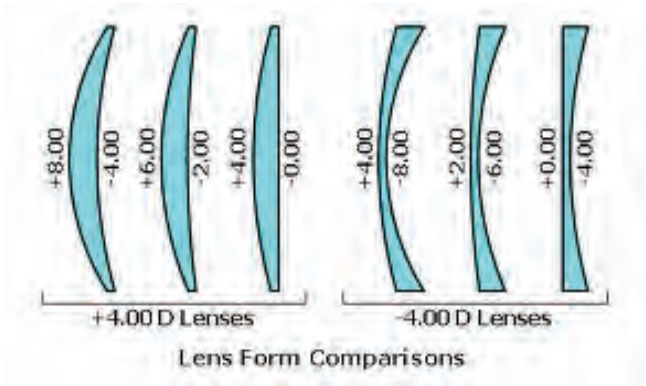

Figure 99: Lens form comparisons

Elevation is more analogous to using a Geneva lens clock and a caliper. With these, both anterior and posterior surfaces can be measured as well as lens thickness. Knowing both surfaces and lens thickness would allow one to reconstruct an identical lens. Knowing the distinct shape of the lens would also allow you to secondarily compute lens power.

The Pentacam® uses a technique of optical cross-sectioning to identify the anterior and posterior corneal surface, the anterior iris, and the anterior and posterior surface of the lens (Figure 100). By measuring these surfaces and their relative position elevation maps of the anterior and posterior cornea can be produced as well as a full corneal thickness map (additionally lens measurements, but these will not be discussed here).

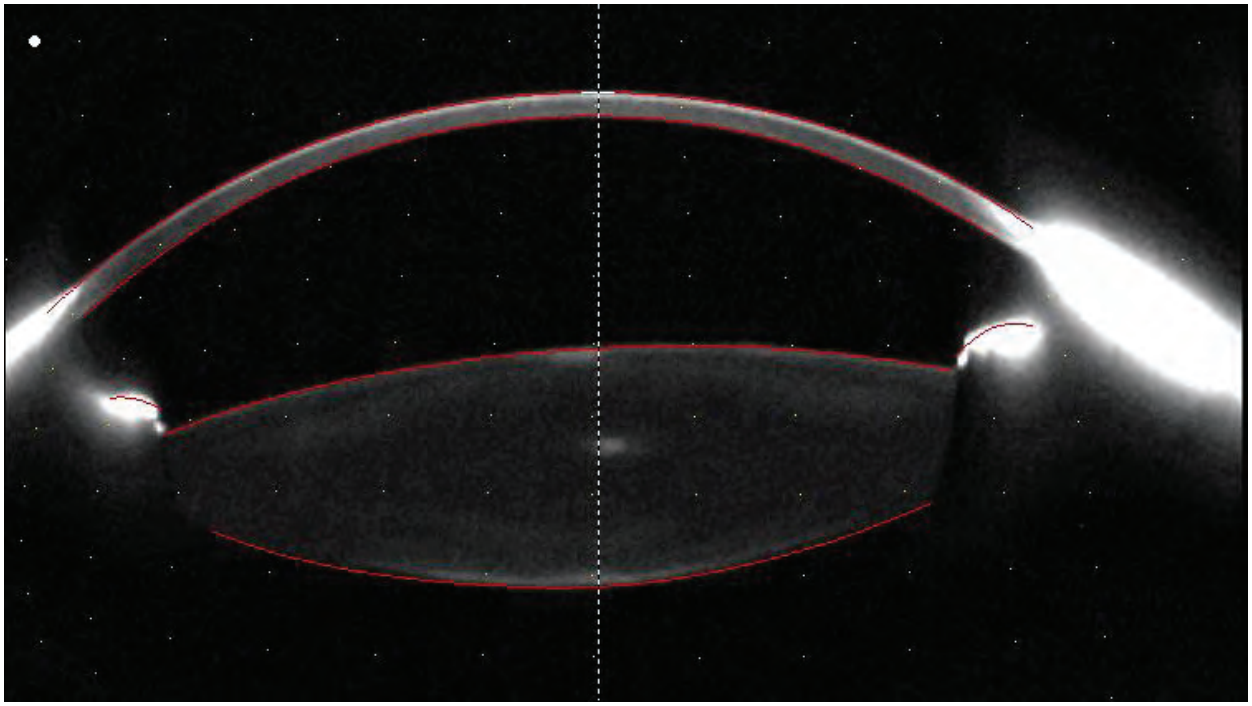

Figure 100: Scheimpflug image

Corneal thickness maps are easy to comprehend. Corneal thickness is an absolute measurement representing the distance between the anterior and posterior surface. Corneal thickness is reference independent. Elevation is different. Elevation is measured by locating points in space and is displayed relative to a reference surface. Raw elevation data is displayed (measured) against a planar reference surface. This represents the "raw" elevation data (Figure 101).

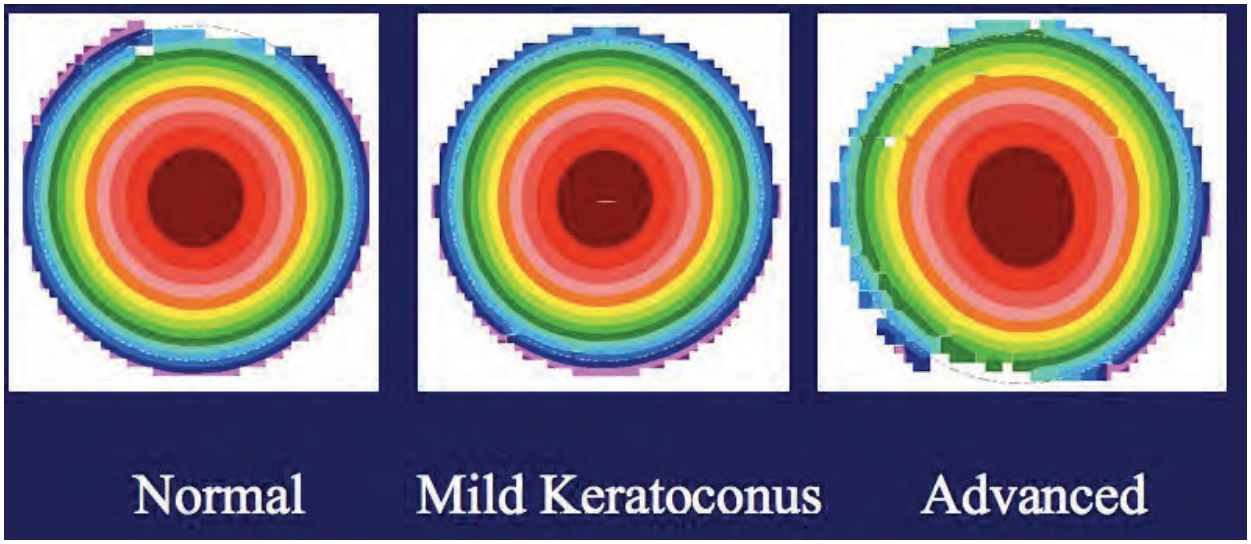

Figure 101: Raw elevation data

The problem with raw elevation data is that it lacks sufficient surface variation for the observer to easily separate normal eyes from abnormal. In order to make elevation qualitatively useful, we need to display the data in a more clinically relevant manner. To do this we typically display the elevation data against a non-planar reference surface. It needs to be understood that the reference surface, while affecting the qualitative appearance of the maps, does nothing to alter the quantitative accuracy. The reference surface alters the appearance, but not the accuracy, sensitivity or specificity (for the computer). The reference surface is chosen to allow us to make a clinically useful and rapid visual inspection.

The most commonly used reference surface is a best-fit sphere (BFS). Other surfaces can be chosen (e.g. best fit ellipse (BFE), best fit toric ellipse (BFTE), best fit toric ellipse fixed (BFTEF)), and while some of these surfaces may have some utility, they lack the intuitive ease of visual inspection of a BFS. Figure 102, depicts an early cone using a BFS (upper left), a BFE (upper right), a BFTEF (lower left) and a BFTE (lower right). The cone is easily identified as a positive island of elevation using the BFS, but is almost completely masked by the BFE and BFTE and, to a lesser degree, in the BFTEF.

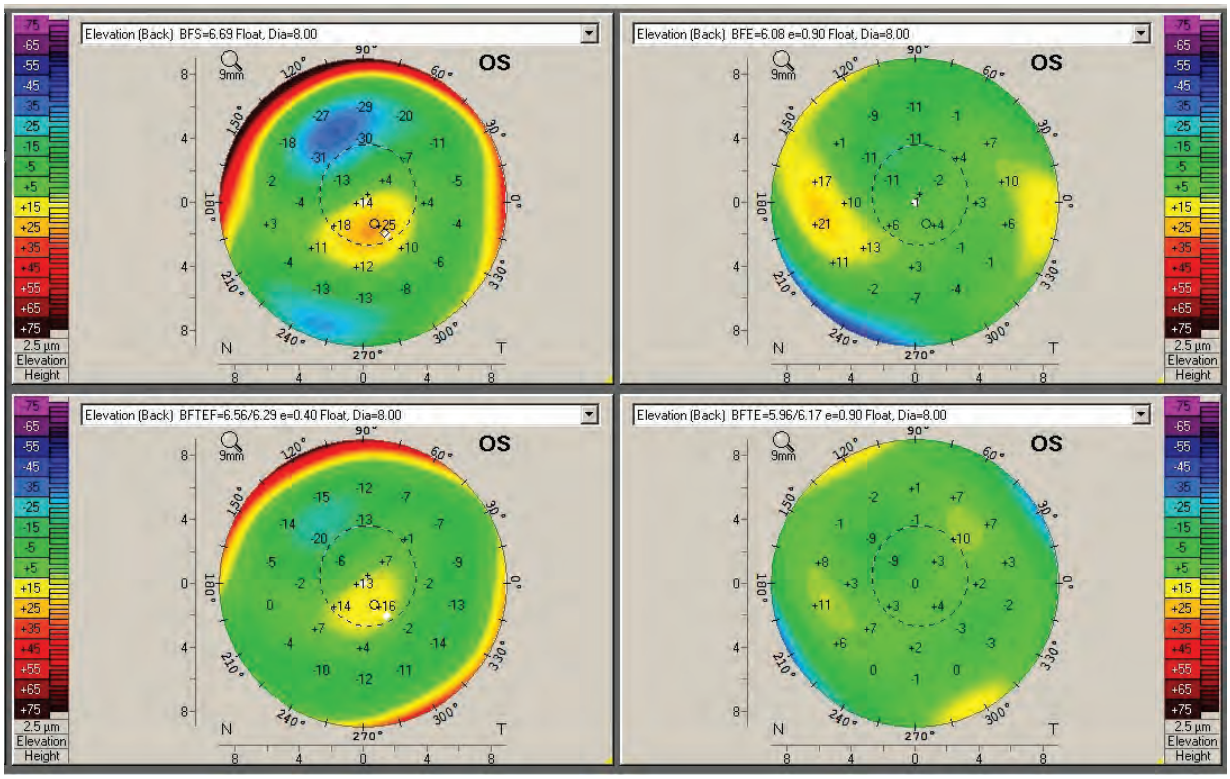

Figure 102: Eelevation maps based on different reference surfaces: BFS, BFE, BFTE, BFTEF

The BFS provides the most clinically useful qualitative maps and is recommended for refractive screening, as conditions such as astigmatism and ectatic change are easily identified with it.

While the BFS is the most clinically useful reference shape, it is important to realize that the normal cornea is aspherical and the BFS will vary depending on how much of the cornea is used to compute it. Since the normal cornea is steeper centrally and flatter in the periphery, the BFS will increase in radius of curvature (flatten) as the corneal area used for its computation is enlargened. Changing the reference surface will change the qualitative appearance of the maps. A larger area will cause the reference surface to be flatter and will accentuate the normal asphericity of the cornea, while a smaller area will cause the reference surface to be steeper and will mask the normal asphericity (Figure 103).

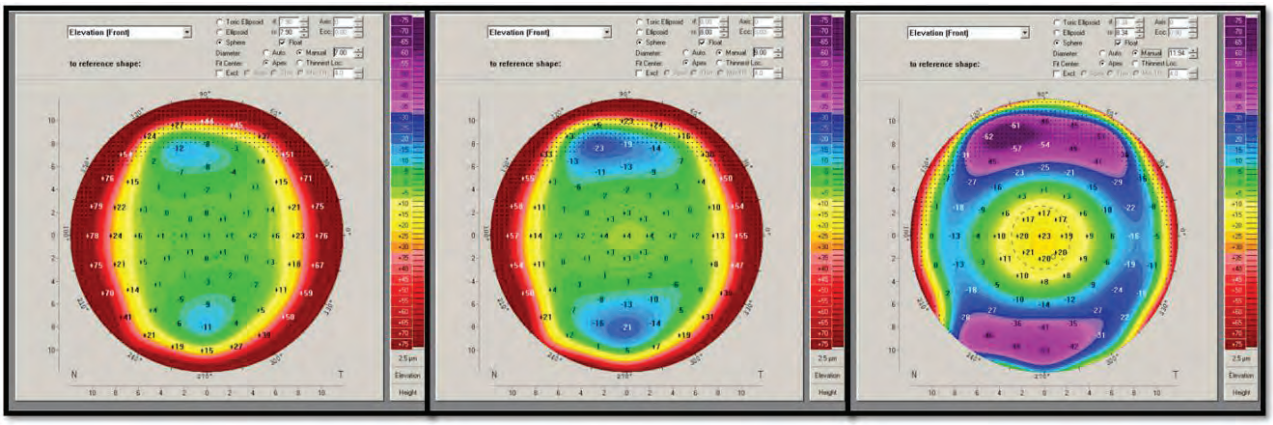

Figure 103: Elevation maps based on different diameters

Since the goal of refractive screening is to allow the physician to easily separate normal from abnormal, it works out that a BFS set at the 8.0 mm optical zone is optimal. A BFS computed from the central 8.0 mm will mask (i.e. normalize) the normal asphericity and allow easy detection of pathologic ectatic change. An 8.0 mm optical zone also provides a sufficient number of data points, while still being in a range where most exams will not include any extrapolated data. For almost all clinical uses we recommend setting the reference surface to a fixed best fit sphere computed from the central 8.0 mm optical zone (setting Manual= 8.0 mm). Fixing the area used to compute the reference surface is also necessary to allow comparisons over time.

When using a BFS patterns such as astigmatism (Figure 104) and keratoconus (Figure 105) are easily identified. An astigmatic pattern will have the flat meridian raised above the BFS and the steep meridian below. The magnitude of the elevation change will increase with increasing distance from the apex and will increase with greater degrees of astigmatism.

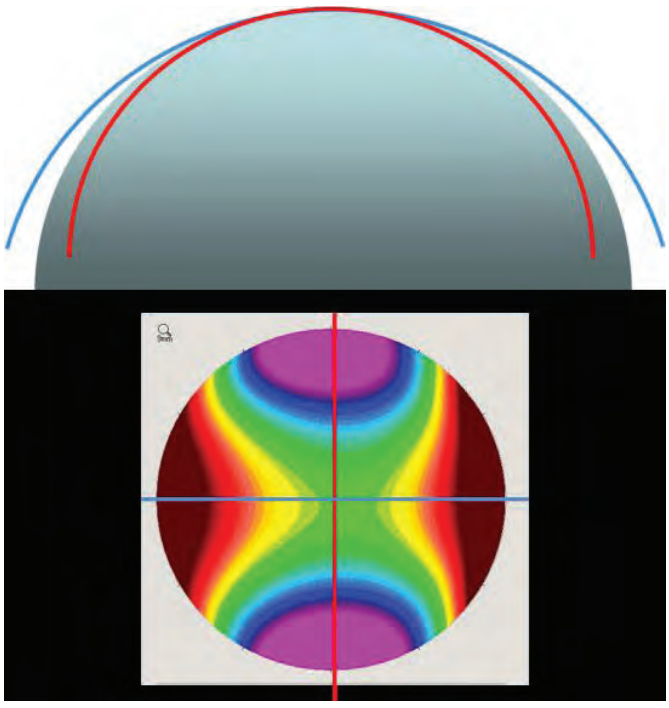

Figure 104: BFS-based elevation map of an astigmatic eye

Keratoconus will show a positive island of elevation, as the conical protrusion is above the BFS. The location of the island and its magnitude will correspond to the location of the cone and the severity of the ectatic change.

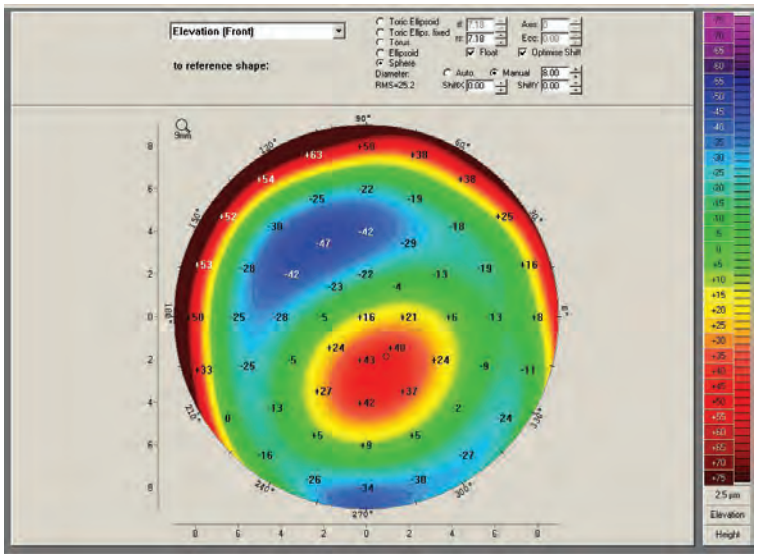

Figure 105: Elevation map of a keratoconic cornea

Most patients with keratoconus have in addition to a conical cornea a significant amount of astigmatism and one will typically see a positive island of elevation superimposed on an astigmatic pattern (Figure 106).

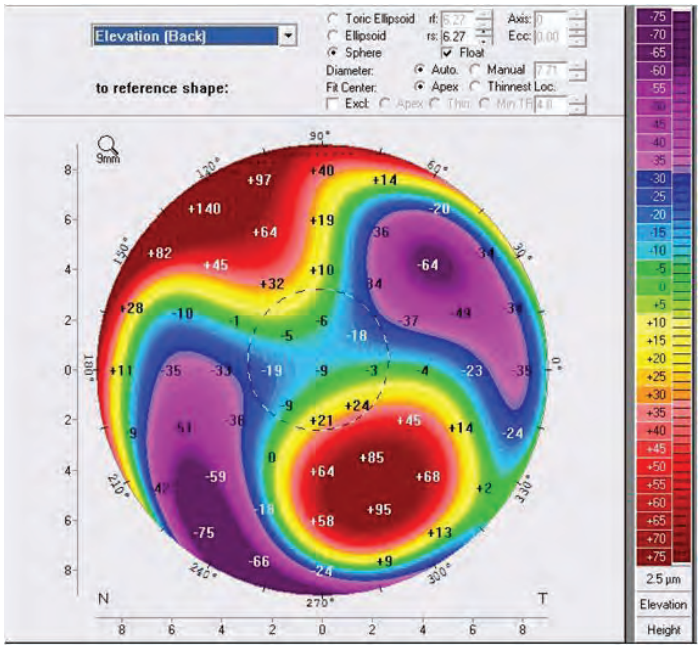

Figure 106: Elevation superimposed on an astigmatic pattern

While the BFS gives easily interpretable qualitative information, early or subtle ectatic change can at times be hard to visually identify. Part of the reason for this is that the BFS is influenced by the ectatic region causing the BFS to steepen and partially masking the cone. A modification of the BFS called the "enhanced reference surface" utilizes the same 8.0 mm central optical zone, but excludes a small portion of this data surrounding the TP on the cornea, effectively minimizing the cone's influence on the best-fit reference surface (Figure 107).

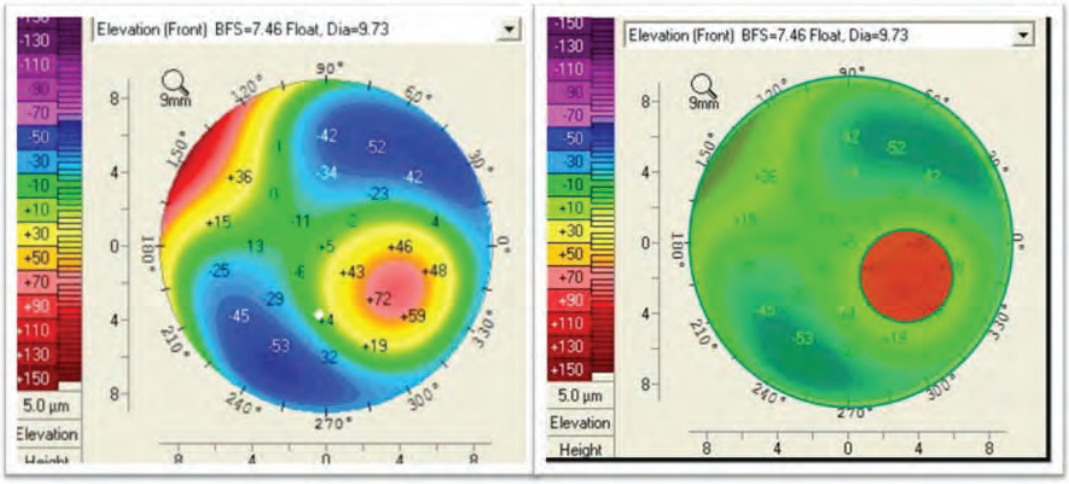

Figure 107: Elevation map of a keratoconic cornea using an enhanced reference shape with an exclusion zone to improve detectability

The enhanced reference surface more closely resembles the more normal periphery (Figure 108) and allows for easier identification of ectatic regions.

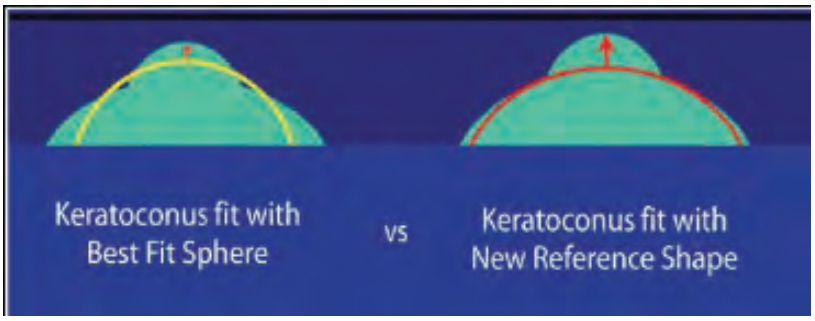

Figure 108: Enhanced reference surface

In Figure 109, the standard BFS is shown on the left, while the enhanced reference surface on the right accentuates the ectatic region, yielding an island of greater magnitude.

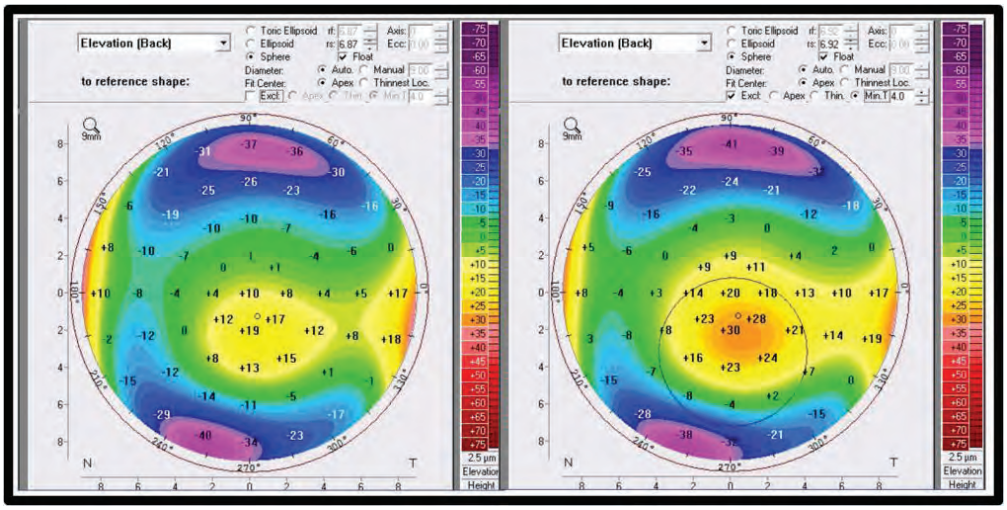

Figure 109: Standard BFS on the left, enhanced reference surface on the right

The enhanced reference surface is one component of the Belin/Ambrósio Enhanced Ectasia Display, a comprehensive tool for preoperative refractive surgery screening.

12.2 Simplifying preoperative keratoconus screening by Prof. Michael W. Belin, Prof. Renato Ambrósio Jr, Andreas Steinmüller, MSc

The original version of the Belin/Ambrósio Enhanced Ectasia Display changed the way we screened patients for sub-clinical ectatic disease. It was the first screening tool to fully exploit the benefits of Scheimpflug derived optical cross-sectioning tomography. It has been shown that anterior curvature and ultrasonic pachymetry, alone, do not provide enough information to detect early disease. The Belin/Ambrósio Enhanced Ectasia Display (BAD display) was designed to utilize the data supplied by a Pentacam® rotating Scheimpflug camera and provide a comprehensive keratoconus screening display. The display combines the anterior and posterior elevation and pachymetric data into one all-inclusive display giving the clinician a more complete overview of the corneal shape and allowing for quick and effective screening of refractive surgery patients. The combination of anterior and posterior elevation and complete pachymetric data gives the clinician a more complete view of the structure of the cornea and allows for earlier detection and more effective screening than was possible with previous systems.

The original display (Belin/Ambrósio Enhanced Ectasia Display – software release # 1-16b96) showed both anterior and posterior elevation data relative to a standard BFS calculated at a fixed optical zone of 8.0 mm. Fitting a BFS to the central 8.0 mm zone has been shown best for clinical interpretation and allows for the generation of standardized normal values. The original display also showed anterior and posterior elevation values relative to the 'enhanced reference surface' computed by determining the BFS from the central 8.0 mm zone after excluding all the data from a 3.5 mm optical zone centered on the TP of the cornea. In the case of keratoconus or ectasia, the cone will have the effect of steepening the BFS. This steepened BFS will actually minimise the elevation difference between the apex of the cone and the BFS. By eliminating the conical portion of the cornea from the BFS computation, the "enhanced reference surface" serves to further accentuate ectatic or conical protrusion, while having little if any effect on normal corneas. The Belin/Ambrósio Enhanced Ectasia Display then computes the change in elevation values going from the standard BFS and the enhanced BFS. This change (elevation change between the standard BFS and enhanced BFS) has been shown to be a key differentiator between normal and ectatic corneas.

The second component of the Belin/Ambrósio Enhanced Ectasia Display is a comprehensive pachymetric evaluation. Both pachymetric values at the apex and TP are displayed and the displacement of the TP from the corneal apex is calculated along with the direction of the displacement. The distance between the TP and the geometric central point is significantly higher in keratoconus. Graphical representations of the progressive thickening of the cornea from the TP to the periphery are depicted in the CTSP. The PIT refers to the percentage of increase in thickness from the TP to the periphery. The data from both graphs are calculated from the pachymetric values at 22 concentric rings centred on the TP. Corneas with ectatic disease (e.g. keratoconus, post LASIK ectasia) show a more rapid progression of thickening from the TP to the periphery. This increase follows a normal pattern and is a strong differentiator between normal and keratoconic corneas.
A more intuitive way of saying the same is that ectatic corneas thin more rapidly than normal eyes going from the periphery to the thinnest part of the cornea. The CTSP and PIT display provides the average progression derived from a normal population (centre line) and 95% confidence interval (upper and lower black lines) against the patient's own data shown in red. This allows the clinician to differentiate a normal thin cornea from one with early ectatic disease. The 'progression index' is calculated as the progression value at each meridian from the TP. The average of all meridians and the meridian with maximal and minimal progressions are displayed. These parameters allow for the differentiation of a normal thin cornea versus one with ectasia, as well as of a normal thick cornea versus one with early edema.

The combination of the pachymetric graphs and indices and elevation maps which utilize an enhanced reference sphere make possible an increased sensitivity and specificity in the screening of patients for ectatic disease. Each of these values (change in anterior elevation, change in posterior elevation, corneal thickness at the TP, TP displacement, and pachymetric progression) can be evaluated against a previously determined set of normal values to assist the physician in determining 'normal,' 'suspicious' and 'abnormal' corneas.

The second version of the Belin/Ambrósio Enhanced Ectasia Display (Release II) (Belin/Ambrósio Enhanced Ectasia Display II – software # 1-17b37) simplifies the physicians' evaluation and was updated in response to inquiries from Pentacam® users. The new display reports five differential parameters individually change in anterior elevation from standard to enhanced reference surface, change in posterior elevation, corneal thickness at the TP, TP displacement, and pachymetric progression) (Df (front), Db(back), Dp (pach progession), Dt (thinnest value), and Da (thinnest displacement)). Each of these values is shown on the bottom right of the display and is reported in numerical form giving the SD from the population mean for that individual parameter. These numbers are colour-coded to turn yellow when ≥1.6 SD from the mean and red when ≥ 2.6 SD from the mean and are white when < 1.6 SD. The final parameter "D" represents an overall reading of all five parameters. This is calculated by performing a regression analysis against a standard data base of normal and keratoconic corneas.

The major advance is that while an individual parameter(s) may fall outside the norm the final overall comprehensive reading may still be viewed as normal (Figure 110, Figure 111). Conversely, multiple yellow or suspicious parameters may be significant enough for the final reading D to be red or abnormal (Figure 112), while more advanced cases of keratoconus may show with multiple yellow and red parameters (Figure 113).

The Belin/Ambrósio Enhanced Ectasia Display is a valuable tool but is never a substitute for clinical judgment. Each surgeon should evaluate each component of the map in addition to the final overall reading. This information needs to be evaluated taking into account the patient's age, history, correction and residual bed thickness. It should be understood that the normal values are generated from a "normal" myopic population and that geographic and ethnic variations do exist. Additionally, hyperopic individuals have been observed to have greater variability, particularly on the posterior corneal surface.

Conclusion

The Belin/Ambrósio Enhanced Ectasia Display was the first comprehensive refractive surgical screening tool to be fully based on elevation tomography and to incorporate data from the posterior corneal surface and corneal thickness map. The second release (version II) takes the analysis one step further by normalising each parameter (allowing for an easier interpretation of relative risk) and provides a final overview reading ("D" value) of the entire map. It is hoped that this additional information will simplify the interpretation of the maps and provide greater specificity and sensitivity in detecting early ectatic disease.

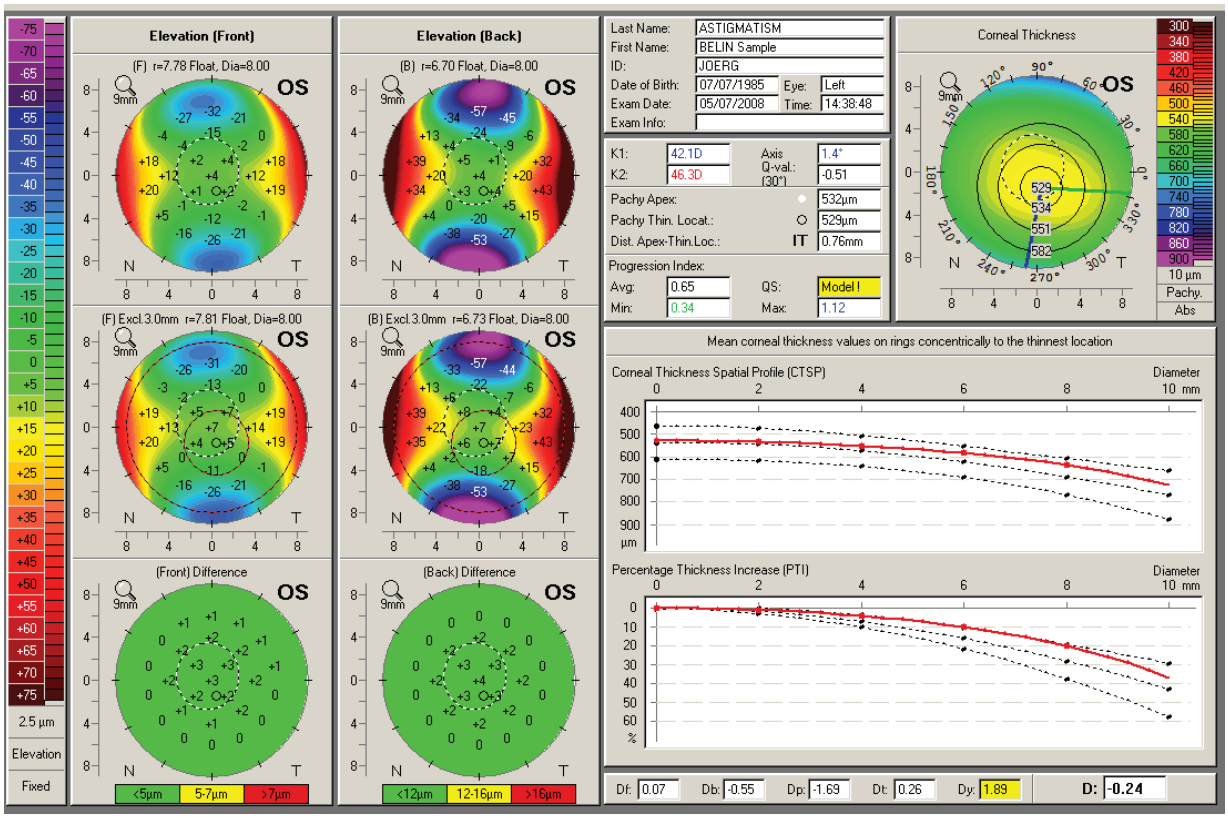

Figure 110: Belin/Ambrósio Enhanced Ectasia Display (version II) of a normal highly astigmatic eye

Both anterior and posterior elevations are normal and show a typical astigmatic pattern. The central cornea has a normal thickness at the apex of 532 µm but shows little progression towards the periphery causing the PIT tracing to be relatively flat (opposite of what you would see in ectasia). The TP is moderately displaced (Dy = 1.89 SD), but the overall reading "D" value is within the normal range.

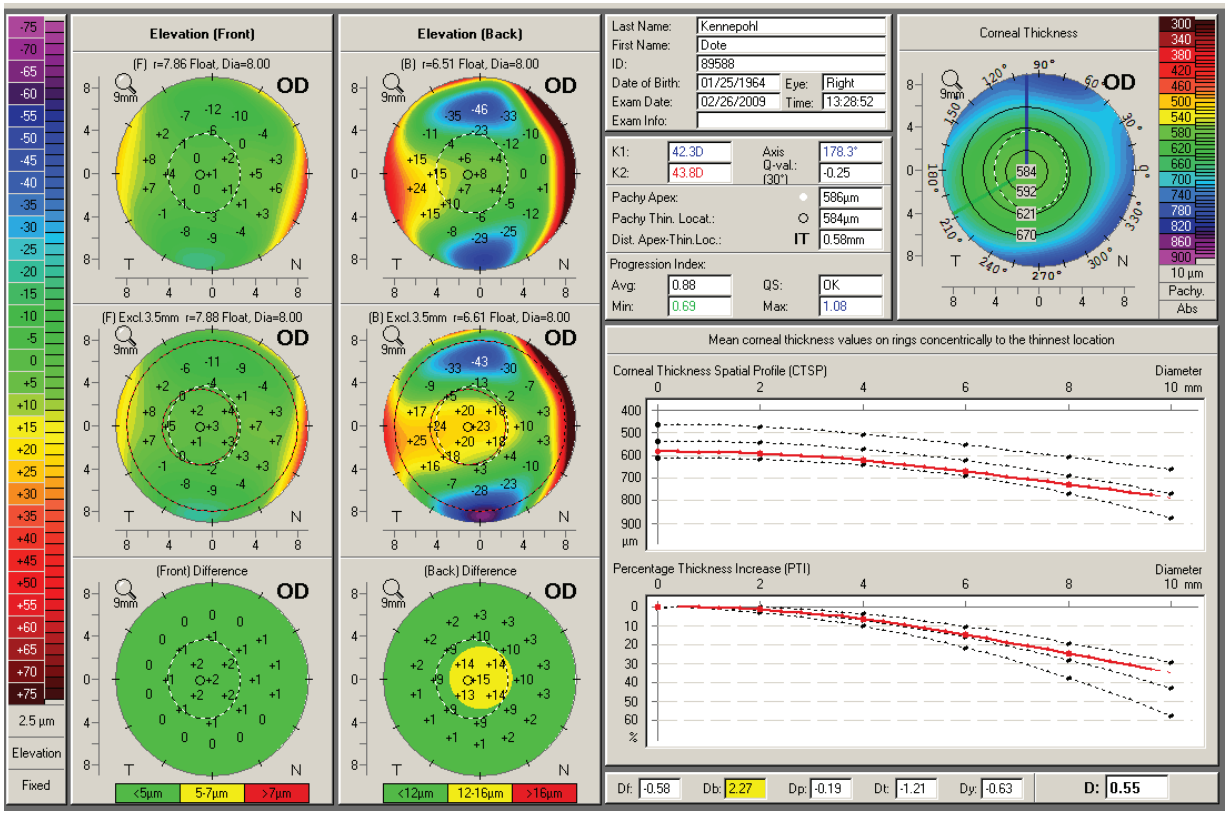

Figure 111: Belin/Ambrósio Enhanced Ectasia Display (version II) of a cornea with an isolated suspicious area on the posterior cornea

The anterior elevation shows a very low degree of astigmatism, and the pachymetric progression, thinnest value and TP displacement are all within normal limits. The posterior elevation change is further heightened by the enhanced reference surface, and the bottom display for the posterior elevation reveals a yellow zone. The Db is 2.27 SD from the mean which puts this in the yellow zone, but because this is an isolated finding the final overall reading "D" is still within normal range at 0.55 SD.

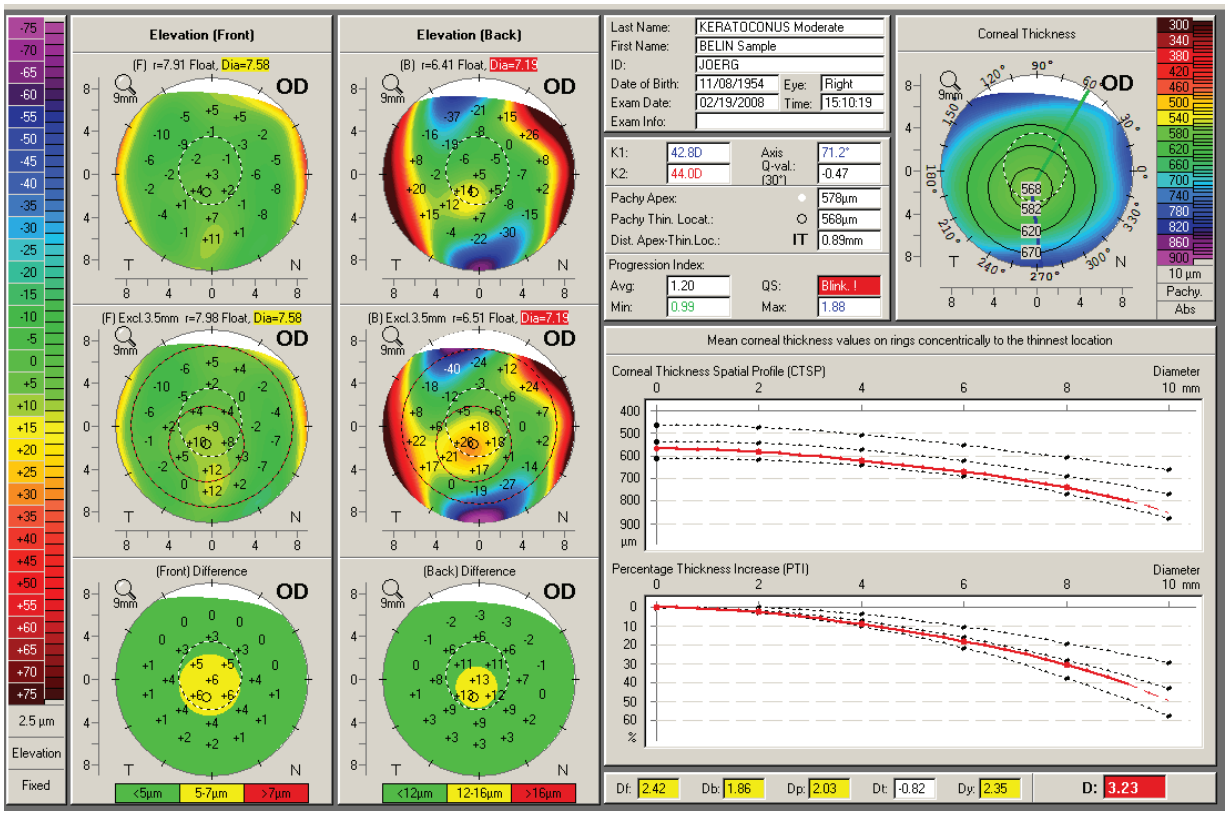

Figure 112: Interesting example of the value of the Belin/Ambrósio Enhanced Ectasia Display (version II) and the "D" values

This cornea has a number of variables that fall in the suspicious area. Both the anterior and posterior elevations show small central yellow zones and the pachymetric progression and TP displacement are also in the yellow zone. Only the thinnest value at 568 µm is normal. The combination of a number of suspicious values, however, is enough to put the overall reading "D" well outside of the normal range at 3.23 SD from the norm and it is therefore displayed in red. Additionally, this display warns the user that there is insufficient corneal coverage (the BFS on the anterior surface is boxed in yellow and the posterior surface in red) and the user should attempt a repeat image which would give a full 8.0 mm of analyzable data for the BFS computation.

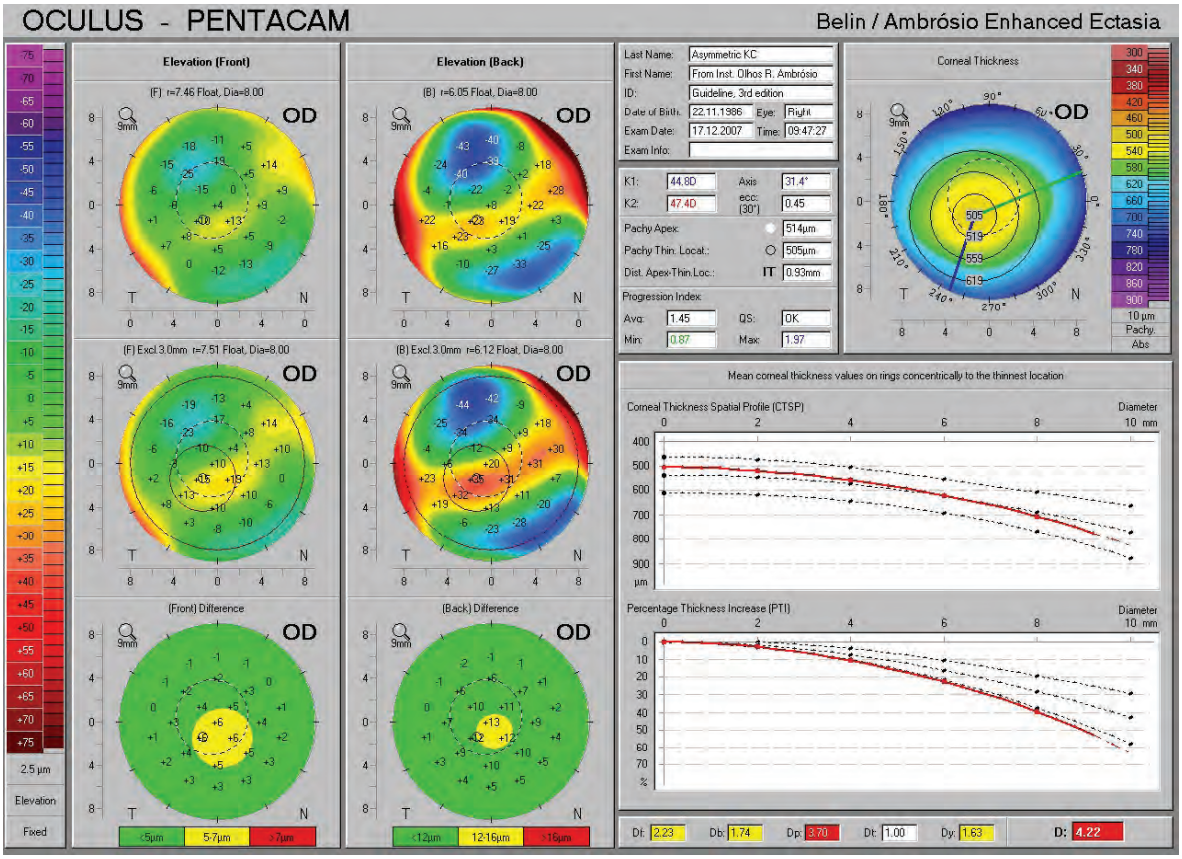

Figure 113: Belin/Ambrósio Enhanced Ectasia Display (version II) of a case diagnosed as "mild" keratoconus based only on the anterior cornea. A fuller picture is obtained by tomography

There are also changes on the posterior surface (both yellow), more dramatic changes in the pachymetric progression "Dp", which is red at 3.70 SD from the mean, and a mild displacement of the TP (yellow). The combination of these, however, is well outside the normal range with a final "D" value clearly in the red zone at 4.22 SD from the mean.

12.3 Interpretation of the Belin/Ambrósio Enhanced Ectasia Display

Standard elevation maps:

The left half of the Belin/Ambrósio Enhanced Ectasia Display the elevation data is shown please refer to Figure 113. The first two elevation maps (placed side by side) display the baseline relative elevation of the cornea of the best fit sph. This map is displayed for the front surface (left map) and back surface (right map) of the cornea. The radius of curvature of the BFS in millimeters and the diameter of the zone used to compute the BFS is noted above each map.

Exclusion elevation maps

Below the standard anterior and posterior elevation maps are the anterior and posterior exclusion maps. These are enhanced elevation maps, which display the same elevation data as the baseline maps, , but the method used to calculate the best fit sph (the reference surface) has been.

In these maps (both anterior and posterior) the BFS is calculated using all the raw elevation data located outside a 4 mm circle centered on the TP of the cornea. This area of excluded data is called the exclusion zone and the map is an exclusion map.

The location of the exclusion zone is indicated by a 4 mm red circle and cannot be modified. The newly calculated BFS is known as the enhanced BFS. An exclusion map may be significantly different from its corresponding baseline elevation map, or it may be very similar, depending on the relative impact of the 4 mm exclusion zone in the original (standard) BFS computation.

Difference elevation maps

The bottom 2 maps are difference maps, i.e. they show the relative change in elevation going from the standard (baseline) elevation map to the exclusion map. The bottom maps are based on a three-colour scale showing the amount of elevation change that occurs when moving between the baseline elevation map and the exclusion map:

- ➔ The green on the difference map represents a change in elevation (from the baseline to the exclusion map) of less than 6 µm on the front surface and 8 µm on the back surface of the cornea and are typically within the range seen in normal eyes.
- ➔ The yellow areas represent a change between 6 and 12 µm for the front surface and 8 to 20 µm for the back surface. These eyes fall in the suspicious or suspect zone.
- ➔ The red represents areas where the elevation difference between the 2 maps is 12 µm anteriorly or 20 µm posteriorly and are the magnitude typically seen in eyes with known keratoconus.

In Figure 114, the front surface does not show much change going from the baseline to the exclusion elevation map (the map is all green), while the posterior surface shows substantial change (red central area).

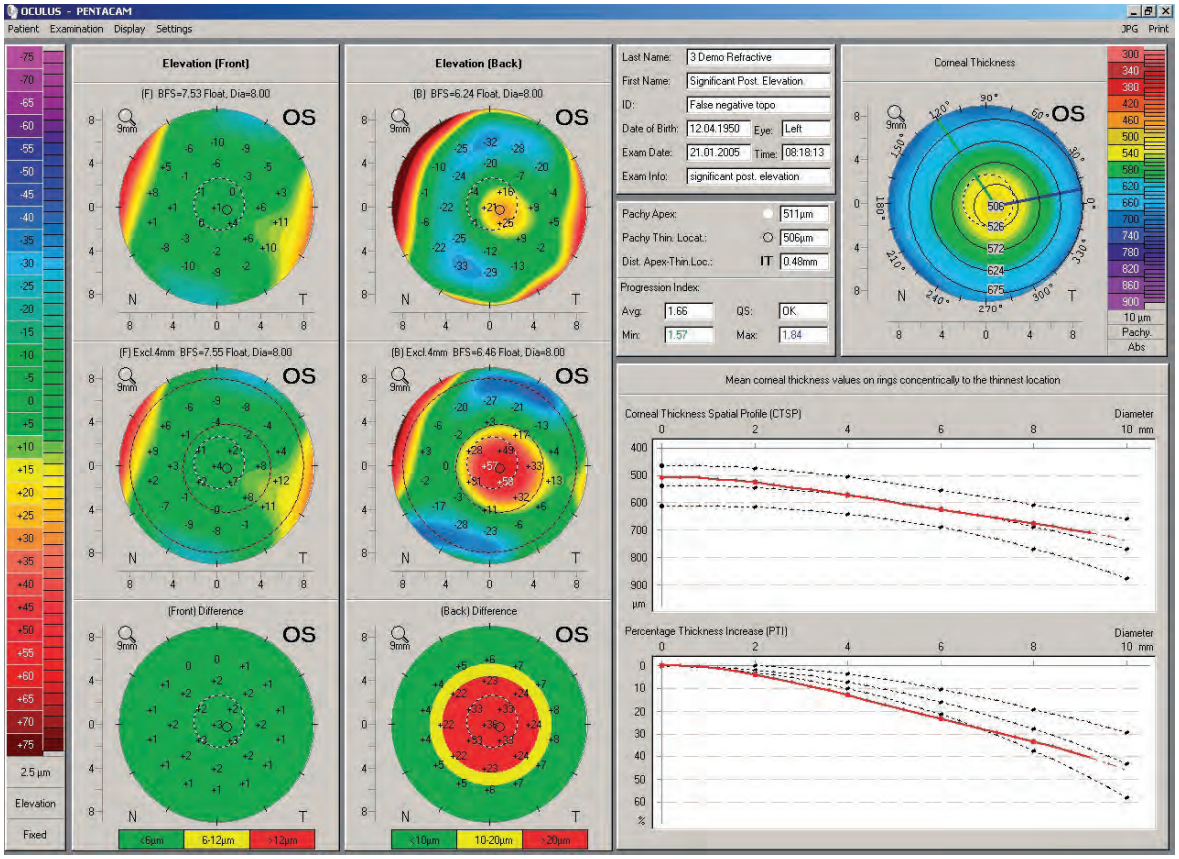

Figure 114: Belin/Ambrósio Enhanced Ectasia Display (version I) showing elevation data on the left and pachymetry data on the right)

12.4 Pachymetry evaluation

The Pentacam® provides a detailed corneal thickness distribution map with 3 µm accuracy and repeatability.

Display interpretation (pachymetry):

The pachymetric portion of the display includes the pachymetry map (corneal thickness), the two graphs showing the current of this patient thickness progression versus a normal population and the pachymetric indices. These identify the corneal thickness at the apex (the point on which the exam is centered), the TP and the location and distance of the TP from the apex.

The location of the TP relative to the apex is described as temporal (T), nasal (N), superior (S) and inferior (I) or intermediate (e.g. IT = inferior-temporal). The pachymetric difference between the TP and the apex is > 10 µm in only about 12% of normal corneas.

We have found a positive correlation (r2 = 0.61) between the distance and the pachymetric difference between the apex and the TP. The distance between the apex and the TP is significantly higher (1.52 ± 0.58 mm) in keratoconic eyes than it is in normals (0.9 ± 0.23 mm) ($p < 0.05$).

Along with the TP the pachymetric display also evaluates the thickness profile of the cornea. The basics and interpretation of the CTSP (Corneal Thickness Spatial Profile) and the PIT (Percentage of Increase in Thickness) are explained in **chapter 11**.

12.5 Ectasia susceptibility revealed in the Belin/Ambrósio Enhanced Ectasia Display by Prof. Michael W. Belin

The case was sent over the internet from a colleague and I advised not to proceed with LASIK and later this wise colleague said "if there are too many doubts, there is no doubt!"

So that, based on the evidences found in the tomography, we agreed to avoid corneal refractive surgery and to wait for evaluating stability before going for custom surface ablation. It is a 28-year-old female, candidate for LASIK

Refraction:

- OD: sph -3.00 cyl -1.25 A 105° VA 20/20
- OS: sph -3.00 cyl -1.00 A 70° VA 20/20
- Central corneal thickness (CCT) was 515 µm in OD and 501 µm in OS.

Interestingly, the case was also documented on a very good Placido topographer with a good artificial intelligence system, which classified it as "green" in both eyes, as shown in Figure 115 and Figure 116.

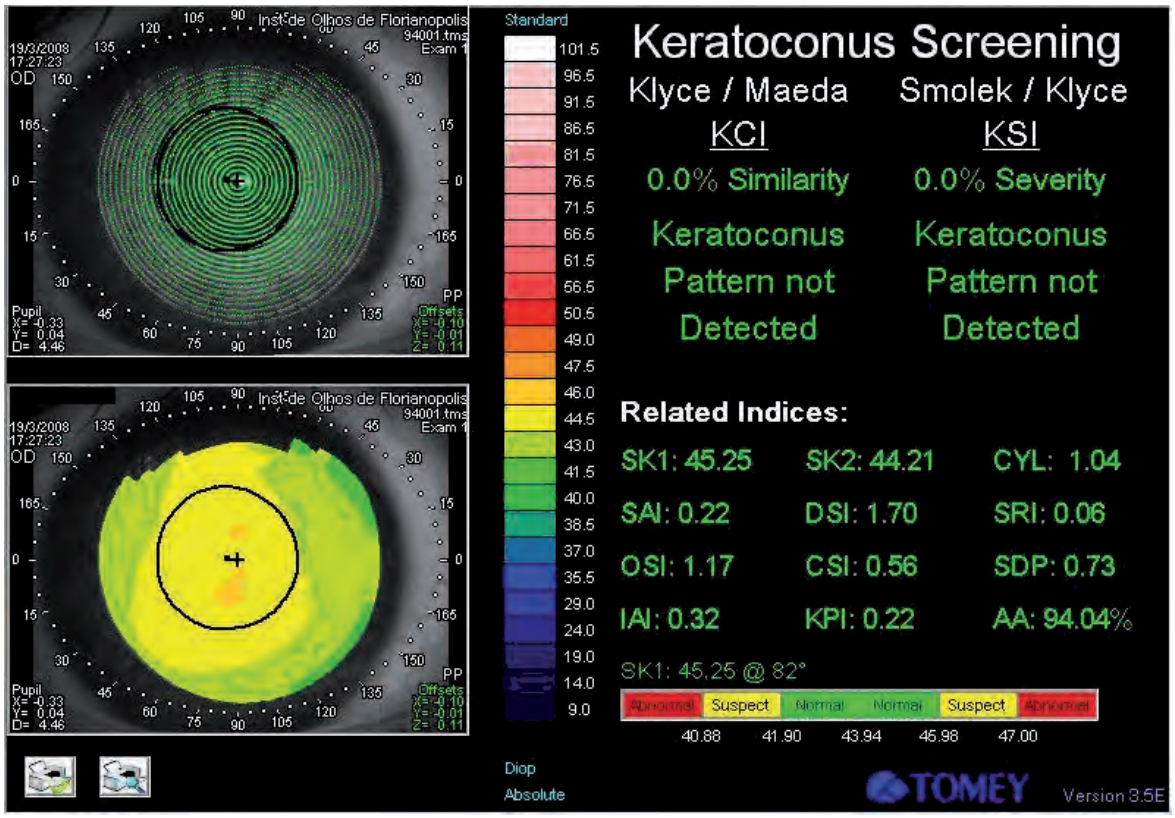

Figure 115: Placido topopraphy in OD showing no keratoconus

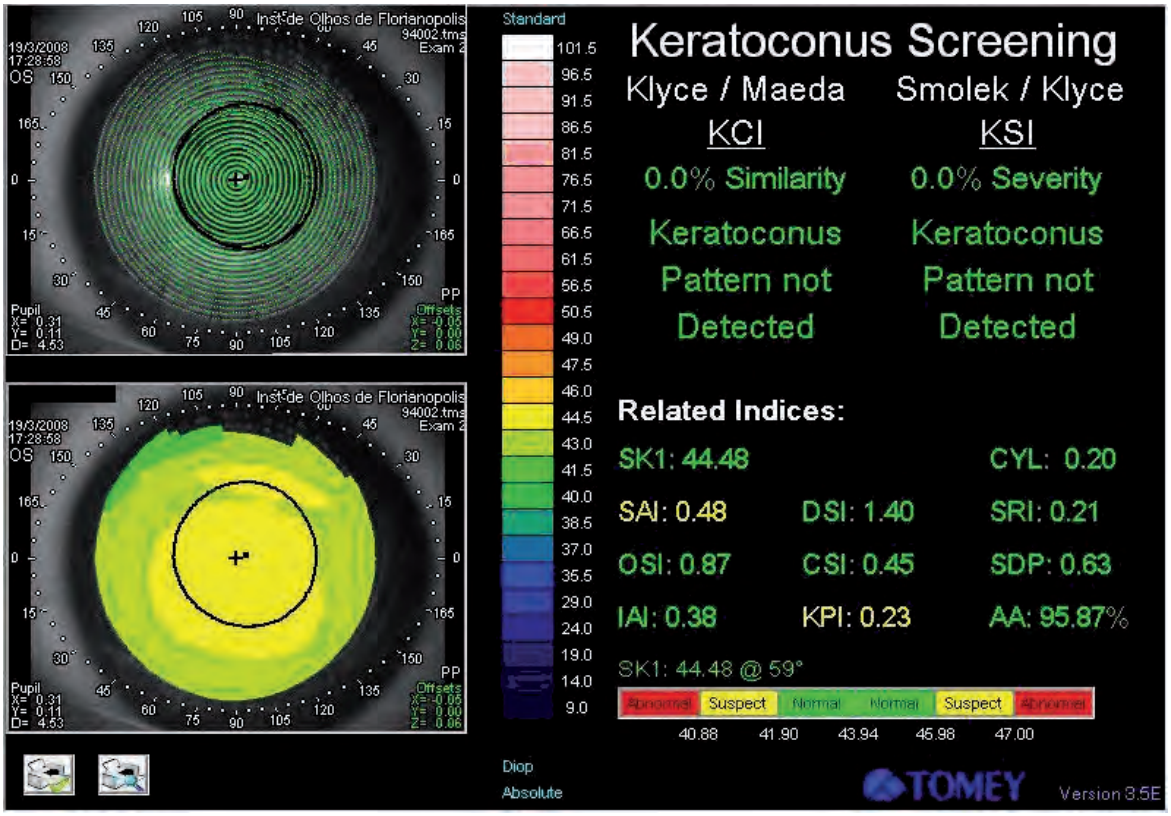

Figure 116: Placido topography in OS showing no keratoconus

Had it only been judged on the basis of Placido topography, CCT and the clinical parameters, the case would have qualified as a good candidate for LASIK. However, the Pentacam® exam revealed some telling characteristics of the cornea which in our view constituted a high risk case for ectasia. This case is a good example of ectasia susceptibility.

In the Belin/Ambrósio Enhanced Ectasia Display, shown in Figure 117, Figure 118, the distance of the TP from the apex is greater than 0.5 mm in both eyes. There is an "S" shape line in the thickness profile graphs in both eyes, more evident in the lower graph (PIT).

The enhanced elevation map of the back surface is also abnormal in both eyes.

This case illustrates the importance of not only relying on central corneal thickness and anterior curvature. The thinnest corneal reading in OS is below 500 µm, the pachymetric progression graphs are borderline in OD and abnormal in OS, and the enhanced elevation maps show changes (red) on the posterior surface, while the anterior surface appears normal. Patients with changes limited to the posterior surface and/or pachymetric progression may retain excellent visual acuity in spite of these abnormalities.

Discussing these findings with Dr. Cunha, I advised not to proceed with LASIK. Interestingly, she mentioned "If there are too many doubts, there is no doubt!".

In view of the tomographic evidence we agreed to refrain from corneal refractive surgery and to first evaluate topographic and refractive stability before going for custom surface ablation. This is a case of subclinical keratoconus.

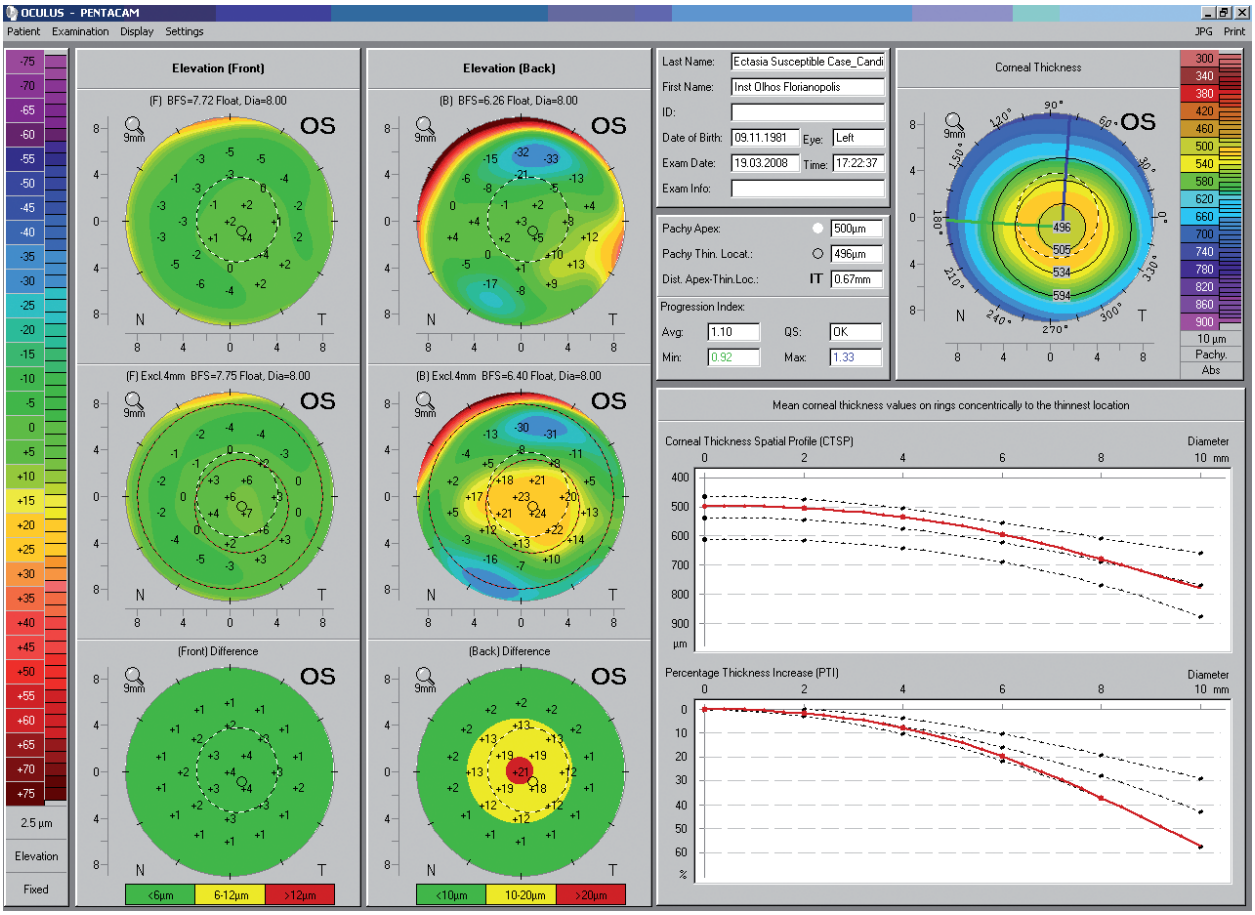

Figure 117: Belin/Ambrósio Enhanced Ectasia Display (version I) showing subclinical keratoconus in OS

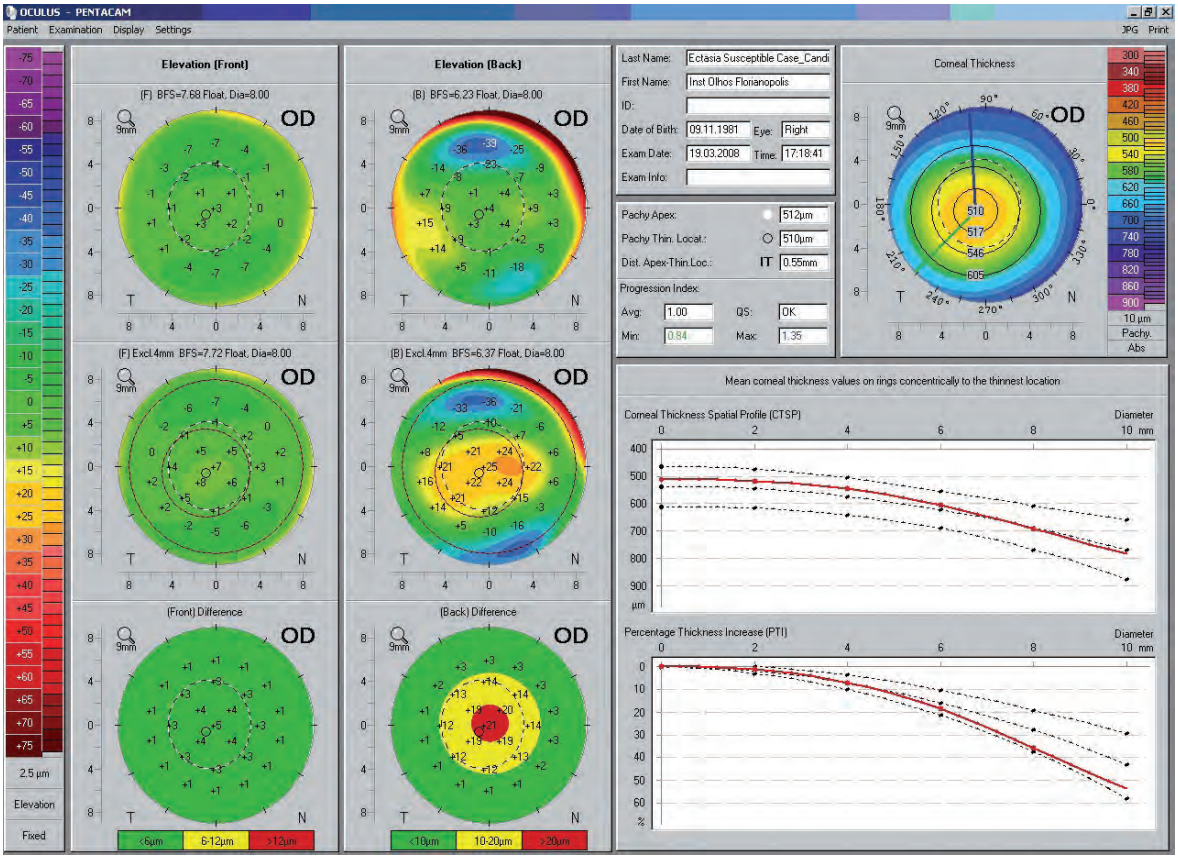

Figure 118: Belin/Ambrósio Enhanced Ectasia Display (version I) showing subclinical keratoconus in OD

12.6 Early ectasia with asymmetric keratoconus by Prof. Renato Ambrósio Jr, Fernando Faria-Correia, MD, Allan Luz, MD

A 20-year-old male patient with asymmetric keratoconus presented with BCVA 20/20 in OD and 20/15 in OS. The data in OS show a relatively normal topography pattern, while those in OD reveal mild keratoconus (Figure 119). Combining tomographic elevation and thickness data as it is done in the Belin/Ambrósio Enhanced Ectasia Display improves the ability to detect ectatic disease [7,8]. The Ambrósio relational thickness maximum (ARTmax) [9] was 259 µm in both eyes (Figure 120, Figure 121). The final deviation value D was 3.50 in OD and 1.77 in OS, which is consistent with the clinical diagnosis. This is an example of a very mild forme fruste keratoconus in OS with still relatively normal curvature topography and moderate tomographic changes [10,11,12,13].

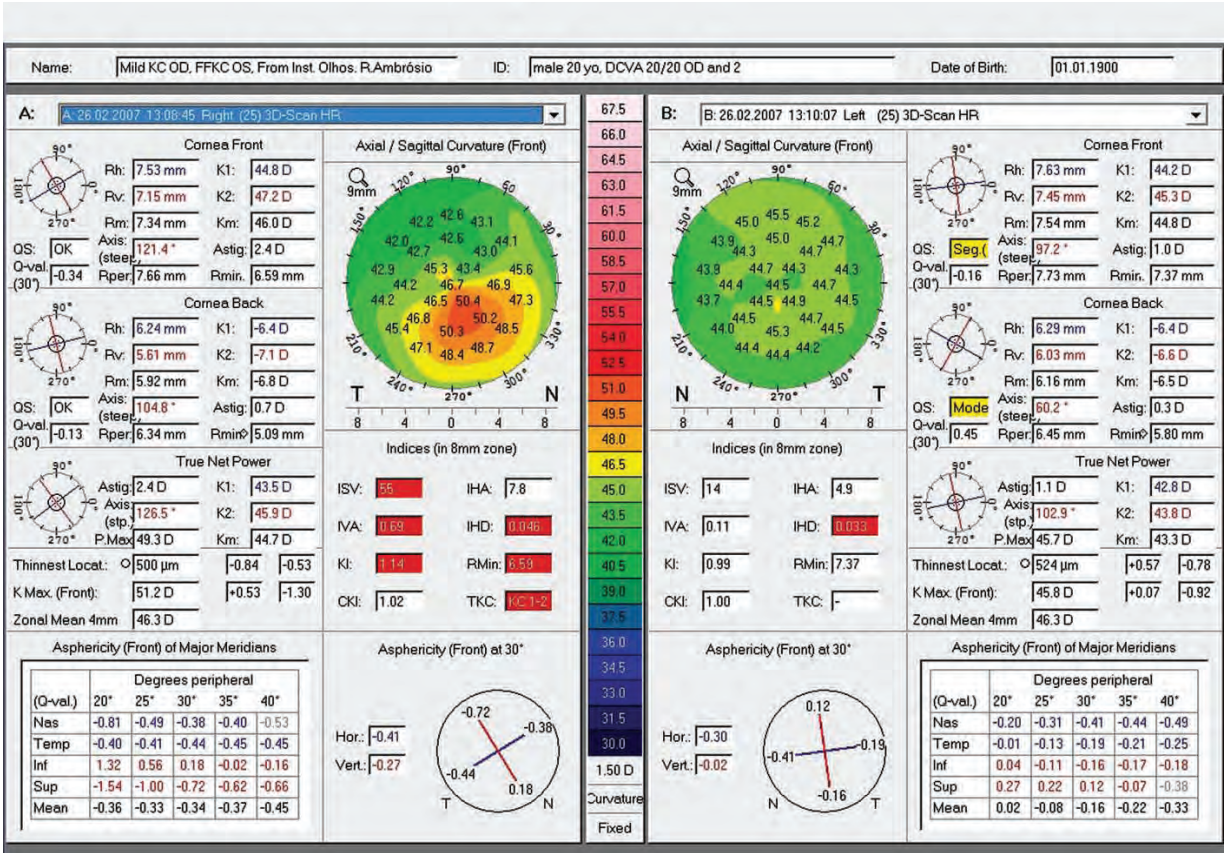

Figure 119: Show 2 Exams anterior curvature sagittal map showing mild keratoconus in OD and forme fruste keratoconus in OS

The Belin/Ambrósio Enhanced Ectasia Display shows abnormal values for posterior elevation and thickness distribution.

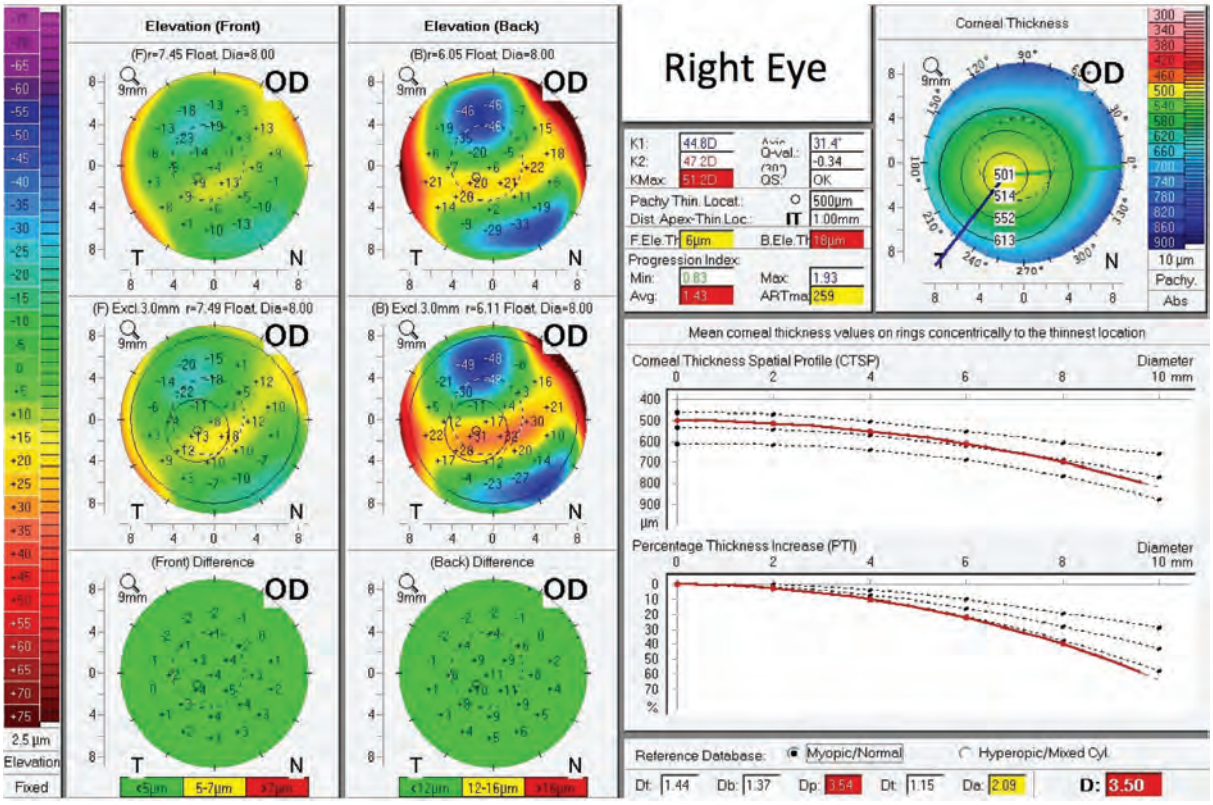

Figure 120: Belin/Ambrósio Enhanced Ectasia Display (version III) showing mild keratoconus in OD

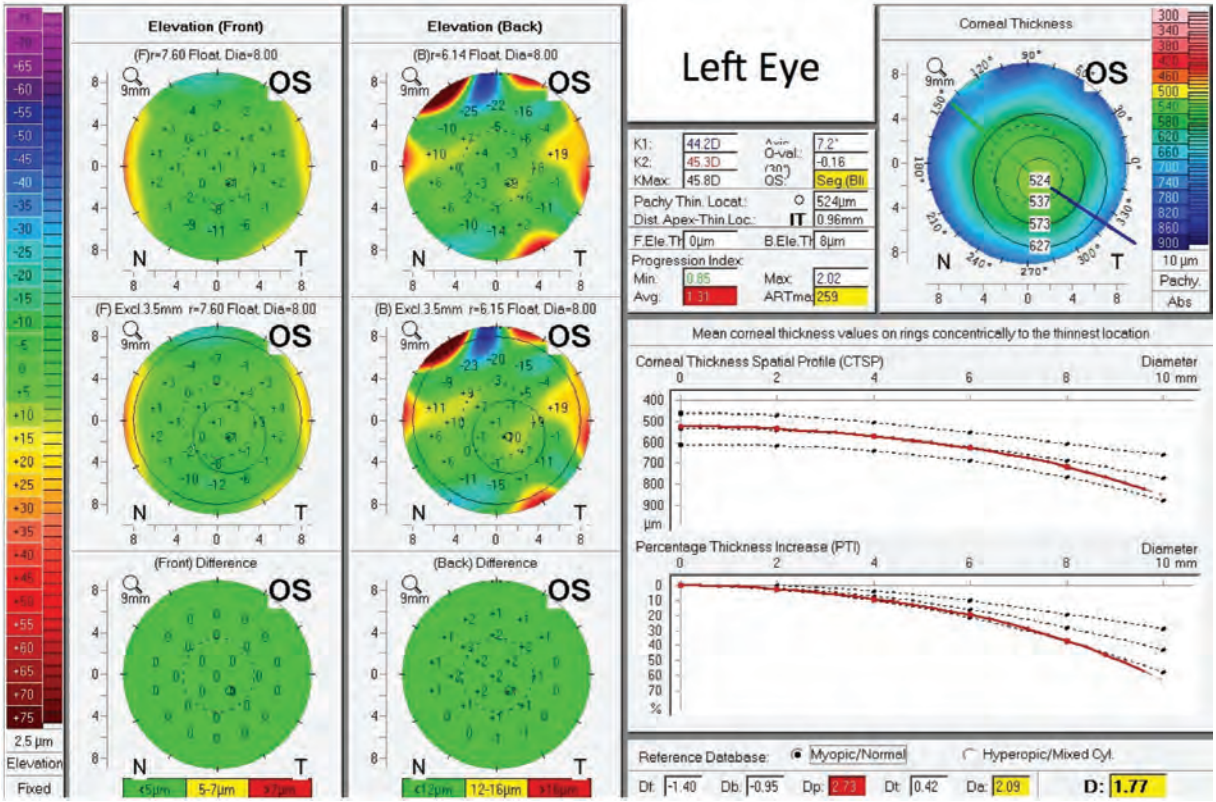

Figure 121: Belin/Ambrósio Enhanced Ectasia Display (version III) showing forme fruste keratoconus in OS

Refractive surgery screening commonly involves Placido disk based corneal topography and central corneal thickness measurement by ultrasound [14,15,16]. At the time of its introduction the ectasia risk score system, which is based on a topographic classification, proved to be an improvement of the refractive surgery screening process [17,18]. However, some studies have shown this scoring system to have drawbacks, revealing high false positive as well as high false negative rates [19, 20, 21, 22, 23]. There are well defined risks for ectasia after LVC, and these may be related to the presence of (typically mild) ectasia preoperatively, or a procedure that determined important changes in corneal biomechanics [24]. From the viewpoint of these concepts any cornea may evolve into ectasia if surgery or trauma weakens its biomechanical structure. This can occur as a result of LASIK due to a thick flap or excess tissue ablation, or simply after a blunt trauma. The likelihood of ectasia developing depends not only on the structural susceptibility of the cornea but also on the impact of surgery [25, 26]. The process of screening for the risk of ectasia developing must therefore do more than only detect mild forms of keratoconus or related diseases [27, 28, 29].

13 Locating the cone by Prof. Michael W. Belin

Most clinicians have characterized keratoconus based on the appearance on curvature maps. This leads to inaccurate placement of the cone and a high incidence of supposed "pellucid marginal degeneration", which is a relatively rare occurrence. Elevation and pachymetry maps are more reliable in locating the apex of the cone. The example below shows such a case.

Judging from the sagittal curvature map you would expect the cone between 6 and 7 o'clock. The elevation maps of the anterior and posterior corneal surface show the rather position (Figure 122).

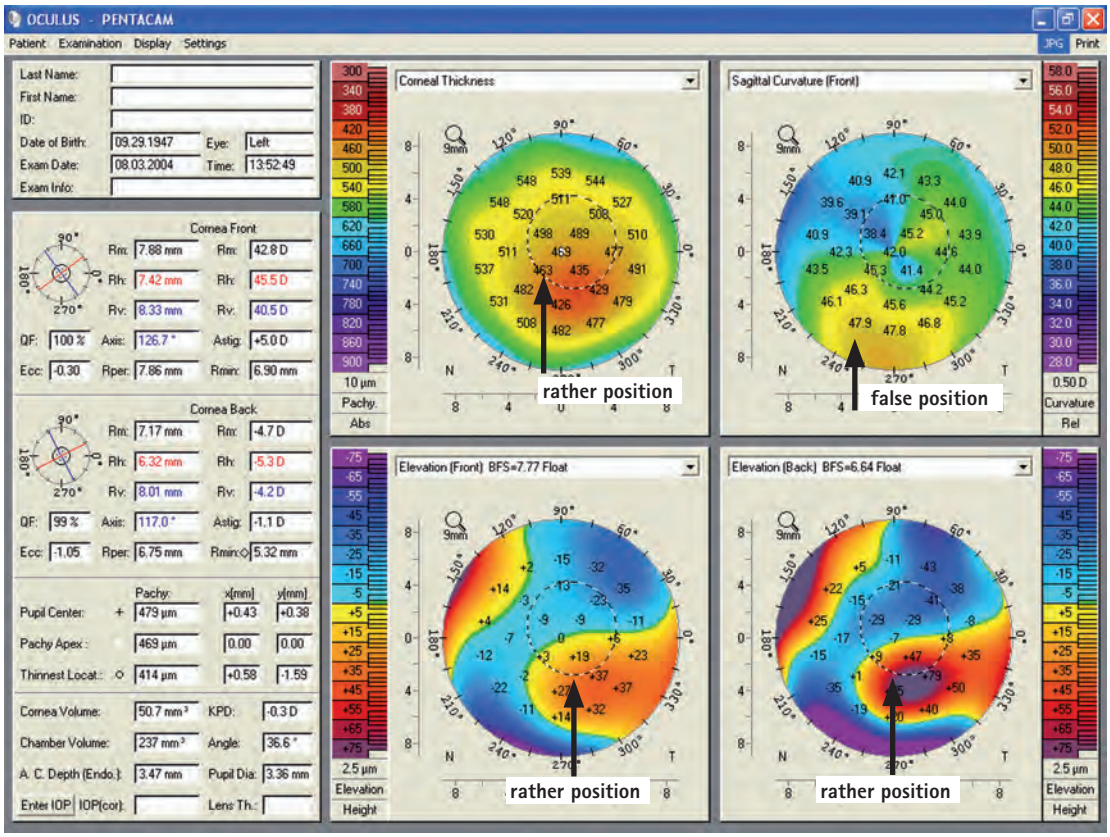

Figure 122: 4 Maps Selectable with different representations suggesting different cone locations

14 The Corneal Optical Densitometry display, by Sorcha S. Ní Dhubhghaill, MB, PhD, Jos J. Rozema, MSc, PhD

Gaining a sense of the structural situation in corneal pathologies can be difficult based on raw Scheimpflug images alone. For this reason the method of tomographic reconstruction was introduced, which provides cross-sections along the three cardinal axes. However, as ocular structures often do not lie within a flat plane, structures at similar depths in the cornea often can appear at different depths in the tomography, hindering their assessment.

This is where the corneal densitometry screen comes in useful in that it presents scatter data over a curved plane that is interpolated between the anterior and posterior corneal surfaces. This means that all structures visible in the map are located at the same relative distance from the corneal surfaces, making it a useful tool for assessing the depth and position of scattering phenomena that may occur within the cornea.

What is the clinical utility of corneal densitometry?

If performed in uniform conditions, densitometry assessment can be used for making repeatable, reproducible measuremements of corneal haze. Densitometry measurements have been used for following up corneal haze in patients post LASIK or post PRK, or with infectious keratitis, corneal mucopolusaccharidosis and keratoconus. The scan protocol is simple and does not lengthen the Pentacam® scan time. We will here describe some of our experiences using this technique.

Applications and Limitations

Any condition that induces a corneal haze or opacity can be objectively assessed using the densitometry approach, provided that the cornea is not opaque. If the cornea is very hazy or opaque, the backscatter will be too high and the measurements unreliable. Corneal densitometry also increases with age in the periphery but remains stable centrally [30].

Note

Densitometry values near the limbus (10 mm – 12 mm from central fixation) should also be interpreted with caution, as scleral backscatter can artificially elevate the values in this area.

14.1 Keratic precipitates

A 50-year-old patient presented with a history of granulomatous uveitis due to a toxoplasmosis infection. At initial presentation he had numerous large keratic precipitates deposited on the endothelial surface. In Figure 123 the large precipitates are prominent on the innermost layer of the densitometry scan. Slit lamp photography was less successful in imaging the precipitates due to the impossibility of targetingthe endothelial surface with retroillumination (Figure 124). Once the patient had been started on a course of antibiotics and corticosteroids he showed significant clinical improvement (Figure 125) and at his two week appointment there was no trace of the previous keratic precipitates (Figure 126).

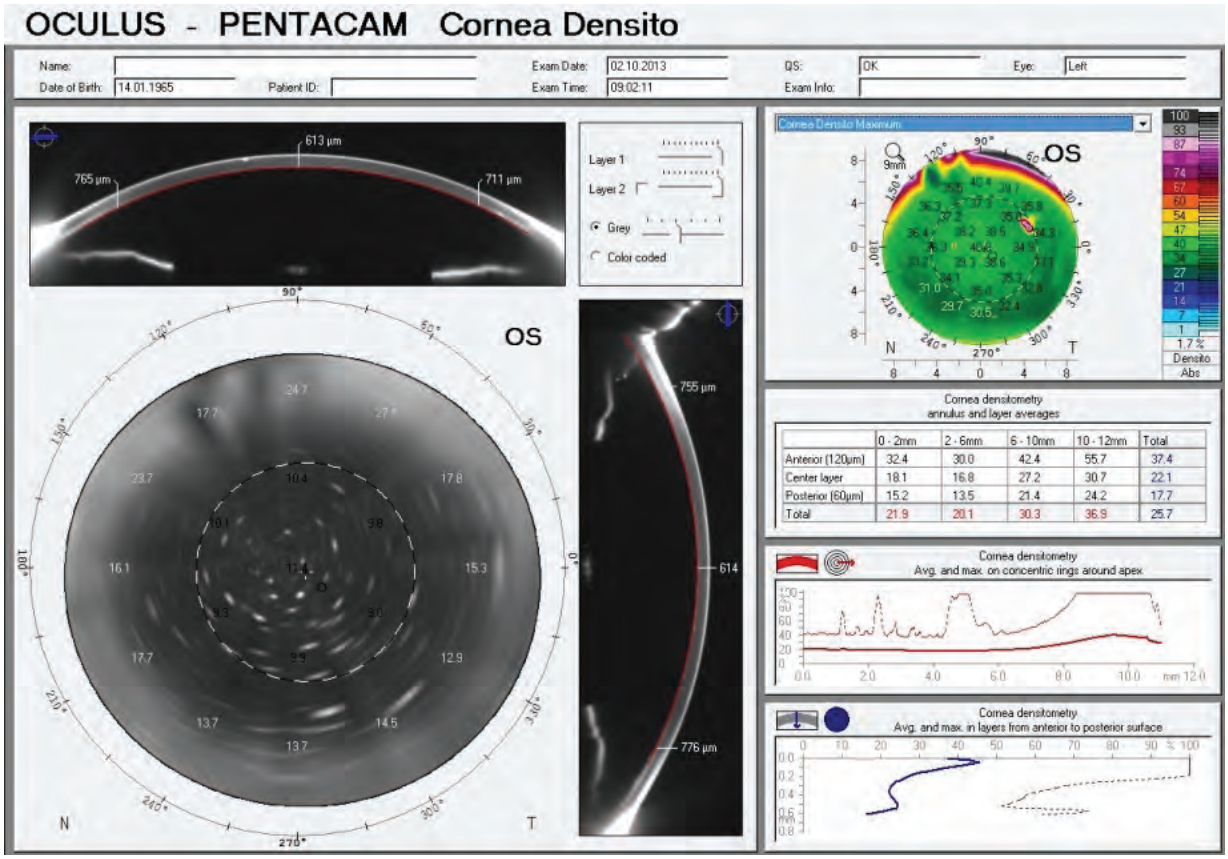

Figure 123: Corneal Optical Densitometry display showing a patient's endothelial densitometry at his initial presentation

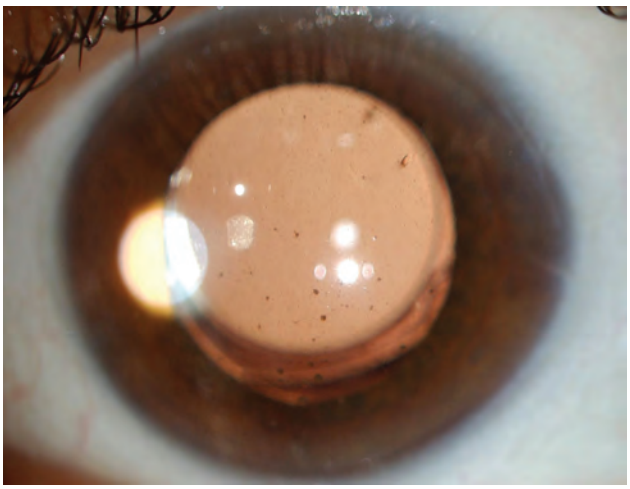

Figure 124: Slit lamp photo of the same eye at the patient's initial presentation

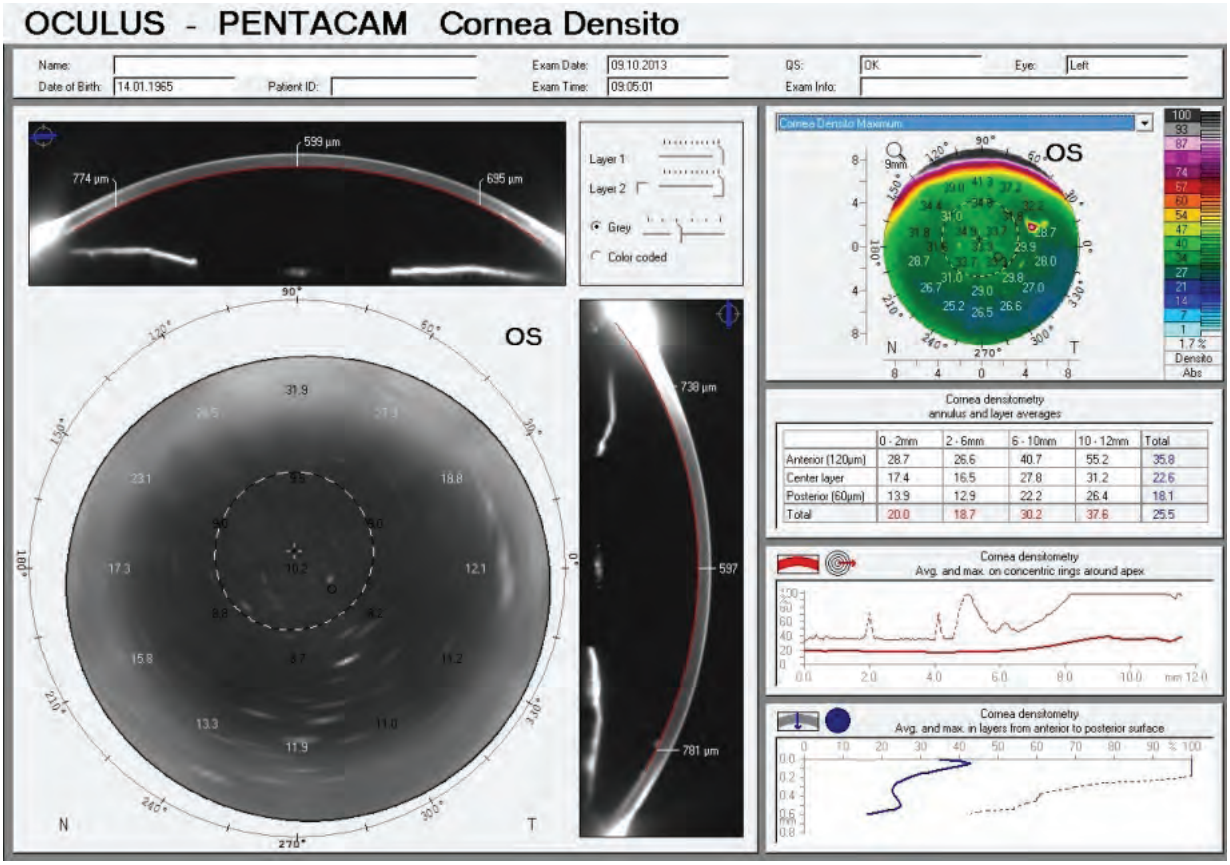

Figure 125: Corneal Optical Densitometry display showing keratic precipitates after one week of therapy

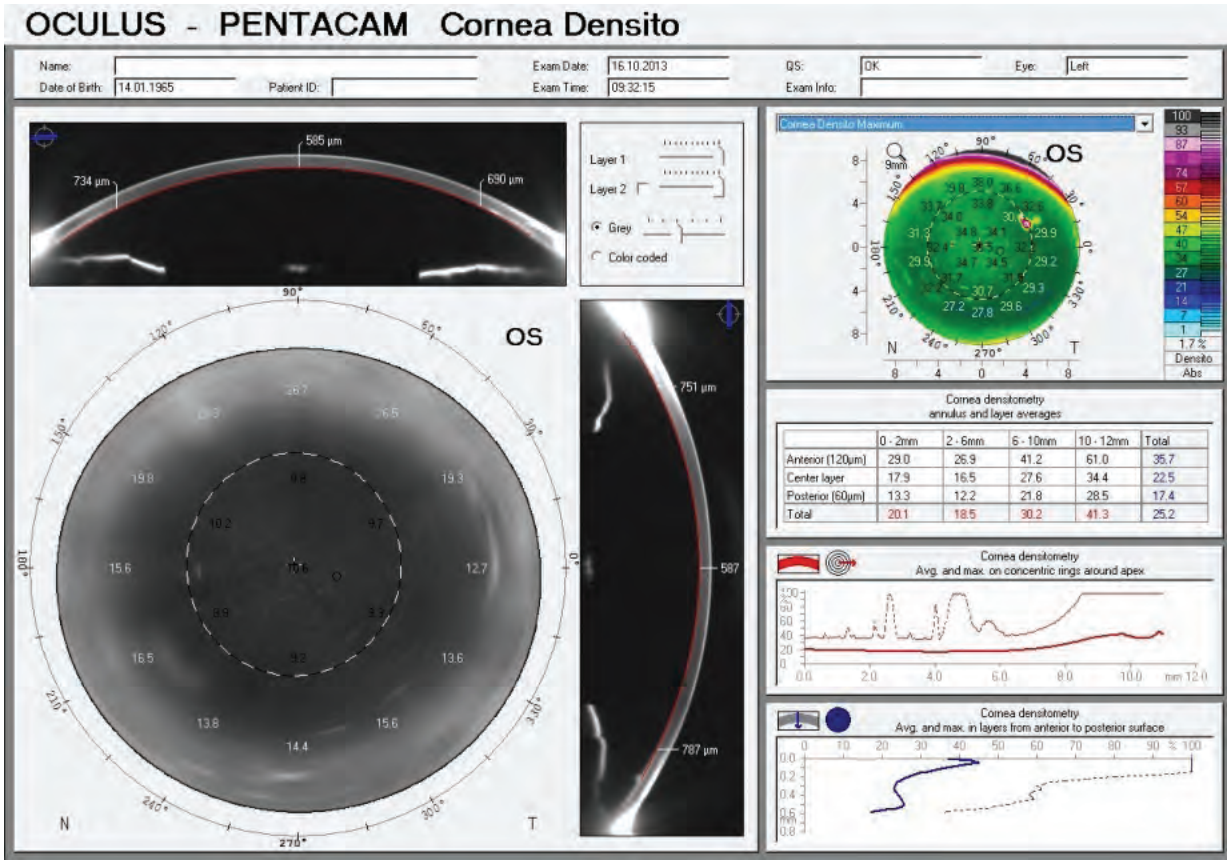

Figure 126: Corneal Optical Densitometry display showing keratic precipitates after two weeks of therapy

14.2 Position and depth of INTACS® rings

As described elsewhere in this Interpretation Guide, Pentacam® examinations can be extremely useful both in planning for surgery and following up patients. The densitometry screen can add an extra dimension to the follow-up. A 35-year-old patient with a history of stable keratoconus was treated by implantation of INTACS® corneal ring segments. The segments are readily visible in the densitometry screen (Figure 127). The depth of the rings can also be seen, measured and followed up over time, and all measurements can be made from a single Pentacam® scan.

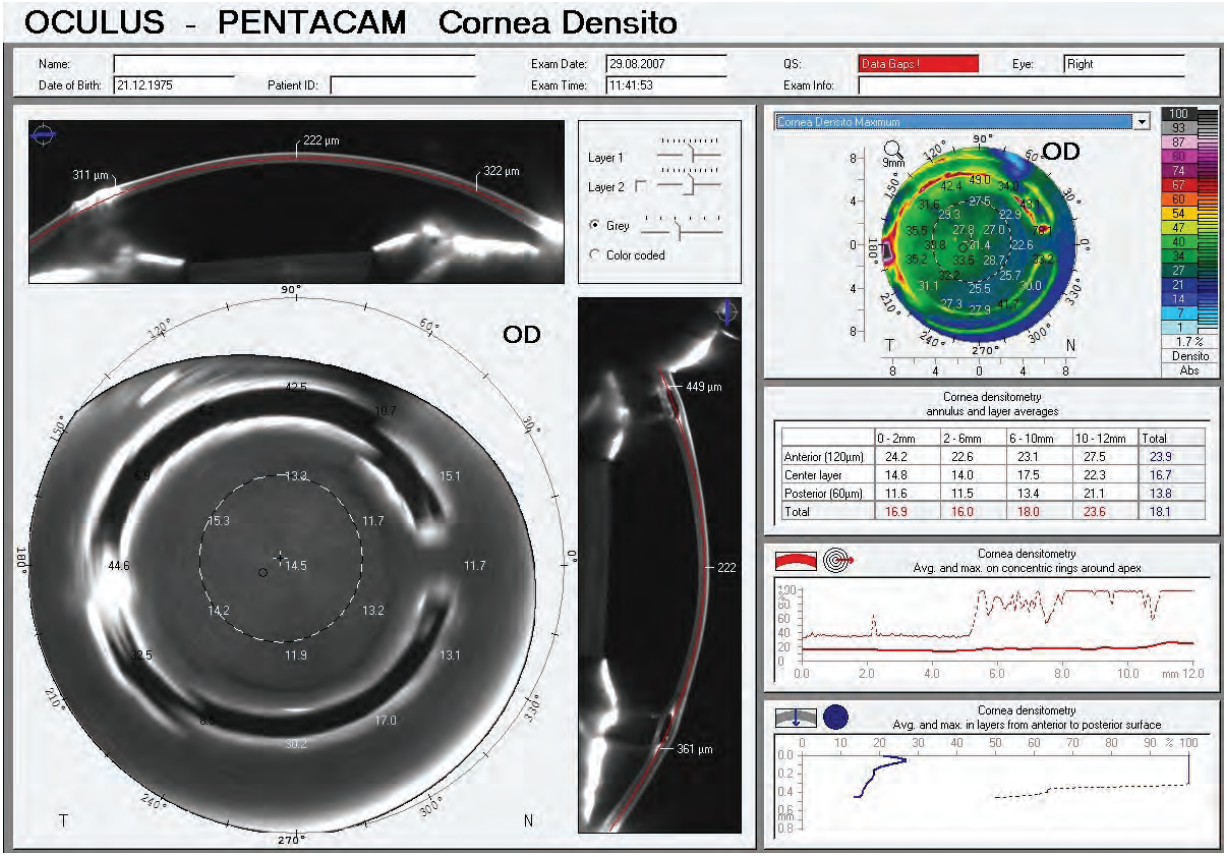

Figure 127: Corneal Optical Densitometry display showing the position and depth of INTACS® corneal ring segments

14.3 DSAEK with specks at the interface

One of the complications associated with a reduced visual outcome in DSAEK surgery is haze at the interface between the donor cornea and the recipient cornea. The capacity of the densitometry screen to depict any desired layer makes it possible to examine the lamellar interface in greater detail. When the visual outcome in the case of this 80-year-old lady was slightly less than expected, there were found to be specks or deposits of inflammatory material at the interface. The densitometry technique allowed for objective measurements of this layer (Figure 128).

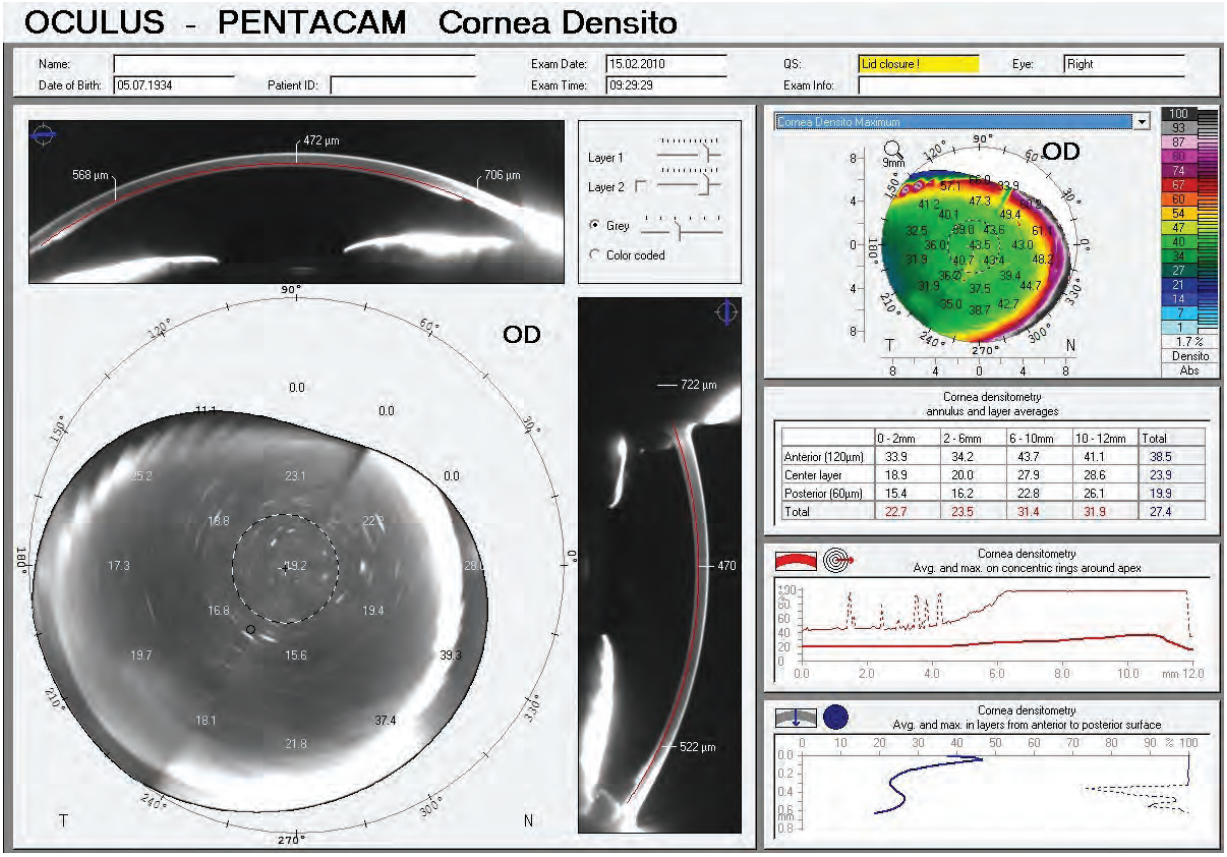

Figure 128: Corneal Optical Densitometry display showing specks and precipitates at the lamellar interface post DSAEK

15 Using Pentacam® technology to evaluate corneal scars, planning and documenting surgery outcomes by Arun C. Gulani, MD, MS

I'd like to present the cornea as an elegant, optically powerful, and visually focused organ which is readily accessible for shape modification aimed at achieving unaided vision. Unless there is a severe and pervasive corneal pathology/perforation a penetrating corneal transplant should be in my opinion the last resort of corneal rehabilitative techniques.

When looking at a corneal scar our inherent mindset is: "There is the culprit. Let's eradicate it".

What I suggest instead is to study the corneal scar and its impact on vision and the Pentacam® technology, especially its corneal densitometry program is a dominant diagnostic in this direction. It can essentially visualize the scar, its depth in the cornea; correlate it to corneal shape (topography) and its consequent impact on refraction. In each and every patient with corneal scarring I begin my quest by using the Pentacam® to determine the depth and density of the scar and its correlation with topography. This helps me decide whether the scars are superficial (less dense) or whether they are denser and deeper. For clinical ease, I have divided corneal scars into "on-cornea" scars (Figure 129, Figure 130), which are located above Bowman's membrane and lead to a camouflaged topography and misleading refractive error, and "in-cornea" scars (Figure 131, Figure 132), which actually become part of the cornea, directly influencing its topography and hence its refractive error. This helps me to decide which treatment method to choose.

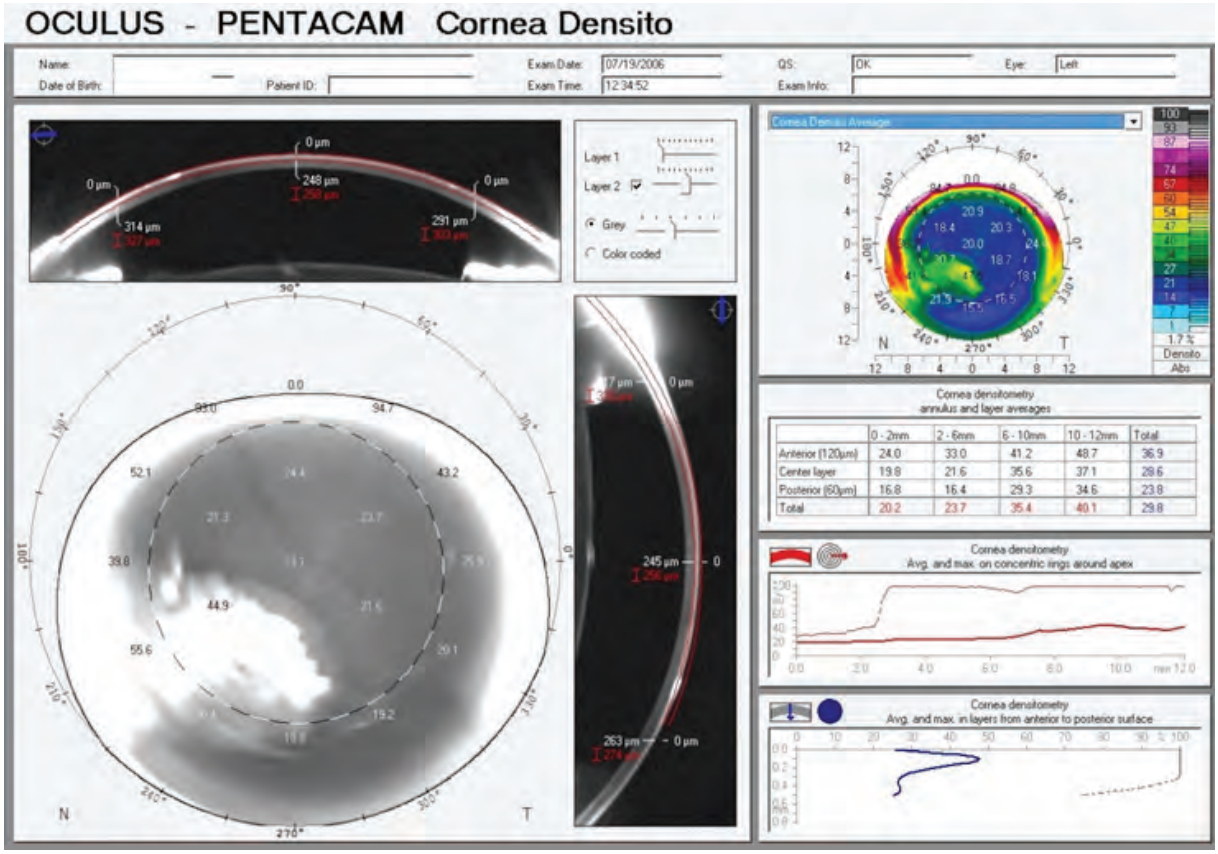

Figure 129: Corneal Optical Densitometry display showing findings on an on-cornea scar

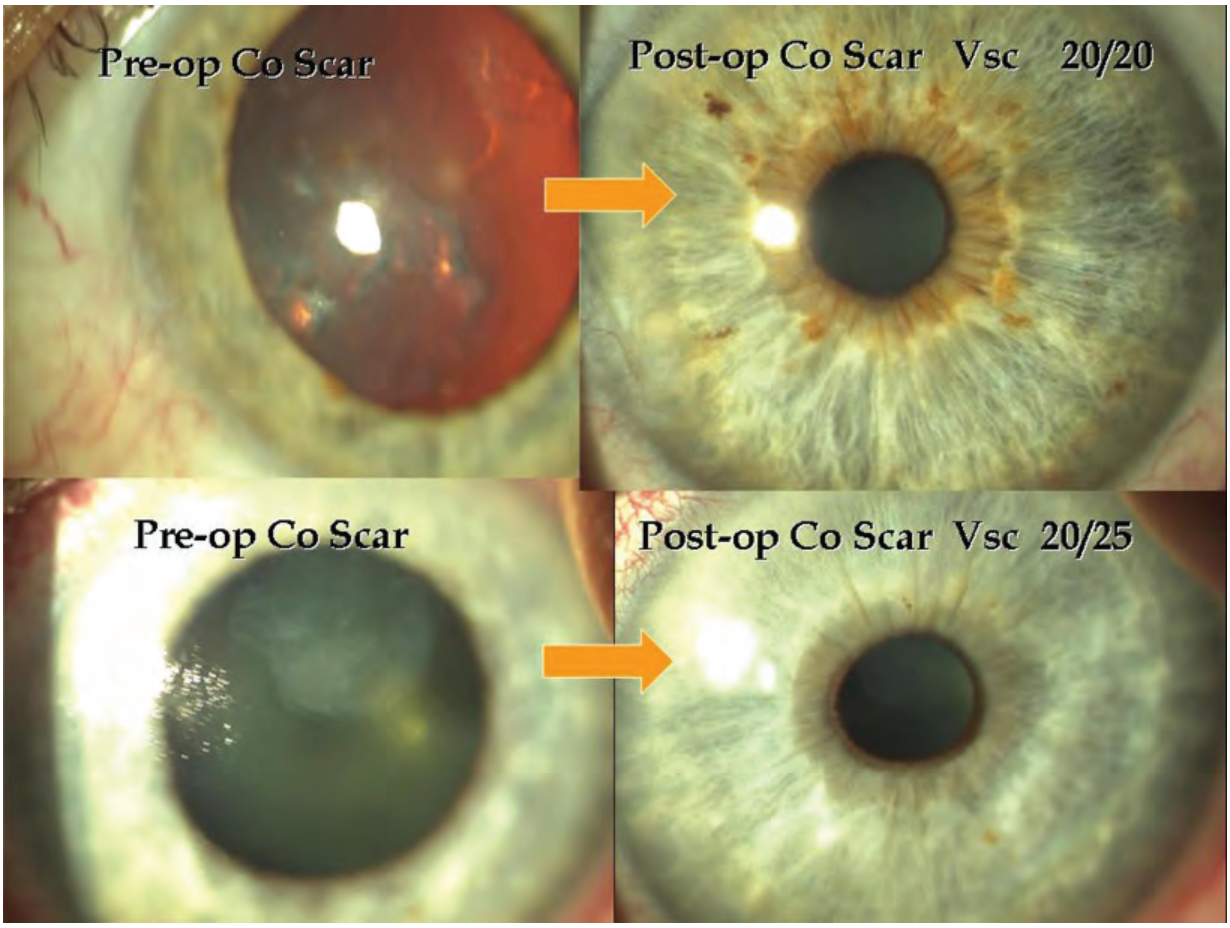

Figure 130: Post- and pre-op slit lamp images of an on-cornea scar

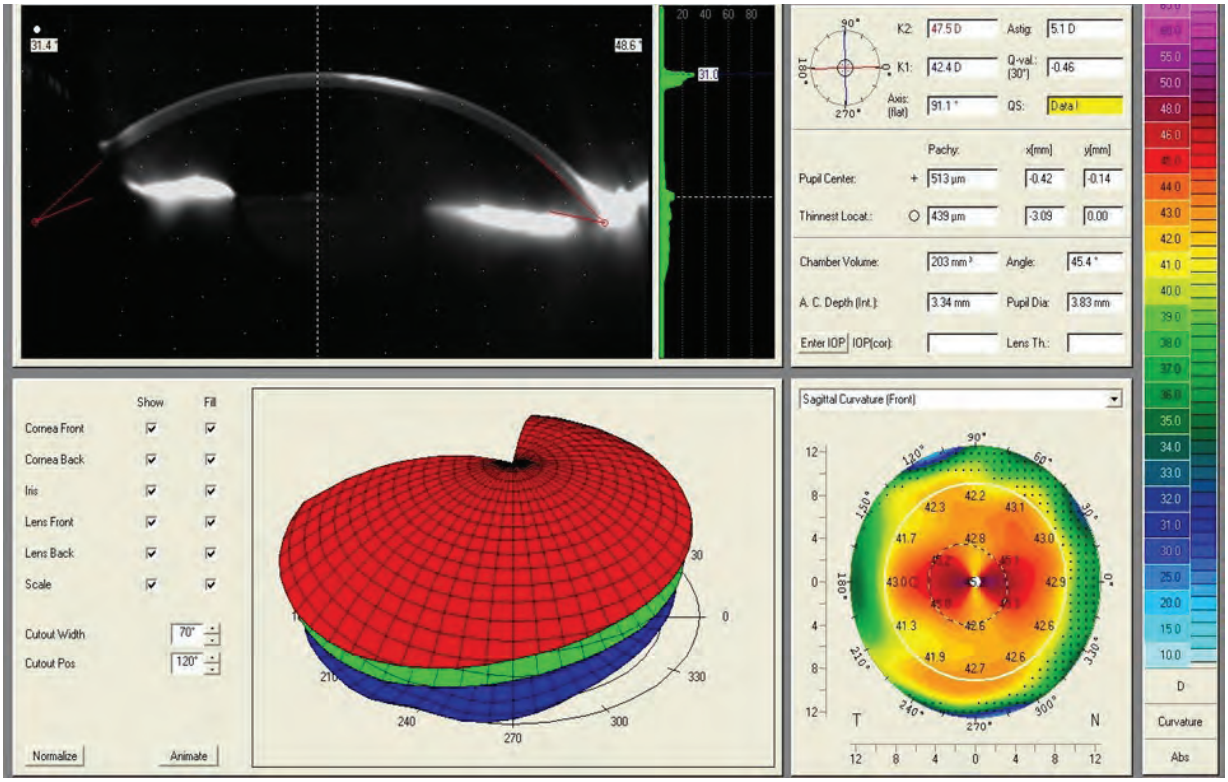

Figure 131: General Overview showing findings on an in-cornea scar in the Scheimpflug image

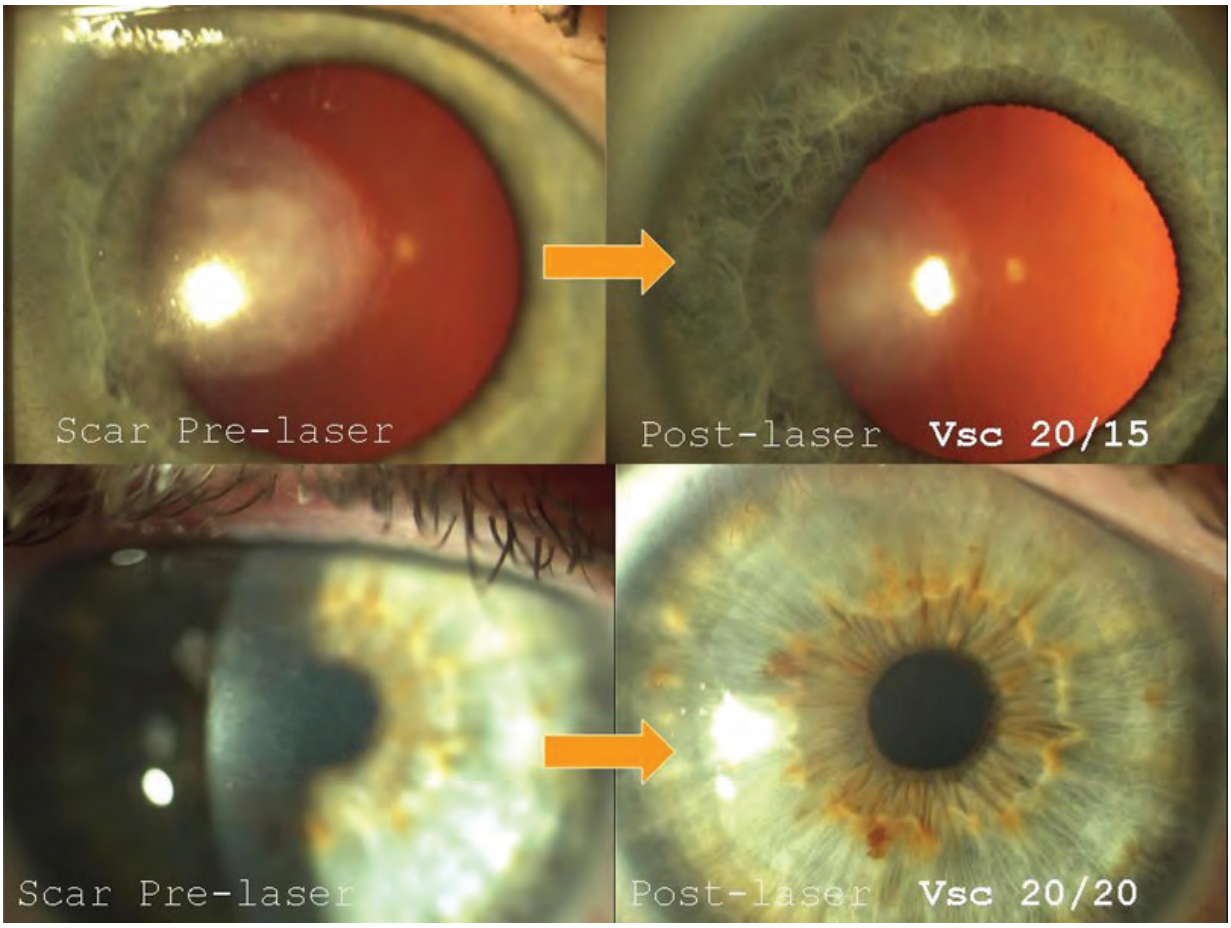

Figure 132: Pre- and post-op slit lamp images of an in-cornea scar

The Pentacam® corneal densitometry function is indispensable to me not only in selecting specific techniques but also as a means of educating my patients with a visual aid that they can understand. In cases of moderate anatomical abnormality with structural instability (i.e. keratoconus, keratoglobus, pellucid marginal degeneration or LASIK ectasia), INTACS can be used (Figure 133).

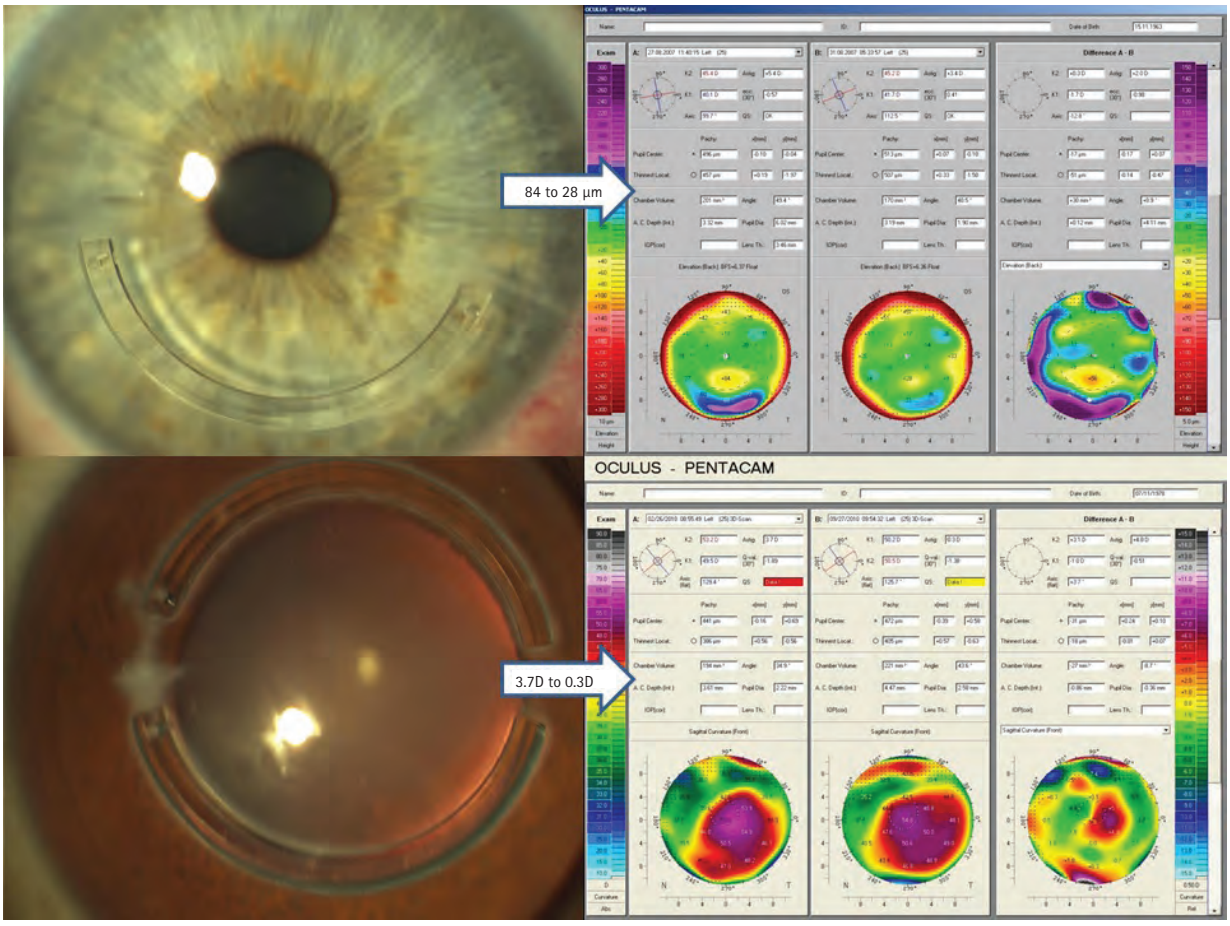

Figure 133: INTACS® for optical manipulation and laser refractive combinations

In Figure 133 the upper two images show the topography after asymmetric implantation of INTACS in the Compare 2 Exams display with a significant decrease of posterior corneal elevation from 84 µm to 28 µm. The lower 2 images show the impact after Laser PRK following previous INTACS to result in decrease in corneal astigmatism from 3.7 D to 0.3 D.

After corneal visual rehabilitation, collagen-cross-linking can be used to further stabilize this restored cornea. Here the Pentacam® can be used not only in planning but also in documenting successful outcomes.

[51, 52, 53, 54, 55, 56, 57]

15.1 Case 1: Corneal scar with RK incisions and cataract

This patient was referred with a central on-corneal scar with multiple RK incisions and cataract. As a first step, he underwent scar peel with excimer laser myopic ablation to clear the cornea and make it measurable. After IOL power calculation, he then underwent cataract surgery with a precisely calculated lens implant and was brought to emmetropia and unaided 20/20 vision.

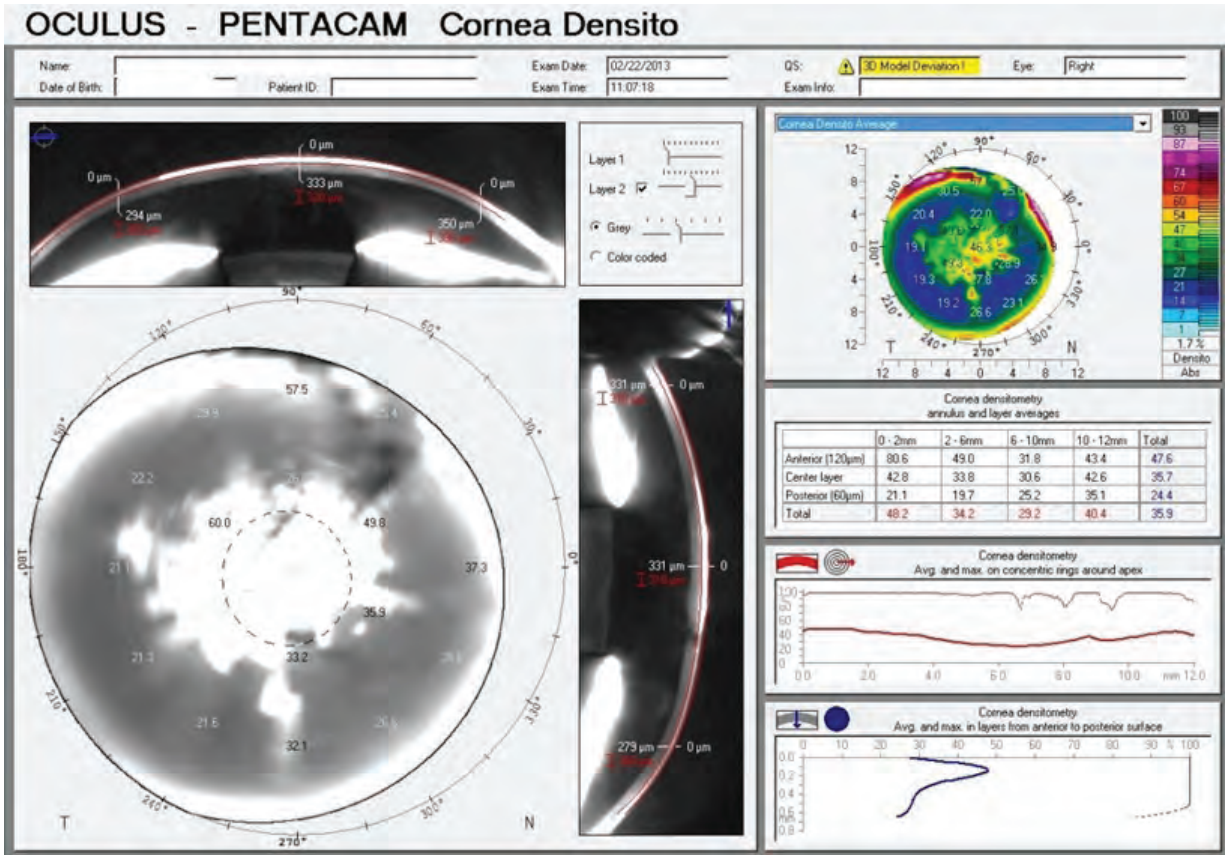

Figure 134: Corneal Optical Densitometry display showing a central corneal scar with RK incisions and cataract

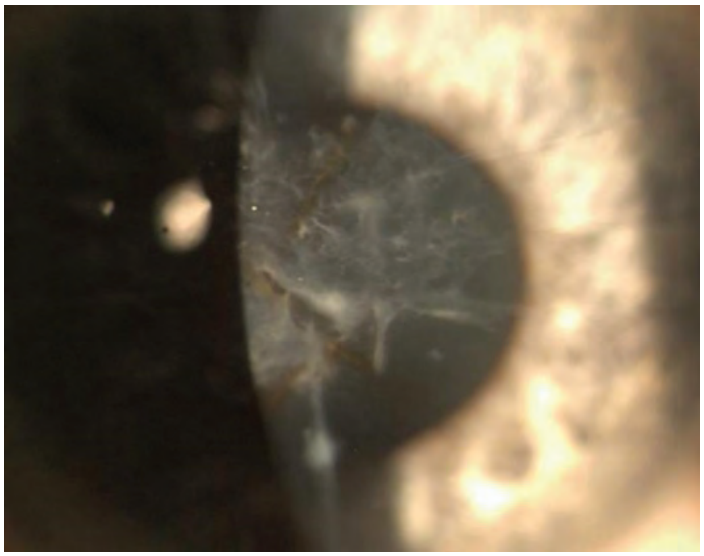

Figure 135: Slit lamp image of a central corneal scar with RK incisions and cataract

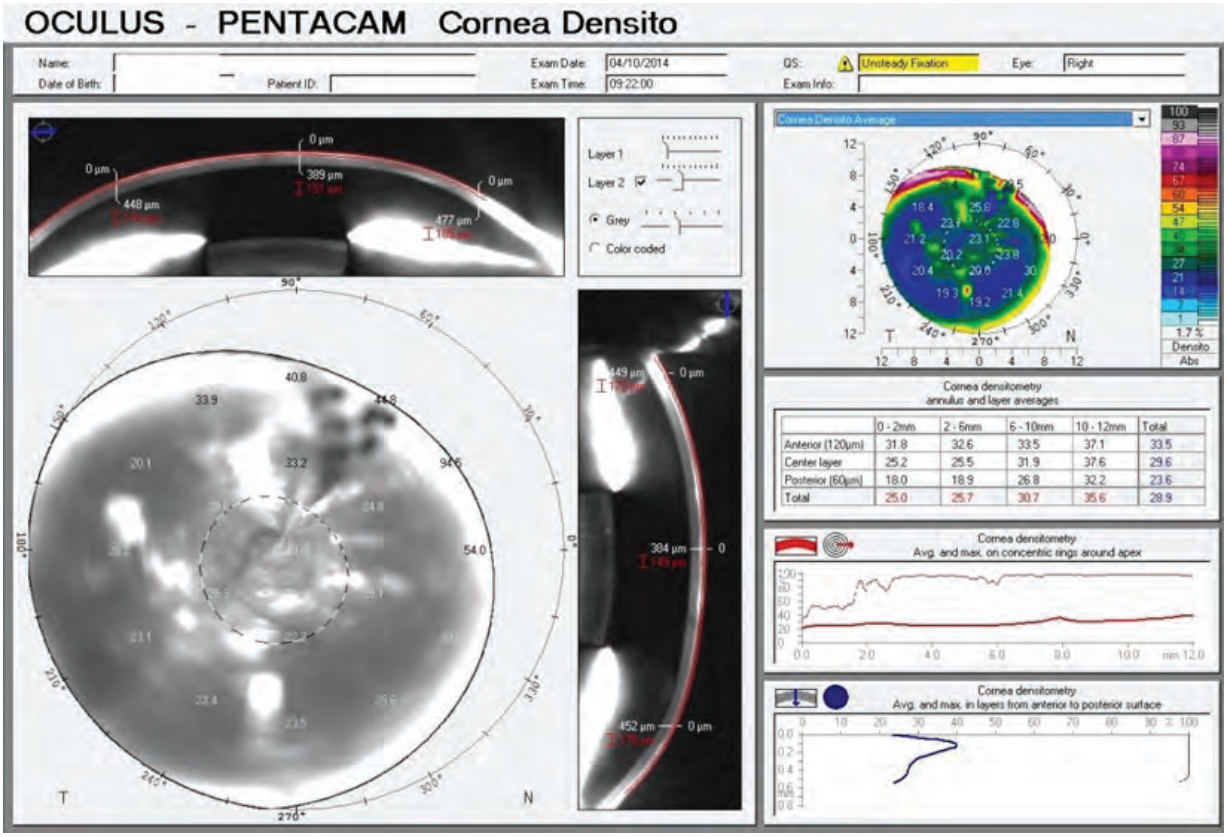

Figure 136: Corneal Optical Densitometry display showing a clear cornea following laser scar peel; cataract present

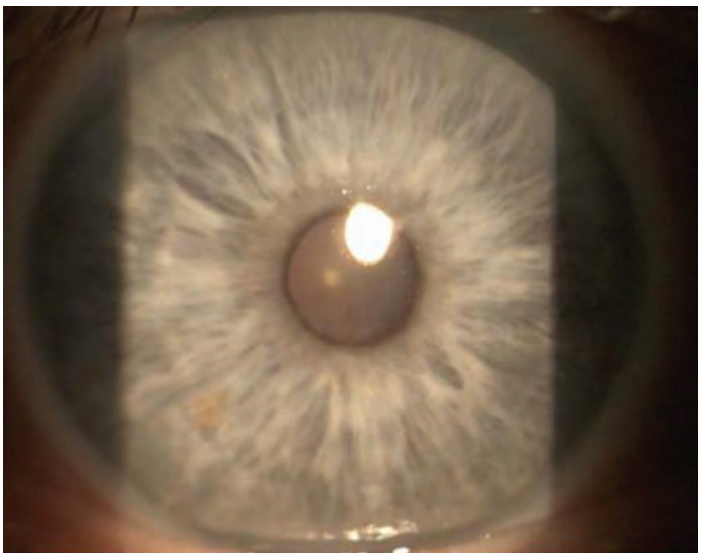

Figure 137: Slit lamp image showing a clear cornea following laser scar peel; cataract present

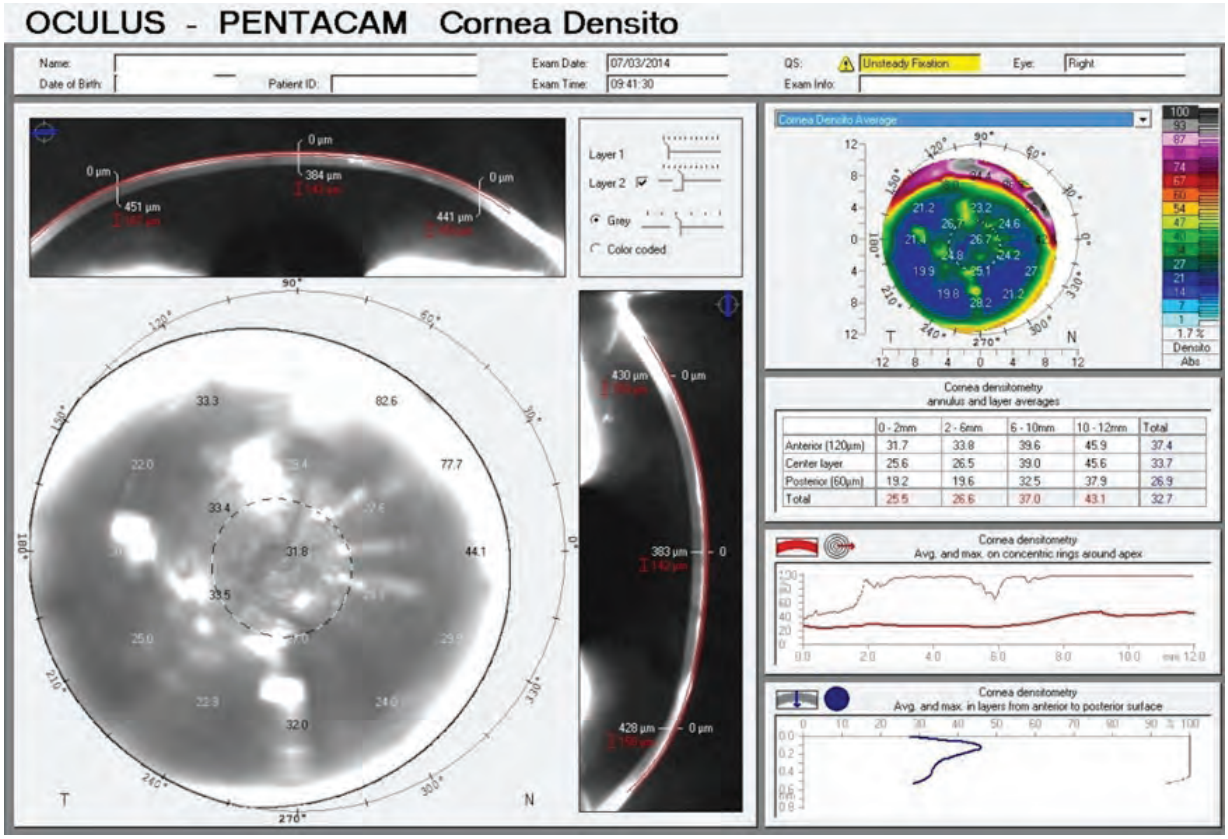

Figure 138: Corneal Optical Densitometry display showing status post cataract surgery with toric lens implant giving 20/20 vision

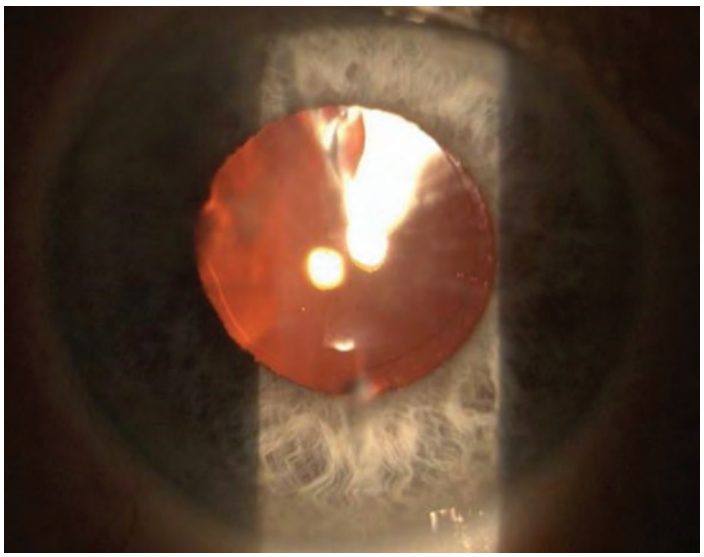

Figure 139: Slit lamp image showing status post cataract surgery with toric lens implant giving 20/20 vision

15.2 Case 2: Keratoconus with congenital cataract, high myopia and high astigmatism

This patient was referred with keratoconus, congenital cataracts, high myopia, high astigmatism and presbyopia. As planned first stage, assymetric INTACS® were implanted in preparation of lens exchange surgery using a toric lens implant in the second stage, which eventually brought the patient to emmetropia and unaided 20/20 vision.

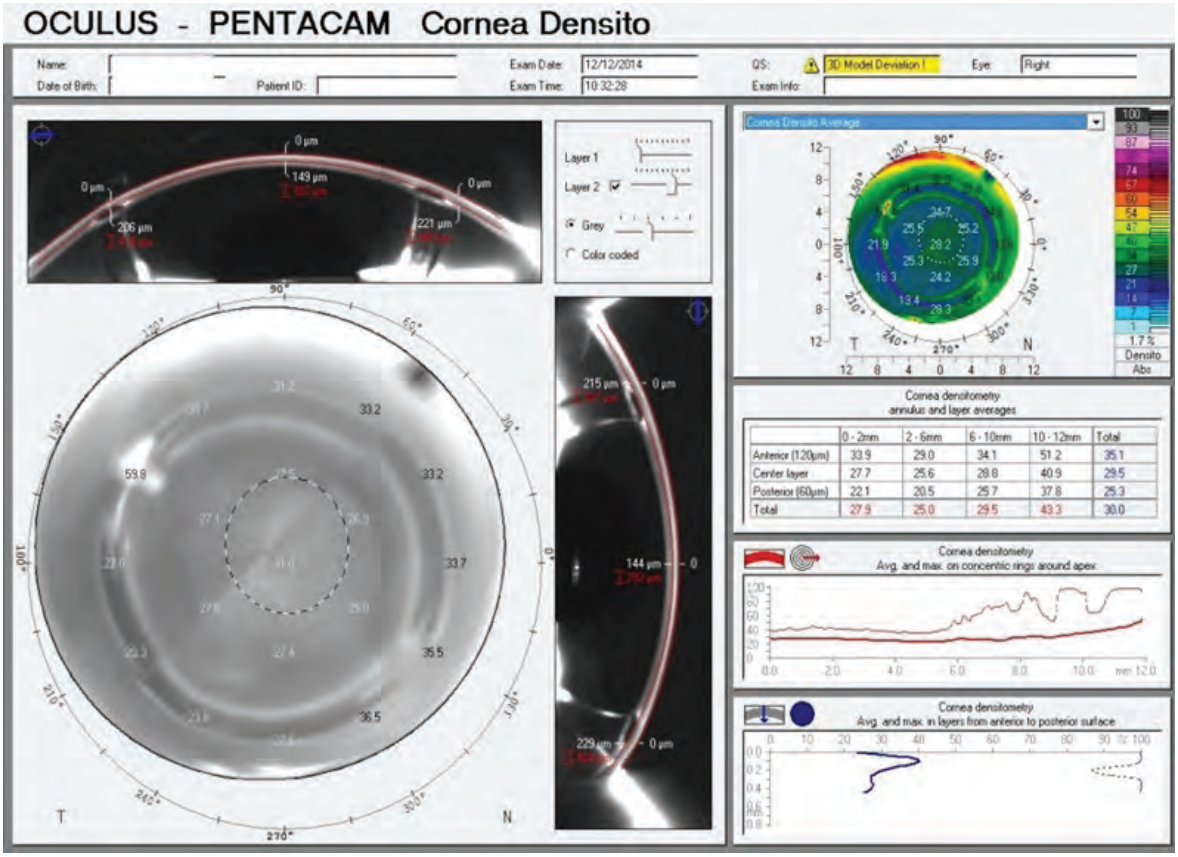

Figure 140: Corneal Optical Densitometry display after strategic INTACS® placement in preparation of lens exchange surgery

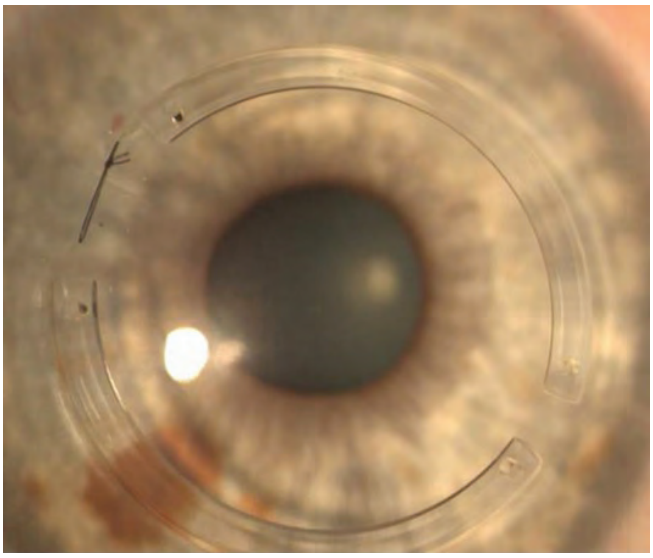

Figure 141: Slit lamp image after strategic INTACS® placement in preparation of lens exchange surgery

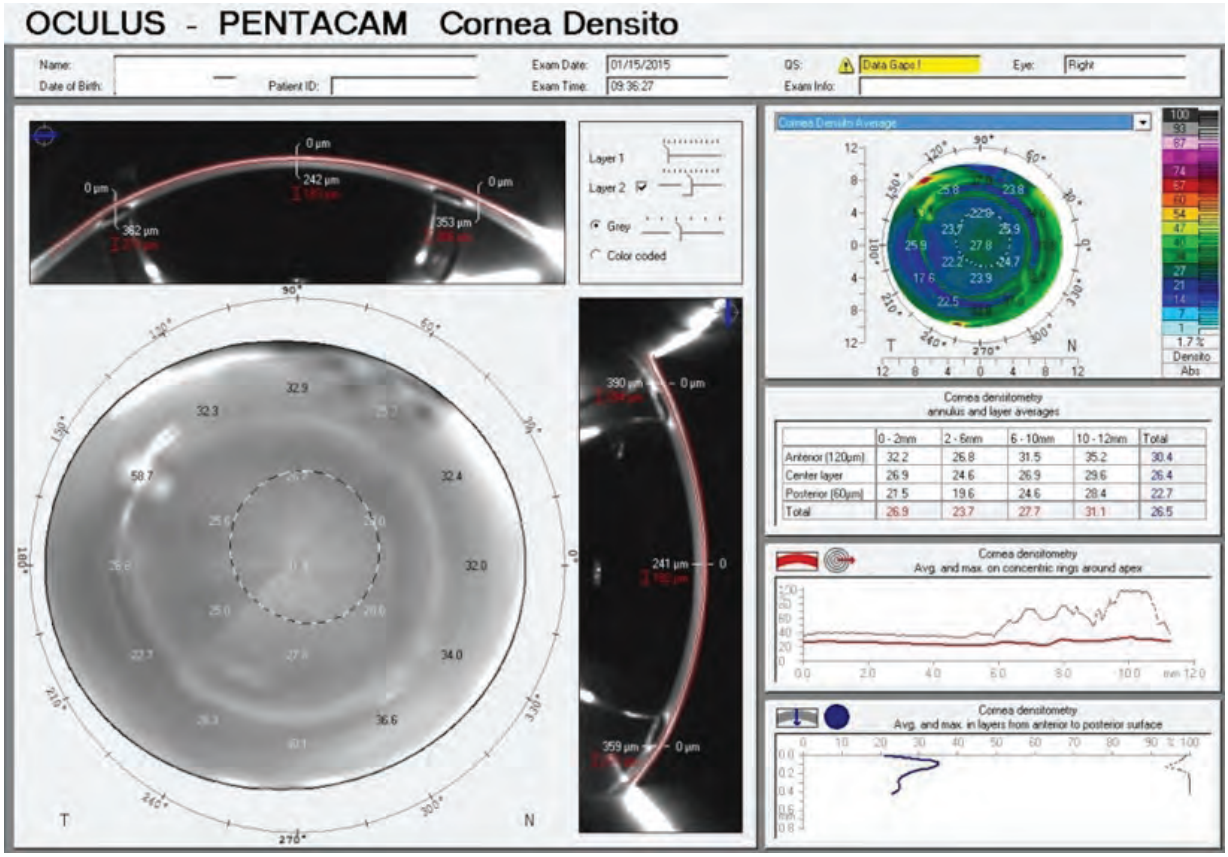

Figure 142: Corneal Optical Densitometry display showing the emmetropic outcome after lens exchange surgery; INTACS® in place.

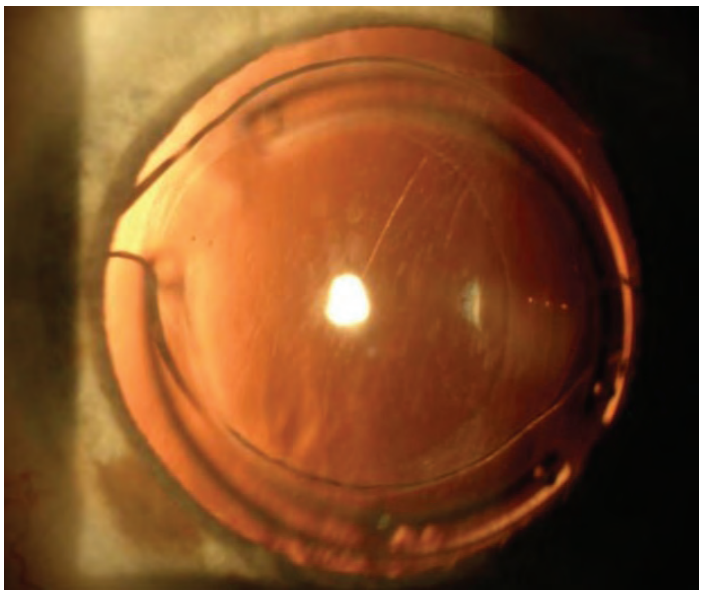

Figure 143: Slit lamp image after lens exchange surgery with an emmetropic outcome; INTACS® in place

16 INTACS® implantation

16.1 Case 1: INTACS® implantation by Prof. Michael W. Belin

A 27-year-old female was referred by her optometrist because of poor vision OD secondary to keratoconus. Her BSCVA was 20/200 OD and with RGP over-refraction 20/30. The patient complained of poor contact lens tolerance with less than 3 hours of daily wearing time. The patient was being considered for intrastromal corneal ring segment implantation (ICRS, commonly referred to as INTACS® in the US)

Anterior corneal curvature analysis showed significant inferior cone displacement and a maximum steepness of > 50 D, with the steepest part of the cone well below the pupillary margin (Figure 144). A presumptive diagnosis of pellucid marginal degeneration (PMD) was made, and the initial surgical plan was to implant dissimilar INTACS® for PMD.

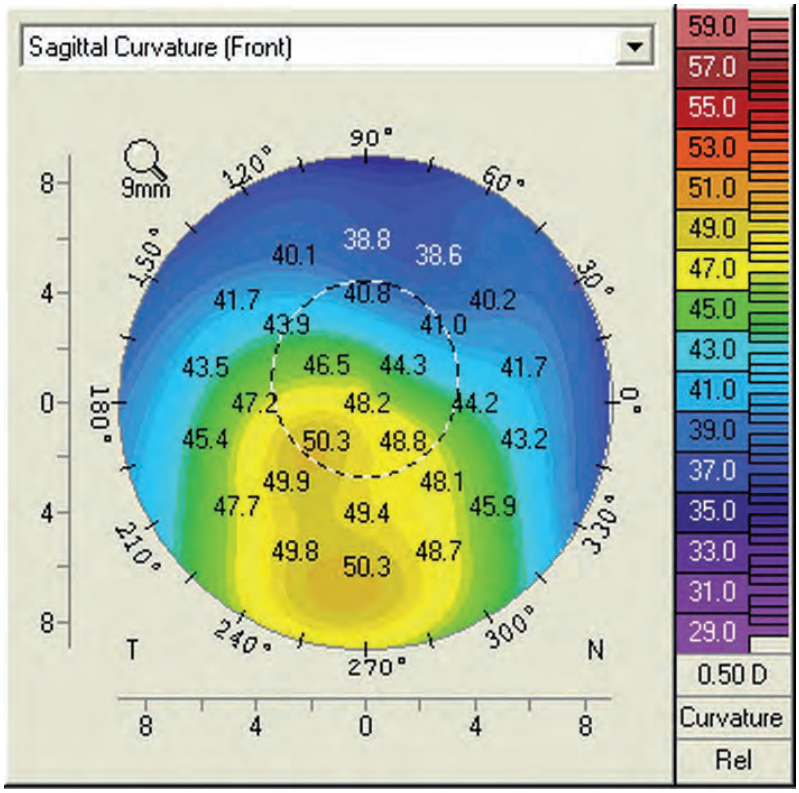

Figure 144: Topography in a case of suspected PMD

Surgical planning also included identifying the steep axis for the incision and looking at the pachymetry over the incision location to determine the incision depth (Figure 145).

Surgical planning included:

- implantation of 0.35 INTACS®
- incision at axis 155°
- incision depth 440 µm

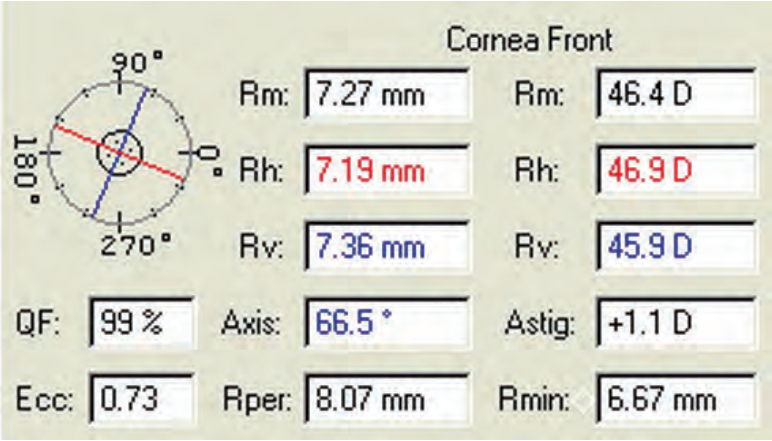

Figure 145: Keratometer values

Then a complete Pentacam® anterior segment analysis was performed, revealing the shortcomings of cone location and keratoconus classification based solely on anterior curvature.

Both the anterior and posterior elevation map, as well as the pachymetry map locates the cone just at the inferior pupillary border, giving a picture typical of traditional keratoconus (Figure 145).

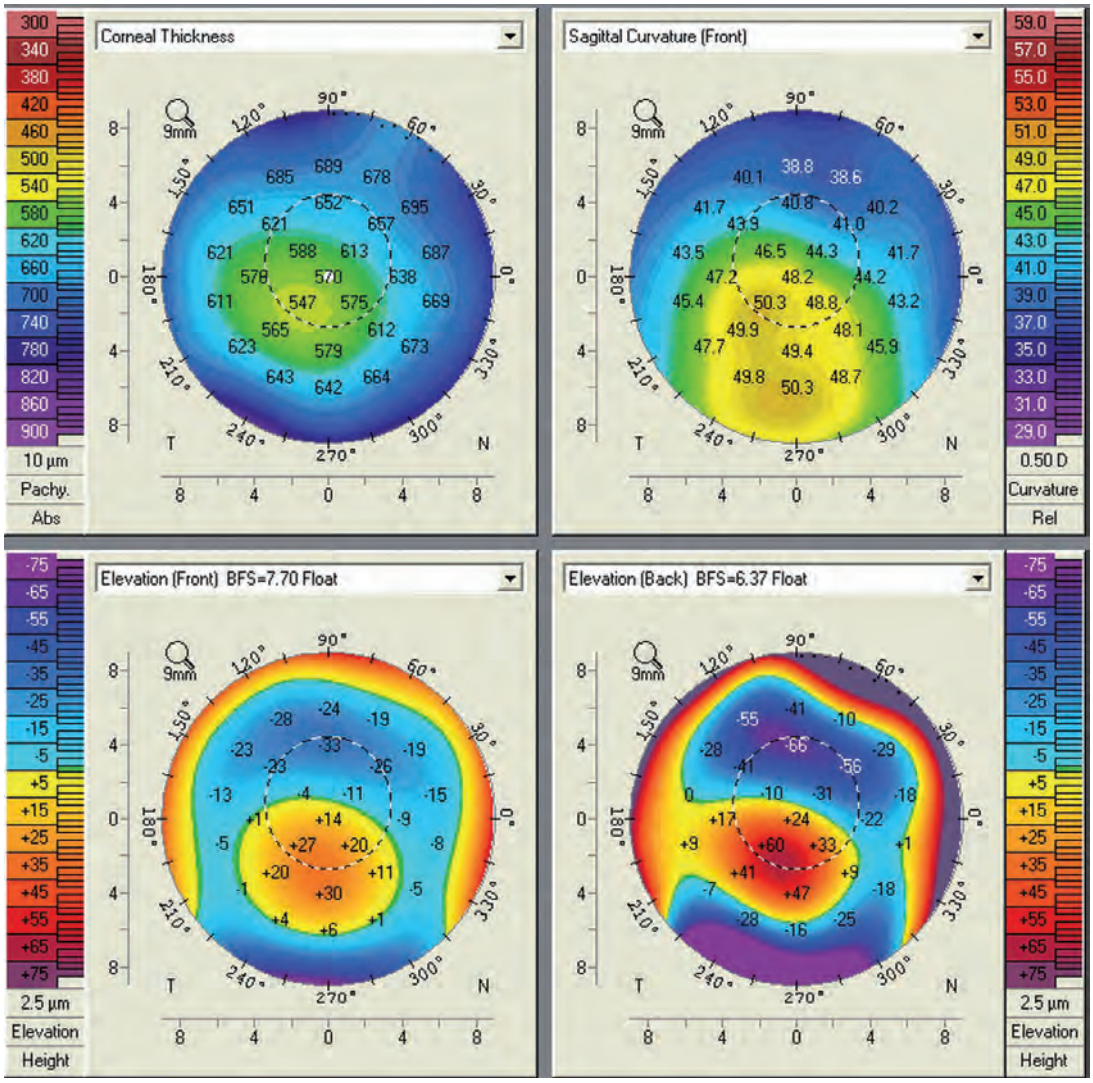

Figure 146: Part of 4 Maps Selectable showing a typical case of keratoconus

16.2 Case 2: INTACS® after PRK by Alain-Nicolas Gilg, MD

A 45-year-old female had had photorefractive keratectomy (PRK) in both eyes 7 years earlier. Before the laser surgery her visual acuity had been

- OD: sph -7.50 cyl -0.50 A 170°
- OS: sph -6.75 cyl -1.00 A 10°

She was referred for blurred vision, photophobia, and poor intermediate VA. Zernike analysis confirmed the functional disorders of her vision, showing them to be due to abnormal spherical and high order aberrations (HOA), |Z|4° (spherical), |Z|5³ (trefoil 5th order) |Z|6² (astigmatism 6th order) (Figure 147).

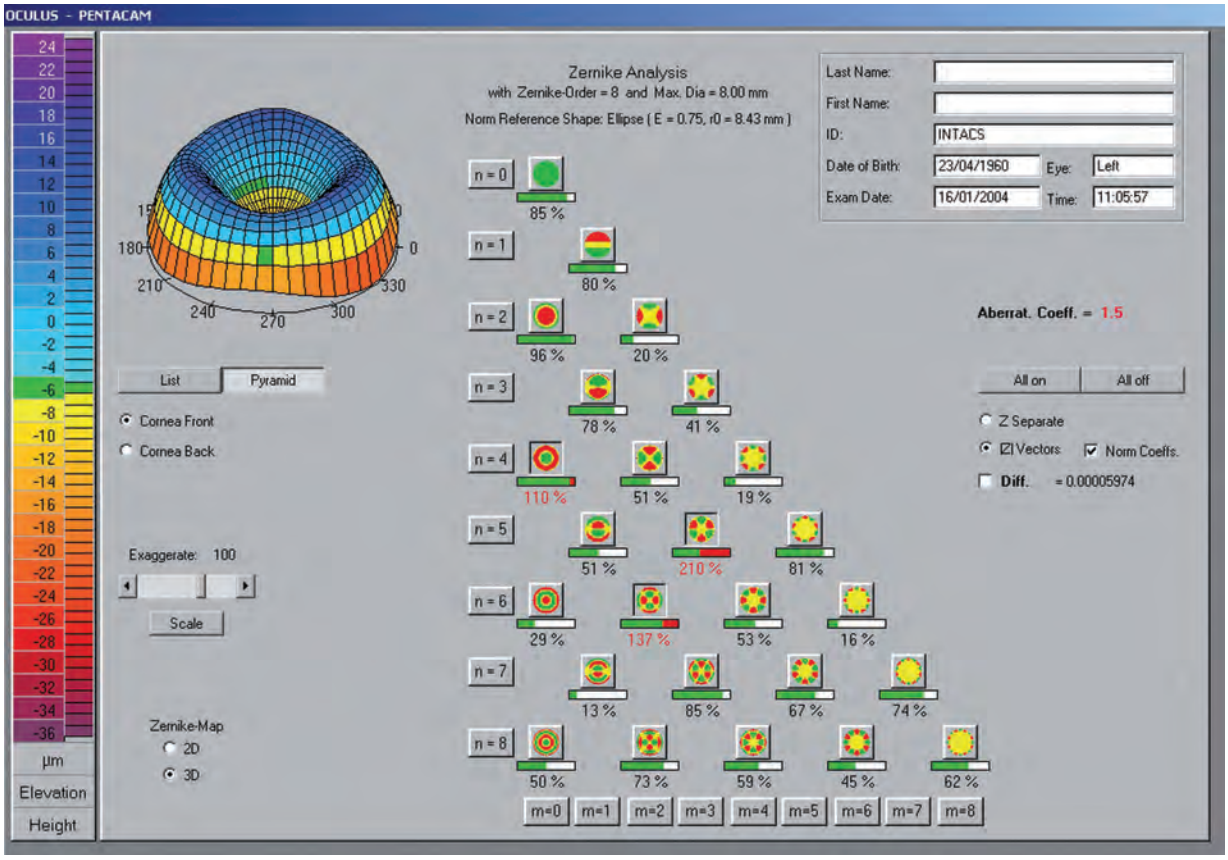

Figure 147: Zernike Analysis topography pre INTACS®

The keratoconus menu of the Pentacam® identifies this cornea as an oblate postoperative cornea. Note the negative eccentricity and the abnormally high aberration coefficient due to the HOA (Figure 148).

The pachymetry map shows a smooth progression with a thick area for the implantation of the INTACS® in the 7 mm zone. This made her a good candidate for INTACS® implantation.

Before the implantation of corneal INTACS® her visual acuity was:

- OD: sph -1.25, cyl -0.50 A 175° VA 20/25
- OS: sph -1.50, cyl -0.50 A 55° VA 20/40

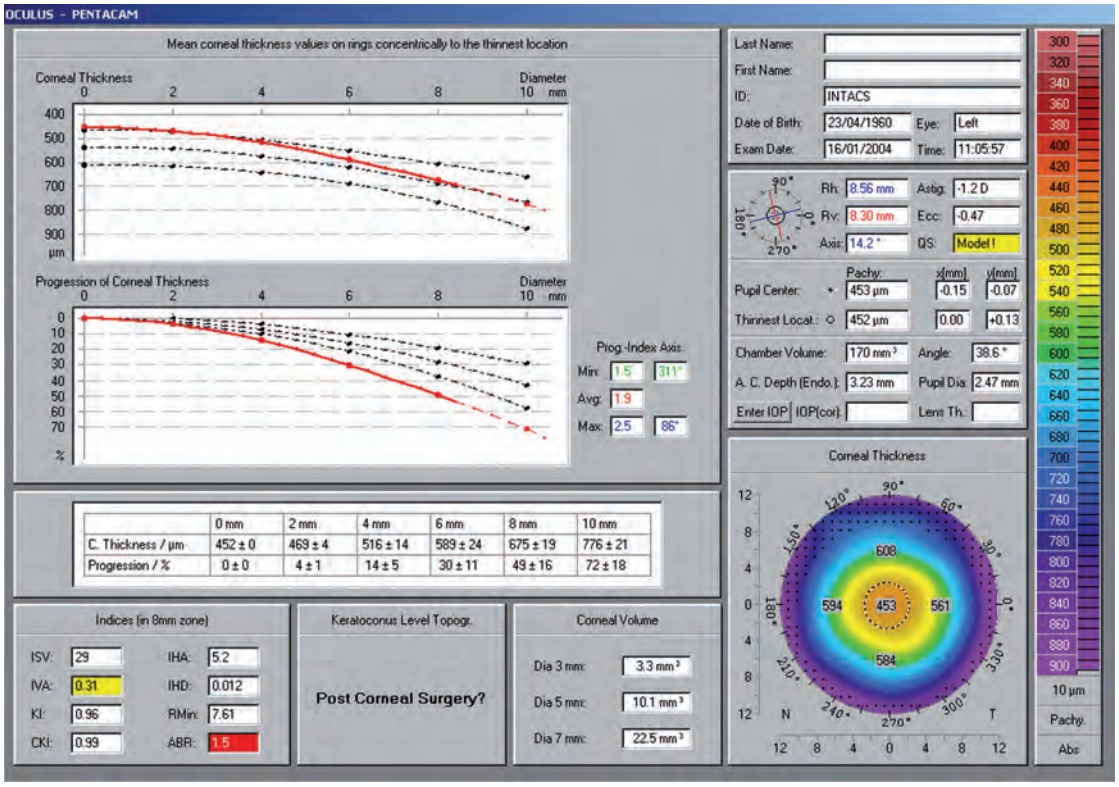

Figure 148: Pachymetric showing the pachymetry progression in an oblate postoperative cornea

After the implantation of INTACS® her visual acuity was

- OS: sph +0.50 cyl -1.25 A 30° VA 20/20

The Scheimpflug image shows a successful fit of the implanted INTACS® (Figure 149).

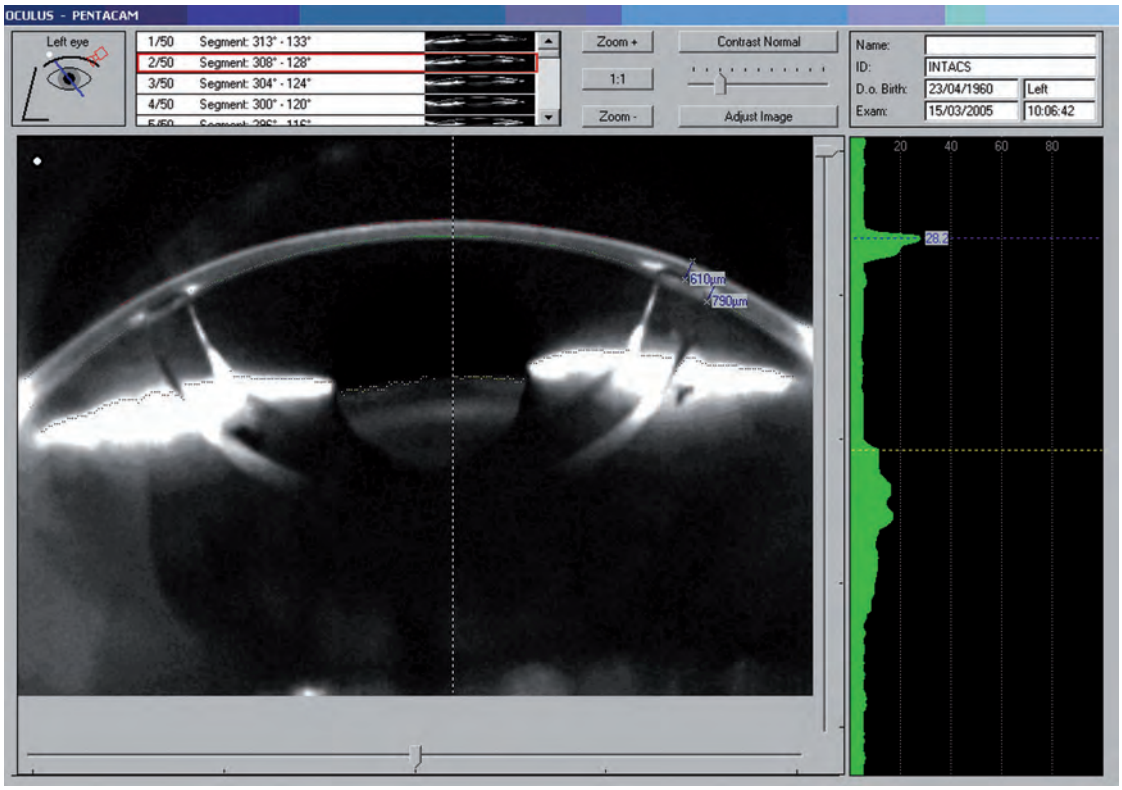

Figure 149: Scheimpflug Image after INTACS® implantation

16.3 Case 3: INTACS® & crosslinking by Prof. Renato Ambrósio Jr, Fernando Faria-Correia, MD, Allan Luz, MD

A 24-year-old male patient presented with progressive keratoconus in OS and anisometropia. Uncorrected visual acuity (UCVA) was 20/20 in OD and 20/200 in OS. Wavefront assisted manifest refraction was sph -0.75 cyl -5.25 A 175°, giving 20/30 in OS. Femtosecond laser assisted (FS-200, Alcon, Fort Worth) INTACS® implantation was performed using Keraring (Mediphacos, Belo Horizonte, Brazil) SI6 150[o] with 250 mm thickness. INTACS® implantation was combined with transepithelial (EpiON) crosslinking using riboflavin 0.22% solution (VibeX Xtra; Avedro Inc., Waltham, MS, USA). The patient was subjected to 8 min. of pulsed UV-A light (1 sec on/1 sec off) at 30 mW/cm^2 (energy dose of 7.2 J/cm^2) with the Avedro KXL. After 6 weeks his UCVA was 20/30 and his BCVA was 20/25+ (sph 0.00 cyl -1.00 A 170°). Figure 150, documents the postoperative corneal flattening, along with the increase in corneal density (optical scattering). Figure 151, Figure 152, show the INTACS® position and demarcation line on the Scheimpflug image.

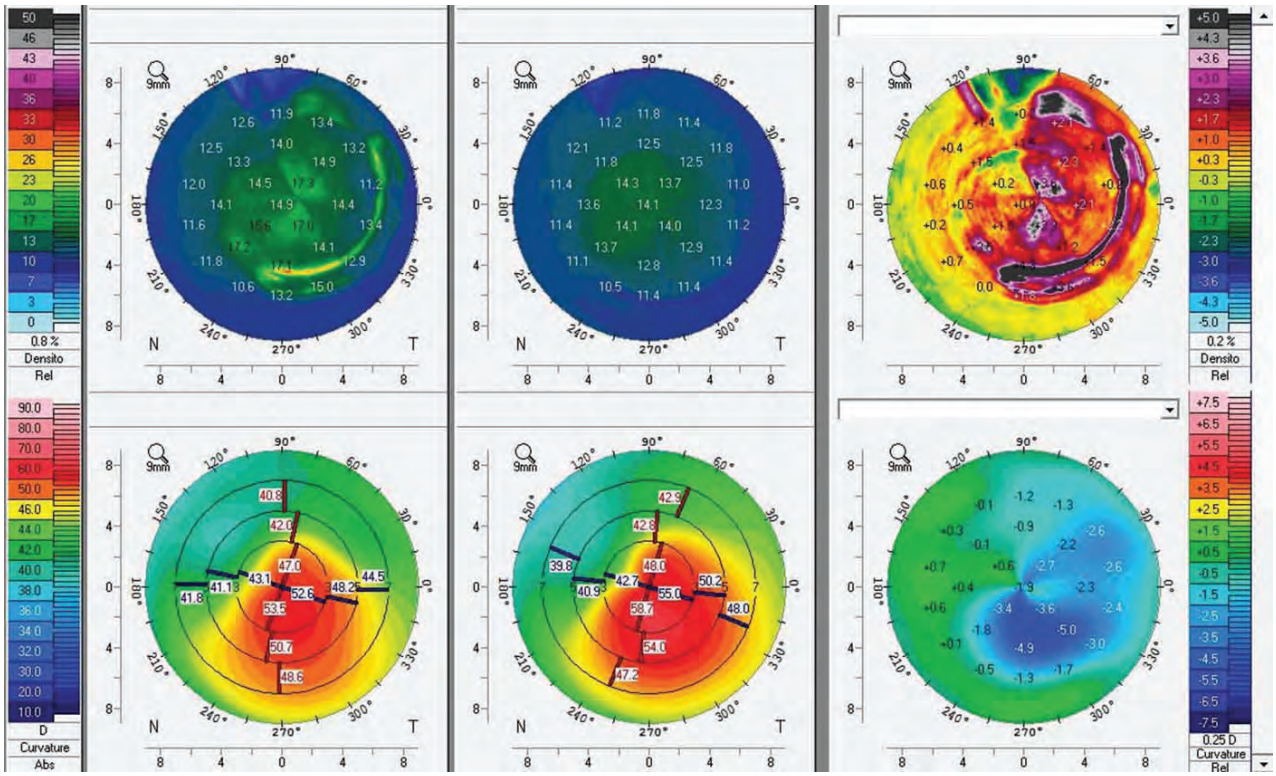

Figure 150: Preoperative, postoperative (6 weeks after femtosecond-assisted intracorneal ring segment and transepithelial crosslinking) and subtraction maps of the average optical density and axial curvature maps

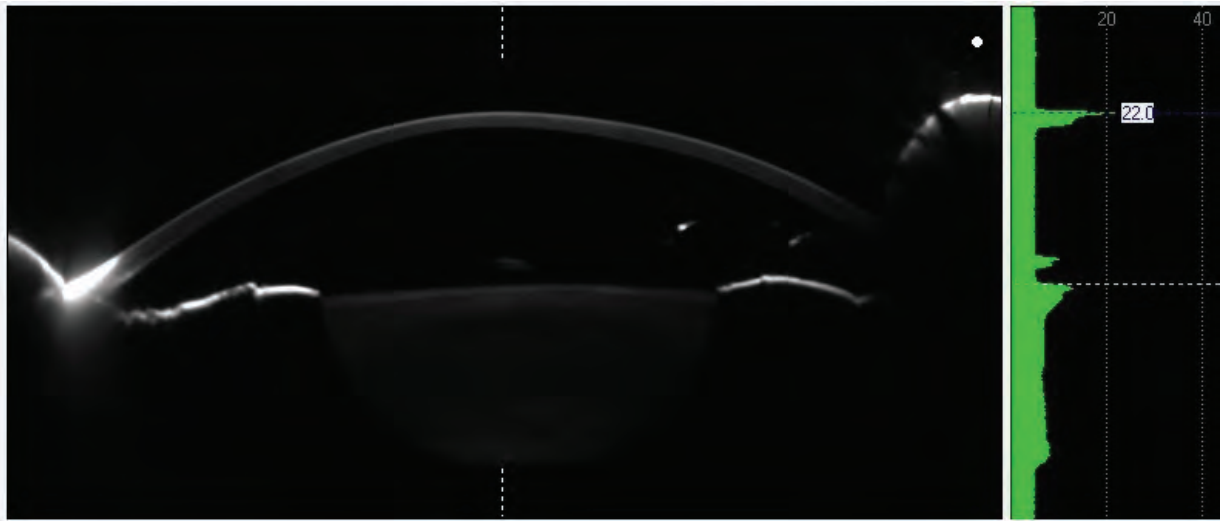

Figure 151: Preoperative Scheimpflug image of the vertical section

Figure 152: Postoperative Scheimpflug image of the vertical section

17 Holladay Report & Holladay EKR65 Detail Report by Jack T. Holladay, MD

17.1 Holladay Report

The Holladay Report was developed together with Jack T. Holladay, MD. The aim was:

- to improve the calculation of IOL for patients who have undergone previous corneal surgery
- to design a display which contains all of the necessary information for screening & treating patients

The proper settings for the Holladay Report are automatically set correctly by default. The settings may be viewed by clicking "Settings" on the tool bar of the Holladay Report and then the color bar settings as shown below in Figure 153.

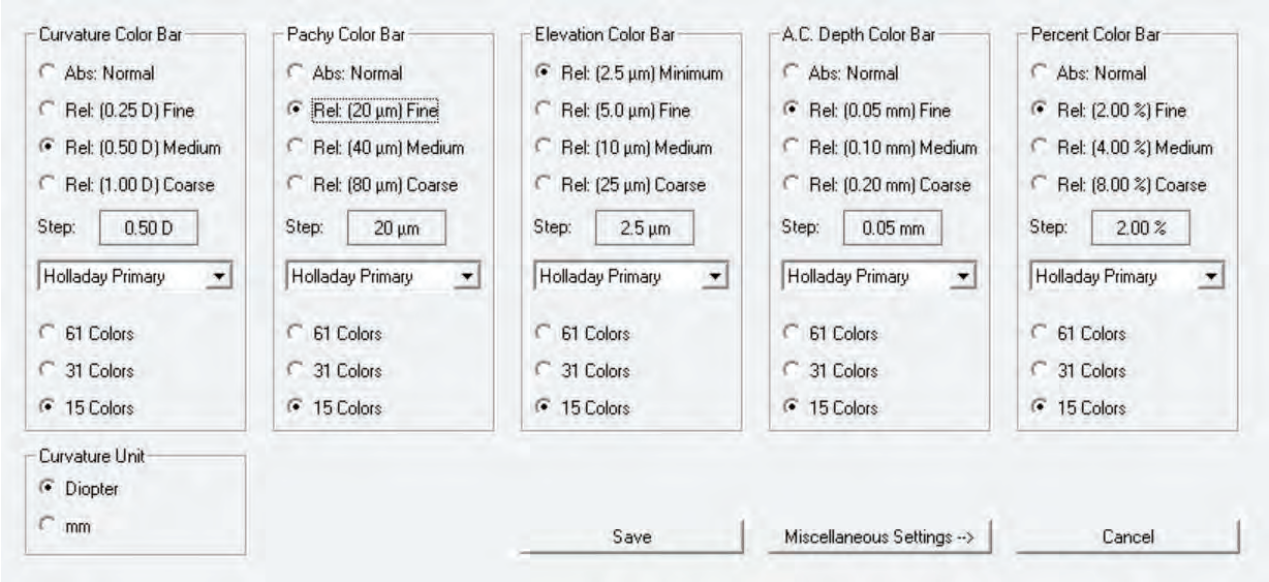

Figure 153: Main color bar settings menu

Then click "Miscellaneous Settings" to confirm all of the other settings. To keep these settings, select "Holladay_Setting" (Figure 154) in the "Load Setting" pull-down menu, then click "Save" and check the "Lock Settings" box.

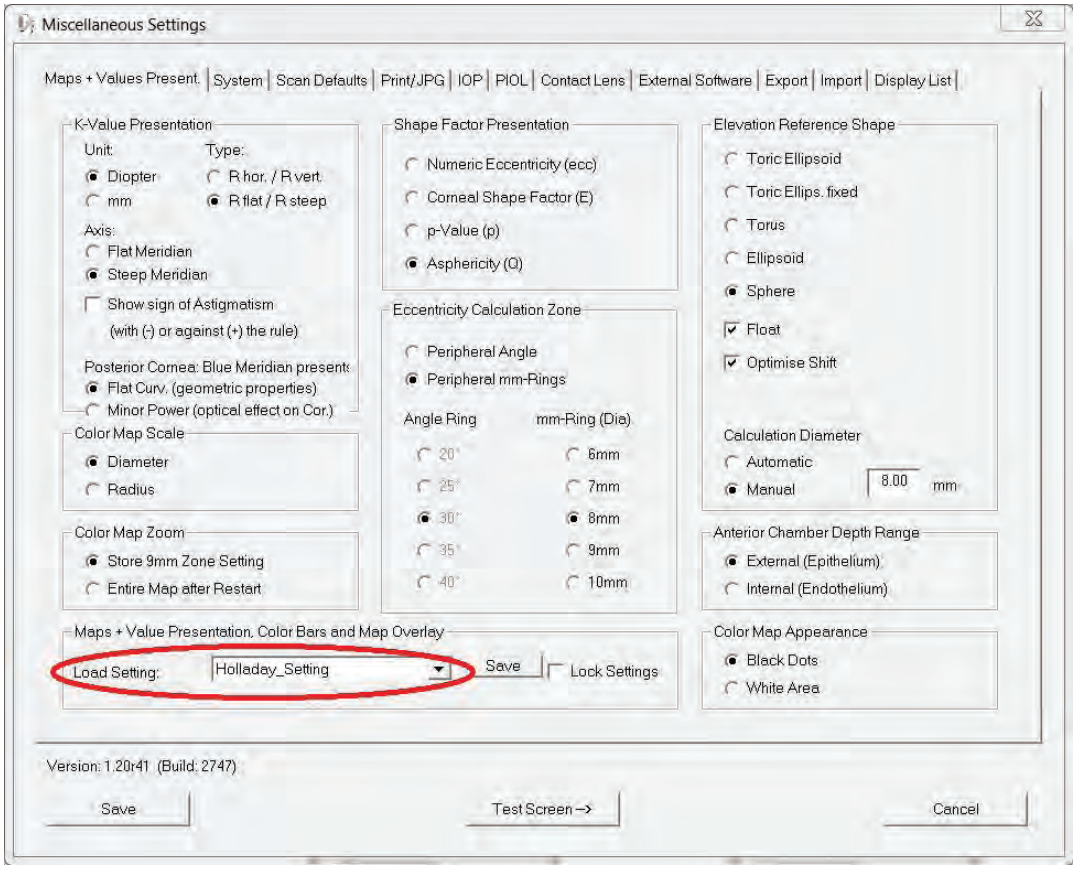

Figure 154: Miscellaneous settings menu

Figure 155 shows the map overlay for the corneal thickness map and Figure 156, the overlay for the other 5 maps.

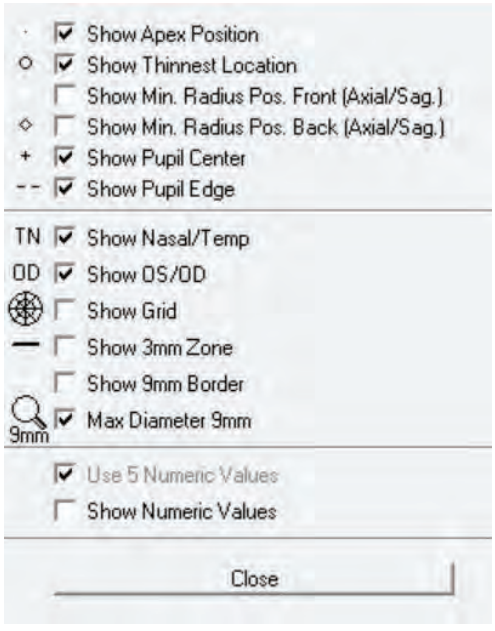

Figure 155: Corneal thickness map overlay

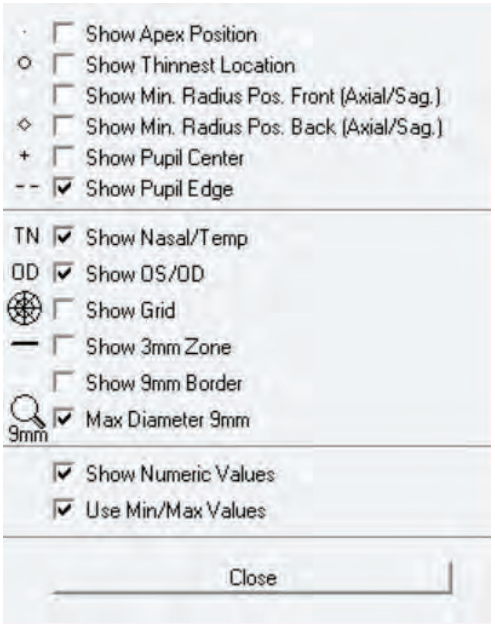

Figure 156: Overlay for the 5 other maps

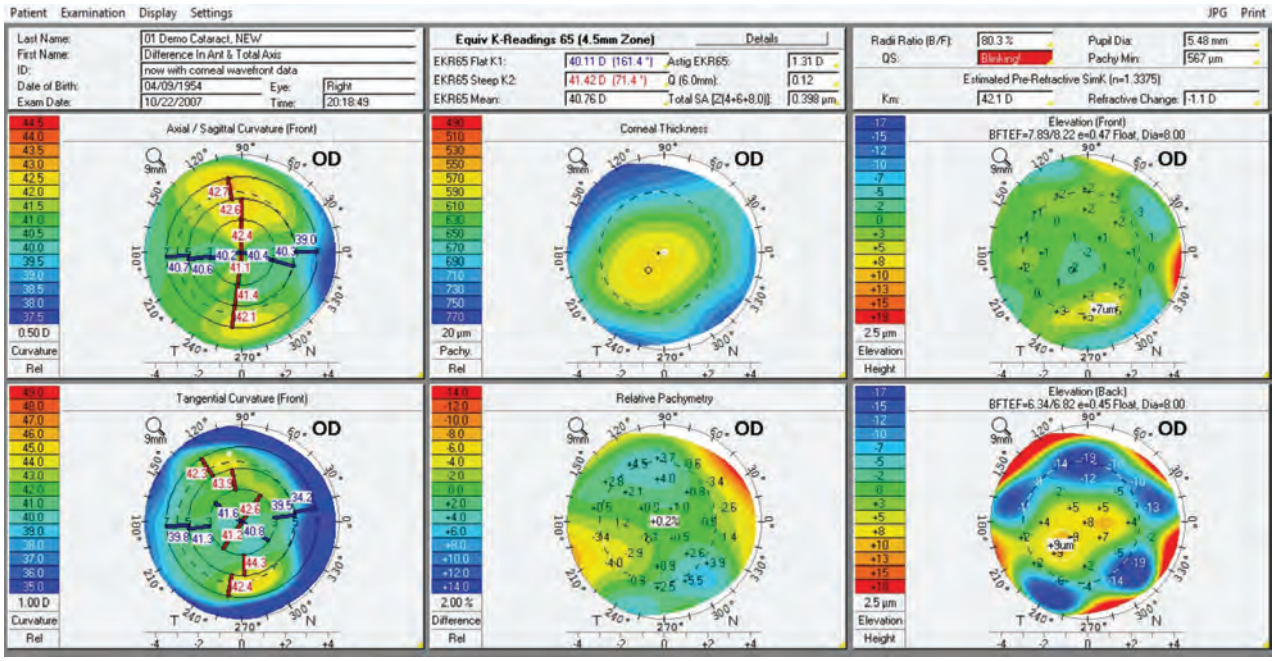

Figure 157: Holladay Report of a normal exam

The **upper left box** in Figure 157 shows the general patient data.

The **center upper box** in Figure 157 shows the Equivalent K-Readings 65 (EKR65) [31] for the 4.5 mm zone along with mean EKR65, astigmatism, Q-value (6 mm zone) and total spherical aberration (SA) [Z(4,0) + Z(6,0) + Z(8,0) for 6.0 mm zone]. The EKR65 values in this have been shown to be optimal values to use in IOL power calculations for K-readings including the amount of corneal astigmatism using the Holladay IOL consultant software. The values include front and back surface power and astigmatism, so no additional adjustments are necessary for the back surface in toric IOL calculations.

The total SA is the sum of the 4th, 6th and 8th order Zernike SA terms and is the best value to use in the selection of aspheric IOLs [32]. Examples of aspheric IOLs are the Tecnis (Advances Medical Optics, Santa Ana, Calif.), with a total SA of 0.27 µm, the Acrysof SN60WF (Alcon Inc., Fort Worth, Texas), which is nominally -0.18 µm and varies with IOL power, and the SofPort AO (Bausch & Lomb, Rochester, New York), which is 0.00 µm [33]. An ocular (corneal + IOL) SA of zero will result in the best visual performance at the target refraction (usually emmetropia). A small amount of residual ocular SA will cause the same amount of blur, whether positive or negative. However, since the pupil constricts in response to near (accommodative) stimuli, negative residual ocular SA results in better near vision, so if there must be a residual SA, slightly negative is preferable.

The **upper right box** in Figure 157 shows the ratio of front to back radii (normal 82.2% ± 2.1%), quality specification QS (i.e. the examination QS of the 3D scan), pupil diameter, pachymetry minimum, estimated k mean before refractive surgery and estimated refractive change due to refractive surgery.

The **upper left map** [axial/sagittal curvature (front)] in Figure 157, shows the axial curvature or power map uses a sph as the reference and the keratometric formula for power (337.5/axial radius in mm). A steel ball with a 7.5 mm radius of curvature would have a uniform power of 45.0 D (337.5/7.5 mm = 45.0 D) at all points. It therefore does not show the refractive power (using Snell's Law) of the cornea except in the central 3 mm, where the difference is negligible. Since the normal shape of the front surface of the cornea is a prolate ellipsoid with the radius of curvature steepest in the center and flattening as we move peripherally, the colors do become cooler (toward blue) by 1 to 2 D , but are less than the actual refractive power using Snell's Law. The mean and SD for central keratometry (axial power in 3.2 mm ring) are shown in Table 1.

Central keratometry (front)*			
		lower limit	upper limit
	central K	central K min	central K max
	(D)	(D)	(D)
mean	43.82	--	--
± SD	1.51	42.31	45.33
±2 SD	3.02	40.80	46.84
±3 SD	4.53	39.29	48.35

Table 1: Central keratometry (front) (*N = 1243 normal eyes, internal, unpublished data by J. T. Holladay)

Tables 1-8 (N = 1243 normal eyes, internal, unpublished data from J. T. Holladay's refractive surgical practice) give the mean, SD, 2 SD and 3 SD upper and/or lower limits for each variable assuming a normal distribution. For 1 SD, 68% would be between the lower and upper limit, 16% would be above 45.33 D and 16% below 42.31 D. Similarly, for 2 SD 2.3% would be below 40.80 D and 2.3% would be above 46.8 D (1 in 44 cases) and for 3 SD 0.1% would be below 39.29 D and 0.1% would be above 48.35 (1 in 769 cases). In general, values beyond 2 SD are suspicious of pathology and those beyond 3 SD are considered abnormal statistically.

The steep (red) and flat (blue) semi-meridians (principal) are shown in the 3 mm, the 3 – 5 mm and 5 – 7 mm diameter zones. If these semi-meridians do not form single meridians (one line) and are not orthogonal, then irregular astigmatism is present and the axis and magnitude are less accurate.

The **lower left map** [tangential curvature (front)] in Figure 157 shows the front tangential curvature (or instantaneous curvature) map does not depend on a reference axis (axis through vertex normal), and the radius is not the distance from the surface to the axis, as with axial radius. It is the radius of curvature (reciprocal the curvature) relative to the surface at that point. For example, if the earth has an average radius of 4000 miles and if there was a semicircular mountain of 6 miles, the axial radius would be 4006 miles from the center of the earth to the top of the mountain but the tangential radius would be only 6 miles ... a significant difference. The tangential curvature or power is much more sensitive and shows geometrical changes much more sensitively. Because of this increased sensitivity the default scale is in 1 D steps, whereas the axial map is in 0.50 D steps [34] (Table 2).

maximum tangential K (front)*			
		lower limit	upper limit
	central K	central K min	central K max
	(D)	(D)	(D)
mean	45.55	--	--
± SD	1.84	43.71	47.40
±2 SD	3.69	41.87	49.24
±3 SD	5.53	40.02	51.08

Table 2: Maximum tangential K (front) (*N = 1243 normal eyes, internal, unpublished data by J. T. Holladay)

The **central upper map** (corneal thickness) in Figure 157, shows that the shape of a normal cornea is a negative meniscus lens (i.e., the back surface radius of curvature is steeper than the front) which is thinnest at its optical center and thickens by the square of the distance from the center. The positive total power is a result of air in front and aqueous behind. The shape of the central color zones should be circular if no significant astigmatism is present and elliptical if there is astigmatism. In either case the small black circle (TP) should be at the center of the ellipse (or circle). It will be temporal and either inferior or superiorly to the apex (vertex normal of Purkinje-Sanson Reflex I, white circle), which is the normal center of all maps. This point is also very near the visual axis and is usually considered to be this point. The dashed black circle is the border of the pupil and the black dot is the centroid of the pupil. The pupil center is also temporal to the apex and may also be inferior or superior. The angle between the apex (visual axis) and optical center (TP of the cornea) is referred to as angle alpha and has both a horizontal and a vertical component. The angle between the apex (visual axis) and the pupil center is known as angle kappa and also has a horizontal and a vertical component. The normal values for TP of the cornea are shown in Table 3.

Thinnest pachymetry*			
	thinnest	lower limit	upper limit
	pach	thinnest pach	thinnest pach
	(µm)	(µm)	(µm)
mean	543	--	--
± SD	33	509	576
±2 SD	67	476	609
±3 SD	100	442	643

Table 3: Thinnest pachymetry (*N = 1243 normal eyes, internal, unpublished data by J. T. Holladay)

The central lower map (relative pachymetry)(RP) (Figure 157) shows why a negative meniscus lens has a predictable thickness from its center to periphery, the percentage above or below this value at each point may be calculated. The RP map shows these values at all points. . The minimum RP values are shown in Table 4.

Minimum RP*		
	thinnest	lower limit
	pach	thinnest pach
	(µm)	(µm)
mean	-2.5	--
-SD	-2.6	-5.1
-2 SD	-5.1	-7.7
-3 SD	-7.7	-10.2

Table 4: Min RP (*N = 1243 normal eyes, internal, unpublished data by J. T. Holladay)

The **upper right map** [elevation (front)] in Figure 157, shows the elevation in µm above the BFTEF determined over an 8 mm zone. The Q-value of the ellipsoid for the front surface is fixed at -0.22 (eccentricity =+0.47) and the principal radii are varied for the best least square fit of the surface. The Q-value of the ellipsoid for the back surface is fixed at -0.20 (eccentricity =+0.45) and the principal radii are varied for the best least square fit of the surface. Plus (+) values for elevation are above the reference surface and negative values (-) are below and are all given in µm. The Q-values for the BFTEF are slightly less (-0.22 versus -0.26 for the front and -0.20 versus -0.24 for the back) for both elevation maps because it is the average value for the population when "fit" over an 8 mm zone rather than the normal 6 mm zone. Normal values for front elevations near the minimum RP (Table 5) and maximum elevations at any location (Table 6) for the front surface are given.

Front elevation near min RP*		
	elevation	upper limit
	(µm)	(µm)
mean	+1.0	--
+SD	+2.1	+3.1
+2 SD	+4.2	+5.2
+3 SD	+6.2	+7.2

Table 5: Front elevation near min RP (*N = 1243 normal eyes, internal, unpublished data by J. T. Holladay)

Maximum front elevation*		
	elevation	upper limit
	(µm)	(µm)
mean	+1.0	--
+SD	+1.3	+4.3
+2 SD	+2.6	+5.5
+3 SD	+3.8	+6.8

Table 6: Maximum front elevation (*N = 1243 normal eyes, internal, unpublished data by J. T. Holladay)

The **lower right map** [elevation (back)] (Figure 157) shows the elevation of the back surface in µm relative to the BFTEF over an 8 mm zone. The eccentricity of the ellipsoid is fixed at 0.45 (Q-value = -0.20) and the principal radii are again varied for the best least square fit of the surface. Plus (+) values are above the reference surface and negative values (-) are below, and are all given in µm. Normal values for back elevations near the minimum RP (Table 7) and maximum elevations at any location on the back surface (Table 8) are given.

Back elevation near min RP*		
	elevation	upper limit
	(µm)	(µm)
mean	+6.8	--
+SD	+4.2	+11.0
+2 SD	+8.4	+15.2
+3 SD	+12.6	+19.4

Table 7: Back elevation near min RP (*N = 1243 normal eyes, internal, unpublished data by J. T. Holladay)

Maximum back elevation*		
	elevation	upper limit
	(µm)	(µm)
mean	+8.5	--
+SD	+3.3	+11.8
+2 SD	+6.5	+15.0
+3 SD	+9.8	+18.3

Table 8: Maximum back elevation (*N = 1243 normal eyes, internal, unpublished data by J. T. Holladay)

The asphericity quotient (Q-value) and eccentricity (ε) describe the shape of the elliptical surface ($Q = -\varepsilon^2$). These and the computed Zernike as well as the Seidel Longitudinal SA for a 6 mm zone are shown in Table 9.

Variables indicating shape and SA of cornea front surface*			
Q-value	Eccentricity (ε)	Zernike (4,0) -- SA	Seidel Longitudinal SA (D)
-0.54	+0.73 ($Q = -\varepsilon^2$)	0.00	0.00
-0.26	+0.51 ($Q = -\varepsilon^2$)	+0.19	+1.03
0.00	0.00	+0.38	+2.10
+0.26	0.51 ($Q = -\varepsilon^2$)	+0.59	+3.24
+0.54	0.73 ($Q = -\varepsilon^2$)	+0.81	+4.46

Table 9: Variables indicating the shape and SA of the corneal front surface (* All variables are computed over a 6 mm corneal zone based on an anterior corneal apical radius of 7.71 mm, a corneal index of refraction of 1.376 and a wavelength of 0.555 µm, using an elliptical model.)

17.2 Holladay EKR65 Detail Report

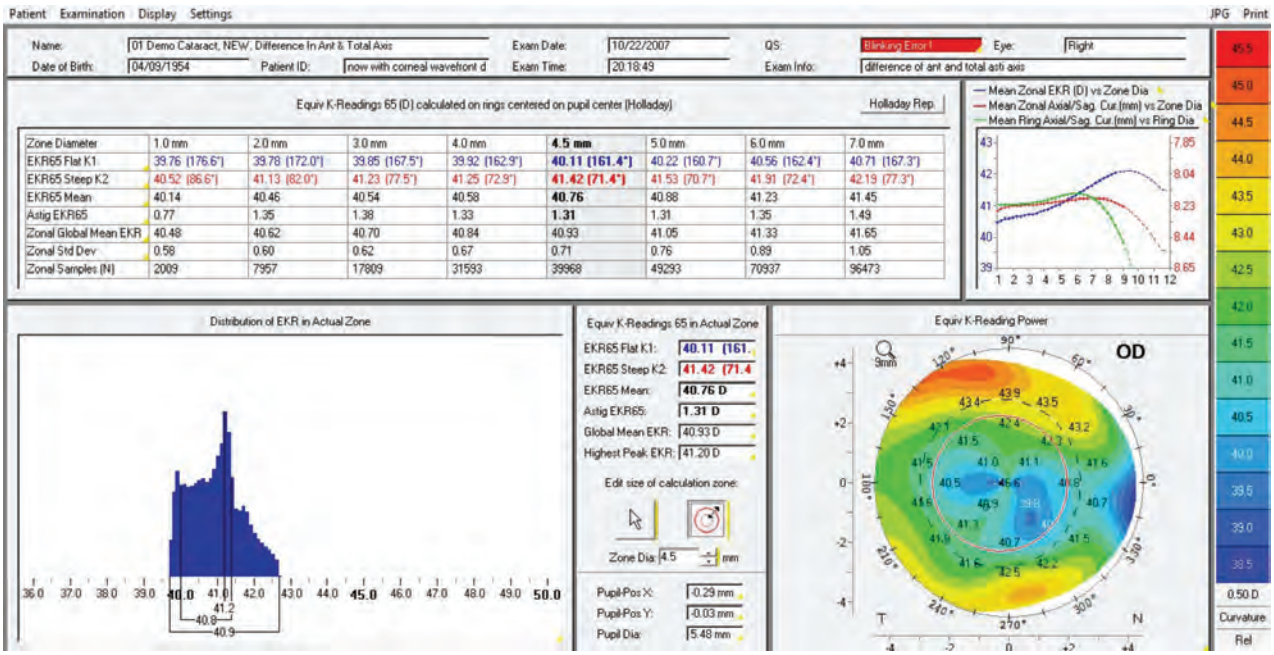

Figure 158: Holladay EKR65 Detail Report of a normal exam

The **upper box** in Figure 158, shows the demographic information regarding the patient is in the box at the top of the Page 2.

The **upper left box** (Figure 158) shows the table for the EKR65 (D) for various parameters from 1.0 to 7.0 mm [35,36,37]. All values are calculated from the pupil center, so that only rays actually contributing to the retinal image are used.

The **upper right graph** (Figure 158) shows the mean zonal EKR (D) versus zone diameter (blue), the mean zonal axial radius of curvature (mm) versus zone diameter (red) and the mean ring axial radius of curvature (mm) versus zone diameter (green). The blue values represent refractive power (D) of a zone as one moves from the center of the pupil. The increase in power reflects the normal presence of positive SA in the human cornea (approximately 2 D from center to periphery).

The **lower left graph** in Figure 158, is a histogram showing the relative frequency of EKR power over the selected zone (default is 4.5 mm zone). The graph is rarely symmetrical and often has multiple peaks with a nominal 2 to 3 D range.

The **lower central table** in Figure 158, shows the EKR65 mean, is the weighted mean where 65% of the values are represented using the smallest range of points. In the above graph this value is 40.76 D (40.8 D) for the range indicated. Note that this value is less than the 40.93 D global mean of EKR that results when all points are used. The highest peak is at 41.20 D. In a normal cornea these three values will vary by less than 0.50 D. The actual size of the pupil during the exam is shown with a dashed circle. The zone diameter may be changed by using the up or down arrow button or by clicking the red graphic and dragging the red circle larger or smaller diameter. The new values are calculated instantaneously.

The **lower right map** (Figure 158) shows the EKR power map uses both front and back power, "Snell's law, and represents the values that are appropriate for IOL power calculations. The EKR65 flat K1 (40.11 A 161) and EKR65 steep K2 values (41.42 A 71.4) are the appropriate values to enter for K-readings. No additional adjustment needs to be made for back surface power or toricity. The 4.5 mm zone has been shown to be the best value for large data sets, but for a specific patient the value may be customized to the individual patient (values from 3.0 to 4.5 mm zonal diameter may be used). For example, if a patient has an unusually small pupil (3.0 mm) at mesopic light levels and the EKR65.

17.3 Case 1: Holladay Report & Holladay EKR65 Detail Report of a normal exam

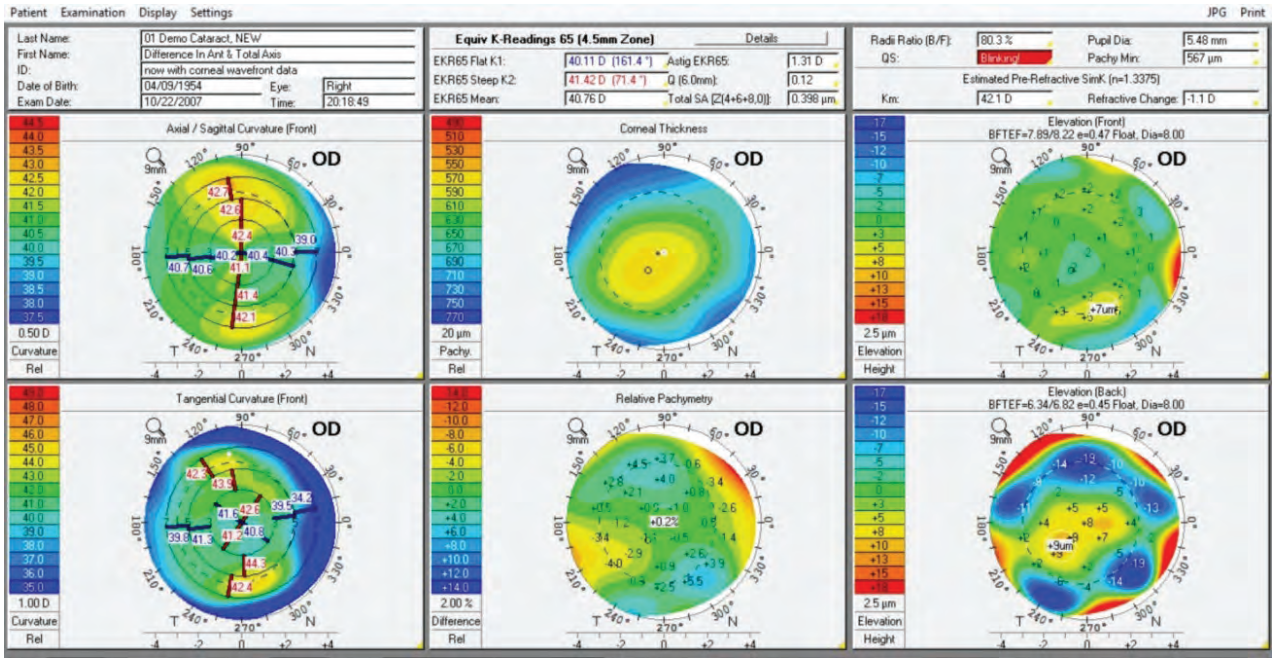

Figure 159: Holladay Report of a normal exam

The EKR65 values at the top center (Figure 159) are approximately 3.0 D flatter than average with 1.31 D of astigmatism. In the axial power map corneal power is steeper above than it is below by around 1.0 D, which is not unusual. The broken semi-meridian lines show mild irregular astigmatism which have been orthogonalized to the best least squares fit of 161.4° for the flat meridian and 71.4° for the steep meridian axes for both the front and back surface. Since the irregular astigmatism is mild and the magnitude of 1.31 D relatively low, this orientation is desired for a toric IOL. It should be noted, however, that repeated measures and using the average magnitude and axis would improve results even more. The tangential curvature map also illustrates the irregular astigmatism component due to the broken semi meridian lines.

The Q-value over the 6.0 mm zone is 0.12, which is more positive than normal (-0.26), so more SA is expected. Table 10 shows the normal values for the Q-value, eccentricity, total Zernike SA (µm) at the corneal vertex and Seidel SA (D) at the retina plane. The total SA confirms the increased SA with a value of 0.398 µm, which is much higher than the average of 0.27 µm. The total SA is the value that should be used for the selection of an aspheric IOL for a specific patient [38]. The radii ratio (back/front) is 80.3%, which is lower than the normal ratio. Although this cornea has not had myopic refractive surgery (LASIK or PRK), the percentage gets lower the greater the amount of the treatment. In this case the estimated K pre-refractive surgery is 42.1 D, and a refractive change is -1.1 D. These are the values that would be used for the historical method from traditional keratometry for comparison with the EKR65, when no historical information is available regarding the refractive surgery. The pupil diameter is 5.48 mm and taken with low light levels, but depending on the location of the device (illuminated room), the value is usually smaller than the scotopic pupil size one obtains with infrared pupillometers that would in complete darkness. In this case, the value is larger than 4.5 mm, so this zone would be appropriate for the EKR65 values for this patient. When the patient's pupil is 3.0 or 4.0 mm, then going to the appropriate columns for the EKR65 valueis recommended. The pachymetry min is 567 µm, which is thicker than average (555 µm). Note that the QS shows "blinking" and should be repeated. The Scheimpflug images may be reviewed to see how many were corrupted by the blink.

In the corneal thickness map the TP of the cornea (small black circle and optical center) is at the centroid of the elliptical colour zones, as it should be. The pupillary center (black and white cross hair) and apex (small white spot with black dot) are located temporally. Angle alpha is the angle or distance between optical center and apex (visual axis), which has both a significant vertical and horizontal component. Diffractive and refractive multifocal IOL perform best when located at the pupillary center and visual axis. If these IOLs are to be used, the surgeon should note these locations because the IOL will normally center in the bag at the optical center, rather than the pupil center and visual axis. The IOL haptics will need to be "nudged" to achieve the optimal lens performance. The RP is normal with a distribution that parallels the steep and flat meridians. The flatter meridian usually has negative values (thinner) that are similar to the positive values (thicker) in the steeper meridian. The elevation maps are normal, even with the lobulated pattern on the elevation (back), since these values would result in thicker corneal pachymetry in these areas. Positive elevations on the back surface are the most important values indicating the possibility of a thinning disorder.

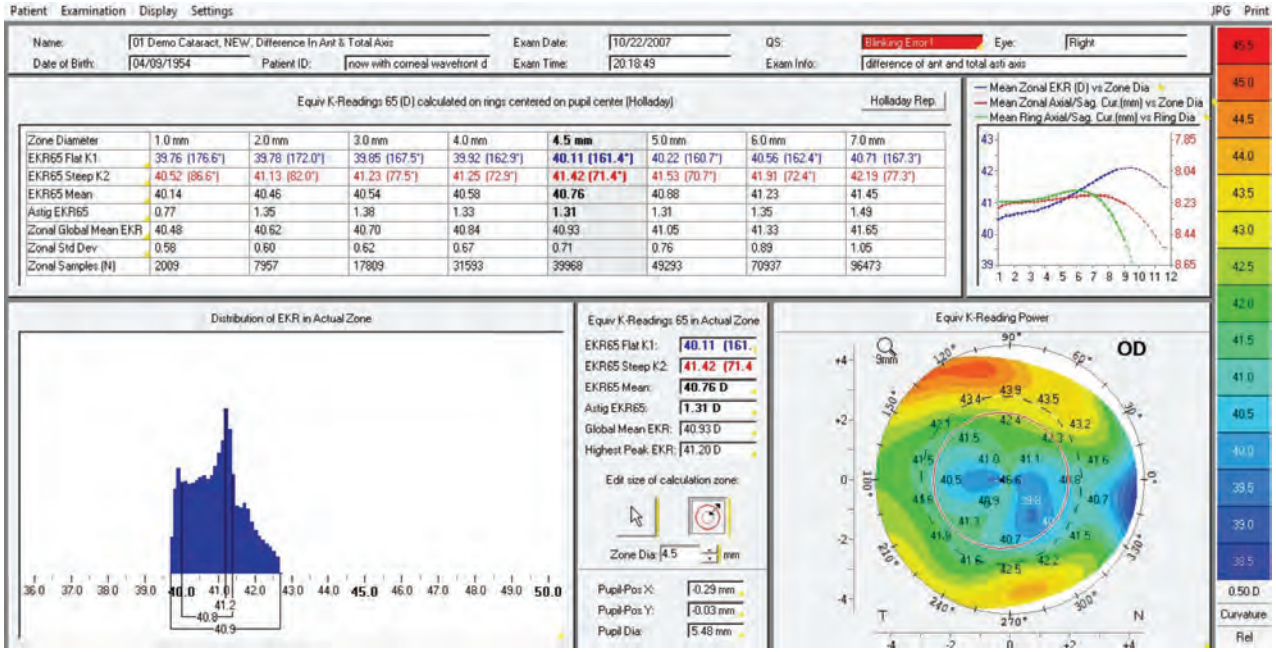

Figure 160: Holladay EKR65 Detail Report of a normal exam

With a normal pupil of 5.48 mm the 4.5 mm grey column, with EKR65 flat K1 = 40.11 A 161° and steep K2 = 41.42 A 71° (Figure 160), would provide the correct keratometric values to enter into an IOL calculator for the proper spheroequivalent power and toricity of the IOL. An exact toric calculator such as the one provided in the "Holladay IOL Consultant Program" (www.hicsoap.com) which does not use a constant ratio of the corneal astigmatism to the ideal toricity of the IOL [39]. When EKR65 values are used and an exact toric calculator, the back surface power and astigmatism have been already been implemented and there is no need for additional adjustments!

The blue line in the upper right graph demonstrates that there is approximately a 0.75 D increase in power from the 1 to 4.5 mm zone. This was also confirmed by the Q-value and total SA values on page 1. Note the EKR65 uses "Snell's law, whereas the axial power lines (green and red) are not and therefore do not reflect actual refractive power changes due to the cornea.

The distribution of EKR in the 4.5 mm zone shows that the EKR65 mean (40.76), global mean (40.93) and the highest peak (41.20) are all within 0.50 D of each other. The difference in these values is a measure of the irregular astigmatism as well as a measure of the precision of the EKR65, which is the best value to use. The greater the differences, the broader the range of the distribution and the greater the number of individual peaks, the lower is the reliability of the EKR65 which results in a lower predictability of the IOL power outcome. Multiple examinations are helpful for repeatability, but when the range is large the patient should be prepared for the possibility of a "fine tune" to achieve the exact refractive spheroequivalent power target and elimination of astigmatism. The EKR map in the lower right allows the clinician to see the EKR distribution graphically.

17.4 Case 2: Holladay Report & Holladay EKR65 Detail Report of a keratoconus exam

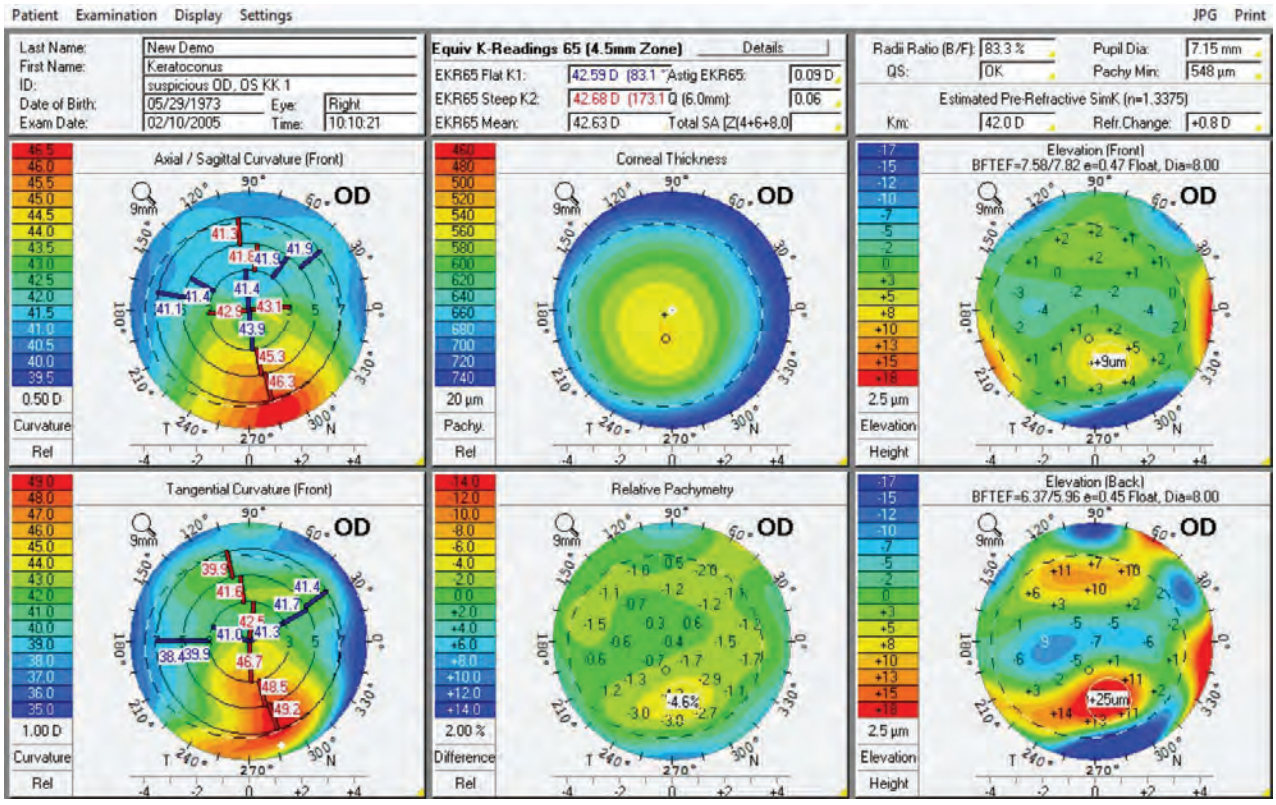

Figure 161: Holladay Report from a keratoconus exam

The axial power map scale is centered at 43.0 D (green), which is normal. The axial and tangential curvature maps show a "hot spot" with the peak at 8 mm on the axial map and 6 mm on the tangential map (Figure 161). The peak is geometrically more accurately located on the tangential map. The corneal thickness map shows the TP is displaced inferiorly by almost 1 mm, slightly nasally and is not at the center of the vertical ellipse. A vertical ellipse with the TP inferior is suggestive of keratoconus. The ellipse may also be egg-shaped in severe cases, with the small end of the ellipse pointing in the direction of the "hot spot" on the curvature maps. On the RP map the minimum -4.6% is at the limit of suspicious and is also located at the point of peak power on the tangential curvature map. The elevation (front) is +9 µm and located at the "hot spot" and minimum of the RP. The elevation (back) is highly elevated, at 25 µm above the reference BFTEF, and also at the same location as the peak on the front. It is typical in keratoconus for the back elevation to be higher than the front, due to epithelial remodeling on the front. The average thickness of the epithelium is 50 µm, and 6 – 8 epithelial cell s thick. The 16 µm higher on the back (25 – 9 µm) indicates that the epithelium is ~2 cells thinner than normal due to the protrusion and physiologic smoothing of the surface.

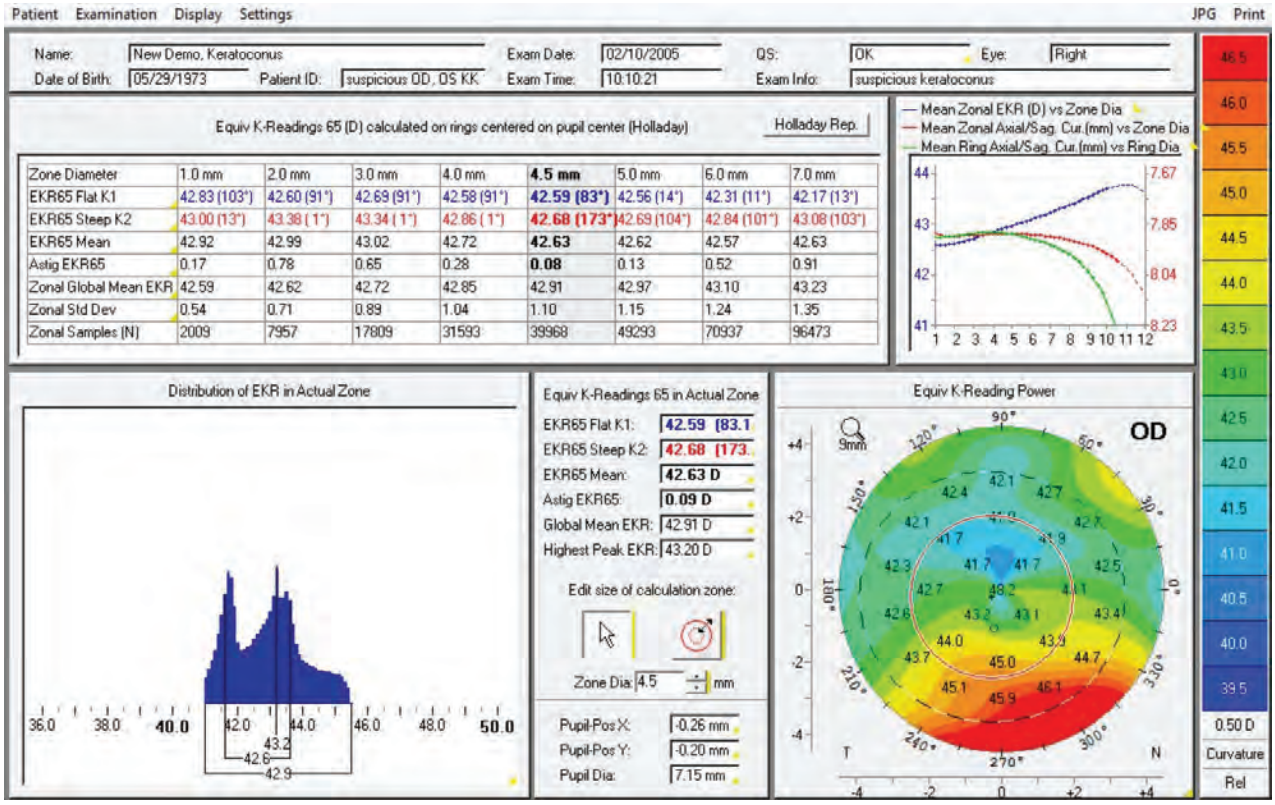

Figure 162: Holladay EKR65 Detail Report from a keratoconus exam

The distribution of EKR is a bimodal (2 peaks) (Figure 162) distribution, and the EKR65 of 42.63 D is 0.57 D less than the 43.20 D peak. Standard keratometry usually measures nearer the peak and will over-estimate the power in keratoconus, leaving the patient with a hyperopic surprise. In severe cases, this difference may be up to 3 or 4 D. The K values that should be used for this case are the EKR65 flat K1 = 42.59 A 83° and EKR65 steep K2 = 42.68 A 173°. In the EKR65 table the EKR65 mean varies very little, from 43.02 to 42.63 (0.39 D), from the 3 to 4.5 mm zone. The EKR65 power increases SA as the pupillary diameter increases. This visual performance is also affected by KC and is limited by the irregular astigmatism in the cornea. Regular astigmatism is also often present, but determining the ideal toricity is ambiguous at best, and stability of the astigmatism is also a problem. In our experience, determining the optimal toric IOL power almost always involves an intra-operative refraction or postoperative refraction and a secondary procedure to achieve the optimal toric IOL.

17.5 Case 3: Holladay Report & Holladay EKR65 Detail Report of a post LASIK exam

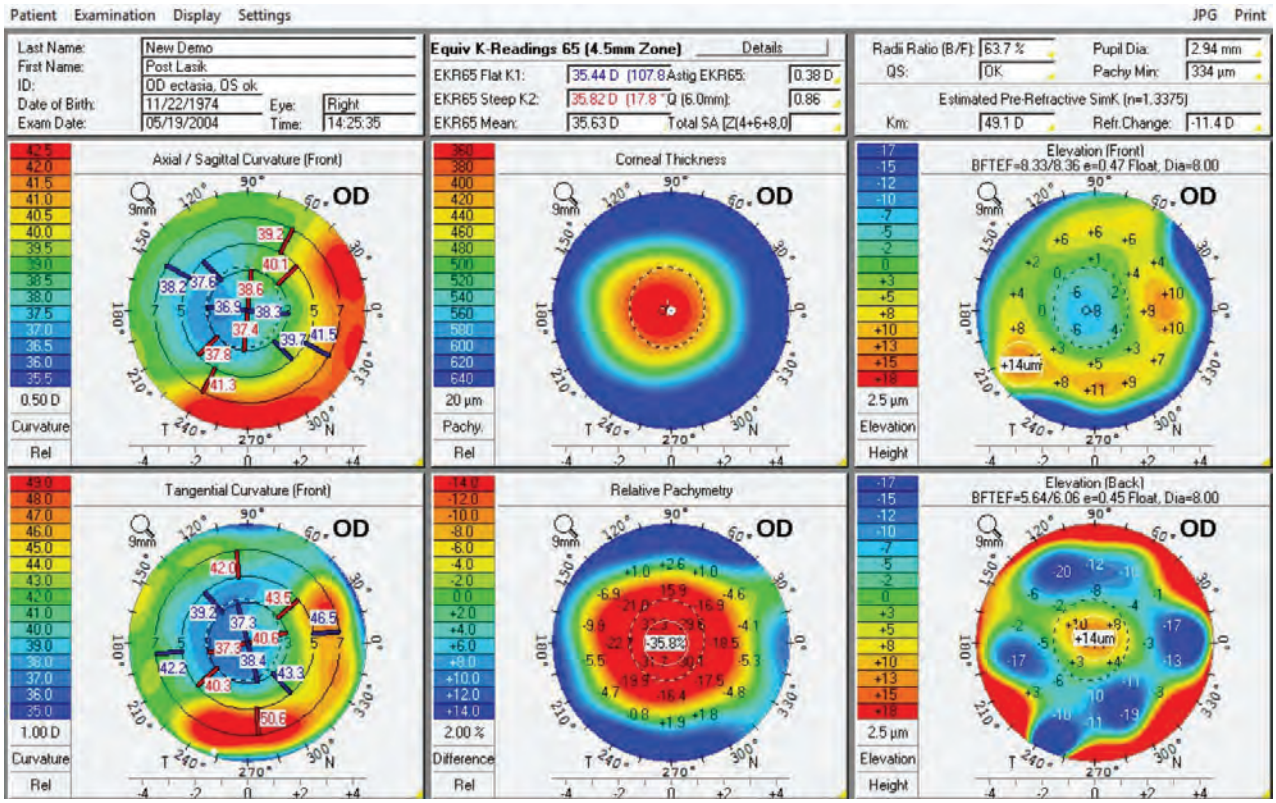

Figure 163: Holladay Report of a post LASIK exam

The mean value of the color scale (green) is 39.0 D, which is 4.5 D flatter than normal, and the semi-meridian lines are extremely segmented, demonstrating a large amount of irregular astigmatism. The EKR65 mean is 35.63 D, which is ~ 8 D flatter than normal (Figure 163). The corneal thickness map shows that the TP, pupillary center and vertex normal are almost coincident and at the center of the almost circular color rings. The RP map is also circular, 35.8% thinner than normal at the center and gradually returning to normal (green) at the 6 mm diameter. The center has a front elevation (front) is -8 µm at the center and on the elevation (back) is + 14 µm. This elevation on the back is suggestive of ectasia.

The steepened radius on the back surface of the cornea from the ectasia results in a 63.7% radii ratio (back/front) and results in the program determining the estimated refractive change to have been -11.4 D, with a pre-op mean K = 49.1 D. The actual measured pre-op K mean before surgery was 45.5 D, and the actual refractive change was -7.8 D. The ectasia has thus caused the program to overestimate the change. In normal refractive surgery the estimated refractive change and estimated pre-op mean K are much more accurate.

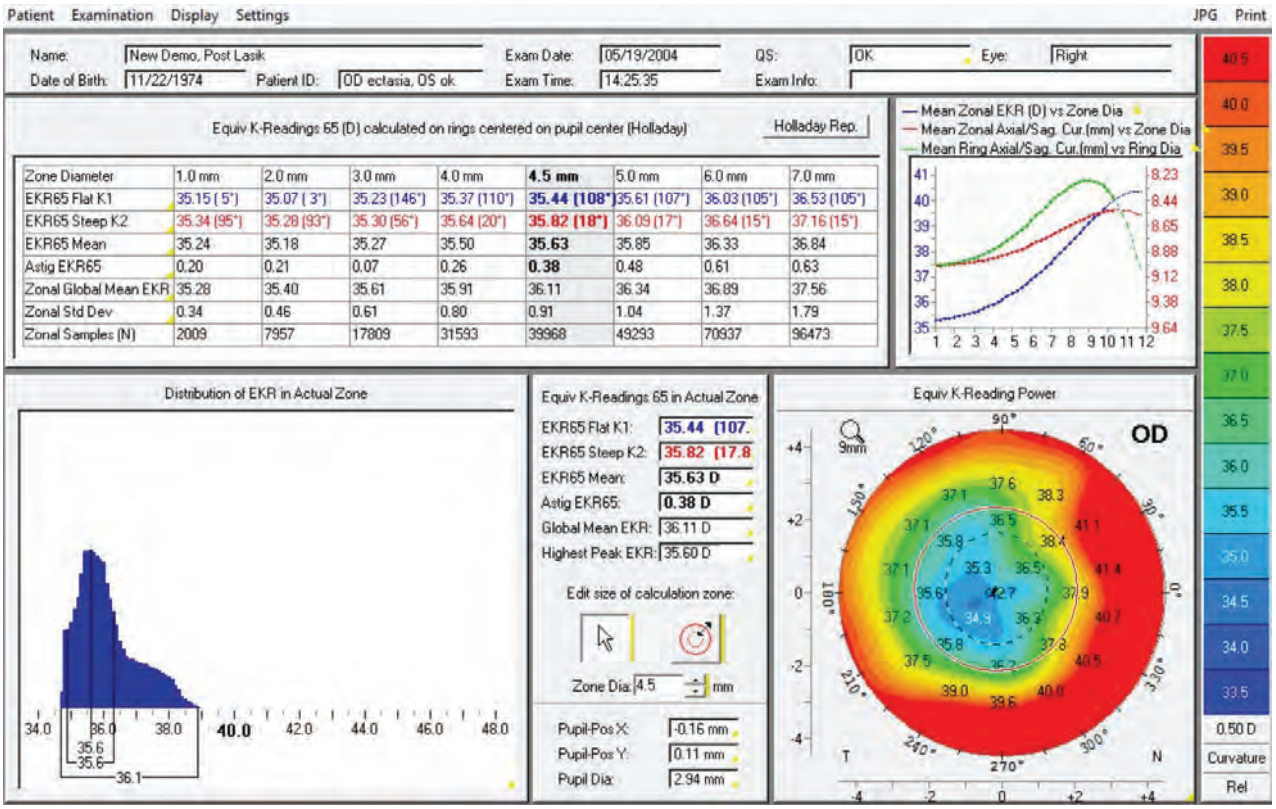

Figure 164: Holladay EKR65 Detail Report of a post LASIK exam

The EKR65 mean is 35.63 D at the 4.5 mm zone and 35.27 D at the 3.0 mm zone (Figure 164). The pupil diameter was 2.94 mm and confirmed with scotopic pupillometry done with another device. Due to the small pupil, the appropriate Ks for IOL calculation would be at the 3.0 mm zone and are EKR65 flat K1 = 35.23 A 146° and EKR65 steep K2 = 35.30 A 56°. The axes are quite different from the 4.5 mm zone, but this is due to the small magnitude of the astigmatism and is seen in the segmented semi-meridian lines in the axial and tangential maps.

18 Corneal tomographic analysis is essential before cataract surgery - 4 steps in screening candidates for premium IOLs by Prof. Naoyuki Maeda

New advancements in surgical techniques have improved the safety and efficacy of cataract procedures to a remarkable level. As a result, indications for cataract surgery have expanded, and cataract patients' expectations for post-surgical results have grown.

The introduction of premium IOL or new technology IOLs such as multifocal IOL, toric IOL, and aspherical IOLs have enabled us to modify the optical properties of the eye postoperatively in tailor-made fashion. While the choice of an IOL, aside from its power, was not so critical from the patient's point of view in the days when only spherical IOLs were available, today, his or her postoperative satisfaction will depend not only on the power but also on the optical characteristics of the IOL.

Therefore, it is important for cataract surgeons to understand the lifestyle of each patient, the ocular pathology, and the optical quality of the eye before surgery. This article explains on the basis of case examples how the Pentacam® can be used for assessing corneal optical quality for the selection of premium IOLs. In the process it conveys the importance of corneal tomographic screening before cataract surgery.

18.1 Corneal topography for selecting premium IOLs

When planning for the implantation of a new technology IOL surgeons have to select one particular IOL from at least four kinds of IOL for the recipient patient. They must evaluate the optical quality of the cornea during the preoperative evaluation, because suboptimal optics of the cornea or could lead to a postoperative refractive error or spoil the outcome in other ways.

We have been proposing four steps for the interpretation of corneal tomography before performing cataract surgery as shown in Table 10.

Step 1: **Evaluation of corneal irregular astigmatism**	Check the irregular astigmatism with the refractive power map qualitatively, and with total HOA quantitatively. The current cut-off value of less than 0.3 µm (RMS, 4mm) for multifocal IOLs, and more than 0.5µm (RMS, 4mm) for the informed consent about significant irregular astigmatism is important.
Step 2: **Detection of abnormal corneal shape**	Check the abnormal corneal shape with the axial power map qualitatively, and with sagittal front-back ratio quantitatively. Determine whether to select the routine method or special method for IOL power calculation.
Step 3: **Evaluation of corneal spherical aberration**	Check the corneal spherical aberration. The tentative cut-off value of 0.1µm (RMS, 6mm) or higher for aspherical IOL and less than 0.1µm (RMS, 6mm) for spherical IOL.
Step 4: **Evaluation of corneal cylinder**	Compare the magnitude and axis of cylinder between K readings and wavefront. Consider surgical correction of regular astigmatism depending on the magnitude and axis.

Table 10: 4 steps in the interpretation of corneal tomography

The Pentacam® is a Scheimpflug based corneal tomographer. We have been able to develop a program which makes it easy to perform the 4 steps of the screening procedure as described above.

Similar to the manual keratometer, it is very important to confirm the reproducibility of the data before attempting an interpretation. Especial attention should be paid to patients of very advanced age, patients with a narrow palpebral fissure, or patients with poor fixation during measurement. If QS (quality specification) in the map is indicated with red color, the data should not be used. In cases of doubt the measurements should be repeated until reproducible topographic maps are obtained for each eye.

Figure 165, Figure 166, Figure 167 are the examples of the output. This display consists of 3 topographic maps, one Scheimpflug image, and one data box. The upper left is the axial power map, which is based on anterior surface data with a keratometric refractive index of 1.3375. This map is used to determine any abnormality in corneal shape. In the upper center is the map of Total Corneal Refractive Power (TCRP). TCRP (n=1.376 for cornea, n=1.336 for aqueous) is calculated from the anterior and posterior refractive power of the cornea while considering corneal thickness and Snells law of refraction. It can be for IOL power calculation for patients with corneal shape abnormality such as in post-LASIK, post-PTK, and post-keratoplasty. In the upper right is the corneal pachymetric map. This map can be used to check the thickness at the main incision and at the side ports. The Scheimpflug image can be used to show the cataract to the patients and also to check the ACD. The data box shows tomographic indices including total corneal refractive power, corneal irregular astigmatism (total higher-order aberration), corneal SA, and corneal cylinder. In addition, simulated K readings, ACD, pupil diameter, corneal thickness and others are available.

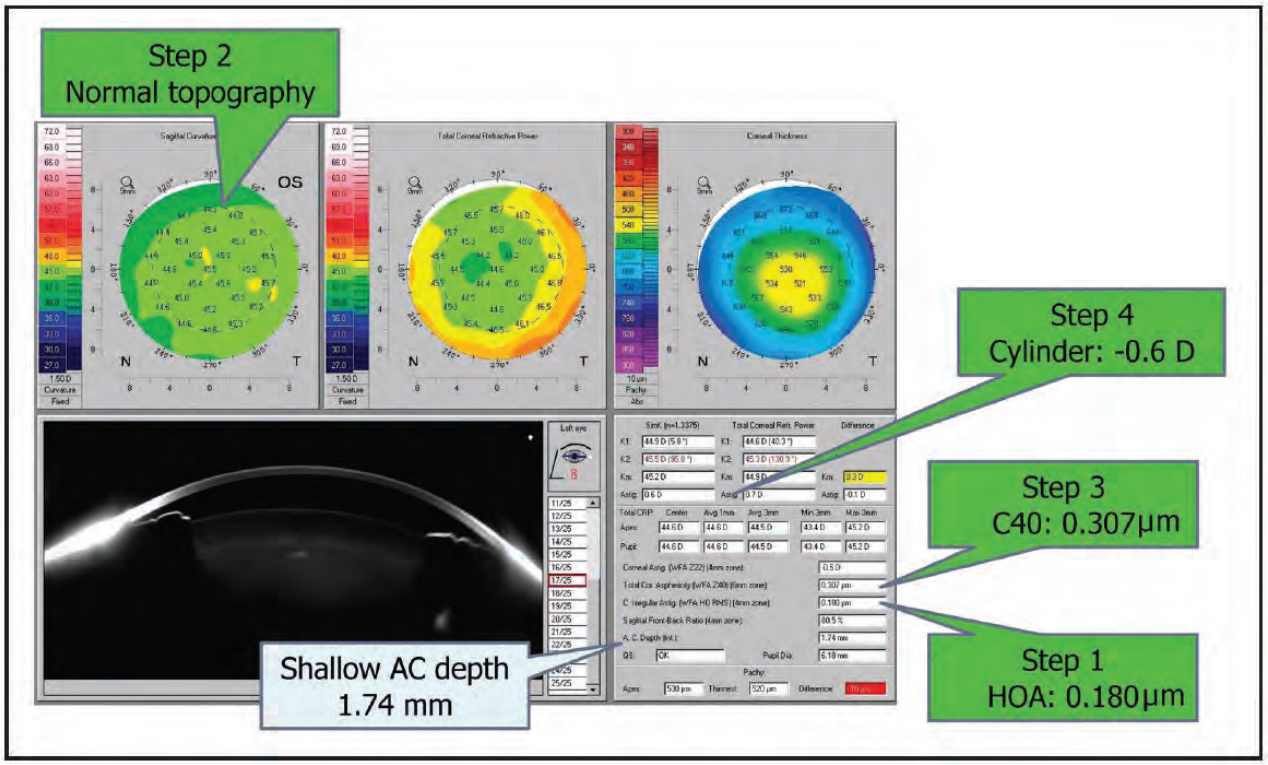

Figure 165: Cataract Pre-OP Display normal cornea with a shallow anterior chamber

Total HOA (0.180 µm), SA (0.307 µm), front-back ratio (80.5 %), and cylinder (-0.5 D) are within normal ranges. Either multifocal aspherical IOL or monofocal aspherical IOL will be fine in terms of optical quality of the cornea, although the anterior chamber is shallow (1.74 mm).

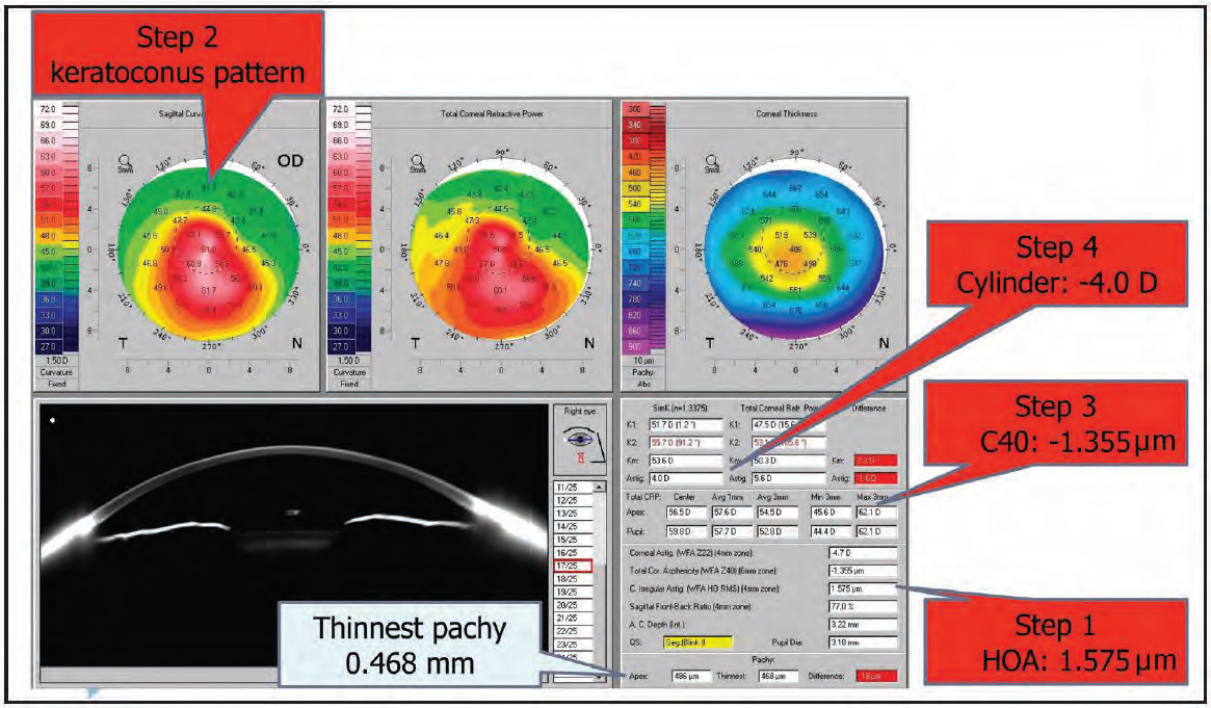

Figure 166: Cataract Pre-OP Display moderate keratoconus

Total HOA (1.575 µm) is high, and SA (-1.355 µm) is too low. Conventional spherical IOL is recommended after obtaining the patient's informed consent regarding the effects of corneal irregular astigmatism on quality of vision.

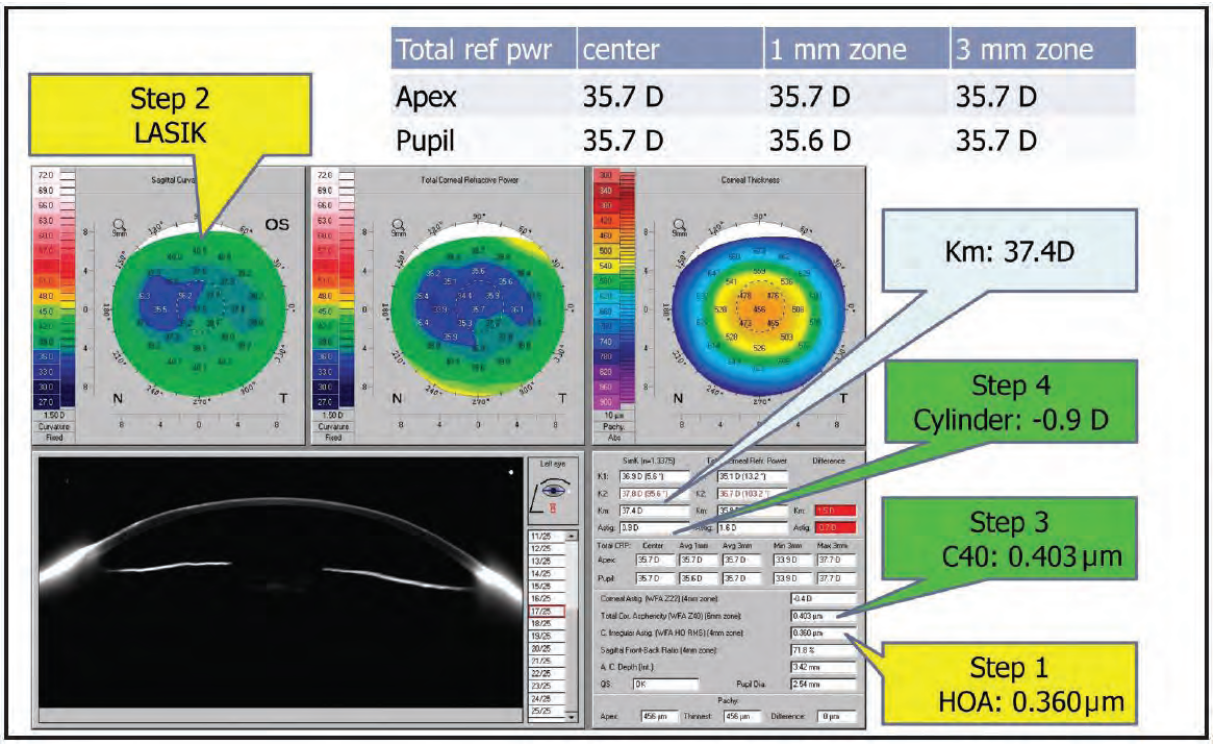

Figure 167: Cataract Pre-OP Display post LASIK

Total HOA (0.360 µm) shows mild irregular astigmatism, and SA (0.403 µm) is relatively high but within the normal range. A monofocal aspherical IOL is recommended and should be calculated using special IOL formulas for post-LASIK.

18.2 Step 1: Evaluation of corneal irregular astigmatism

Although there is no inherent problem in performing cataract surgery in patients with mild pterygium, subclinical keratoconus, or mild corneal scar, it is possible for irregular astigmatism associated with these corneal diseases to affect the quality of vision of the eye after surgery [40]. In times when cataract surgeries were only performed in patients with advanced visual loss surgeons did not need to pay as much attention to conditions of mild irregular astigmatism because this seemed negligible given the remarkable improvement in visual acuity achieved. Today however, in patients with relatively mild cataract or premium IOL recipients, mild irregular astigmatism can be a later cause of dissatisfaction when postoperative visual acuity or contrast sensitivity did not improve as expected.

Preoperative evaluation of corneal irregular astigmatism and obtaining the patient's informed consent regarding the effects of corneal irregular astigmatism on quality of vision can help to avoid claims after surgery also when a conventional IOL is being considered. Even mildly elevated HOAs can be the cause of suboptimal results with multifocal IOLs, as has become clear from the improved outcomes achieved with aspherical multifocal IOLs. Currently we have our cut-off value for total HOAs at 4 mm diameter at 0.3 µm for mild irregular astigmatism and at 0.5 µm for moderate irregular astigmatism.

18.3 Step 2: Detection of abnormal corneal shape

After many years Laser in Situ Keratomileusis (LASIK) has become a popular and well-established method of correcting refractive errors. A current topic of discussion however is how postoperative refractive errors can be avoided following cataract surgery in post-LASIK patients. As is well known, patients for whom IOL power was calculated by conventional methods often experience a hyperopic shift in postoperative refraction, disappointing their hopes for good uncorrected visual acuity following cataract surgery.

To avoid postoperative errors in these patients it is important to review the tomographic map so as not to overlook any abnormality of corneal shape. IOL power should be calculated using suitably modified methods [41], while in the no-history methods one can use total corneal refractive power.

18.4 Step 3: Evaluation of corneal spherical aberration

Aspherical IOLs are widely applied for correcting the average corneal SA [42]. However, corneal SA varies widely even in the normal population. In addition, there are reports of myopic LASIK patients having higher positive SA [43] and hyperopic LASIK and keratoconus patients having lower negative SA. Measuring corneal SA in candidates for an aspherical or spherical IOL is in any case a reasonable approach. At present we use a cut-off value of 0.1 µm or higher for aspherical IOLs.

18.5 Step 4: Evaluation of corneal cylinder

Toric IOLs are effective in obtaining good uncorrected visual acuity in patients with regular corneal astigmatism. However, severe irregular corneal astigmatism is considered as a contraindication to toric IOL implantation. Therefore, it is critical to evaluate not only corneal regular astigmatism with a manual keratometer but also corneal total HOA with a corneal tomographer. Comparisons between manual keratometry and wavefront analysis results on the magnitude and axis of regular astigmatism value may also be helpful in confirming data reproducibility.

19 Dependency of effective phacoemulsification time on Pentacam® nucleus staging (PNS) by Mehdi Shajari MD, Wolfgang Mayer MD, Prof. Thomas Kohnen

19.1 Introduction

The Pentacam® HR Scheimpflug imaging system can be used for cataract grading with the Pentacam® nucleus staging (PNS) classification. It evaluates the optical density of the lens by analyzing the backward scatter. For reliable results it is critical to perform the examination when the eye is dilated. The software automatically calculates the density of a central, 3-dimensional reference block, grading it from 0 to 5.

During conventional cataract surgery phacoemulsification has to be performed. The effective phacoemulsification time (EPT) shows how long the phacoemulsification time would have been if 100% power had been used in continuous mode and is calculated by multiplying the total phacoemulsification time by the average percentage of total power used.

In a previous study [44] we found that EPT increases with increasing PNS both in conventional and femtosecond laser-assisted cataract surgery. Furthermore we found that EPT is significantly less in femtosecond laser-assisted cataract surgery compared to conventional cataract surgery ($p = 0.001$).

19.2 Case 1: Low PNS and low EPT

In OD of this caucasian female patient it can be seen by the relatively high scatter that the lens is not clear. Accordingly, the Pentacam® shows a PNS of 1. Please note also the overview of further details on lens opacification such as average and maximum density. For this patient an EPT of 2.99 seconds was calculated.

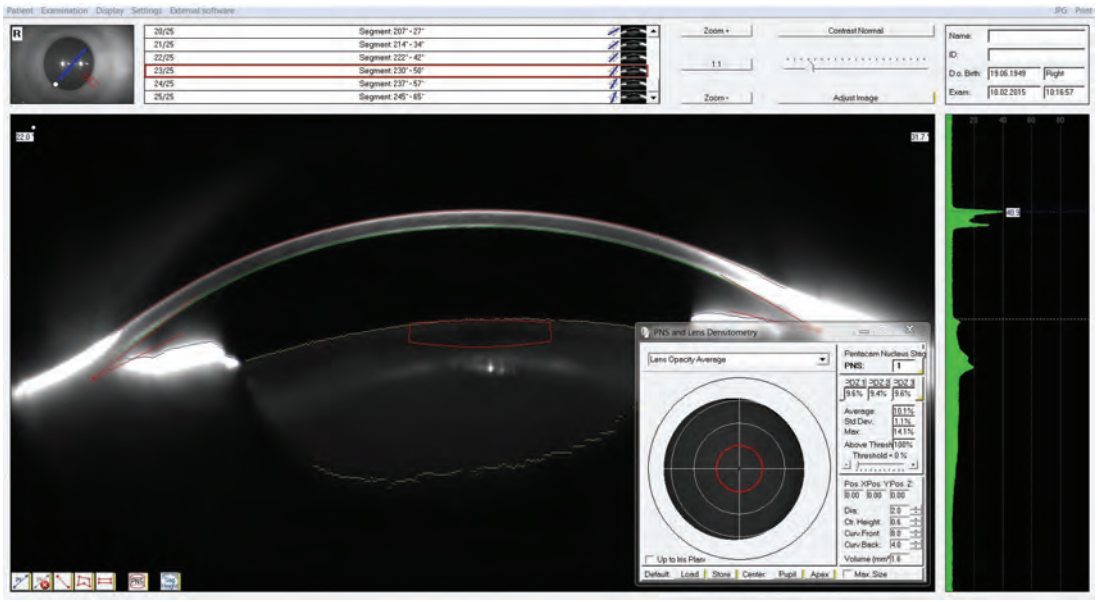

Figure 168: Scheimpflug Image with the PNS module showing a PNS of 1

19.3 Case 2: High PNS and high EPT

In OD of this caucasian male patient one sees immediately that lens clarity is considerably reduced compared to the first patient. This higher opacification level is also reflected in a higher PNS of 3. The average lens density also shows a clear increase. Despite the higher lens density, this surgery was also performed without any complications; however, it required significantly more EPT, at 11.90 seconds.

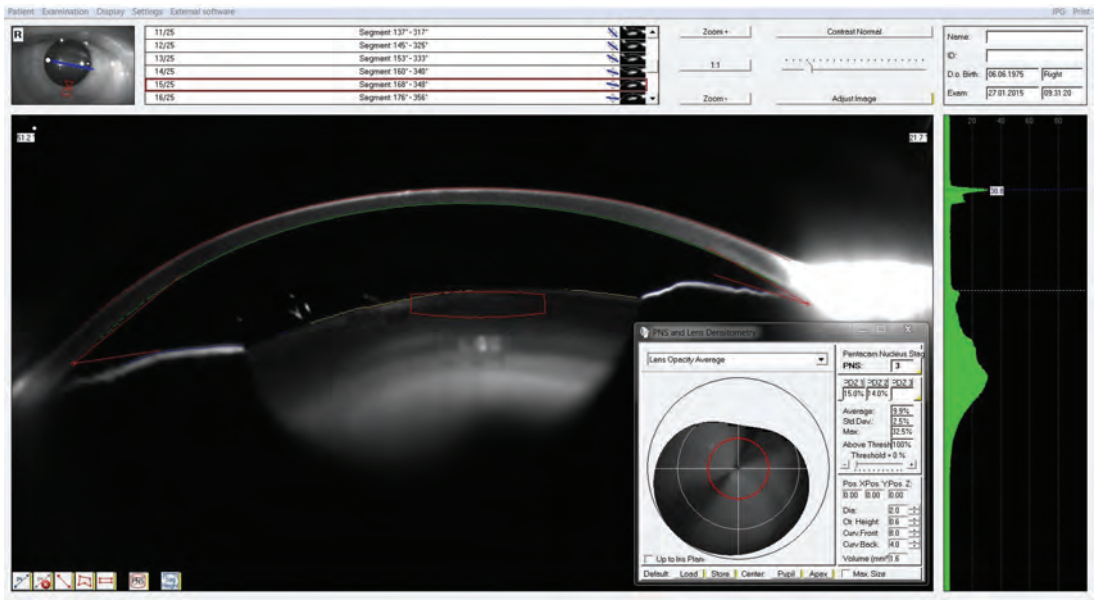

Figure 169: Scheimpflug Image with the PNS module showing a PNS of 3

20 Total corneal astigmatism for toric IOL by Giacomo Savini, MD

The influence of posterior corneal astigmatism on total corneal astigmatism (TCA) has been established by different studies based on Scheimpflug imaging [45, 46, 47]. In the great majority of eyes, the steepest corneal meridian of the posterior corneal surface has a vertical direction and produces an against-the-rule astigmatism (ATRA). In contrast to the anterior corneal surface, which is contact with air and has a positive refractive power, the posterior corneal surface is contact with aqueous and has a negative refractive power. For this reason a vertically aligned steep meridian on the posterior corneal surface generates an ATRA rather than a with-the-rule astigmatism (WTRA). The average magnitude of posterior corneal astigmatism is around 0.50 D, which should be added to anterior ATRA and subtracted from anterior WTRA to get the total corneal astigmatism (TCA). However, the average 0.5 D value is not fixed, but is proportional to the amount of anterior corneal astigmatism, so that a greater contribution can be expected with increasing values of anterior corneal astigmatism.

On the other hand, ophthalmologists are used to dealing with keratometric astigmatism (KA) and not anterior corneal astigmatism. There is a subtle difference: both are calculated from the radii of the anterior corneal surface, but the anterior corneal astigmatism is based on the 1.376 refractive index of cornea, whereas the KA is based on the 1.3375 keratometric index, which was developed to take into account the influence of the posterior corneal surface even when this cannot be measured. For this reason, the difference between KA and TCA is, on average, 0.25 D and not 0.50 D. Some differences in the axis of the steepest meridian may be expected too.

The influence of posterior corneal astigmatism on the refractive outcome of toric IOL implantation should therefore be predictable. However this has been demonstrated only recently [48]. Using the Pentacam® TCRP (i.e. the TCA) to calculate the required cylinder of toric IOLs we were able to lower the error in refractive astigmatism after cataract surgery as compared to calculations based on KA. In eyes with WTRA, KA generated an overcorrection of 0.59 ±0.34 D, which dropped to 0.13 ±0.42 D when using TCA. In eyes with ATRA, KA generated an undercorrection of 0.32 ±0.42 D, which dropped to 0.07 ±0.59 D when using TCA. Minor and clinically non-significant differences were observed in the torsional component of astigmatism, meaning that differences in axis orientation between KA and TCA are less important than differences in magnitude.

TCA measurements by the Pentacam® are shown in the power distribution display as TCRP. For this study we relied on 3 mm measurements centered on the pupil, considering the whole zone inside the ring. This setting provided us with the best results; future studies with larger samples may yet suggest different settings however.

20.1 Case 1: Cylinder overcorrection from measurement of keratometric astigmatism in an eye with WTRA

A 51-year-old woman underwent cataract extraction in OD. Her refraction was sph +4.00 cyl +0.75 A 100°. Axial length was 20.03 mm, and a +33.00 D toric Acrysof (Alcon, Fort Worth, TX) was calculated for emmetropia. The Pentacam® detected a WTRA whose measurements at 3 mm (Figure 170, Figure 171) yielded a 0.8 D difference between KA (1.4 D 110.8°) and TCRP astigmatism, i.e. TCA (0.6 D 14.9°).

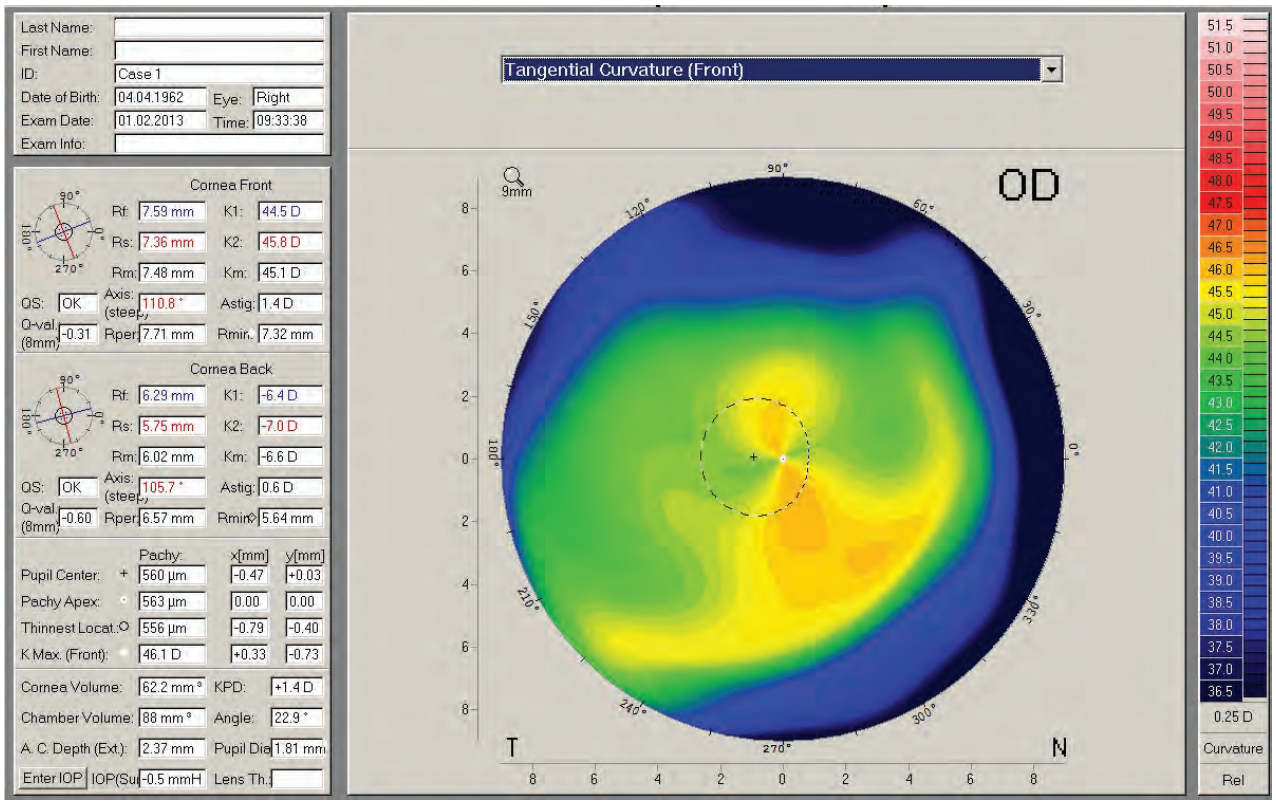

Figure 170: 1 Large Color Map showing keratometric astigmatism with a difference between K1 and K2 of 1.4 D 110.8°

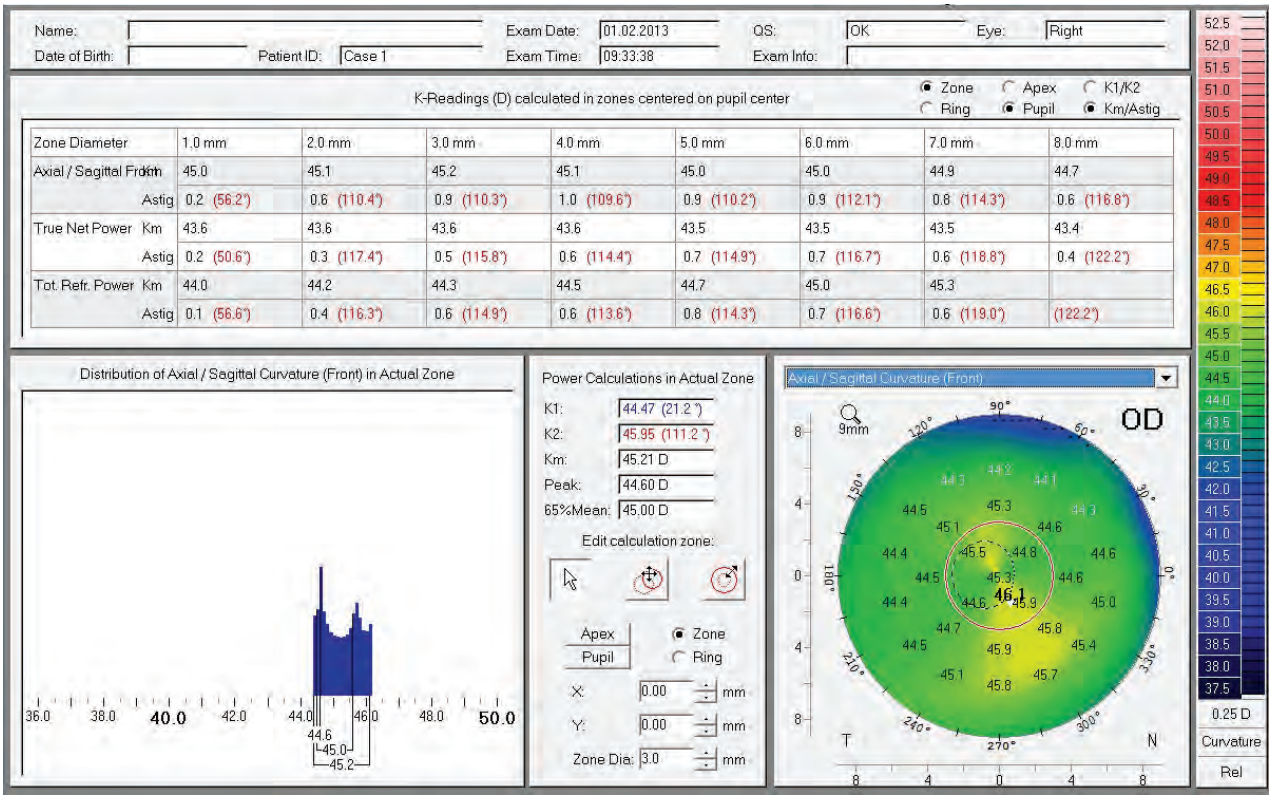

Figure 171: Corneal Power Distribution display showing a lower amount of astigmatism, at 0.6 D 114.9°

The choice of the IOL was between the SN6AT3 and the SN6AT4 models (the T2 model was not available). According to the manufacturer, the SN6AT3 and the SN6AT4 should correct, respectively, 1.03 and 1.55 D at the corneal plane. After including the effect of surgically induced astigmatism (0.2 D 90°), calculations based on meridional analysis [49], which, unlike the manufacturer online calculator, take into consideration the effect of axial length and corneal power [50], suggested a T4 IOL to correct the KA (residual predicted astigmatism = 0.23 D 39°) and a T3 IOL to correct the TCRP astigmatism (residual predicted astigmatism = 0.20 D 36°). We decided to implant the T3 model in order to correct the TCRP astigmatism. The IOL was oriented at 115° and the patient's refraction at one month after surgery revealed no residual refractive cylinder: the refractive outcome showed that our choice to rely on TCA had been correct.

20.2 Case 2: Cylinder undercorrection from measurement of keratometric astigmatism in an eye with ATRA

An 85-year-old man underwent cataract surgery in OS. Axial length was 23.31 mm, and a 21.50 D toric Acrysof was calculated for emmetropia. Traditional KA measurement (Figure 172) showed a value of 1.9 161°, which was significantly lower than the Pentacam® TCRP at 3 mm (Figure 173), measuring 2.8 D 160.3°.

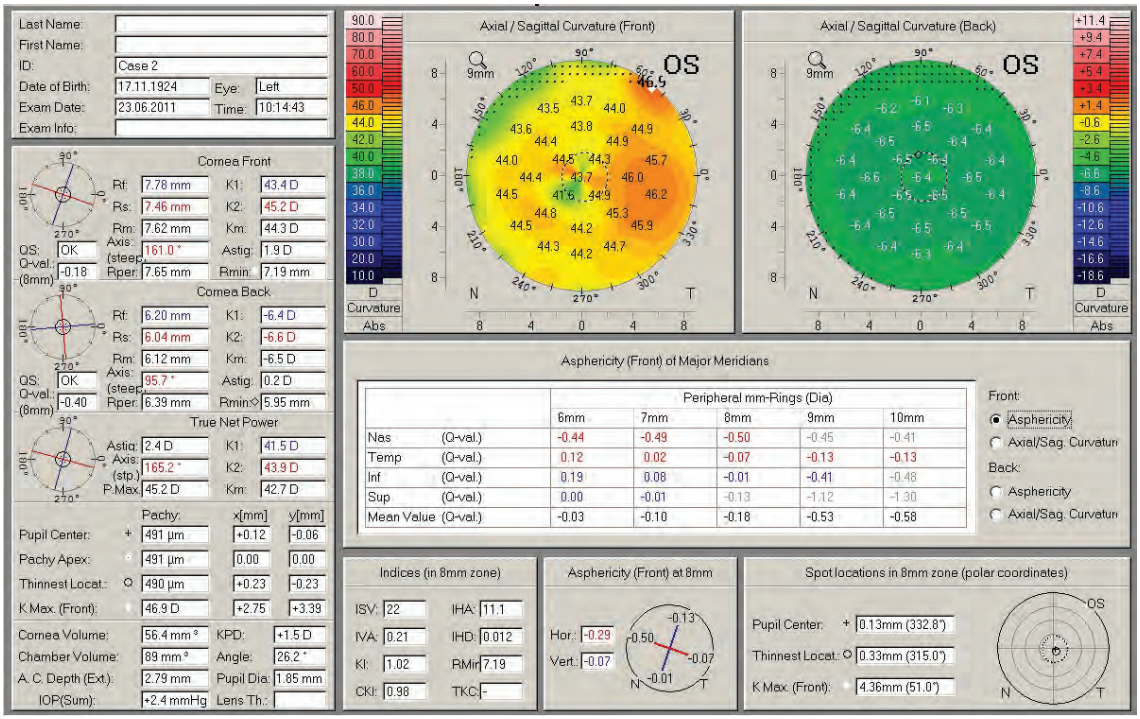

Figure 172: Topometric showing a keratometric astigmatism of 1.9 D 161°

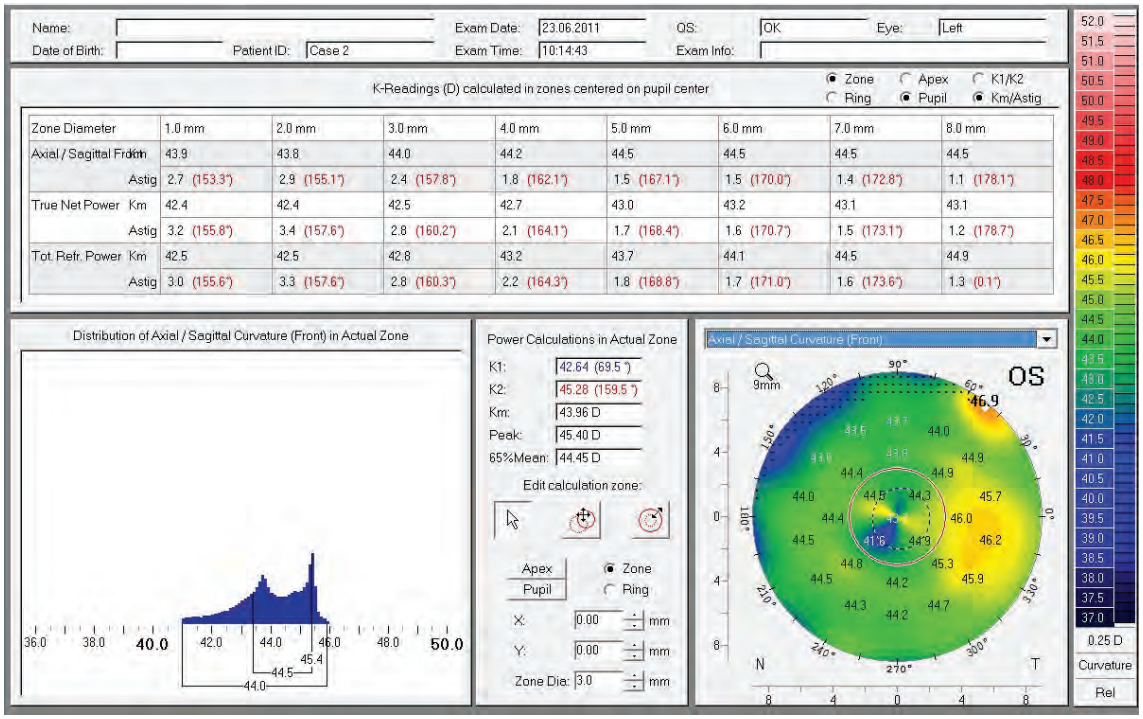

Figure 173: Corneal Power Distribution display with TCRP at 3 mm revealing a higher astigmatism of 2.8 D 160.3°

After considering the SIA = 0.2 D 90° the choice was between a SN6AT4 to correct the KA (predicted residual astigmatism = 0.17 D 138°) and a SN6AT6 to correct the TCA (predicted residual astigmatism = 0.13 D 122°). The former should correct 1.55 D at the corneal plane, the latter 2.57 D. We implanted a SN6AT6 oriented at 160°. One month after surgery, the patient had no residual refractive astigmatism.

20.3 Case 3: Cylinder overcorrection from measurement of keratometric astigmatism

A 71-year-old man underwent cataract surgery in OS. Axial length was 22.87 mm and a 23.50 D toric Acrysof was calculated for emmetropia. Traditional KA measurement (Figure 174) showed a value of 1.9 D 79.2°, which was significantly higher than the Pentacam® TCRP at 3 mm (Figure 175), measuring 1.2 D 74°.

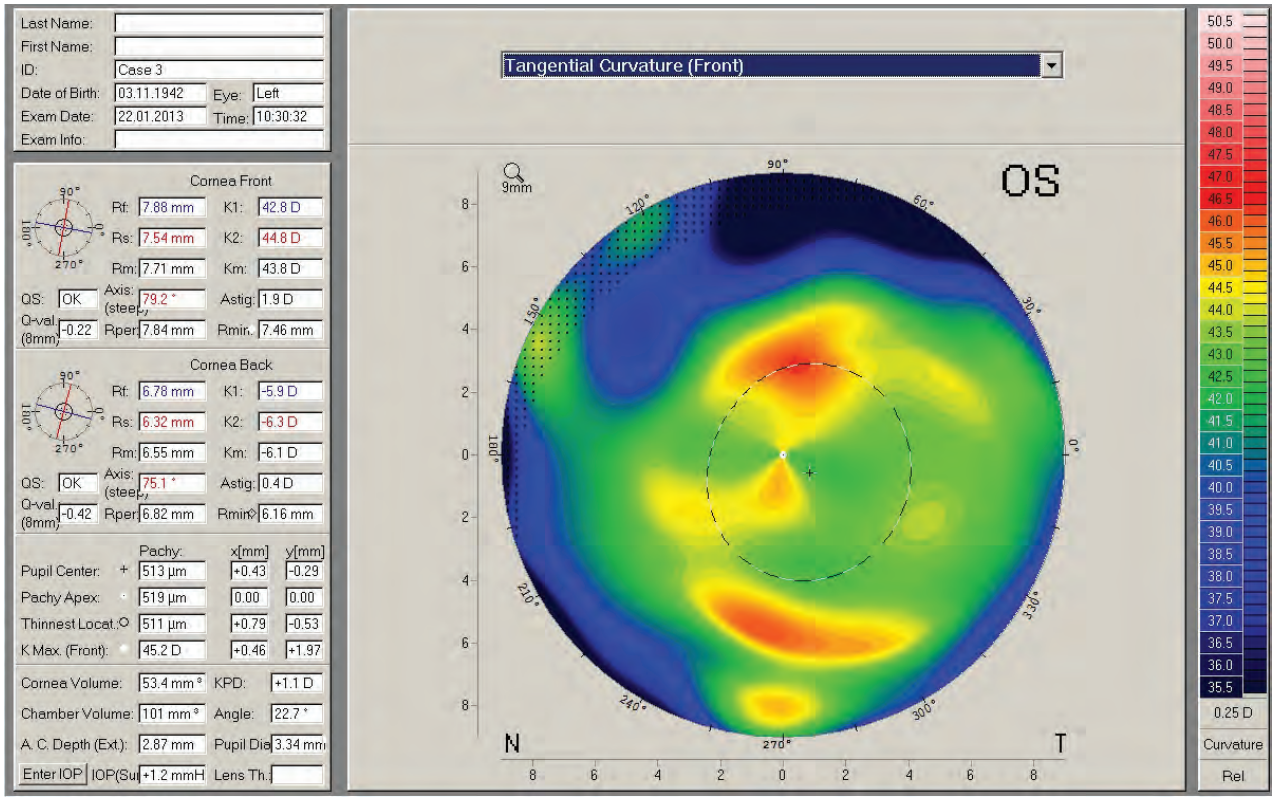

Figure 174: 1 Large Color Map showing a keratometric astigmatism of 1.9 D 79.2°

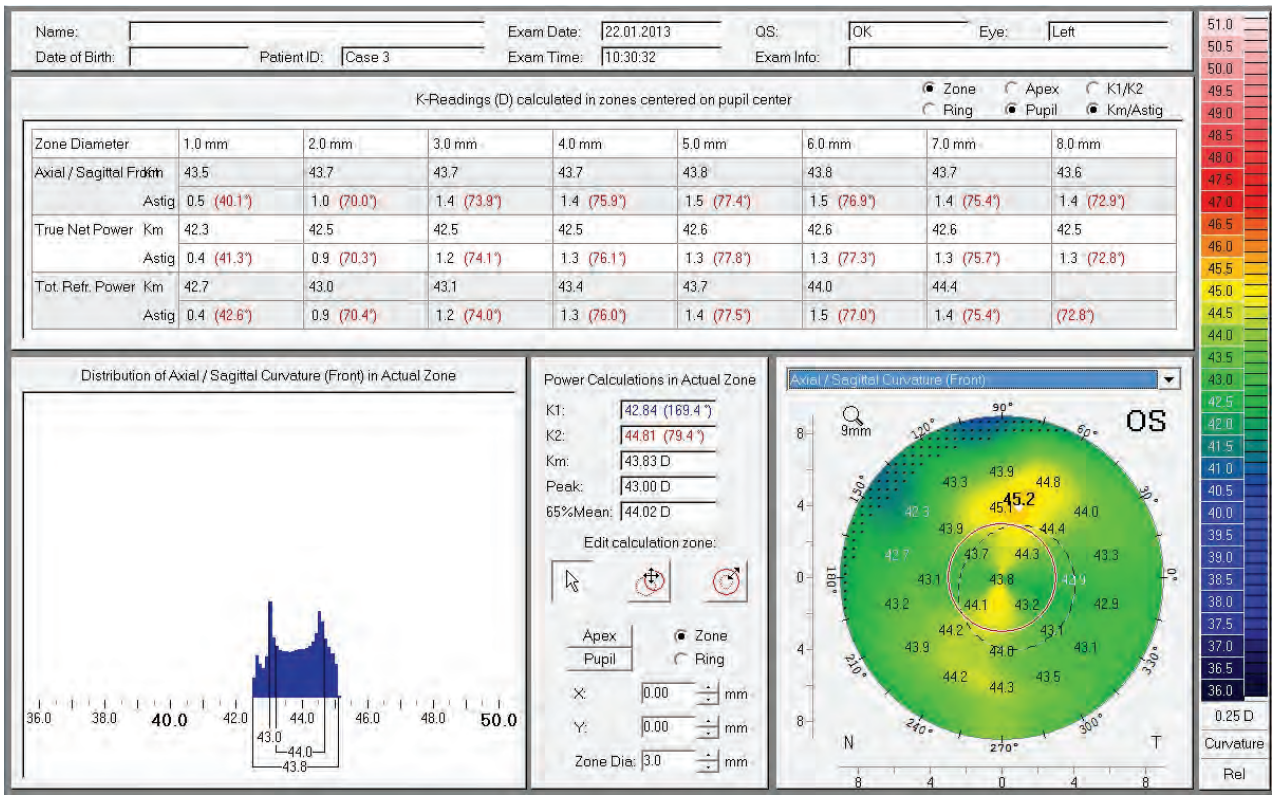

Figure 175: Corneal Power Distribution display showing a TCRP astigmatism of 1.2 D 74°, i.e. lower than KA astigmatism

We aimed to correct the TCA and considering a surgically induced astigmatism of 0.2 D 90°, we targeted a correction of 1.37 D 76°. A SN6AT4 IOL was implanted at 75°. One month after surgery the refraction was sph -0.25 cyl -0.25 A 120°. Using the KA data would have led to cylinder overcorrection.

21 Overview about IOL power calculation formulas for different eye types

patient group	IOL-calculator/formula	where to find	value	paper
normal eyes	standard historical methods (SRK I; SRK II; Hollady I; Holladay II; SRKT; Hoffer Q; Haiges and many others)	Cataract Pre-OP Display	Sim K's and other values depending to the used formula	Scheimpflug Corneal Power Measurements for Intraocular Lens Power Calculation in Cataract Surgery - (Elie Saad, Maya C. Shammes and H. John Shammes) - American Journal of Ophthalmology, Septemner 2013
post RK eyes	ASCRS-calculator: http://www.iolcalc.org/	Corneal Power Distribution display, Cataract Pre-OP Display	Axial/Sagittal Front 4.0 mm; settings: Zone/ Pupil/Km/Asti; CT_Min	New algorithm for post-radial keratotomy intraocular lens power calculations based on rotating Scheimpflug camera data - (Richard Potvin, OD, Warren Hill, MD) - J Cataract Refract Surg 2012; © 2012 ASCRS and ESCRS
post myopic LASIK without history	ASCRS-calculator http://www.iolcalc.org/ (Potvin/Shammas/ Hill) no history, BESST II, ray-traycing formulas (Phaco Optics & Okulix), EKR65 + Holladay consultant, A-P calculator from Dr. Negishi	Corneal Power Distribution display, Cataract Pre-OP Display, Holladay Report	True Net Power (TNP) 4,0 mm; settings: Zone/Apex/Km/Asti; BESSt and ray tracing formulas (Phaco Optics, Okulix) are linked via interface	New algorithm for intraocular lens power calculations after myopic laser in situ keratomileusis based on rotating Scheimpflug camera data - (Richard Potvin, OD, Warren Hill, MD) - J Cataract Refract Surg 2015; 41:339–347 © 2015 ASCRS and ESCRS
post myopic LASIK with history	double K-methode, BESST II, ray-traycing formulas (Phaco Optics & Okulix), EKR65 + Holladay consultant	Cataract Pre-OP Display, Holladay Report	Sim K's or EKR65 + other values depending to the formula, BESSt and ray tracing formulas (Phaco Optics, Okulix) are linked via interface	
for every eye	theoretically ray tracing formulas like Oculix, Phaco Optics, EKR65 + Holladay consultant	Corneal Power Distribution display, Cataract Pre-OP Display, Holladay Report	Sim K's or EKR65 + other values depending to the formula, BESSt and ray tracing formulas (Phaco Optics, Okulix) are linked via interface	
Alcon toric IOL	Alcon-calculator: http://www.acrysoftoriccalculator.com/	Corneal Power Distribution display	Total Cornea Refractiv Power (TCRP) 3,0 mm; settings: Zone/Pupil/ Km/Asti	An Analysis of the Factors Influencing the Residual Refractive Astigmatism After Cataract Surgery With Toric Intraocular Lenses - (Giacomo Savini and Kristian Næser) - Investigative Ophthalmology & Visual Science, February 2015, Vol. 56, No. 2, 829

status September 2015

Table 11: Overview about IOL power calculation formulas for different eye types

22 Phakic IOL implantation

22.1 Manual pre-op simulation and post-op control by Eduardo Viteri, MD

22.1.1 Preoperative evaluation

A high myopic, 20-year-old patient entered the office; refraction data:

- OD: sph -12.00 (cyl -1.50 A 180°)
- OS: sph -12.50 (cyl -1.50 A 10°)

She complained of poor contact lens tolerance with less than 4 hours of daily wearing time. We discussed several treatments and the possibility of implanting a pIOL. The Pentacam® allows us to measure very easily and accurately the anterior chamber and so determine if there is enough space to implant an iris-fixated Artisan phakic IOL.

One can measure not only the distance from the endothelium to the anterior surface of the crystalline lens but also the available space at the point where the claws will grasp the iris (Figure 176). Most important are minimum distances, which are in most cases not perpendicular to the iris, but diagonal.

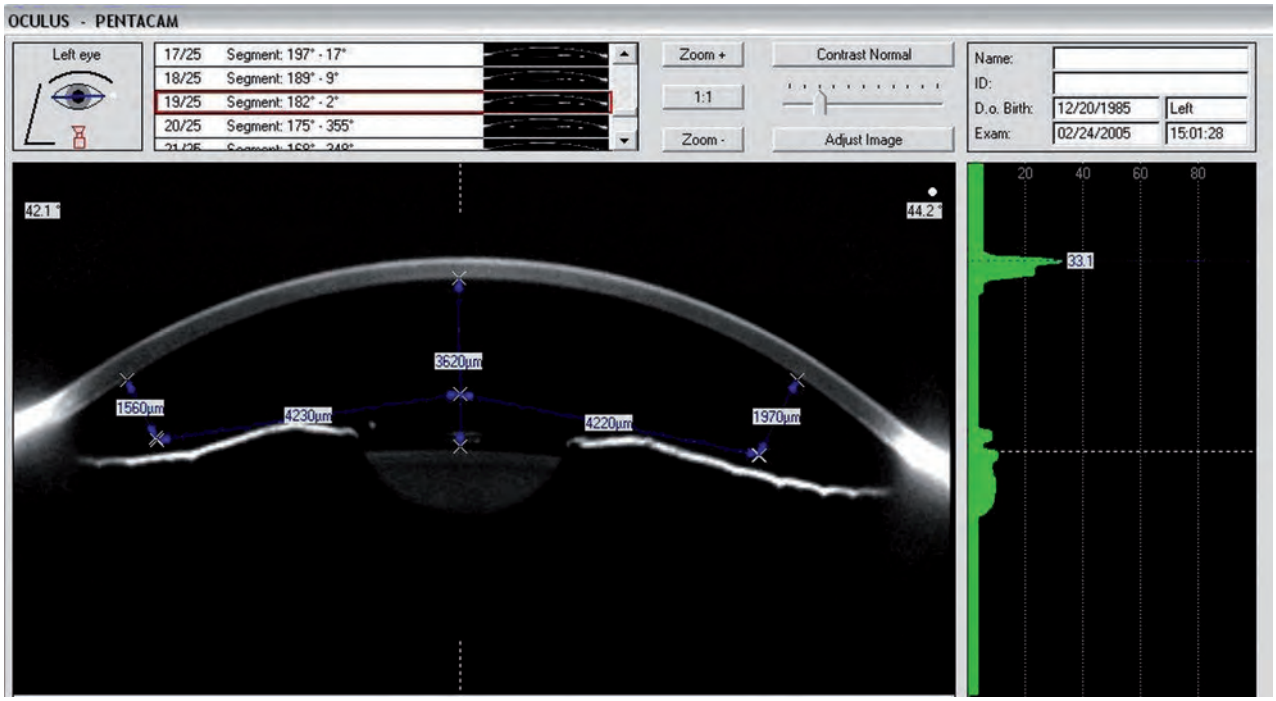

Figure 176: Scheimpflug Image with pre-op measurements

A Pentacam® examination for the pre-op planning of the surgery showed there was enough space for the Artisan pIOL implant.

22.1.2 Postoperative evaluation

The Scheimpflug image shown below displays the same case after successful Artisan pIOL implantation. It is evident there is space from the anterior pIOL surface to the endothelium centrally and at the periphery (Figure 177). The posterior of the pIOL also has enough distance to the iris and to the crystalline lens. Her post-op refraction:

- OD: sph +0.25 cyl -1.00 A 180°
- OS: sph +0.50 cyl -1.00 A 180°

We had a good pre-op planning process and a happy post-op patient.

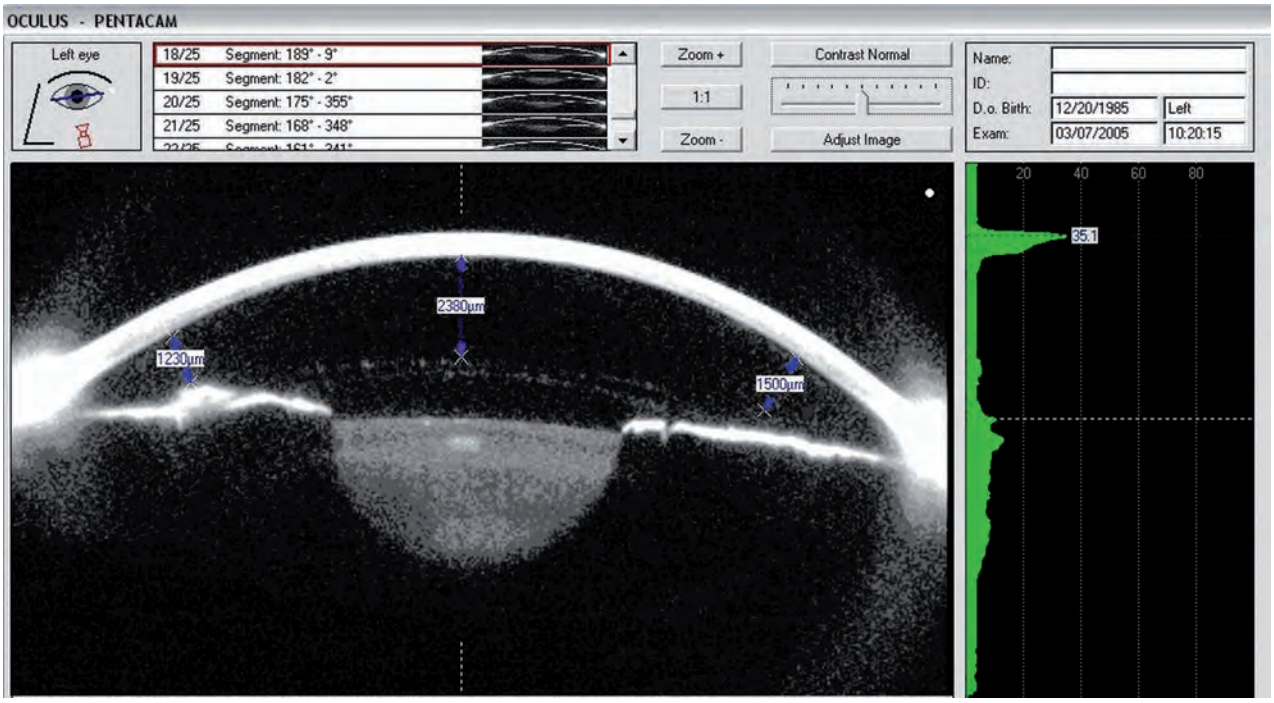

Figure 177: Scheimpflug Image after Artisan IOL implantation

22.2 3D pIOL Simulation and Aging Prediction by Prof. Burkhard Dick, Sabine Buchner, Optometrist

22.2.1 Myopic Artisan/Verisyse 6/8.5 mm

A 40-year-old female:

- OD: sph -15,00 cyl -1.25 A 82° VA 20/30
- OS: sph -14.75 cyl -1.75 A 83° VA 20/30

She complained of poor contact lens tolerance because of dry eyes with less than 3 hours daily wearing time. In view of her high ametropia in both eyes and her age we considered pIOL implantation to preserve her ability to accommodate.

Her pupil sizes were:

- scotopic: OD 6.24 mm, OS 6.27 mm
- mesopic low: OD 4.74 mm, OS 4.78 mm
- mesopic high: OD 3.62 mm, OS 3.56 mm.

Because of her high ametropia, LASIK and PRK were not an option. Therefore we checked the possibility of a pIOL implantation. A 3D simulation of the fit of a pIOL gave a swift answer to this.

Because of her big pupil size it was clear that only the Artisan/Verisyse with the 6 mm optic would be suitable.

The minimum clearance in the anterior chamber between the pIOL optic edge and the endothelium was 1.22 mm.

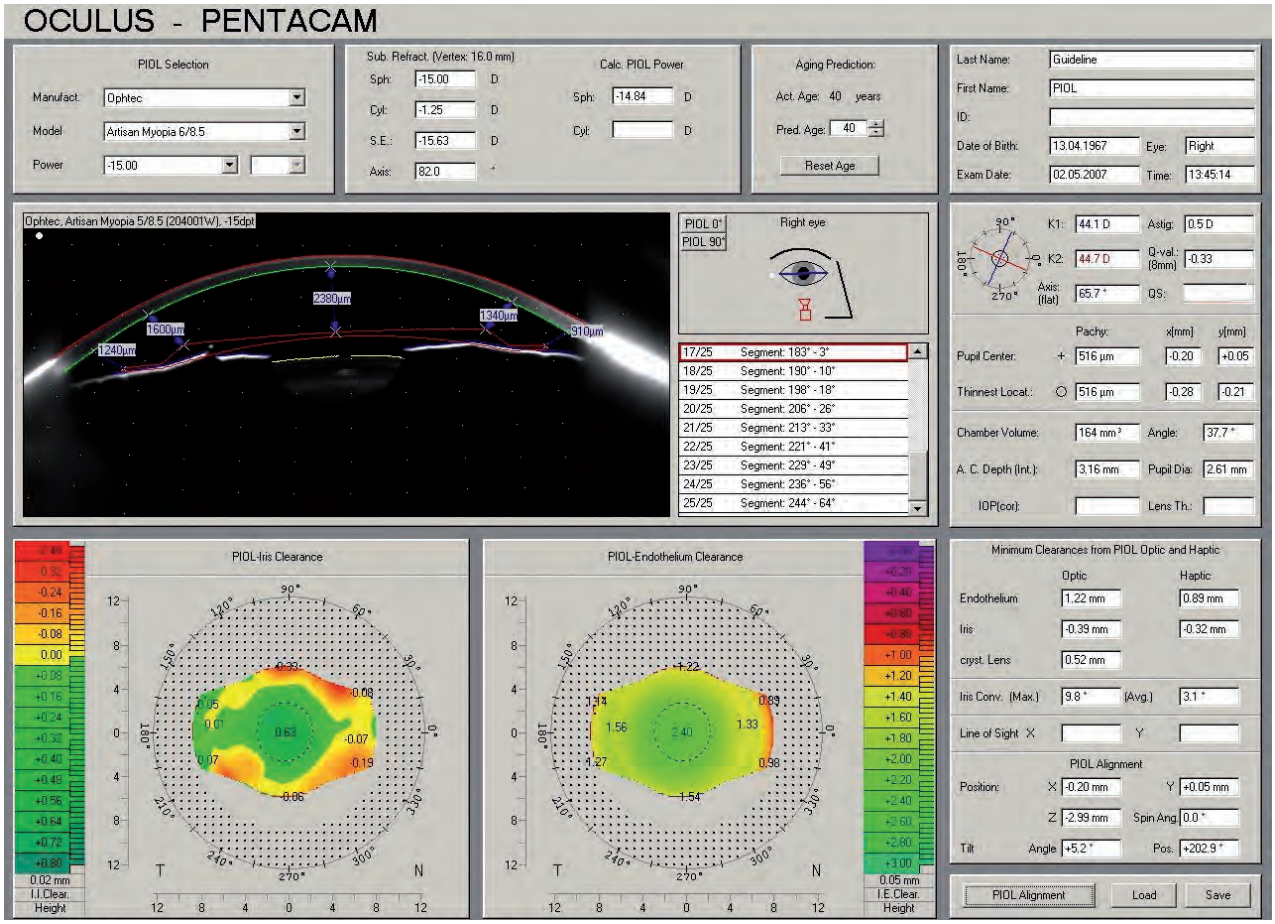

Figure 178: 3D pIOL Simulation and Aging Prediction for the patient's current age

Because of these distances between the pIOL and the endothelium, it would be currently safe. The mimimum clearance between the pIOL and the endothelium was 1.22 mm calculated in 3D. The iris convexity is shown on the lower right hand side of Figure 178.

However, what would happen as the patient grew older?

The crystalline lens grows approximately 19 µm per year. This would necessarily cause a shift of the pIOL towards the endothelium, reducing the distance between them. A possible consequence would be endothelial cell loss, a risk that must be taken into account and avoided. For this purpose the Pentacam® offers unique aging prediction software which simulates the position of the pIOL after 10, 15 or 20 years.

Figure 179 shows the predicted distances ten years after pIOL implantation.

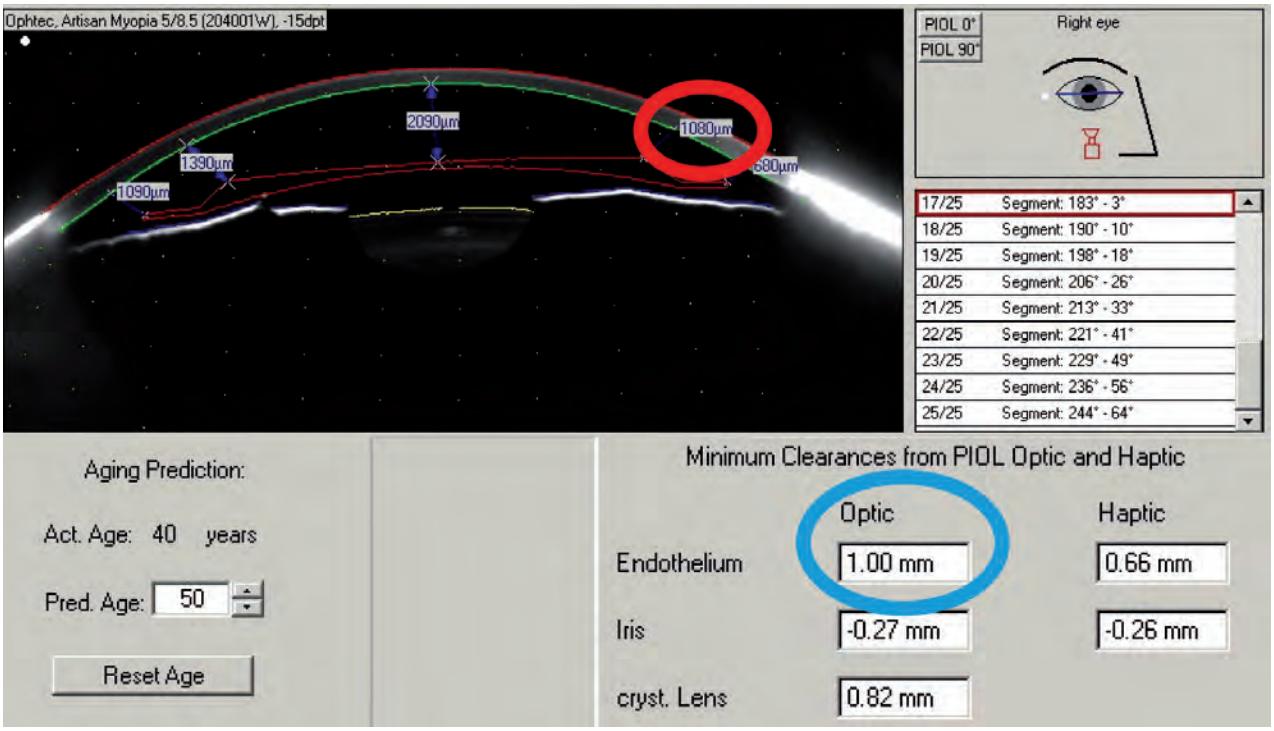

Figure 179: 3D pIOL simulation 10 years after implantation

The horizontal Scheimpflug image shows a minimum clearance between optic edge and endothelium of 1080 µm, but the distinct minimum clearance, derived from the internal 3D-model between the pIOL optic edge and the endothelium is 1.00 mm, which is already borderline.

The image below shows the simulated pIOL position 20 years after implantation.

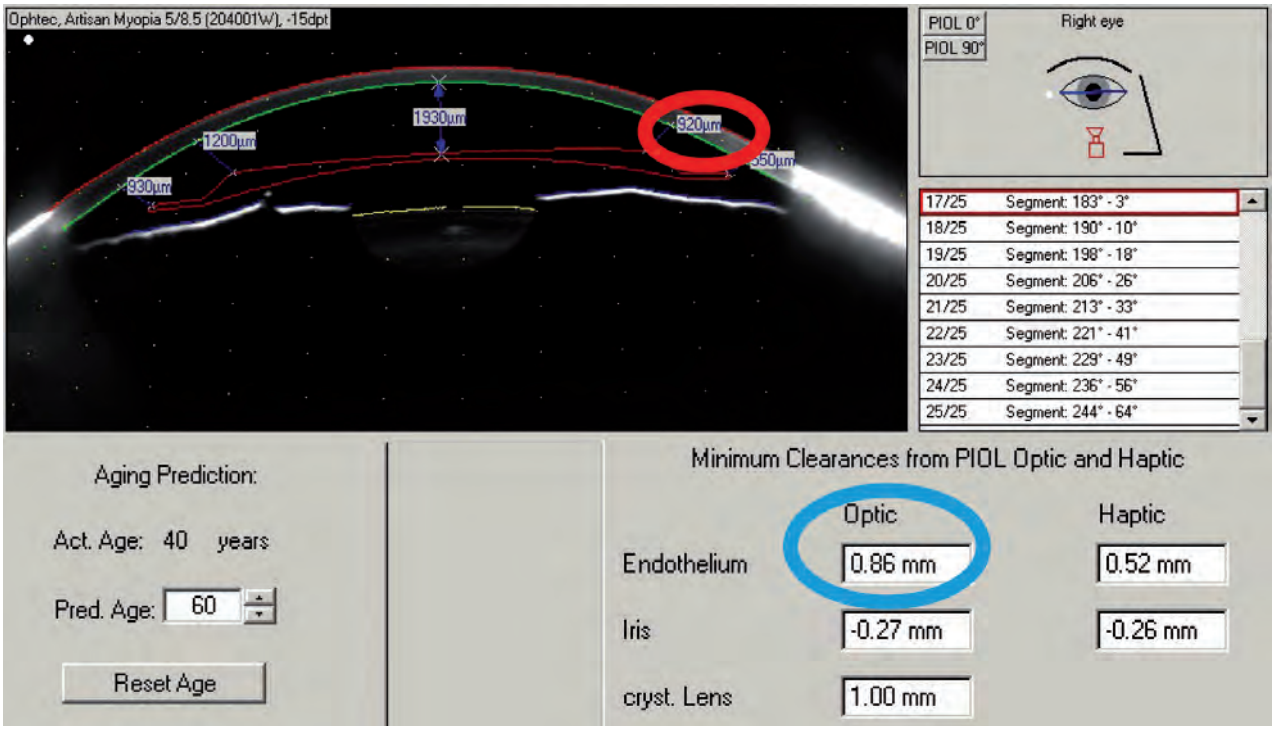

Figure 180: 3D pIOL simulation 20 years after implantation

The horizontal Scheimpflug image shows a minimum clearance between optic edge and endothelim of **920 µm**, but the distinct minimum clearance, derived from the internal 3D-model between the pIOL optic edge and the endothelium is **0.86 mm**, which is too small.

Note:

Judging by the first impression of her anterior chamber conditions this patient appears suitable for pIOL implantation. Without the Pentacam® we would have done the implantation. However, because of the predicted pIOL position after 10 or 20 years, we decided not to perform the surgery. This case demonstrates the big advantage of the Pentacam® in daily clinical practice. Without even touching the patient's eye we were able to make a competent diagnosis and decision followed by thorough consultation with the patient.

22.2.2 Toric Artisan/Verisyse, 5/8.5 mm

A 22-year-old female:

- OD: sph -18.50 cyl 4.00 A 127°
- OS: sph -10.50 cyl 1.50 A 45°

asked for refractive surgery.

On the left cornea a small corneal cicatrix was detected centrally during slit lamp examination. Her pupil sizes were:

- scotopic: OD 7.51 mm, OS 7.34 mm
- mesopic low: OD 5.40 mm, OS 5.24 mm
- mesopic high: OD 4.34 mm, OS 4.27 mm

IOP was 16 mmHg in both eyes. We counted 2318 cells/mm² in OD and 2418 cells/mm² in OS. We used the Pentacam® 3D pIOL Simulation and Aging Prediction to simulate the fit of the pIOL and to check its position over the course of years following surgery using the aging prediction module.

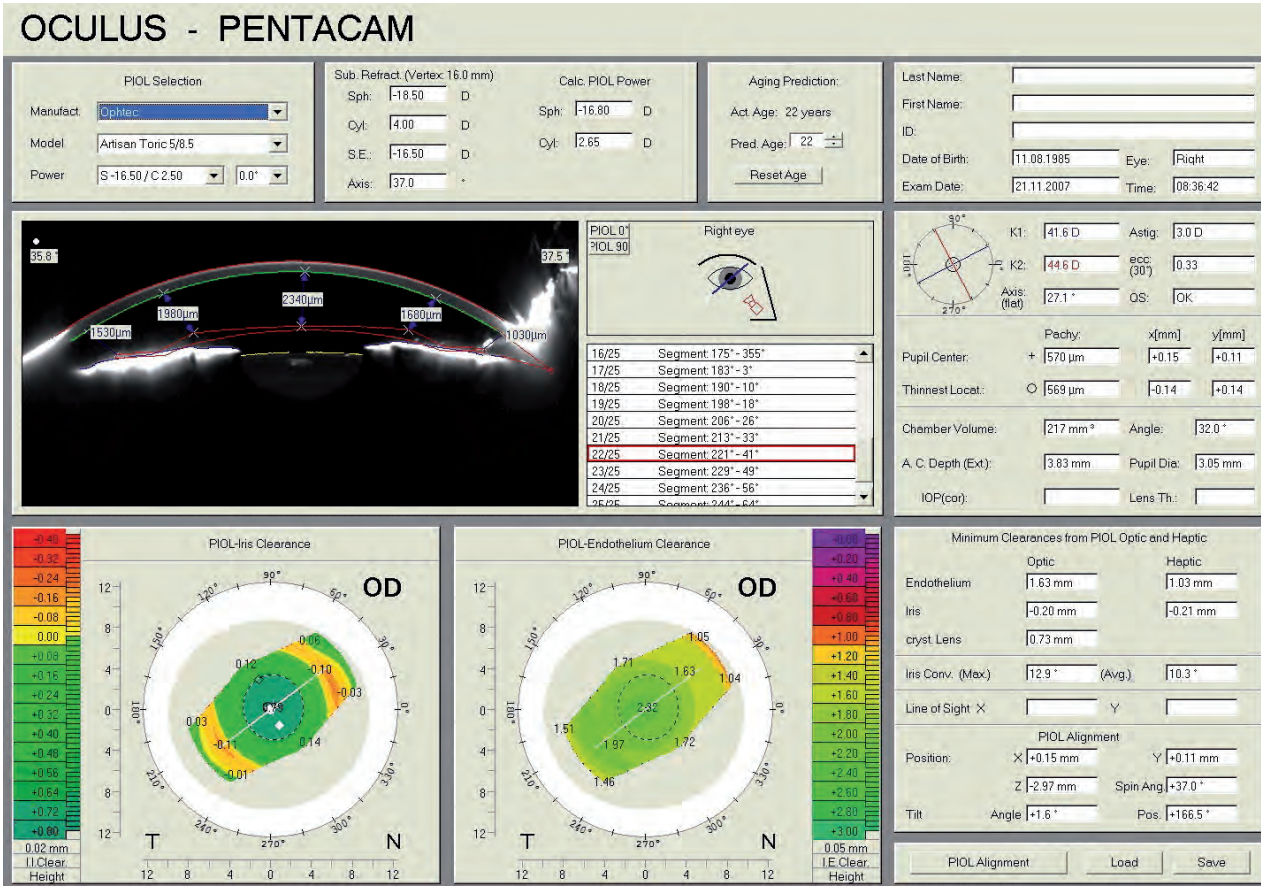

Figure 181: 3D pIOL Simulation and Aging Prediction at the patient's current age

pIOL lens power is calculated automatically on entering the patient's subjective refraction. A toric Artisan/Verisyse was selected and its fit in the axis of the astigmatism was simulated as shown in Figure 181. The maximum iris convexity is 12.9° and the minimum clearance between pIOL optic edge and endothelium is 1.63 mm. From the current point of view everything thus appeared to be within normal limits.

Since the patient was only 22 years old, we wanted to check the pIOL position as to be on the safe side. We checked the predicted pIOL position at 40 years after surgery (Figure 182). Here the simulated minimum clearance is 1 mm.

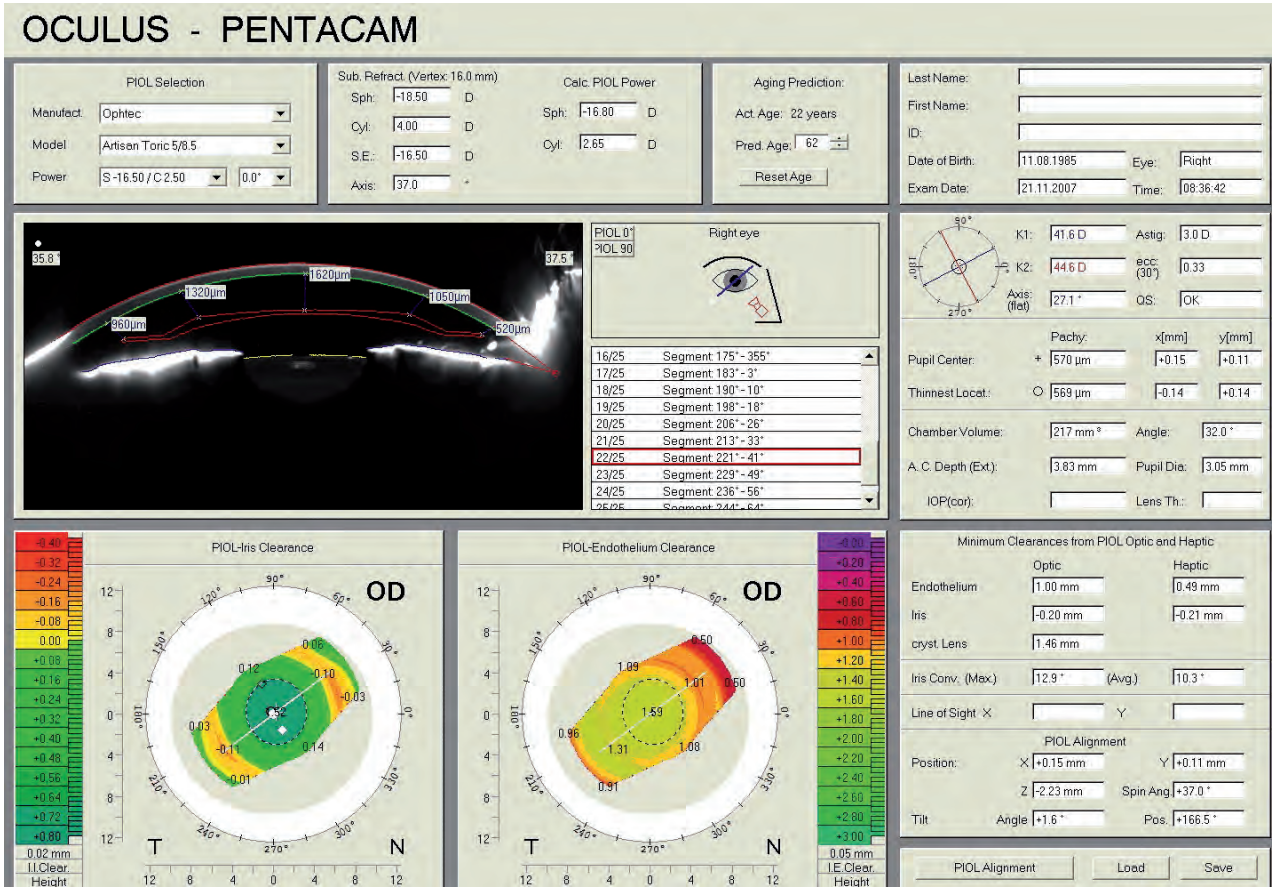

Figure 182: 3D pIOL Simulation and Aging Prediction at 40 years after implantation

Conclusion:

The amount of endothelium cells was in the normal range. The patient was young and her refraction could be expected to remain stable over the next year. The minimum clearance of 1.63 mm between pIOL and endothelium was large enough. The aging prediction showed 1.32 mm clearance after 20 years, which was sufficient.

22.3 Patient selection criteria by Prof. Burkhard Dick, Sabine Buchner, Optometrist

Careful pre-op evaluation and patient selection are essential prerequisites for a successful implantation. There are several criteria that have to be considered. In our clinic, we look at the following:

- The minimum clearance between pIOL and endothelium should be greater than 1 mm;
- Endothelial cell density should be at least 2000 per mm²;
- Dislocation of the pupil should be no greater than 1 mm. The Scheimpflug image in Figure 183 shows a dislocation by approx. 1070 µm;
- The cornea and crystalline lens should be clear;
- Iris convexity: If the iris is very irregular, it is better to refrain from pIOL surgery. The Pentacam® pIOL simulation in Figure 184 shows an iris convexity of more than 15 degrees.

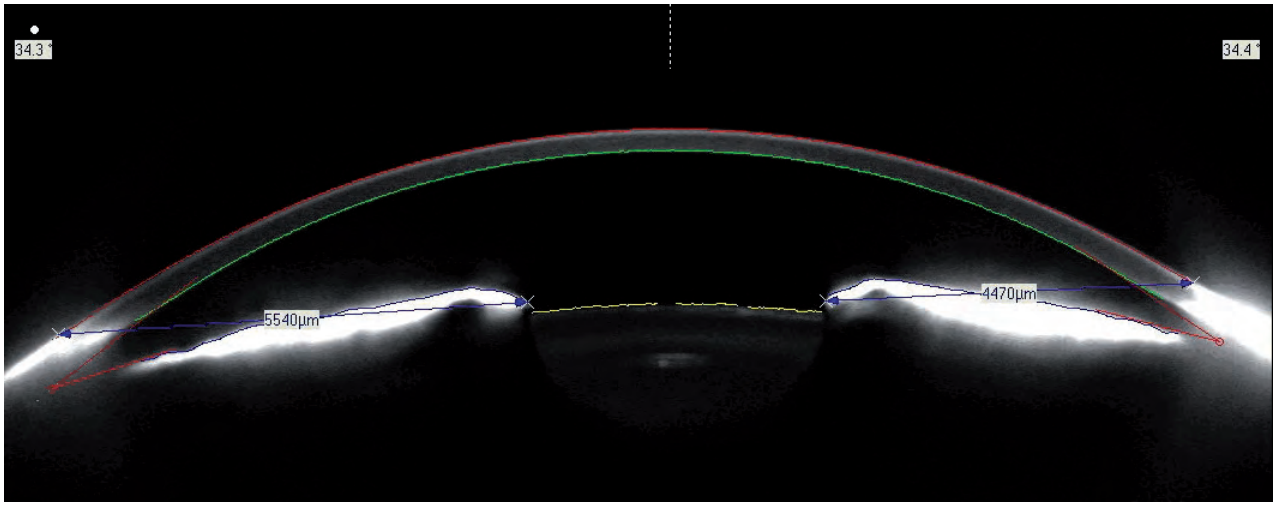

Figure 183: Scheimpflug image showing a both visible and measurable pupil dislocation

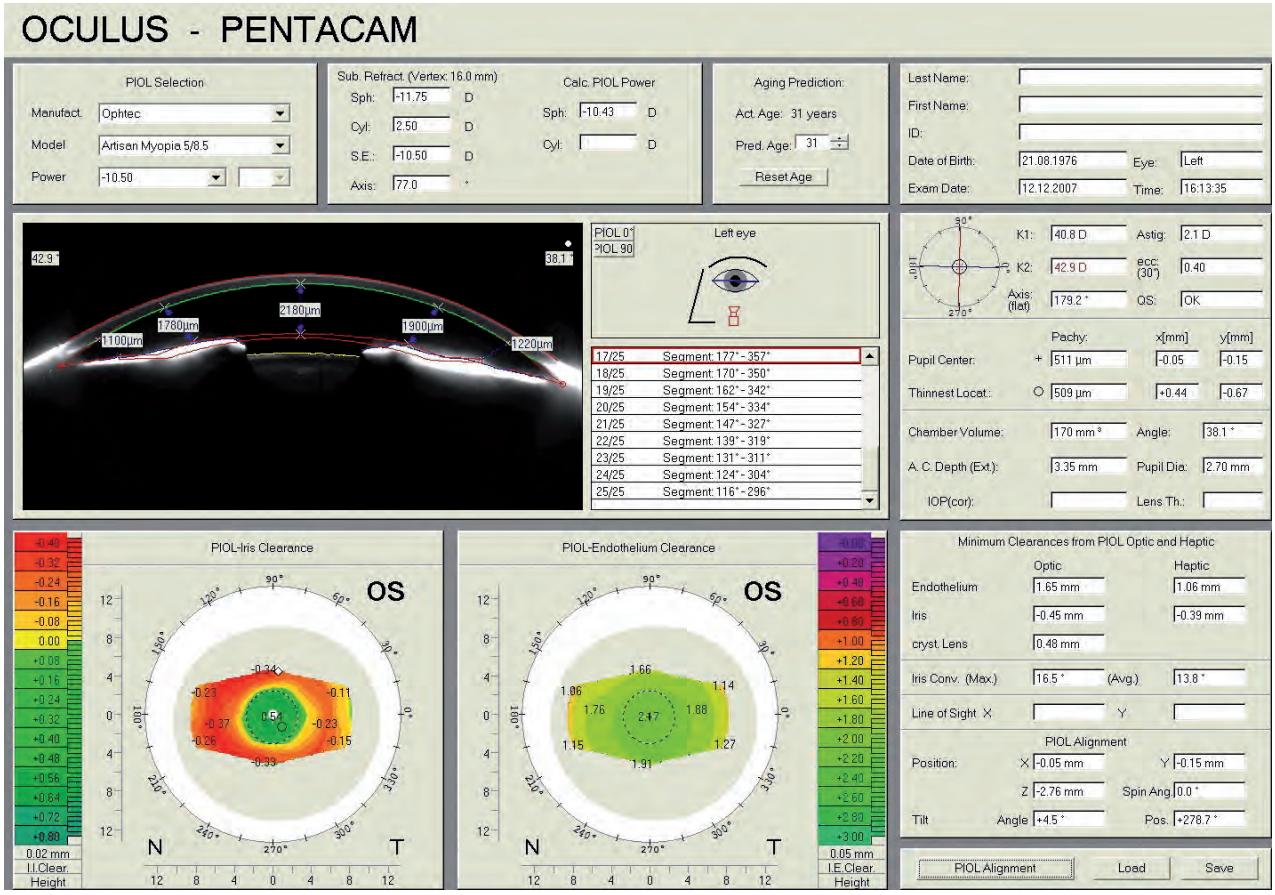

Figure 184: 3D pIOL Simulation and Aging Prediction showing a large iris convexity

The following warning appears: "Automatic pIOL alignment may be negatively influenced by large iris convexity".

22.4 Case example of ectasia after LASIK, crosslinking and pIOL implantation by Prof. Renato Ambrósio Jr, Fernando Faria-Correia, MD, Allan Luz, MD

A 25-year-old male patient presented with severe and progressive visual loss (UCVA of counting fingers at 1 m in both eyes) due to ectasia (Figure 185) following bilateral LASIK in 2006. His BCVA was 20/30 (sph -15.0 cyl -2.50 A 15°) in OD and 20/80 (sph -14.25 cyl -6.0 A 0°) in OS. The thinnest pachymetry value was 408 µm in OD and 395 µm in OS. Given the severity of the clinical picture, the moderately thin cornea and the presence of contact lens intolerance it was decided to perform transepithelial crosslinking in both eyes as an alternative to keratoplasty. After refractive stabilization (with two similar treatments one month apart) pIOLs (AcrySof Cachet) were implanted in both eyes. At two-year follow-up the patient's UCVA had improved to 20/30 in OD and 20/25 in OS (Figure 186).

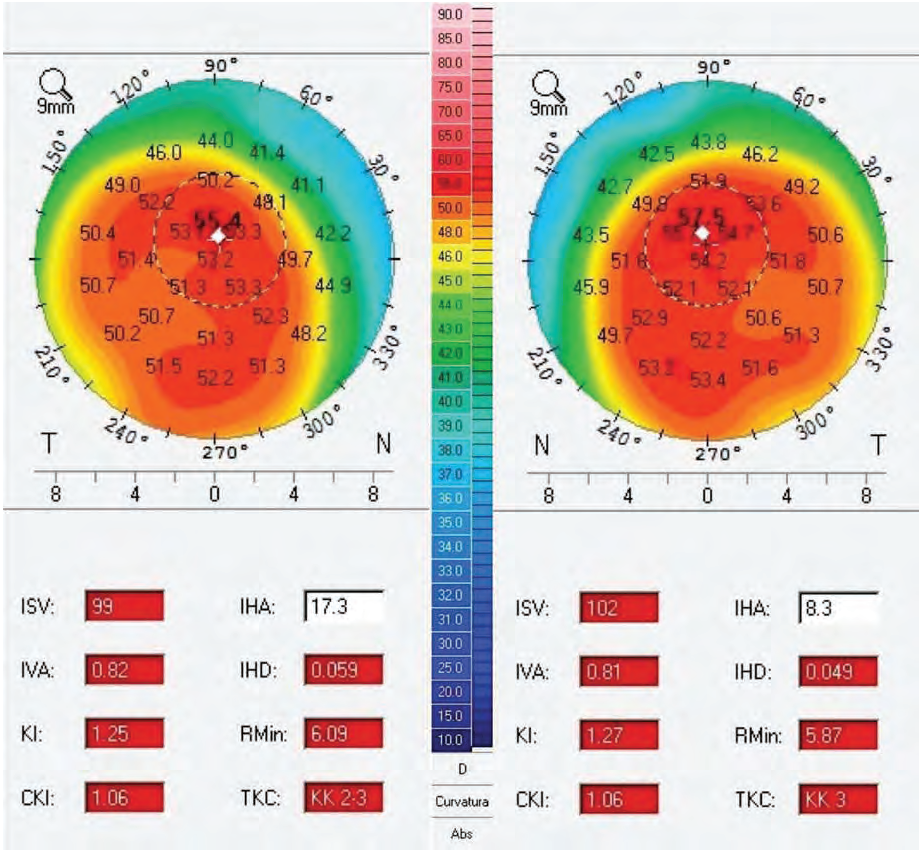

Figure 185: Preoperative axial curvature map of ectasia after LASIK in both eyes

Clinical case of post-LASIK ectasia treated by transepithelial crosslinking followed by phakic intraocular lens implantation in both eyes.

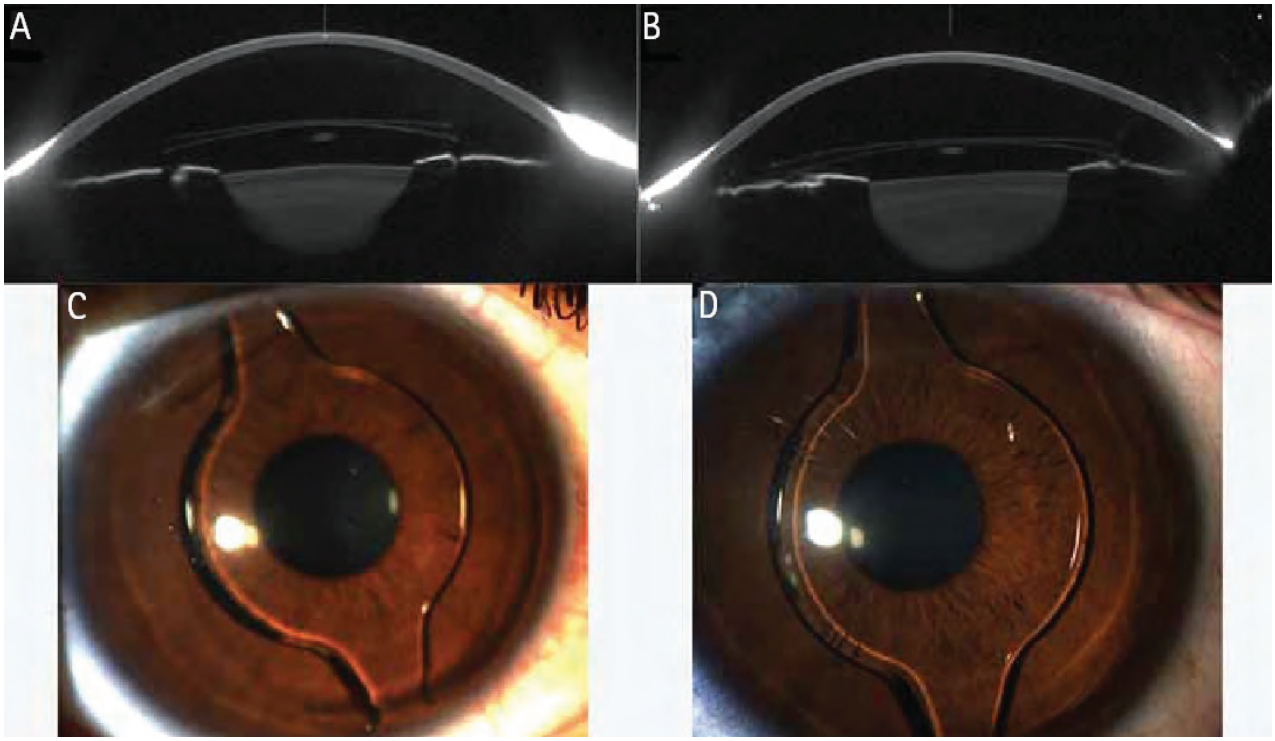

Figure 186: Scheimpflug Image after transepithelial crosslinking in OD (A) and OS (B), slit-lamp photograph showing pIOL implant in OD (C) and OS (D)

23 Case reports from daily practice

23.1 Case 1: Cortical cataract by Tobias H. Neuhann, MD

A 23-year-old, -12.5 D myopic white female underwent a fundus examination at a local eye clinic. Her BSCVA was 20/30, while her best corrected visual acuity with contact lenses was not documented. She was told that cataract surgery would be the only option to improve her visual acuity. She was now presenting at our clinic for a second opinion.

Scheimpflug imaging was successful (Figure 187) in perfectly documenting the peripheral cortical density (yellow arrow). The cause of her reduced BSVCA was corneal warpage caused by the contact lenses. Two weeks later the warpage was found to have changed slightly (Figure 188).

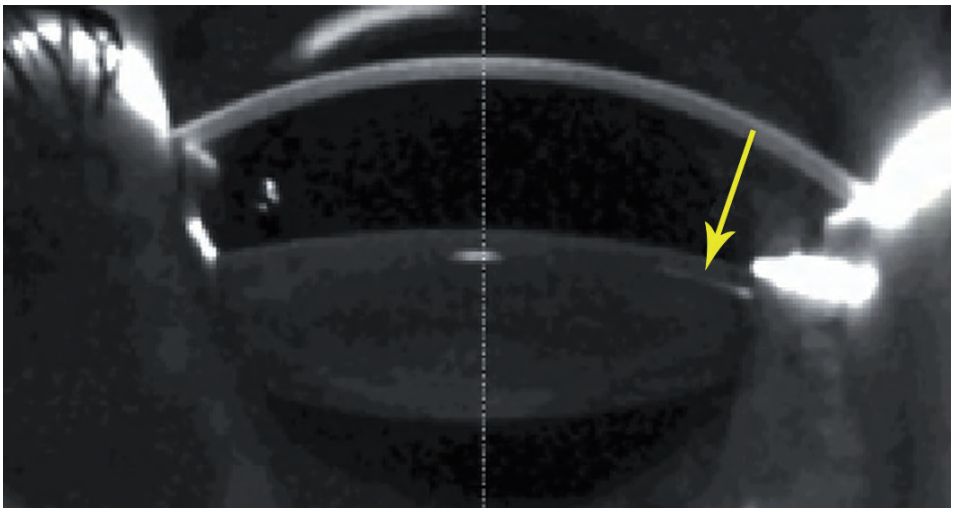

Figure 187: Scheimpflug image showing a cortical cataract

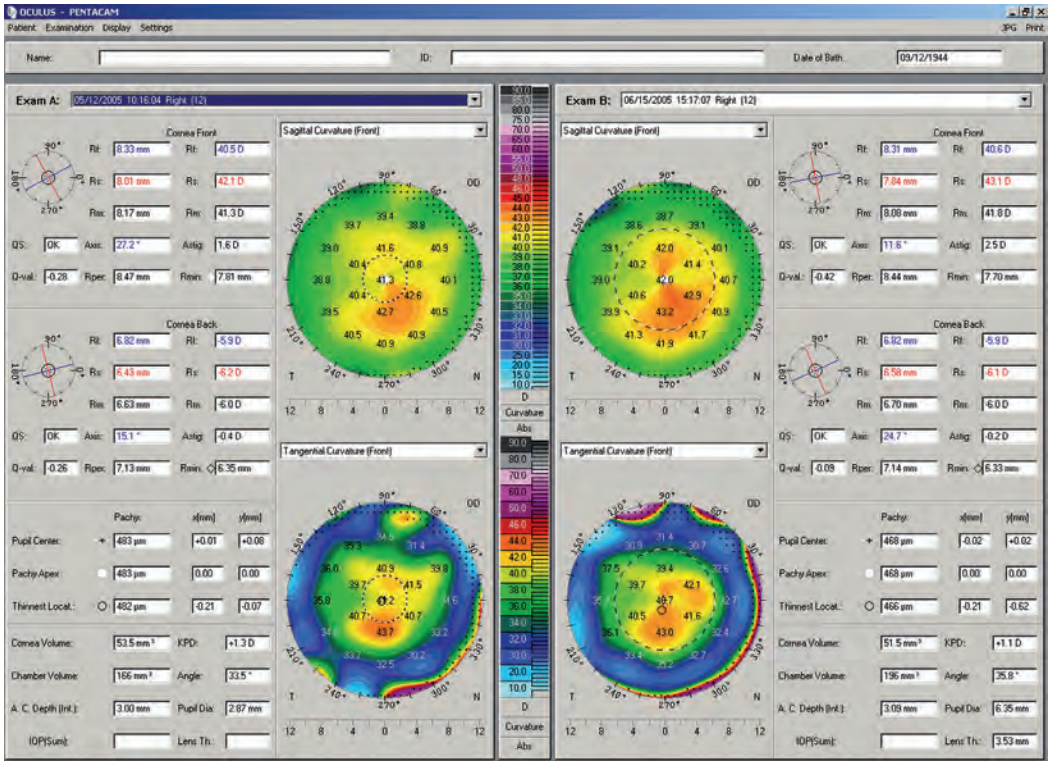

Figure 188: Show 2 Exams

23.2 Case 2: Remove sutures after corneal transplant surgery? by Tobias H. Neuhann, MD

A 22-year-old white male had received a corneal transplant due to keratoconus 12 months earlier. The first suture had already been removed. Examination with the Pentacam® revealed only a small degree of corneal astigmatism (Figure 189), but also a peripheral hot spot (black circle). BSCVA was 20/25 after removing the first sutures. The question now was whether also to remove the remaining?

WHAT WOULD YOU RECOMMEND?

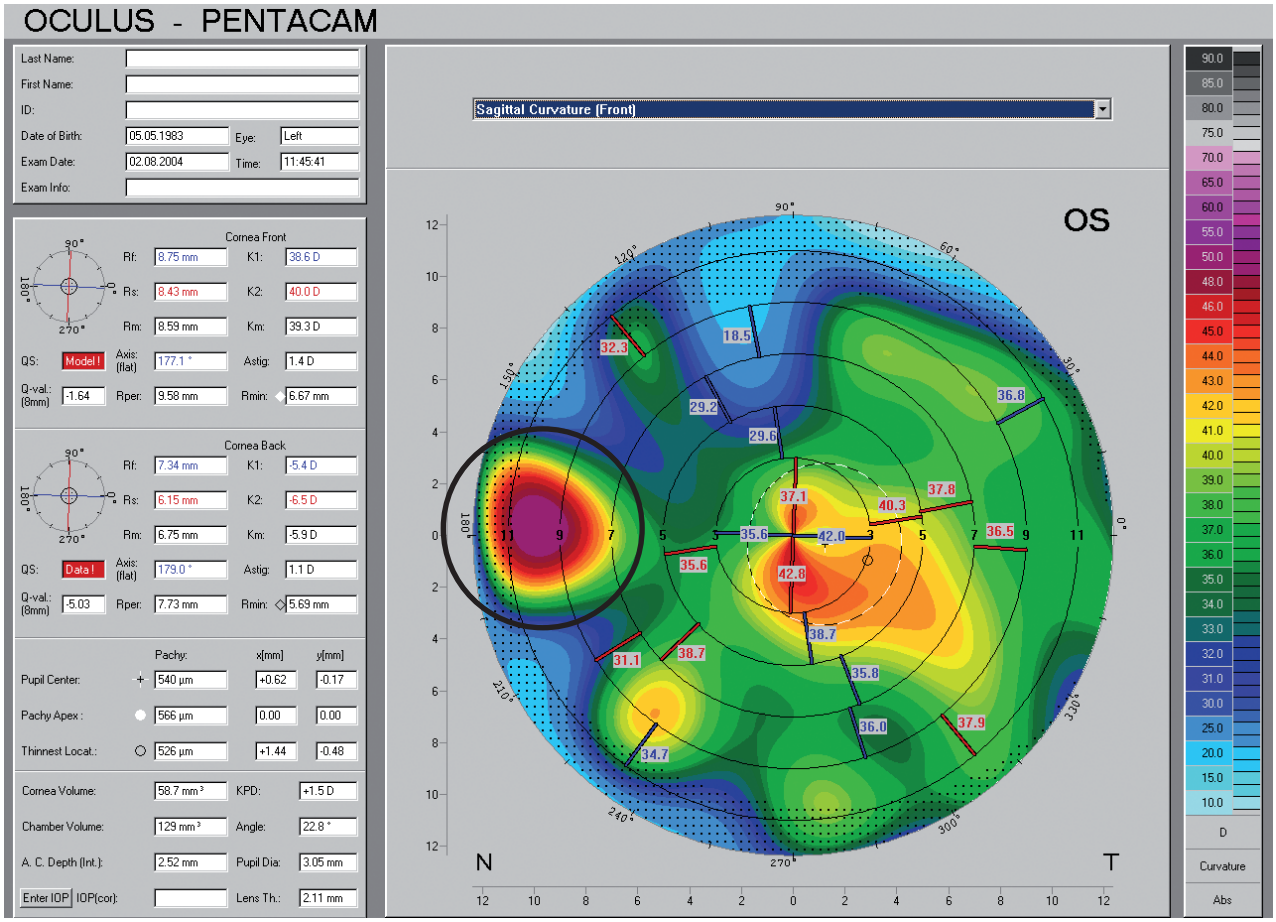

Figure 189: 1 Lage Color Map topography after corneal transplant surgery

We recommended no suture removal because of the „hot spot" temporal of the center and the low astigmatism. The patient only wears his glasses for driving at night.

23.3 Case 3: Keratoconus and cataract by Tobias H. Neuhann, MD

A 54-year-old male asked for glasses. BSCVA was 20/80 in both eyes. The Pentacam® delivered the solution in two seconds. The right eye had a cataract and undetected keratoconus (Figure 190, Figure 192). The left eye had no cataract, but undetected keratoconus (Figure 193, Figure 194, Figure 195).

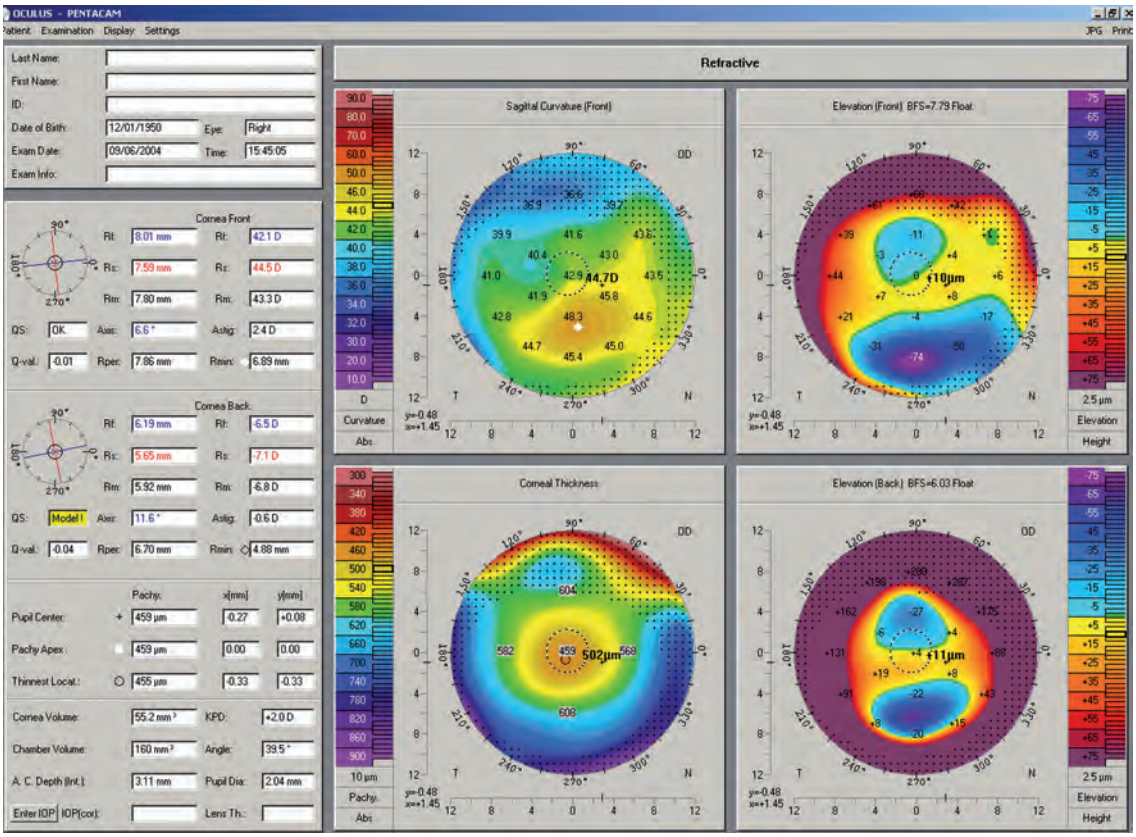

Figure 190: 4 Maps Refractive of OD

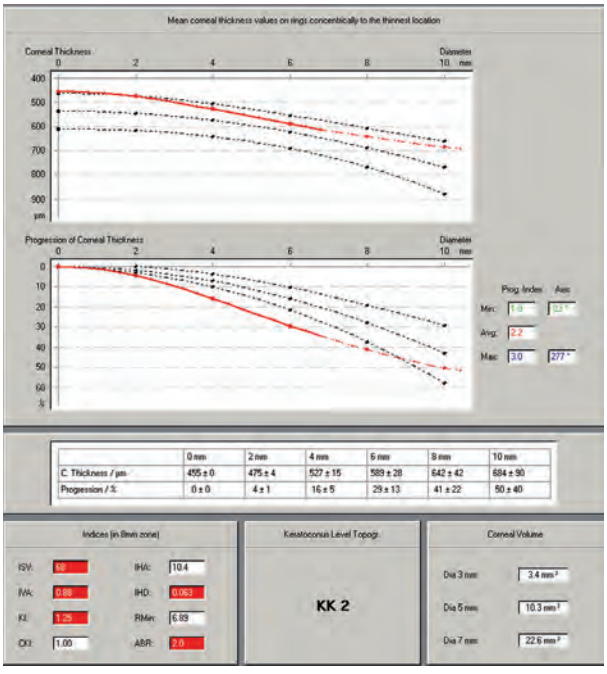

Figure 191: Pachymetry progression in OD

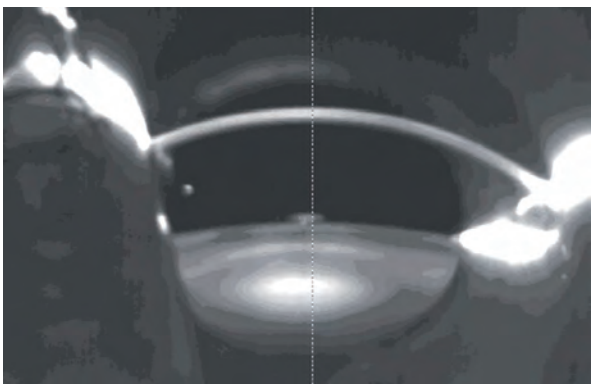

Figure 192: Scheimpflug image of OD

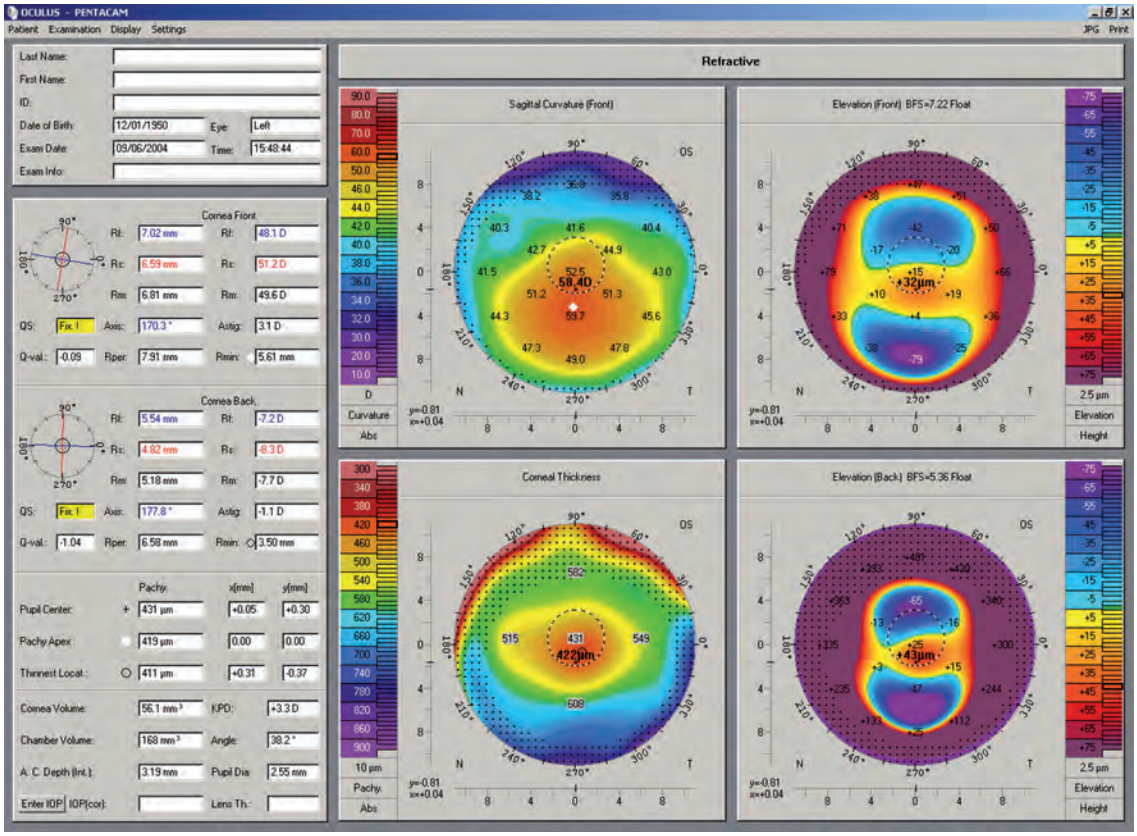

Figure 193: 4 Maps Refractive of OS

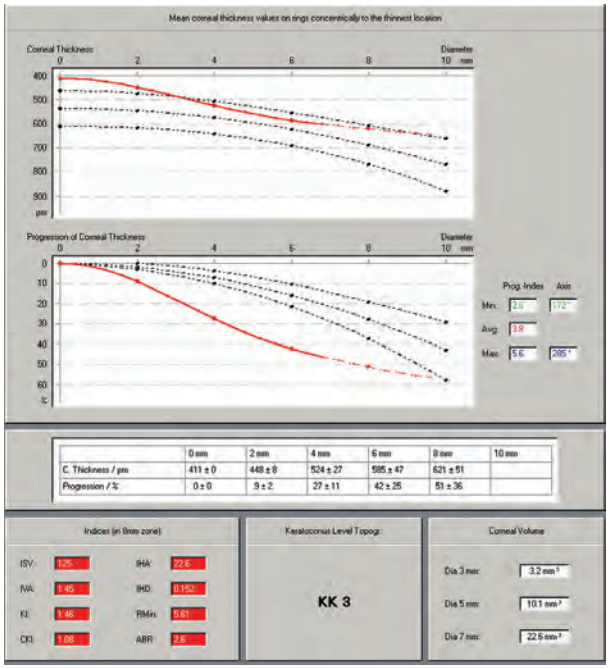

Figure 194: Pachymetry progression in OS

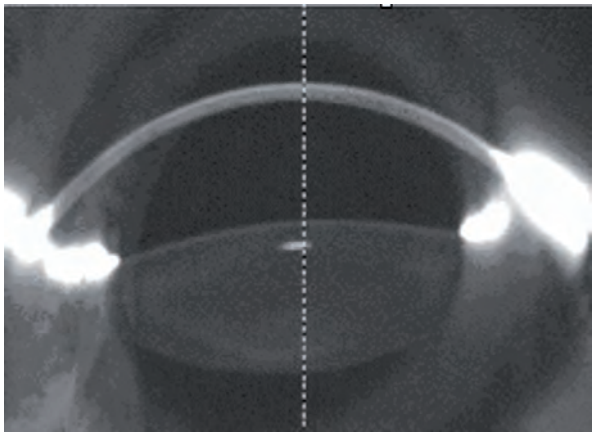

Figure 195: Scheimpflug image of OS

Our recommendation was:

- cataract surgery on the right eye;
- deep lamellar keratoplasty for the left eye; and
- toric IOL implantation in the left eye after suture removal.

This still left one question open regarding the right eye:

Which K reading should we use for the IOL calculation?

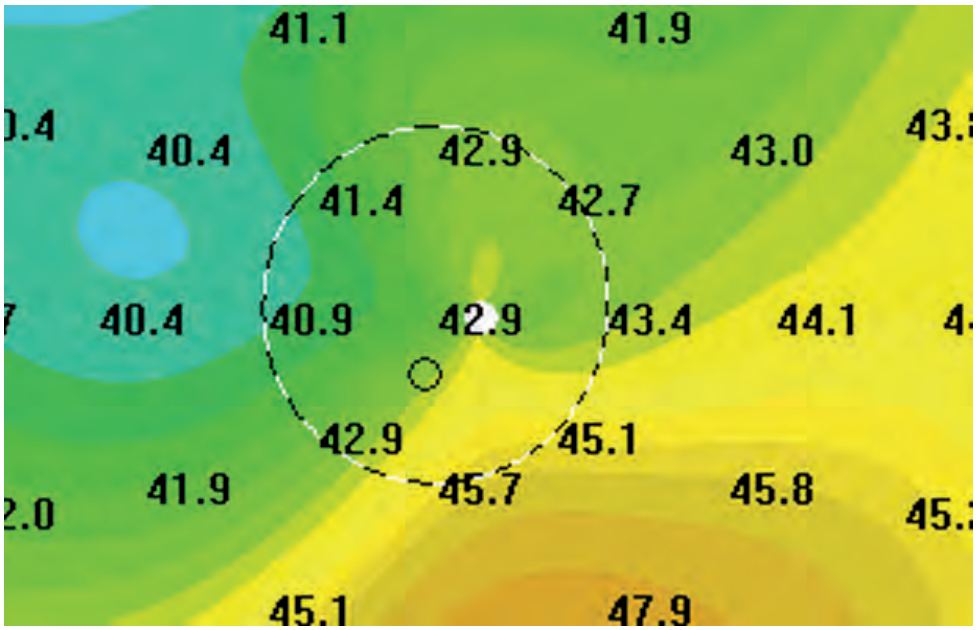

Figure 196: Topography of the central part of the cornea

The Pentacam® gives us an actually measurement ot the central power of the cornea. We used 42.9 for both K1 and K2 (Figure 196). Postoperative refraction turned out at + 0.5 D of the intended refraction.

Note:

The Pentacam® measures the power of the central cornea, whereas topographers have to extrapolate the central power of the cornea because of the blind spot in the center where the camera is located.

23.4 Case 4: Corneal infiltrate by Prof. Renato Ambrósio Jr

A 33-year-old female presented for evaluation of a corneal infiltrate. The patient mentioned having used tap water for cleaning her soft contact lens two days ago. Her symptoms had started after wearing her contact lens 6 hours in OS. She woke up in the next night with moderate secretion.

She complained of photophobia and blurred vision in OS when wearing glasses. A Pentacam® examination was performed in both eyes, revealing an infiltrate in OS, and the findings were with correlated slit lamp biomicroscopy images (Figure 197, Figure 198).

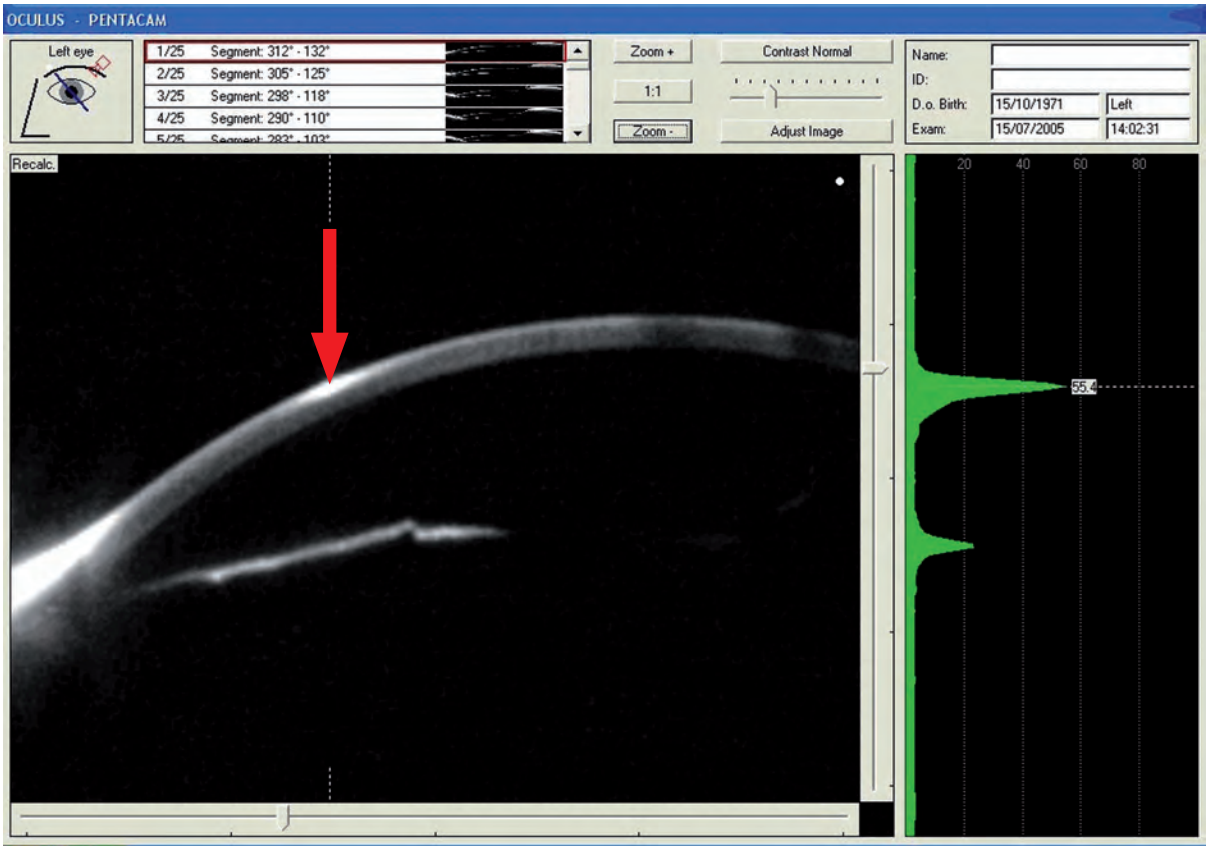

Figure 197: Scheimpflug Image of a corneal infiltrate

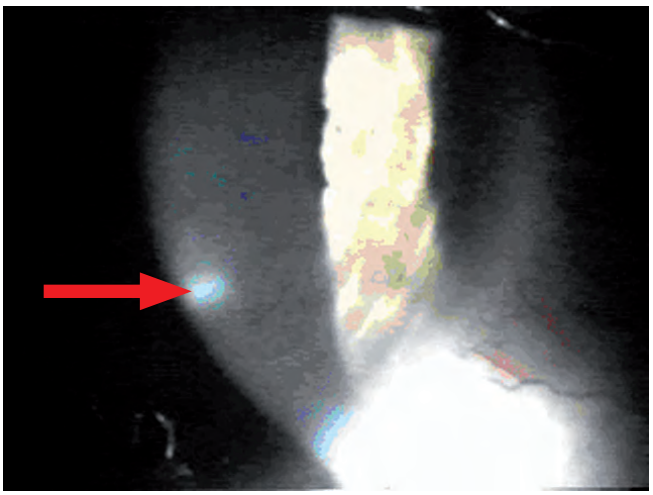

Figure 198: Slit lamp photo of the same corneal infiltrate

She had been prescribed topical drops containing a combination of neomycin, polymixin B and dexametasone, which she had used 4 times since the last night, obtaining mild improvement. The patient was advised to discontinue contact lens use in both eyes and asked to stop the medication. We decided to empirically start her on 4th generation fluoroquinolones, initiating treatment with an attack dose of one drop every ten minutes during the first hour followed by hourly doses around the clock. One day later she reported improvement in her vision as well as her other symptoms.

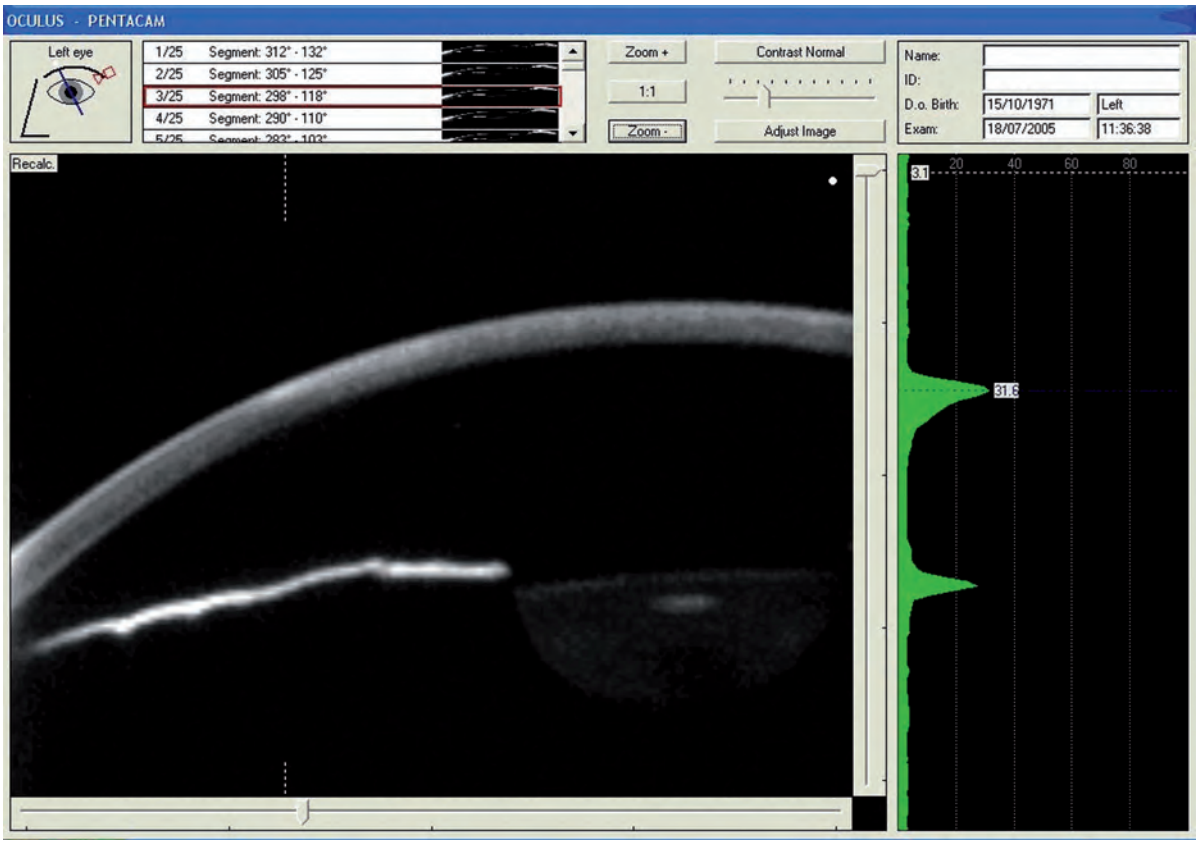

Figure 199: Scheimpflug Image of acorneal infiltrate 3 days later

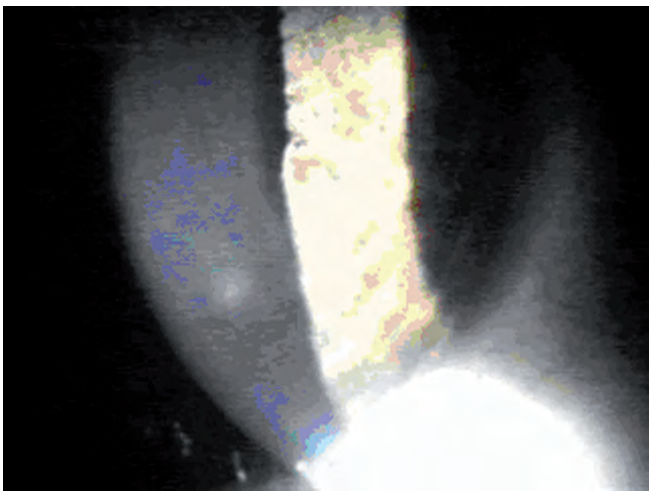

Figure 200: Slit lamp photo of the same corneal infiltrate 3 days later

When the Pentacam® examination was repeated on day 3, the infiltrate was found to have decreased, as seen in the Scheimpflug and slit lamp biomicroscopy images (Figure 199, Figure 200). She also noted improvement in BSCVA in OS.

23.5 Case 5: Incisional edema by Prof. Renato Ambrósio Jr

A 76-year-old female patient presented with incisional edema 12 months after phacoemulsification. Endothelial morphology revealed large cells with pleomorphism and polymegathism. Central cell count was 1.079 cells/mm².

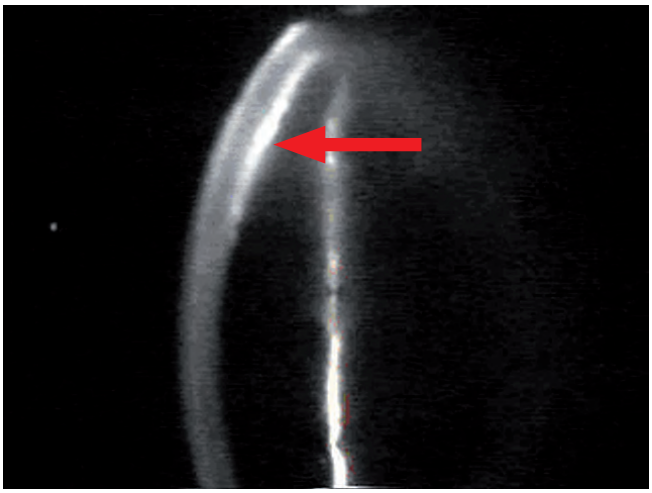

Figure 201: Slit lamp photo showing incisional edema

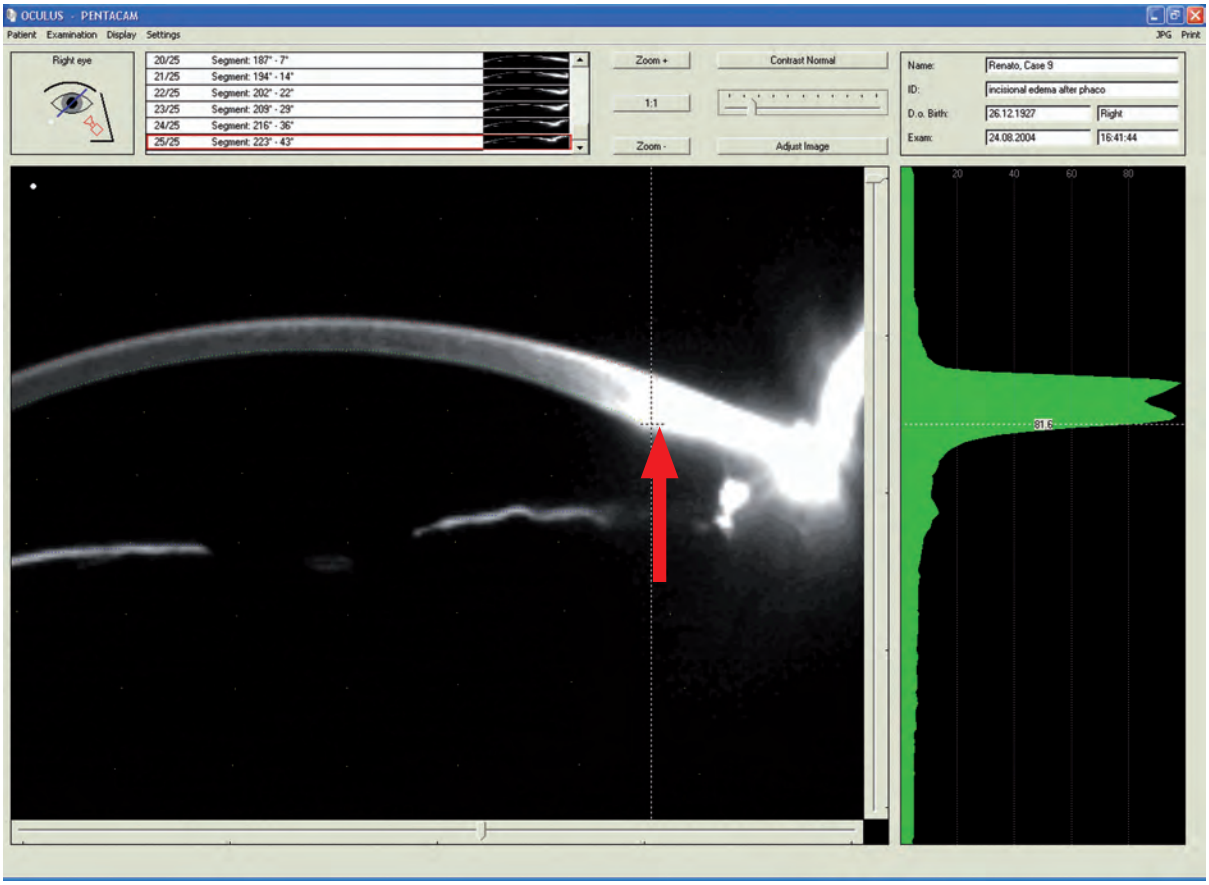

Figure 202: Scheimpflug Image showing incisional edema

A slit lamp exam and a Pentacam® exam were performed, and the findings were correlated with each other (Figure 201, Figure 202). The central cornea was clear with no edema. The peripheral cornea at the incision location was edematous, with formation of small bullae on the surface. The pachymetric map correlates with this finding. Interestingly the Scheimpflug image matches the "U shape" sign or "camel sign" over the edematous area on the densitometry. This is caused by the high reflectivity of the posterior layer of the cornea at the incision level.

23.6 Case 6: Corneal thinning after herpetic keratitis by Prof. Renato Ambrósio Jr

A 68-year-old female patient entered the office with a long history of several episodes of herpes simplex virus stromal keratitis. Careful slit lamp examination (Figure 203) revealed sub-epithelial scarring of the central cornea consistent with the "ghost scarring" known of herpes simplex virus infections.

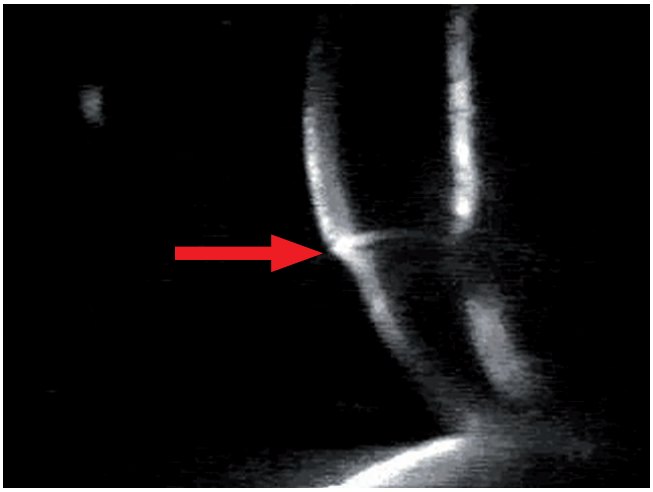

Figure 203: Slit lamp photo revealed sub-epithelial scarring of the central cornea

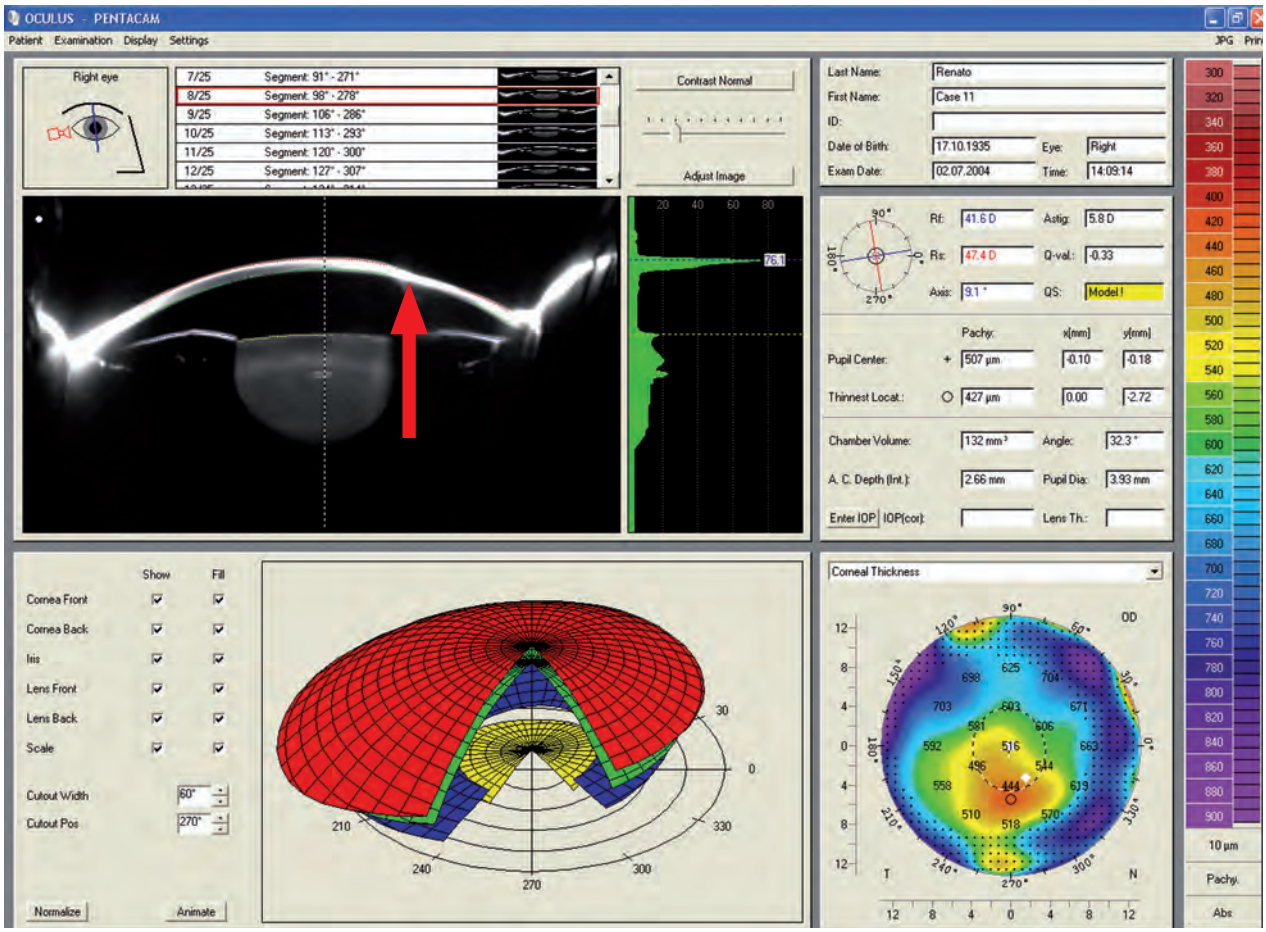

Figure 204: General Overview display revealing corneal thinning

A Pentacam® exam is useful for documenting corneal thickness. The thinnest spot is displayed in the pachymetry map and can also be seen in the Scheimpflug images, facilitating follow-up examination (Figure 204). The patient was kept on prophylactic Acyclovir 800 mg per day, omega 3 essential fatty acid supplementation (flaxseed oil, 1g twice daily) and topical artificial tears.

23.7 Case 7: Epithelial ingrowth after keratomileusis in situ by Prof. Renato Ambrósio Jr

A 41-year-old male patient with a history of in situ keratomileusis in 1991 and one re-treatment for removal of epithelial ingrowth asked for a second opinion.

The slit lamp examination (Figure 205) revealed epithelial ingrowth, under a moderately deep cap, reaching the center of the pupil area in OD.

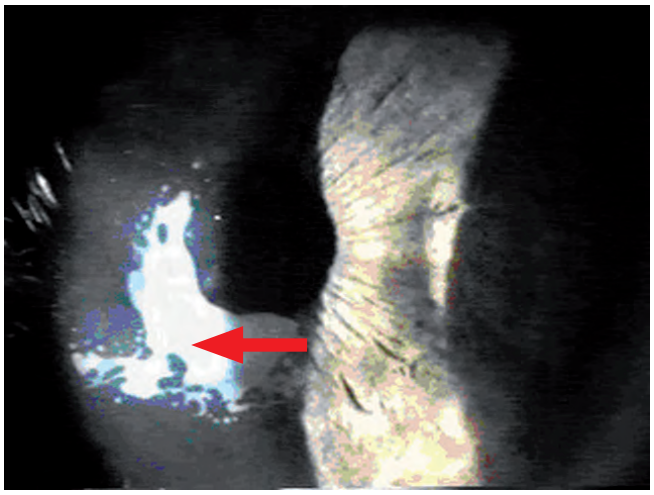

Figure 205: Slit lamp photo revealed epithelial ingrowth

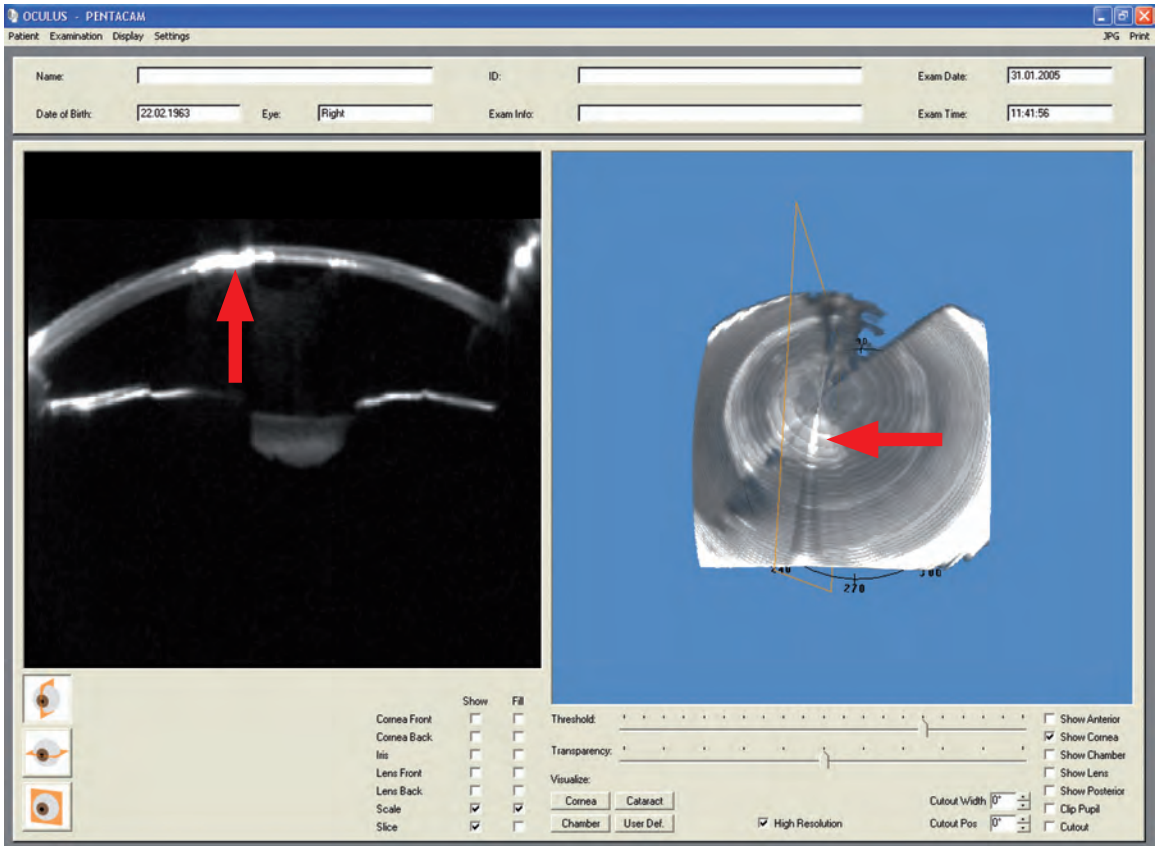

Figure 206: Tomography confirming epithelial ingrowth

Epithelial ingrowth was also easily seen in the Pentacam® Tomography (Figure 206).

The pachymetry map in the 4 Maps Refractive (Figure 207) showed this effect as well, even in the presence of an opaque cornea. The Pentacam® was useful for evaluating corneal elevation, curvature, thickness and opacity.

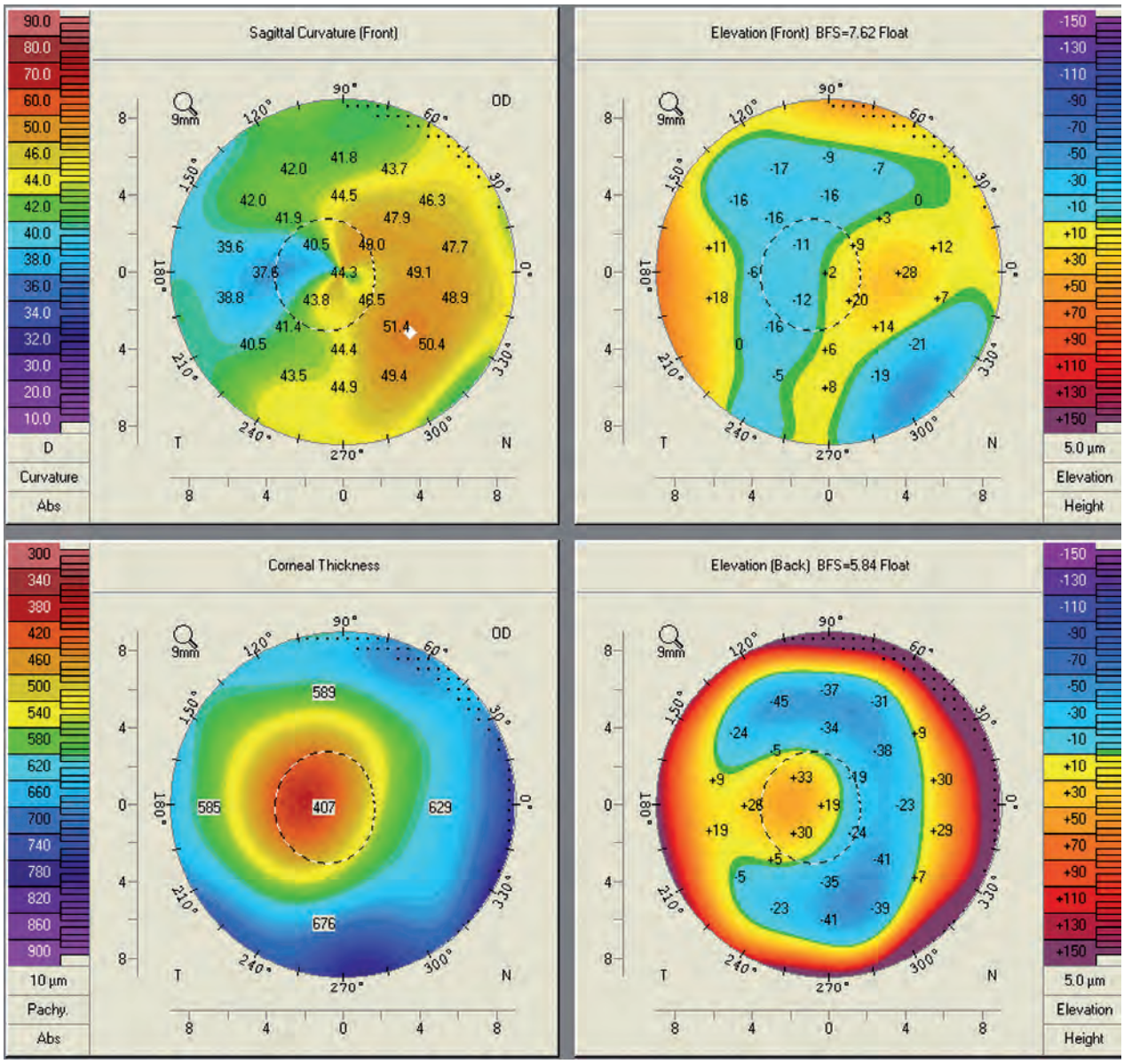

Figure 207: Part of 4 Maps Refractive confirming epithelial ingrowth

24 Scheimpflug and slit lamp images

24.1 Corneal dystrophy

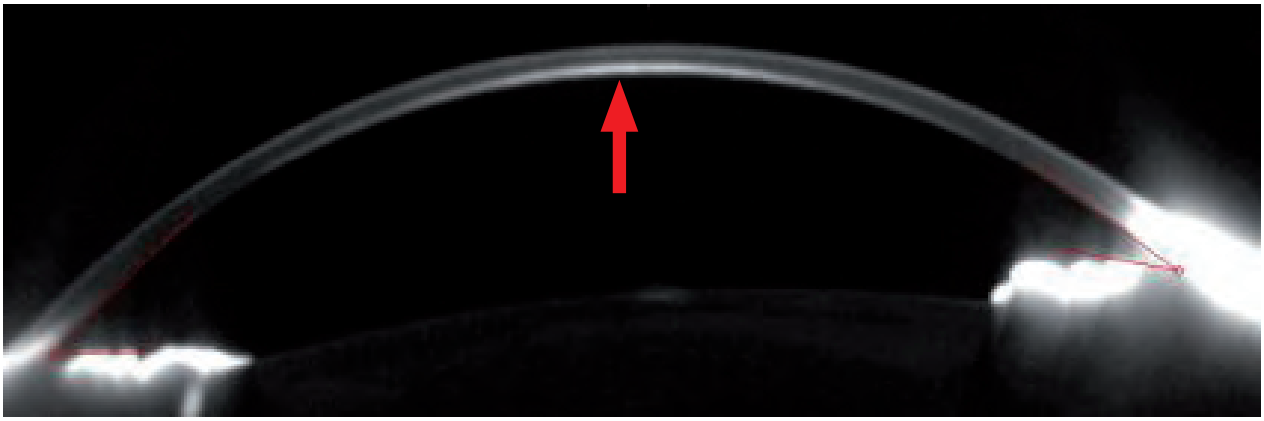

Figure 208: Scheimpflug image revealing, corneal dystrophy on the posterior surface

Figure 209: Slit lamp photo documenting corneal dystrophy on the posterior surface

24.2 Congenital anterior pyramid cataract

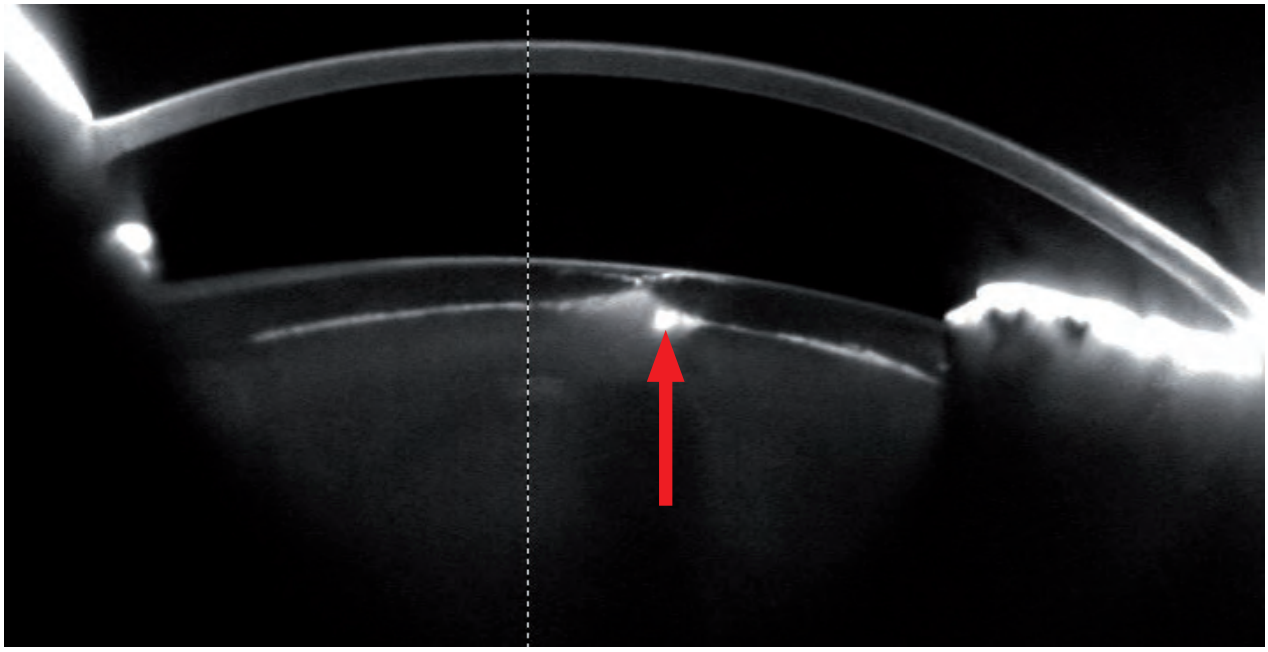

Figure 210: Scheimpflug image showing an anterior pyramid cataract

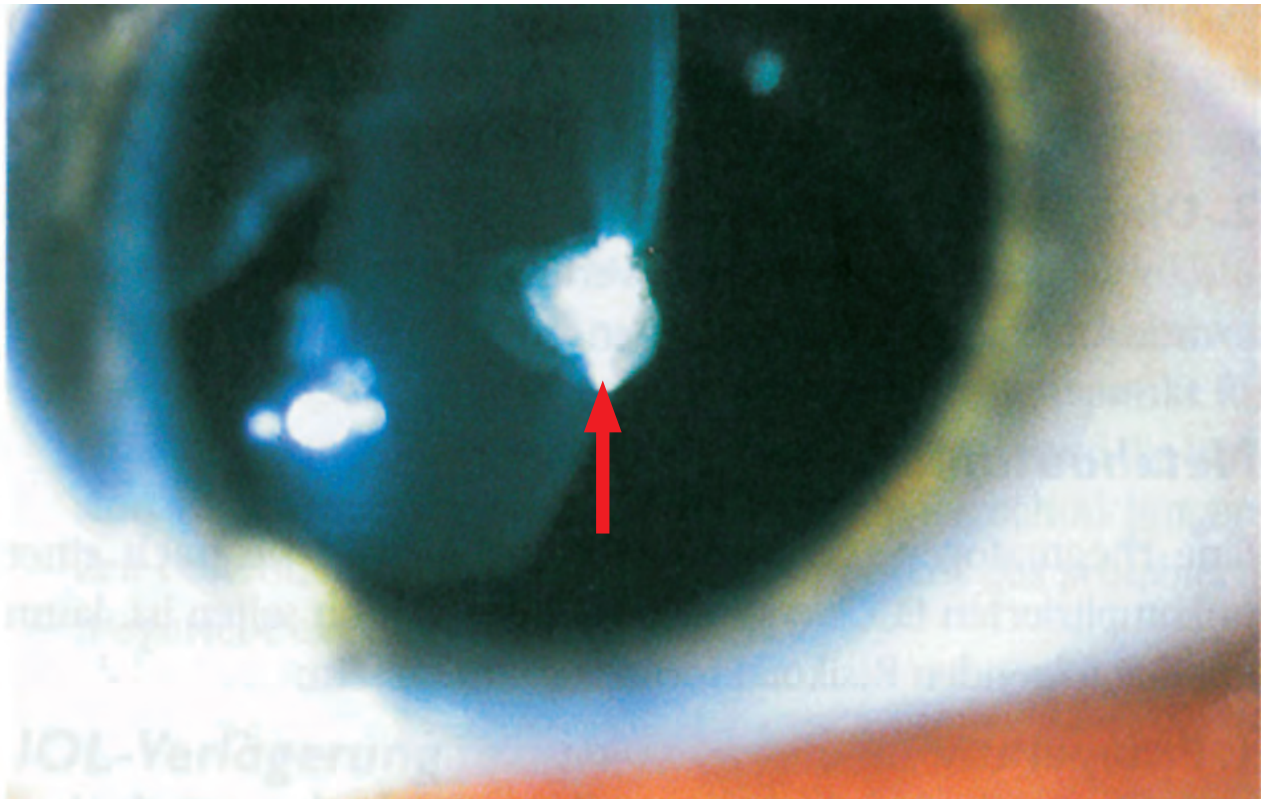

Figure 211: Slit lamp photo showing an anterior pyramid cataract

24.3 Posterior capsular cataract

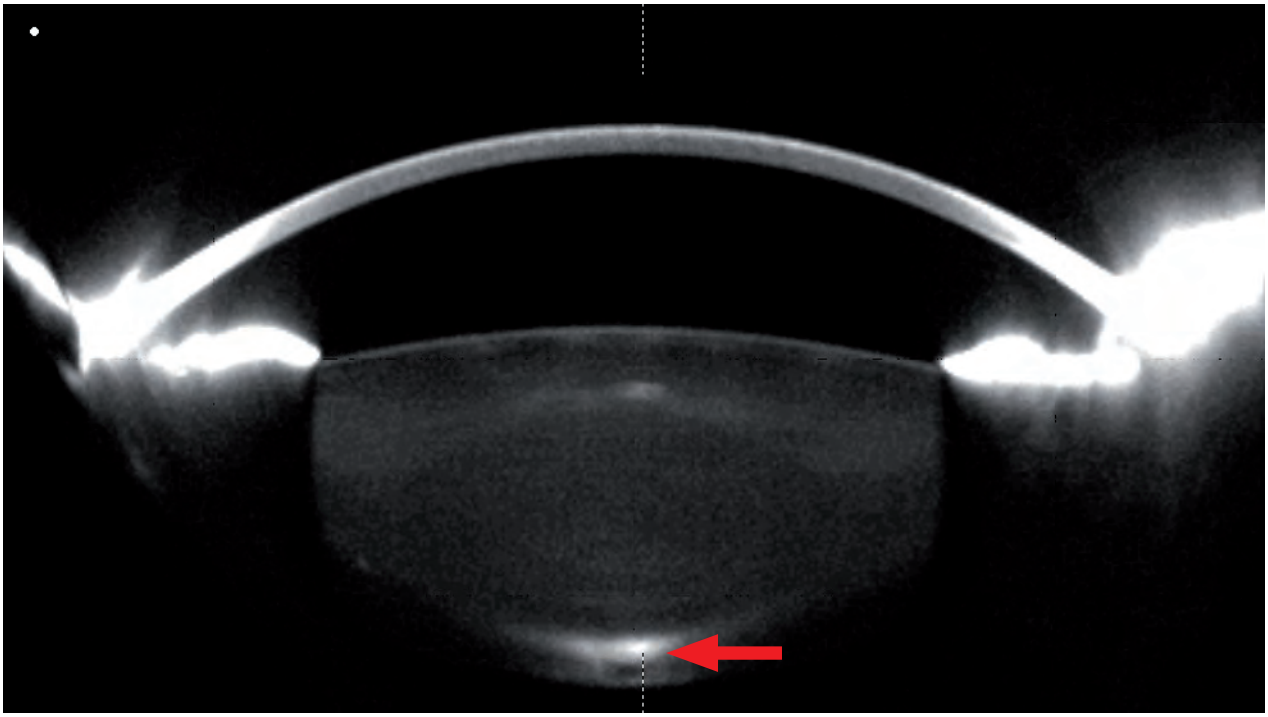

Figure 212: Scheimpflug image showing a posterior capsular cataract

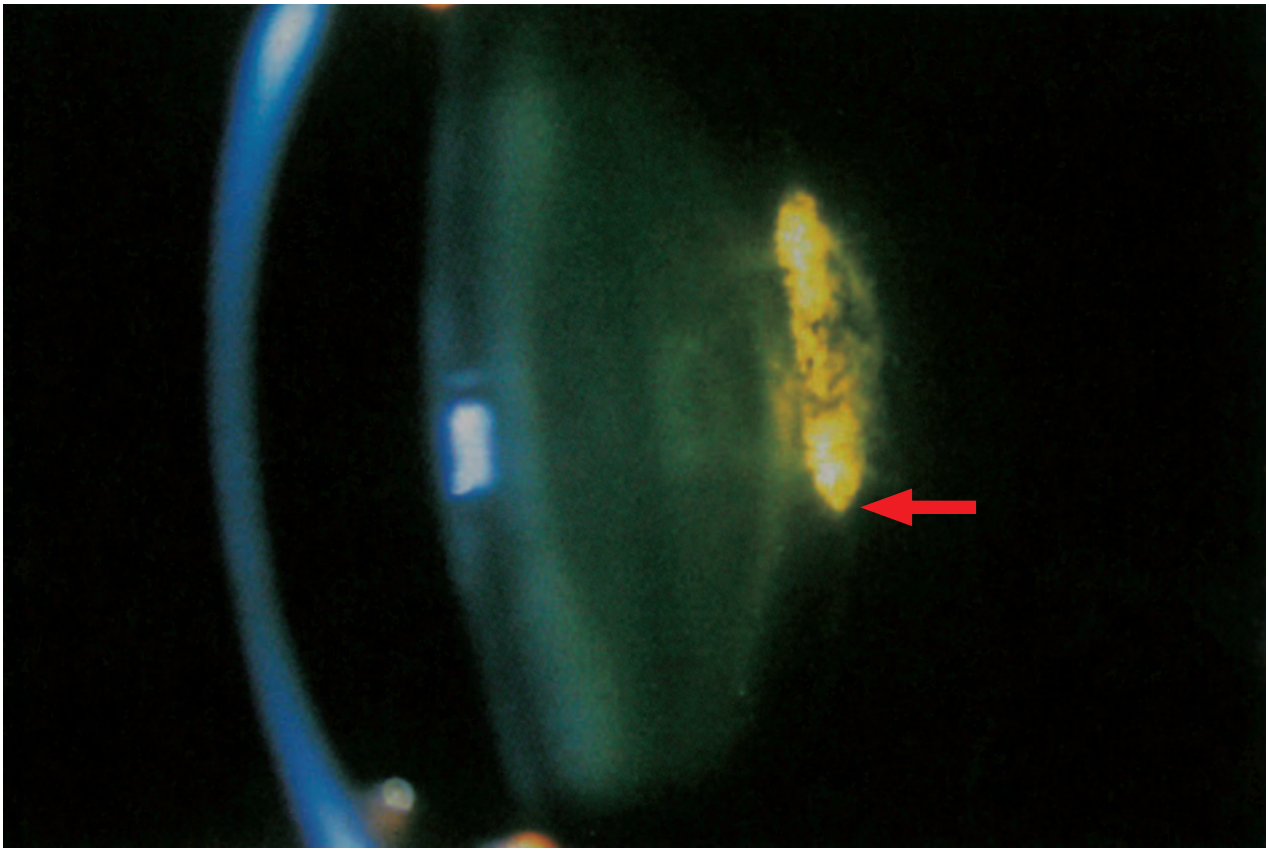

Figure 213: Slit lamp photo showing a posterior capsular cataract

24.4 Nuclear cataract

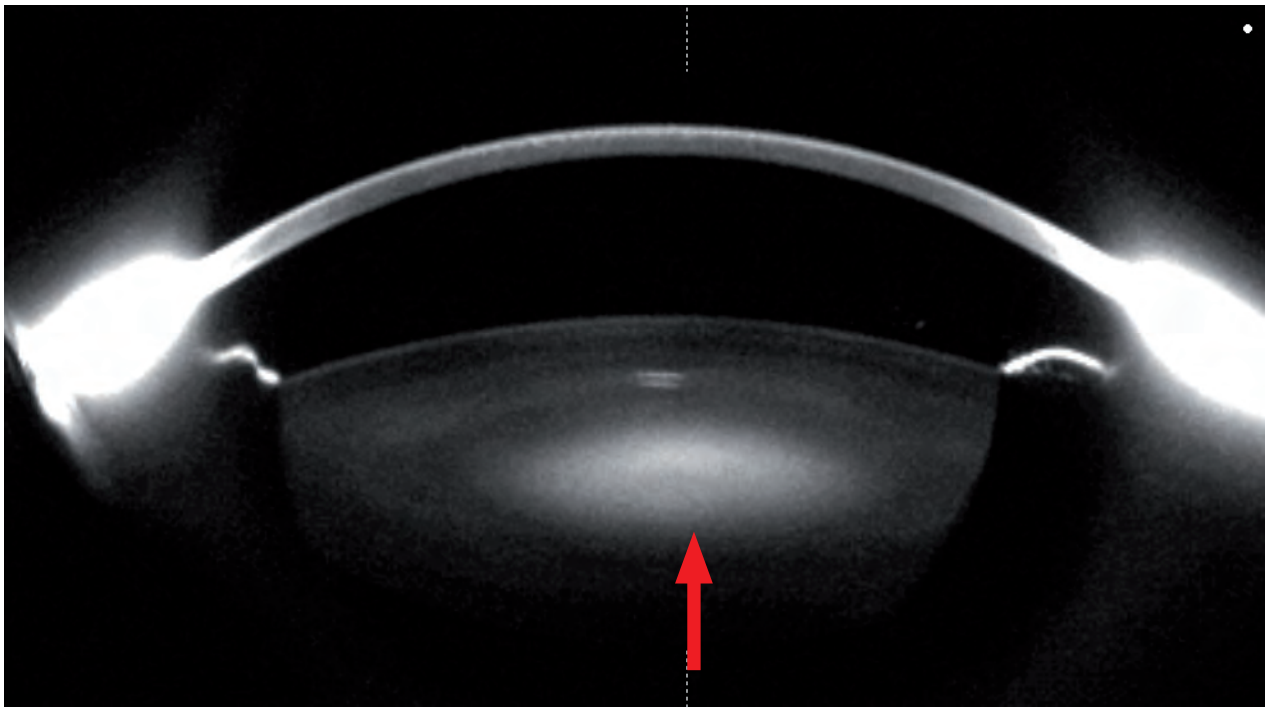

Figure 214: Scheimpflug image showing a nuclear cataract

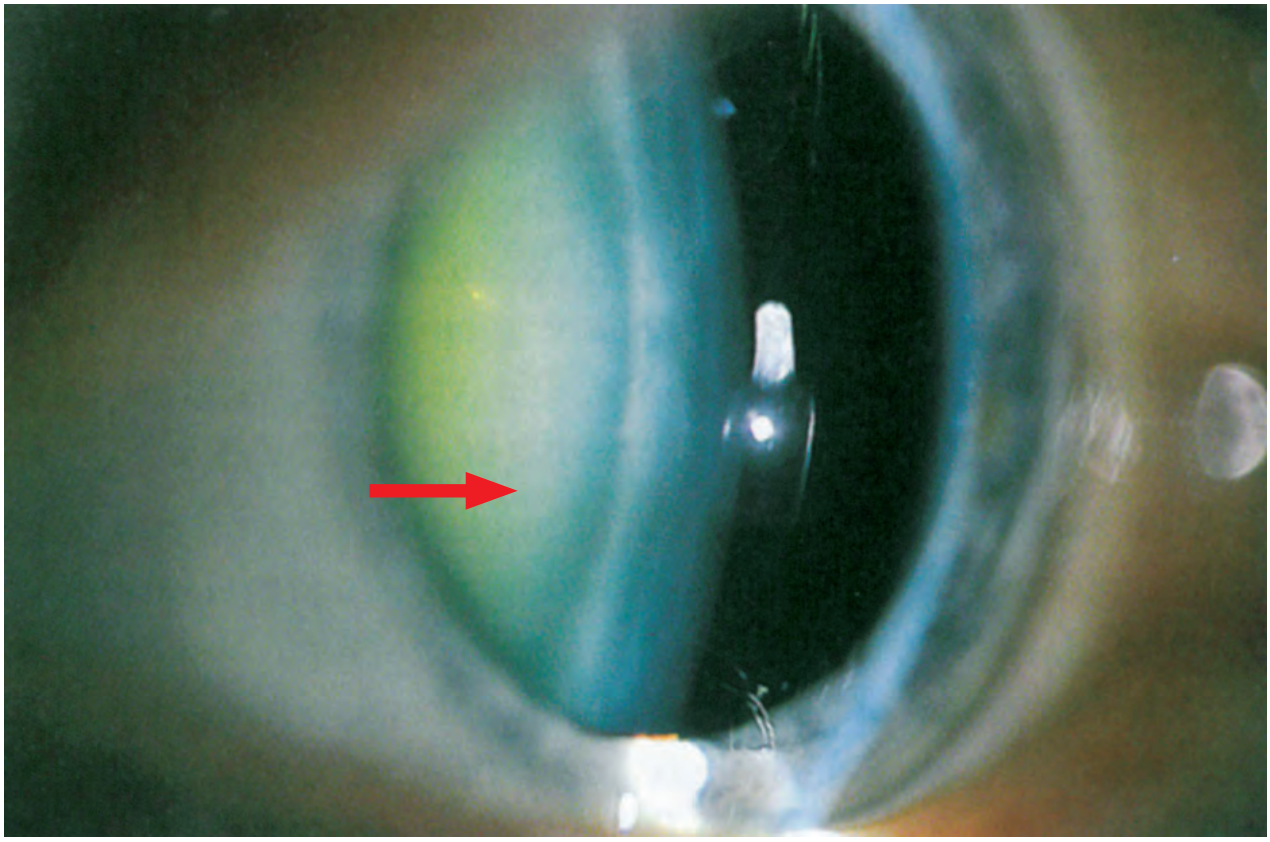

Figure 215: Slit lamp photo showing a nuclear cataract

24.5 Posterior synechia

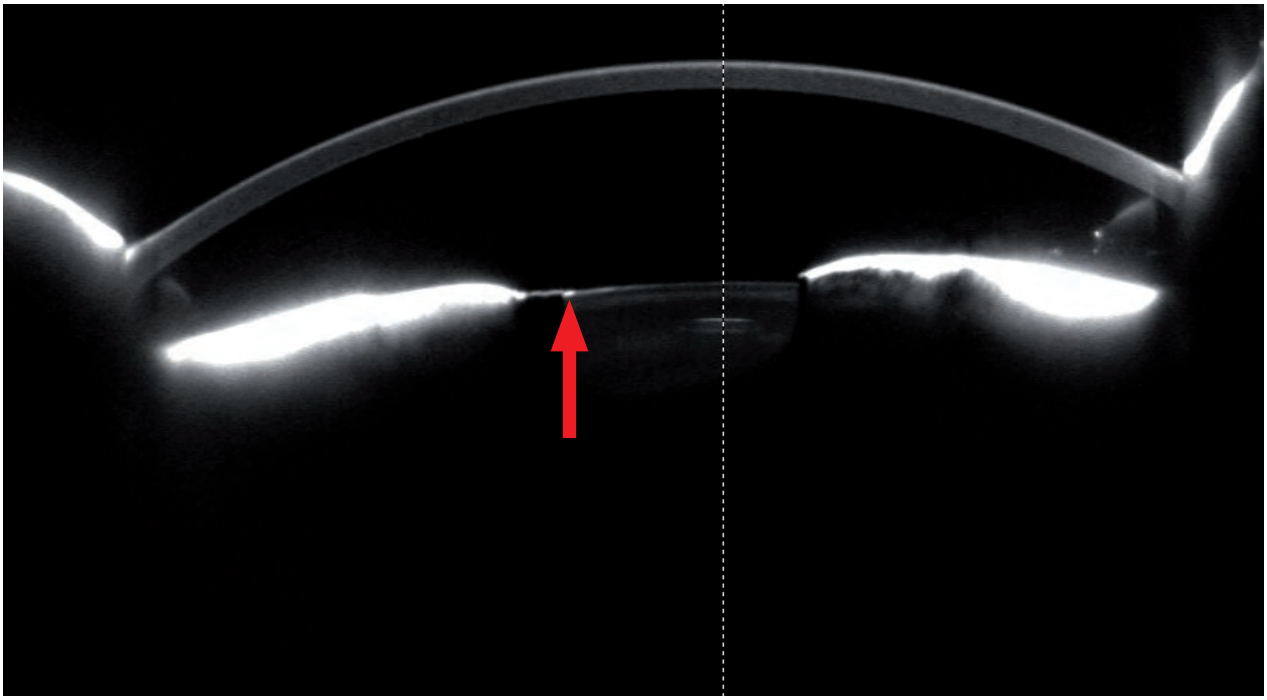

Figure 216: Scheimpflug image showing posterior synechia

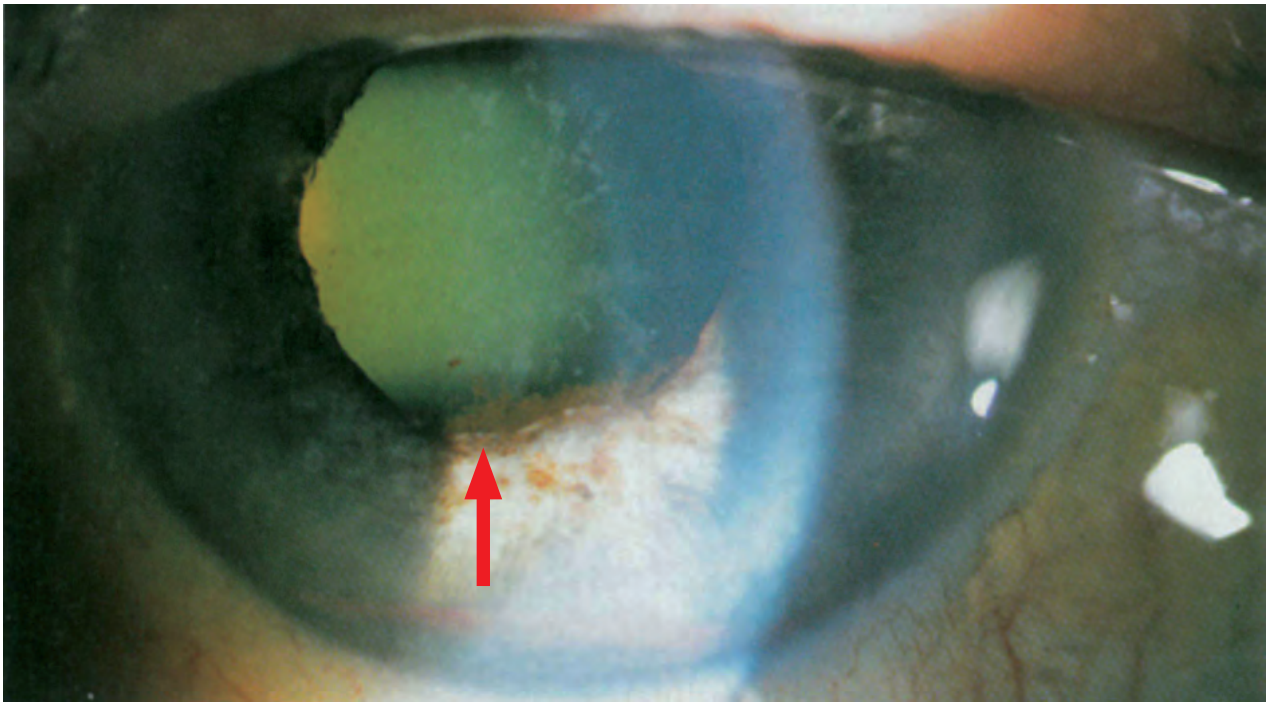

Figure 217: Slit lamp photo showing posterior synechia

24.6 Pterygium

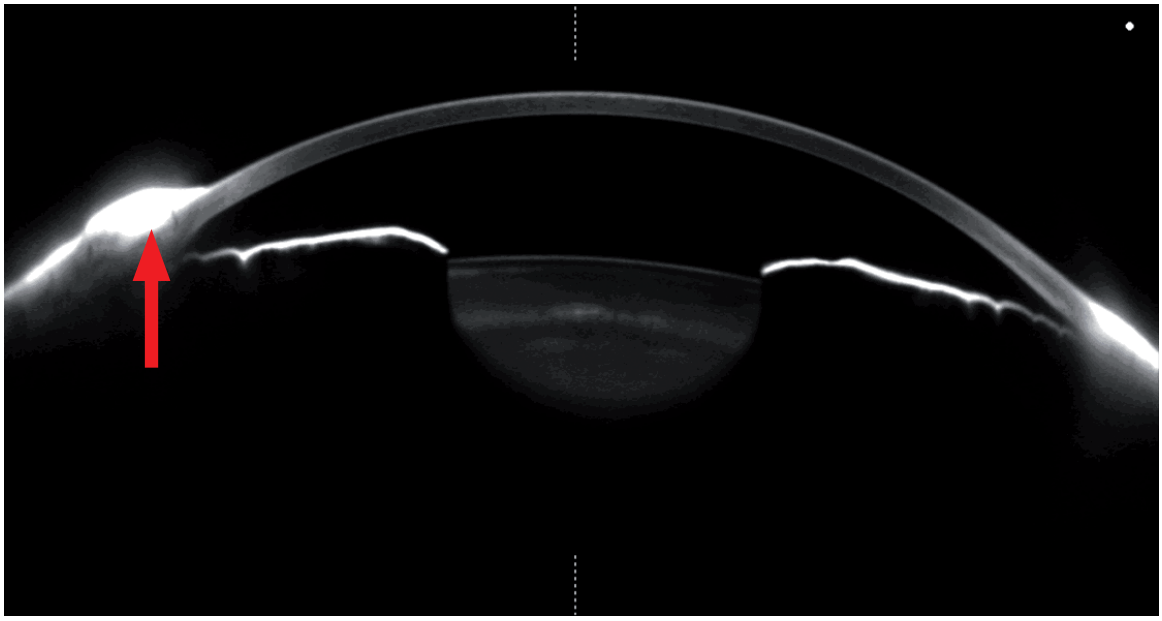

Figure 218: Scheimpflug image in 190° showing a case of pterygium

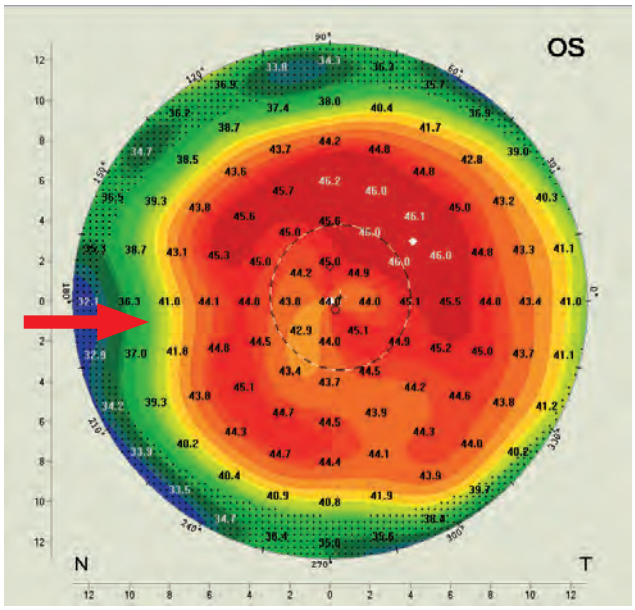

Figure 219: Topography revealing pterygium

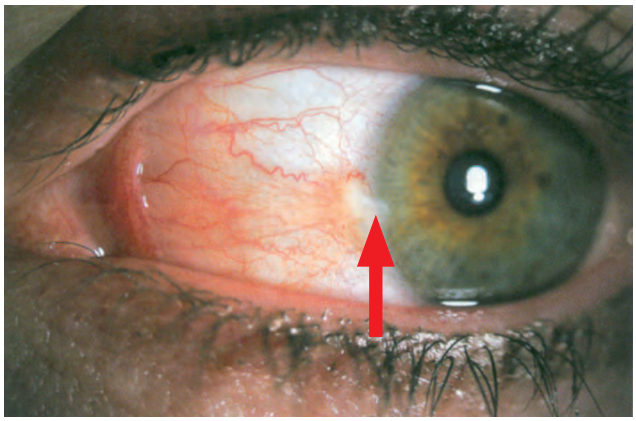

Figure 220: Slit lamp photo of an eye with pterygium

25 Orthokeratology, general screening by Alain-Nicolas Gilg, MD

A 34-year-old male presented with the request to have his soft contact lenses changed because of progressive intolerance during the day.

Subjective refraction resulted in a visual acuity of

- OD: sph -2.50
- OS: sph -1.00

The Pentacam® Show 2 Exams display showed an optimal eccentricity on the 30° meridian of both eyes, namely 0.50 in OD and 0.49 in OS, permitting us to propose an orthokeratology treatment to this patient (Figure 221).

After fitting the lenses, examinations prior to midday revealed a good visual acuity of 0.8 on day 1 and of 1.0 on days 8 and 28.

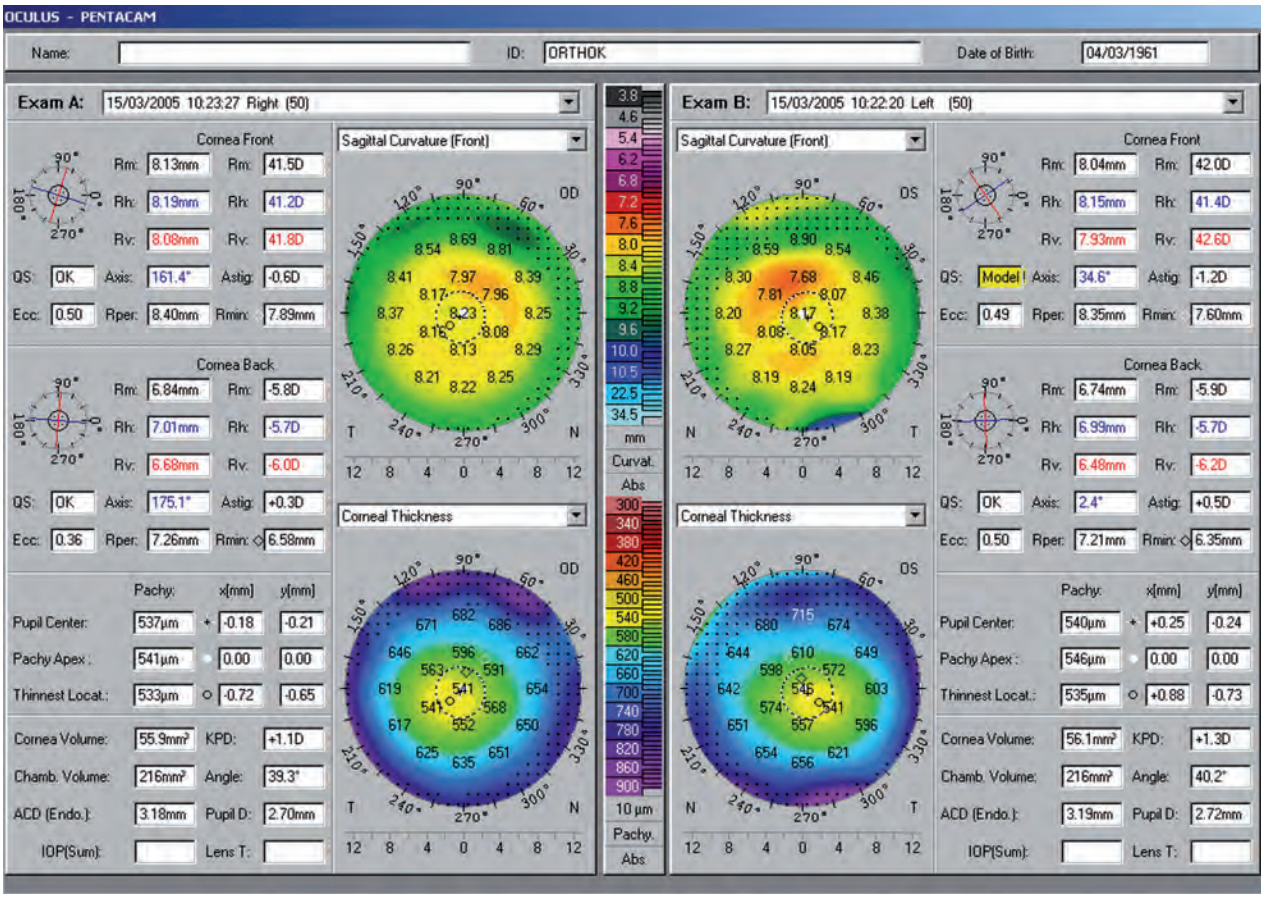

Figure 221: Show 2 Exams of OD & OS prior to orthokeralotogy

The patient was examined 4 times within 2 months to follow up the condition of the cornea, and the efficacy of the treatment was confirmed by a comparison of all four exams (Figure 222).

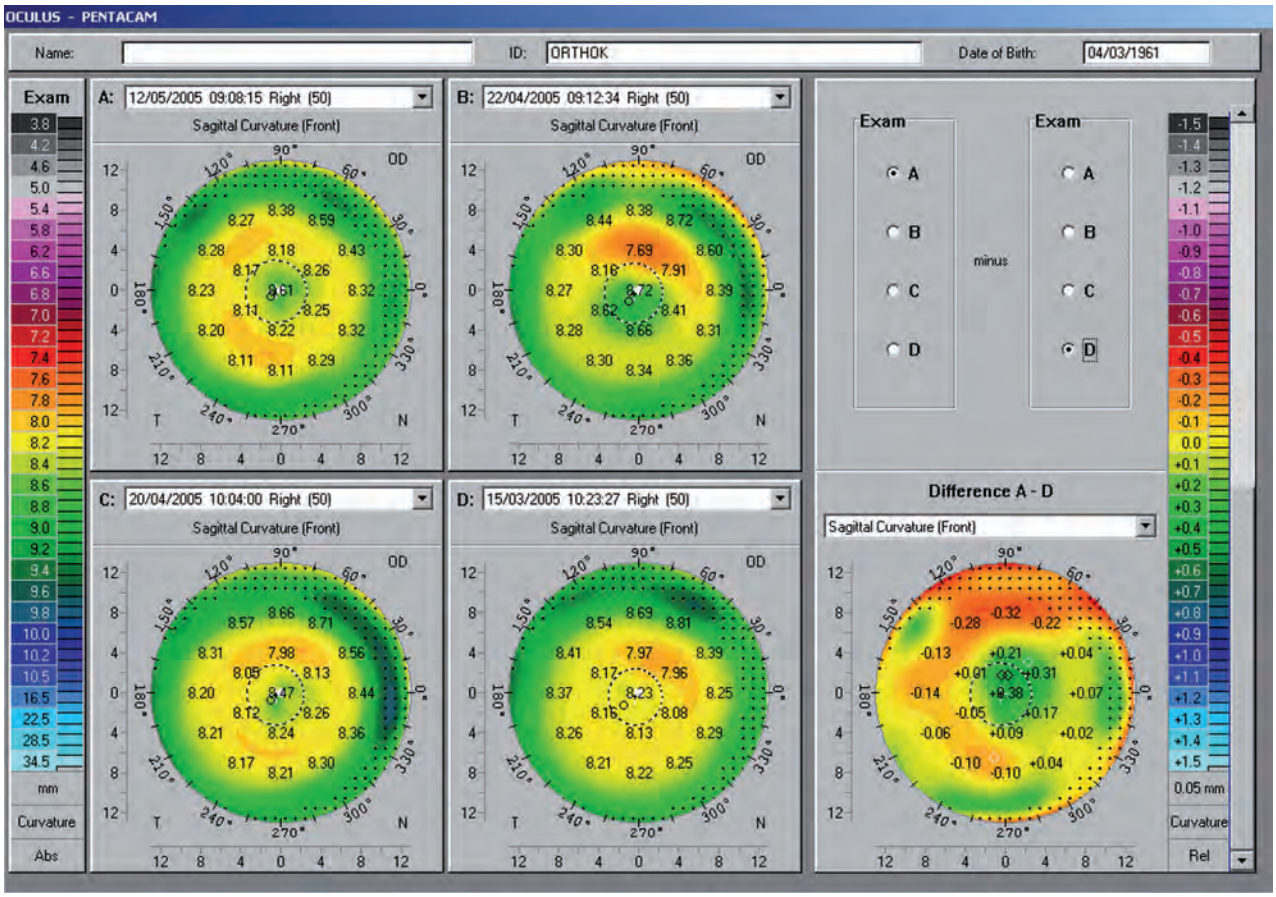

Figure 222: Compare 4 Exams, one prior and three after orthokeratology

On day 28 the patient complained of fluctuations in his visual acuity during the day. Thereupon he was examined in the morning after wearing the lens over night and in the late afternoon. Examination with the Pentacam® using the Compare 2 Exams display confirmed that the effect of the ortho-K lens was reversed during the day, and so it was decided to fit the patient with a more effective ortho-K lens (Figure 223).

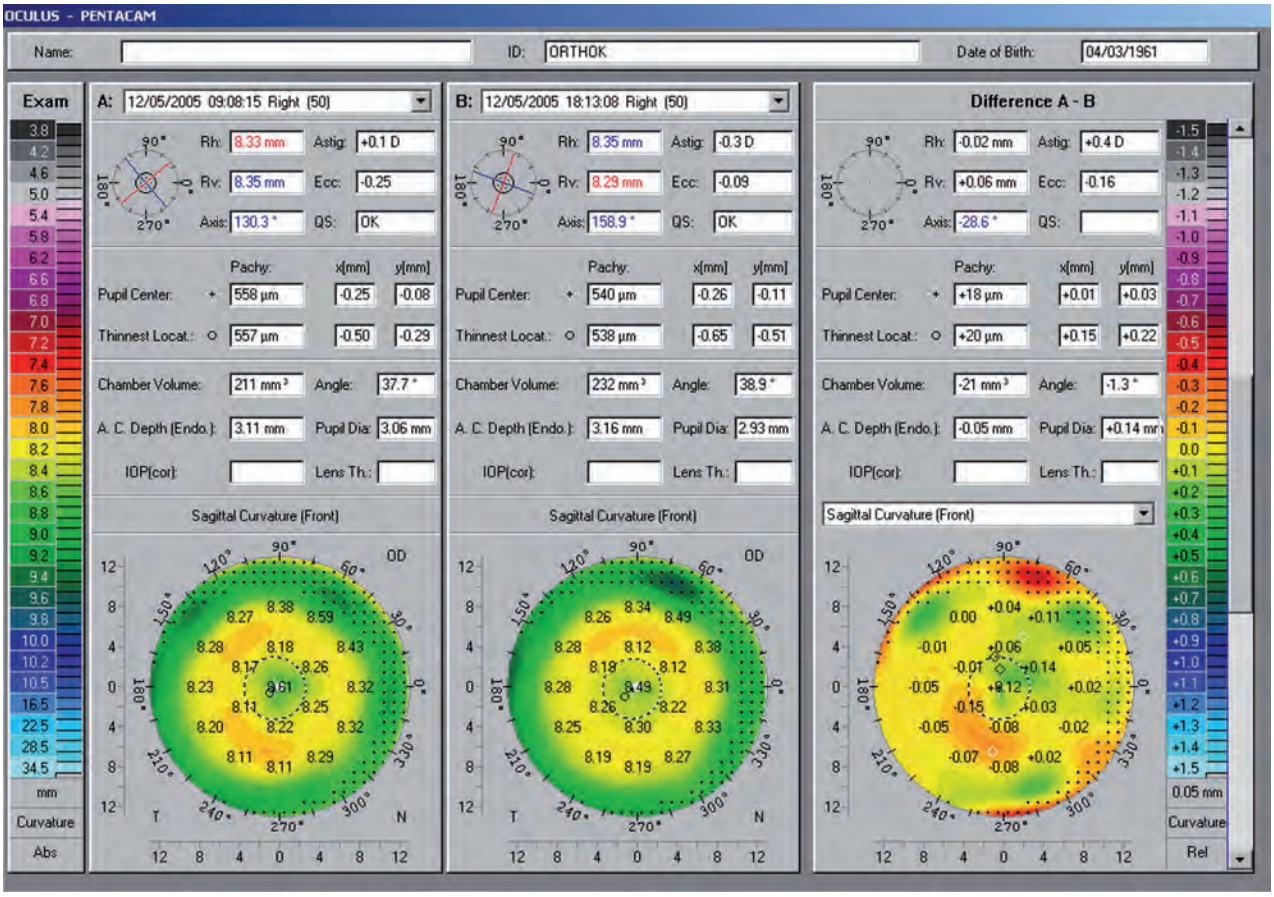

Figure 223: Compare 2 Exams in the morning and evening at the same day

26 Important studies and case reports

26.1 Refractive studies:

2016

- Optical densitometric measurements of the cornea and lens in children with allergic rhinoconjunctivitis - (Gökhan Pekel, MD, Fatih Firinci, MD, Semra Acer, MD, Seher Kasikçi, MD, Ramazan Yagci, MD, Emin Mete, MD, Ebru Nevin Çetin, MD) - Clin Exp Optom 2016; 99: 51–55, DOI:10.1111/cxo.12322
- Application of corneal tomography before keratorefractive procedure for laser vision correction - (Allan Luz, Bernardo Lopes, Marcela Salomão, and Renato Ambrósio) - Journal of BioPhotonics, 1–9 (2016) / DOI 10.1002/jbio.201500236
- Effect of Pseudoexfoliation on Corneal Transparency - (Ali Bulent Cankaya, Kemal Tekin, MD, and Merve Inanc, MD) - Cornea 2016;35:1084–1088
- Central Corneal Thickness Measurement Using Ultrasonic Pachymetry, Rotating Scheimpflug Camera, and Scanning-slit Topography Exclusively in Thin Non-keratoconic Corneas - (Mehrdad Mohammadpour, MD, Kazem Mohammad2, PhD, Nasser Karimi, MD, MPH) - J Ophthalmic Vis Res 2016; 11 (3): 245-251
- Assessing progression of keratoconus: novel tomographic determinants - (Joshua K. Duncan, Michael W. Belin and Mark Borgstrom) - Eye and Vision (2016) 3:6, DOI 10.1186/s40662-016-0038-6
- Keratoconus: The ABCD Grading System - (M.W. Belin, J.K. Duncan) - Klinische Monatsblätter, http://dx.doi.org/10.1055/s-0042-100626
- A new Tomographic Method of Staging/Classifying Keratoconus: The ABCD Grading System - (Michael W. Belin, Josh Duncan, Renato Ambrosio Jr, Jose AP Gomes) - IJKECD, 10.5005/jp-journals-10025-1105
- Corneal Densitometry, Central Corneal Thickness, and Corneal Central-to-Peripheral Thickness Ratio in Patients With Fuchs Endothelial Dystrophy - (Maged Alnawaiseh, MD, Lars Zumhagen, MD, Gabriele Wirths, MD, Maria Eveslage, Nicole Eter, MD, and André Rosentreter, MD) - Cornea 2016;35:358–362

2015

- Comparison of multimetric D index with keratometric, pachymetric, and posterior elevation parameters in diagnosing subclinical keratoconus in fellow eyes of asymmetric keratoconus patients - (Orkun Muftuoglu, MD, Orhan Ayar, MD, Volkan Hurmeric, MD, Faik Orucoglu, MD, Ilkay Kılıc, MD) - Journal of Cataract Refractive Surgery 2015; 41:557–565 Q 2015 ASCRS and ESCRS
- Objective classification of glistenings in implanted intraocular lenses using Scheimpflug tomography - (Heike Biwer, MD, Eva Schuber, MD, Marcus Honig, BSc, Bianca Spratte, MD, Martin Baumeister, MD, Thomas Kohnen, MD, PhD, FEBO) - Journal of Cataract Refractive Surgery 2015; 41:2644–2651 Q 2015 ASCRS and ESCRS
- Comparison of Two Different Scheimpflug Devices in the Detection of Keratoconus, Regular Astigmatism, and Healthy Corneas - (David Finis, Bernhard Ralla, Maria Karbe, Maria Borrelli, Stefan Schrader, and Gerd Geerling) - Hindawi Publishing Corporation, Journal of Ophthalmology, Volume 2015, Article ID 315281, 6 pages, http://dx.doi.org/10.1155/2015/315281

- Accelerated (18 mW/cm2) Corneal Collagen Cross-Linking for Progressive Keratoconus - (Maged Alnawaiseh, MD, André Rosentreter, MD, Michael R. R. Böhm, MD, Maria Eveslage, Nicole Eter, MD, and Lars Zumhagen, MD) - Cornea 2015;34:1427–1431
- Changes in Corneal Transparency After Cross-linking for progressive keratoconus: Long term Follow-Up - (Maged Alnawaiseh, MD, André Rosentreter, MD, Maria Eveslage, Nicole Eter, MD, Lars Zumhagen, MD) - Journal of Refract Surgery. 2015;31(9):614-618

2014

- Overview of the Repeatability, Reproducibility, and Agreement of the Biometry Values Provided by Various Ophthalmic Devices - (Jos J. Rozema, Kristien Wouters, Danny G.P. Mathysen, and Marie-Jose´ Tassignon) - American Journal of Ophthalmology, http://dx.doi.org/10.1016/j.ajo.2014.08.014
- Central and Midperipheral Corneal Thickness Measured with Scheimpflug Imaging and Optical Coherence Tomography - (Jinhai Huang, Xixia Ding, Giacomo Savini, Zhengxuan Jiang, Chao Pan1, Yanjun Hua, Fan Wu, Yifan Feng, Ye Yu, Qinmei Wang) - PLOS ONE, HYPERLINK "http://www.plosone.org" www.plosone.org, May 2014, Volume 9, Issue 5,
- Tomographic Parameters for the Detection of Keratoconus: Suggestions for Screening and Treatment Parameters - (Michael W. Belin, M.D., Ovette F. Villavicencio, M.D., PhD., and Renato R. Ambrósio, Jr M.D., Ph.D.) - Eye & Contact Lens 2014;0: 1–5
- Changes of Corneal Topography Indices After CXL in Progressive Keratoconus Assessed by Scheimpflug Camera - (Kinga Kránitz, MD, Illés Kovács, MD, PhD, Kata Miháltz, MD, PhD, Gábor László Sándor, MD, Éva Juhász, MD, Andrea Gyenes, MD, Zoltán Zsolt Nagy, MD, DSC) - Journal of Refractive Surgery 2014;30(6):374-378;
- A Prospective Study of Pterygium Excision and Conjunctival Autograft with Human Fibrin Tissue Adhesive: Effects on Vision, Refraction, and Corneal Topography - (Stuti Misra, MSc, BOptom, Jennifer P. Craig, PhD, MCOptom, Charles N.J. McGhee, PhD, FRCOphth, Dipika V. Patel, PhD, MRCOphth) - Asia-Pacific Journal of Ophthalmology & Volume 3, Number 4, July/August 2014
- Repeatability and agreement of three Scheimpflug based imaging systems for measuring anterior segment parameters in keratoconus - (Rohit Shetty, Vishal Arora, Chaitra Jayadev, Rudy Nuijts, Mukesh Kumar, Narendra K, Puttaiah, Mathew Kurian Kummelil) - IOVS Papers in Press. Published on July 29, 2014 as Manuscript iovs.14-15055
- Independent Population Validation of the Belin/Ambrosio Enhanced Ectasia Display: Implications for Keratoconus Studies and Screening – (Ovette F Villavicencio, Fatimah Gilani, Maria A Henriquez, Luis IzquierdoJr, Renato Ambrosio Jr, Michael W Belin) - DOI : 10.5005/jp-journals-10025-1069
- Anterior and Posterior Corneal Changes after Crosslinking for Keratoconus – (Johannes Steinberg, Mariam Ahmadiyar, Anika Rost, Andreas Frings, Filip Filev, Toam Katz, and Stephan J. Linke) - Optometry and Vision Science, Vol. 91, No. 2, February 2014
- Keratoconus Management: Long-Term Stability of Topography-Guided Normalization Combined With High-Fluence CXL Stabilization (The Athens Protocol) – (Anastasios John Kanellopoulos, MD; George Asimellis, PhD) - [J Refract Surg. 2014;30(2):88-92.]
- Curvature Analyses of the Corneal Front and Back Surface – (Bo`o Vojnikovi, Nikica Gabri, Iva Dekaris and Branka Juri) - Coll. Antropol. 37 (2013) Suppl. 1: 93–96; Original scientific paper

2013

- Normative values for corneal densitometry analysis by Scheimpflug optical assessment – (Sorcha Ní Dhubhghaill MB PhD, Jos J. Rozema MSc PhD, Sien Jongenelen MD, Irene Ruiz Hidalgo MSc, Nadia Zakaria MD PhD, Marie-José Tassignon, MD PhD.) - IOVS Papers in Press. Published on December 10, 2013 as Manuscript iovs.13-13236
- Anterior segment parameters in Indian young adults using the Pentacam® – (Seyed Mahdi Ahmadi Hosseini; Fereshteh Abolbashari; Norhani Mohidin) - Int Ophthalmol (2013) 33:621–626; DOI 10.1007/s10792-013-9747-1
- Revisiting keratoconus diagnosis and progression classification based on elevation of corneal assymetric indices, derived from Scheimpflug imaging in keratoconic and suspect cases – (Anastasios John Kanellopoulos, George Asimellis) - Clinical Ophthalmology 2013:7 1539-1548
- Comprehensive anterior segment normal values generated by rotating Scheimpflug tomography – (Fatimah Gilani, MD, Michael Cortese, OD, Renato R. Ambr_osio Jr, MD, PhD, Bernardo Lopes, MD, Isaac Ramos, MD, Erin M. Harvey, PhD, Michael W. Belin, MD) - J Cataract Refract Surg. 2013; 39:1707–1712 Q 2013 ASCRS and ESCRS
- Shape of the anterior cornea: Comparison of height data from 4 corneal topographers – (Tim de Jong, MSc, Matthew T. Sheehan, MSc, PhD, Michiel Dubbelman, MSc, PhD, Steven A. Koopmans, MD, PhD, Nomdo M. Jansonius, MD, PhD) - J Cataract Refract Surg. 2013 Oct;39(10):1570-80. doi: 10.1016/j.jcrs.2013.04.032. Epub 2013 Aug 12

2012

- Quality of Vision in Eyes After Selective Lamellar Keratoplasty – (Shizuka Koh, MD, Naoyuki Maeda, MD, Tomoya Nakagawa, MD, and Kohji Nishida, MD) - Cornea _ Volume 31, Number 11, Suppl. 1, November 2012
- Scheimpflug Camera Measurement of Anterior and Posterior Corneal Curvature in Eyes With Previous Radial Keratotomy – (Massimo Camellin, MD; Giacomo Savini, MD; Kenneth J. Hoffer, MD; Michele Carbonelli, MD; Piero Barboni, MD) - J Refract Surg. Vol. 28, No. 4, 2012
- Dual versus single Scheimpflug camera for anterior segment analysis: Precision and agreement – (Jaime Aramberri, MD, Luis Araiz, MS, Ane Garcia, OD, Igor Illarramendi, OD, Jaione Olmos, OD, Izaskun Oyanarte, OD, Amaya Romay, OD, Itxaso Vigara, OD) - J Cataract Refract Surg. 2012; -:--- Q 2012 ASCRS and ESCRS
- Riboflavin injection into the corneal channel for combined collagen crosslinking and intrastromal corneal ring segment implantation – (Aylin Kılıc¸, MD, Gunhal Kamburoglu, MD, Arsen Akıncı, MD) - J Cataract Refract Surg. 2012; 38:878–883 Q 2012 ASCRS and ESCRS
- Variability in Scheimpflug image–derived posterior elevation measurements in keratoconus and collagen-crosslinked corneas – (Georgios Labiris, MD, PhD, Athanassios Giarmoukakis, MD, Haris Sideroudi, PhD; Panagiota Bougatsou, MD, Ilias Lazaridis, MD, Vassilios P. Kozobolis, MD, PhD) - J Cataract Refract Surg. 2012; 38:1616–1625 Q 2012 ASCRS and ESCRS
- Pentacam® based phototherapeutic keratectomy outcome in superficial corneal opacities – (Mohammad A Rashad) - Clinical Ophthalmology 2012:6 885–894; © 2012 Rashad, publisher and licensee Dove Medical Press Ltd.

- Corneal Densitometry as an Indicator of Corneal Health – (Ahmad Muneer Otri, MD, Usama Fares, MD, Mouhamed A. Al-Aqaba, MBChB,Harminder S. Dua, MD, PhD) - Ophthalmology 2012;119:501–508 © 2012 by the American Academy of Ophthalmology
- Correlation of Corneal Elevation With Severity of Keratoconus by Means of Anterior and Posterior Topographic Analysis – (Rie Ishii, MD, Kazutaka Kamiya, MD, PhD, Akihito Igarashi, MD, PhD, Kimiya Shimizu, MD, PhD, Yoshikazu Utsumi, MD, PhD, and Takashi Kumanomido, MD) - Cornea, Volume 31, Number 3, March 2012

2011

- Anterior segment imaging in pediatric ophthalmology – (Kamiar Mireskandari, MBChB, FRCSEd, FRCOphth, PhD, Nasrin N. Tehrani, MBChB, MSc, FRCSEd (Ophth), FRCSC, Cynthia VandenHoven, BAA, CRA, Asim Ali, MD, FRCSC) - J Cataract Refract Surg. 2011; 37:2201–2210 Q 2011 ASCRS and ESCRS
- International values of corneal elevation in normal subjects by rotating Scheimpflug camera – (Matthew T. Feng, MD, Michael W. Belin, MD, Renato Ambr_osio Jr, MD, PhD, Satinder P.S. Grewal, MD, Wang Yan, MD, PhD, Mohamed Shafik Shaheen, MD, PhD, Charlotte A. Jordon, BOptom, Charles McGhee, MD, PhD, Naoyuki Maeda, MD, Tobias H. Neuhann, MD, H. Burkhard Dick, MD, PhD, Andreas Steinmueller, MSc) - J Cataract Refract Surg. 2011; 37:1817–1821 Q 2011 ASCRS and ESCRS
- Corneal topography indices after corneal collagen crosslinking for keratoconus and corneal ectasia: One-year results – (Steven A. Greenstein, BA, Kristen L. Fry, OD, MS, Peter S. Hersh, MD) - J Cataract Refract Surg. 2011; 37:1282–1290 Q 2011 ASCRS and ESCRS
- Corneal thickness changes after corneal collagen crosslinking for keratoconus and corneal ectasia: One-year results – (Steven A. Greenstein, BA, Vinnie P. Shah, MD, Kristen L. Fry, OD, MS, Peter S. Hersh, MD) - J Cataract Refract Surg. 2011; 37:691–700 Q 2011 ASCRS and ESCRS
- Corneal flap assessment with Rondo microkeratome in laser in situ keratomileusis – (Eleftherios I. Paschalis & Antonis P. Aristeidou & Nikitas C. Foudoulakis & Lambros A. Razis) - Graefes Arch Clin Exp Ophthalmol (2011) 249:289–295; DOI 10.1007/s00417-010-1433-7
- Computerized Scheimpflug densitometry as a measure of corneal optical density after excimer laser refractive surgery in myopic eyes – (Gilda Cennamo, MD, PhD, Raimondo Forte, MD, PhD, Bernardino Aufiero, COT, Agostino La Rana,MD) - J Cataract Refract Surg. 2011; 37:1502–1506 Q 2011 ASCRS and ESCRS
- Comparison of anterior segment measurements by 3 Scheimpflug tomographers and 1 Placido corneal topographer – (Giacomo Savini, MD, Michele Carbonelli, MD, Alessandra Sbreglia, OD, Piero Barboni, MD, Giulia Deluigi, MD, Kenneth J. Hoffer, MD) - J Cataract Refract Surg. 2011; 37:1679–1685 Q 2011 ASCRS and ESCRS
- What's in a Name: Keratoconus, Pellucid Marginal Degeneration, and Related Thinning Disorders – (Michael W. Belin, Ijeoma M. Asota, Renato Ambrosio, Jr, and Stephen S. Khachikian) - American Journal of Ophthalmology,August 2011, 2011, Page: 157 – 162
- Novel Pachymetric Parameters Based on Corneal Tomography for Diagnosing Keratoconus – (Renato Ambrósio, Jr, MD, PhD; Ana Laura C. Caiado, MD; Frederico P. Guerra, MD; Ricardo Louzada, MD; Abhijit Sinha Roy, PhD; Allan Luz, MD; William J. Dupps, MD, PhD; Michael W. Belin, MD, FACS) - J Refract Surg., Posted online: July 29, 2011, 2011

- Tomographic Normal Values for Corneal Elevation and Pachymetry in a Hyperopic Population – (Joan T. Kim, Michael Cortese, Michael W. Belin3, Renato Ambrosio Jr and Stephen S. Khachikian;) - J Clinic Experiment Ophthalmol Volume 2 • Issue 2 • 1000130, ISSN:2155-9570
- Estimation of effective lens position using a method independent of preoperative keratometry readings – (Ian Dooley, MRCOphth, Sofia Charalampidou, MRCPI, MRCOphth, John Nolan, PhD, James Loughman, FAOI, PhD, Laura Molloy, BA, Stephen Beatty, FRCOphth, MD) - J Cataract Refract Surg. 2011; 37:506–512 Q 2011 ASCRS and ESCRS
- Comparison of anterior segment measurements with rotating Scheimpflug photography and partial coherence reflectometry – (Jinhai Huang MDa, Konrad Pesudovs PhDa, Daizong Wen MDa, Shihao Chen MD, ODa, Thomas Wright BPsyc (Hons)a, Xiaoyu Wang MDa, Yini Li MDa and Qinmei Wang MD) - J Cataract Refract Surg. 2011; 37:341–348 Q 2011 ASCRS and ESCRS
- Posterior Corneal Elevation After LASIK With Three Flap Techniques as Measured by Pentacam® – (Dilraj S. Grewal, MD; Gagandeep S. Brar, MD; Satinder Pal Singh Grewal, MD) - J Refract Surg. Vol. xx, No. x, 2010 1
- Automated keratometry in routine cataract surgery: Comparison of Scheimpflug and conventional values – (Richard J. Symes, BSc, MRCOphth, Paul G. Ursell, MD, FRCOphth) - J Cataract Refract Surg. 2011; 37:295–301 Q 2011 ASCRS and ESCRS
- Intraocular lens alignment from Purkinje and Scheimpflug imaging – (Patricia Rosales PhD; Alberto de Castro MSc; Ignacio Jiménez-Alfaro MD PhD; Susana Marcos PhD; Instituto de Óptica 'Daza) - Clinical and Experimental Optometry 93.6 November 2010

2010

- Corneal volume, pachymetry, and correlation of anterior and posterior corneal shape in subclinical and different stages of clinical keratoconus – (David P. Pin˜ ero, MSc, Jorge L. Alio´ , MD, PhD, Alicia Aleso´ n, OD, Munir Escaf Vergara, MD, Mauricio Miranda, MD) - J Cataract Refract Surg. 2010; 36:814–825 Q 2010 ASCRS and ESCRS
- Corneal power measurement with a rotating Scheimpflug imaging system after Descemet-stripping automated endothelial keratoplasty – (Pawan Prasher, MD, Orkun Muftuoglu, MD, R. Wayne Bowman, MD, H. Dwight Cavanagh, MD, PhD, James P. McCulley, MD, V. Vinod Mootha, MD) - J Cataract Refract Surg. 2010; 36:1358–1364 Q 2010 ASCRS and ESCRS
- Corneal Higher-Order Aberrations after Descemet's Stripping Automated Endothelial Keratoplasty – (Orkun Muftuoglu, MD, Pawan Prasher, MD, R. Wayne Bowman, MD, James P. McCulley, MD, V. Vinod Mootha, MD) - Ophthalmology 2010;117:878–884 © 2010 by the American Academy of Ophthalmology
- Corneal Biomechanical Metrics and Anterior Segment Parameters in Mild Keratoconus – (Bruno M. Fontes, MD, Renato Ambrósio, Jr, MD, PhD,Daniela Jardim, MD, Guillermo C. Velarde, DSc, Walton Nosé, MD;) - Ophthalmology 2010;117:673–679 © 2010; American Academy of Ophthalmology
- Comparison of Central Corneal Thickness Measurement Using Ultrasonic Pachymetry, Rotating Scheimpflug Camera, and Scanning-Slit Topography – (Mohammed Reza Sedaghat, Ramin Daneshvar, Abbas Kargozar, Akbar Derakhshan and Mona Daraeil) - © 2010 BY ELSEVIER INC. ALL RIGHTS RESERVED. 0002-9394/$36.00

- Anterior Chamber characteristics of keratoconus assessed by rotating Scheimpflug imaging – (Illes Kovacs, MD, PhD, Kata Mihaltz, MD, Janos Nemeth, MD, DSc, Zoltan Z. Nagy, MD, DSc) - J Cataract Refract Surg. 2010; 36:1101–1106 Q 2010 ASCRS and ESCRS
- Marked remodelling of the anterior corneal surface following collagen cross-linking with riboflavin and UVA – (Farhad Hafezi, Tobias Koller, Paolo Vinciguerra, et al.) - Br J Ophthalmol published online October 8, 2010 doi: 10.1136/bjo.2010.184978
- Corneal Collagen Cross-linking for Ectasia After Excimer Laser refractive Surgery: 1-year Results – (Paolo Vinciguerra, MD; Fabrizio I. Camesasca, MD; Elena Albè, MD; Silvia Trazza, BS) - J Refract Surg. 2010;26(7):486-497.]
- Natural history of corneal haze after collagen crosslinking for keratoconus and corneal ectasia: Scheimpflug and biomicroscopic analysis – (Steven A. Greenstein, Kristen L. Fry, OD, MS, Jalpa Bhatt, Peter S. Hersh, MD) - J Cataract Refract Surg. 2010; 36:2105–2114 Q 2010 ASCRS and ESCRS
- Prospective evaluation of changes in anterior segment morphology after laser iridotomy in Chinese eyes by rotating Scheimpflug camera imaging – (Shuning Li MD PhD, Hongtao Wang MD, Dapeng Mu MD PhD, Jing Fu MD, Xiaozhen Wang MD PhD, Jian Wang MD PhD and Ningli Wang MD PhD) - Journal compilation © 2010 Royal Australian and New Zealand College of Ophthalmologists
- Corneal Density With the Pentacam® After Photorefractive Keratectomy – (Agnes I. Takacs, MD; Kata Mihaltz, MD; Zoltan Z. Nagy, MD, DSc, in) - J Refract Surg., 2010
- Central Corneal Thickness, Anterior Chamber Depth, and Pupil Diameter Measurements Using Visante OCT, Orbscan, and Pentacam® – (Ahmet Taylan Yazici, MD; Ercument Bozkurt, MD; Cengiz Alagoz, MD; Nese Alagoz, MD; Gokhan Pekel, MD; Vedat Kaya, MD; Omer Faruk Yilmaz, MD) - J Refract Surg. 2010;26:127-133
- Intra- and Postoperative Variation in Ocular Response Analyzer Parameters in Keratoconic Eyes After Corneal Cross-linking – (Paolo Vinciguerra, MD; Elena Albè, MD; Ashraf M. Mahmoud, PhD; Silvia Trazza, BS;Farhad Hafezi, MD; Cynthia J. Roberts, PhD) - J Refract Surg. 2010;26(9):669-676
- Pentacam® Characterization of Corneas With Fuchs Dystrophy Treated With Descement Menbrane Endothelial Keratoplasty – (Robert O. Kwon, MD; Marianne O. Price, PhD; Francis W. Price, Jr, MD; Renato Ambrosio, Jr, MD; Michael W. Belin, MD) - J Refract Surg. 2010
- Posterior Corneal Elevation After LASIK With Three Flap Techniques as Measured by Pentacam® – (Dilraj S. Grewal, MD; Gagandeep S. Brar, MD; Satinder Pal Singh Grewal, MD) - J Refract Surg. 2010
- Biomechanical and Tomographic Analysis of Unilateral Keratoconus – (Bruno M. Fontes, MD; Renato Ambrósio, Jr, MD, PhD; Marcella Salomão, MD; Guillermo C. Velarde, DSc; Walton Nosé, MD) - J Refract Surg. 2010;26(9):677-681
- Pentacam® Scheimpflug Evaluation of Corneal Volume After LASIK – (Camila M. Gadelha P. Diniz, MD; Rossen M. Hazarbassanov, MD; Ester Yamazaki, MD; Celina Murata, MD; Felipe Mallmann, MD; Mauro Campos, MD) - J Refract Surg. 2010; 26(8):600-604

2009

- Pentacam® Scheimpflug Quantitative Imaging of the Crystalline Lens and Intraoculuar Lens – (Patricia Rosales PhD, Susana Marcos, PhD) - J Refract Surg., Volume 25, may 2009
- Higher-Order Aberrations Due to the Posterior Corneal Surface in Patients with Keratoconus - (Tomoya Nakagawa, Naoyuki Maeda, Ryo Kosaki, Yuichi Hori, Tomoyuki Inoue, Makoto Saika, Toshifumi Mihashi, Takashi Fujikado, Yasuo Tano) - Investigative Ophthalmology & Visual Science, June 2009, Vol. 50, No. 6
- Effect of bottle height on the corneal endothelium during phacoemulsification – (Hisaharu Suzuki, MD, PhD, Kotaro Oki, MD, PhD, Toshihiko Shiwa, MD, PhD, Hideaki Oharazawa, MD, PhD, Hiroshi Takahashi, MD, PhD) - J Cataract Refract Surg. 2009; 35:2014–2017 Q 2009 ASCRS and ESCRS
- Effect of anterior and posterior corneal surface irregularity on vision after Descemet-stripping endothelial keratoplasty – (Takefumi Yamaguchi, MD, Kazuno Negishi, MD, Kazuko Yamaguchi, MD, Dogru Murat, MD, Yuichi Uchino, MD, Shigeto Shimmura, MD, Kazuo Tsubota, MD) - J Cataract Refract Surg. 2009; 35:688–694 Q 2009 ASCRS and ESCRS
- Effect of age on changes in anterior chamber depth and volume after laser in situ keratomileusis – (Ryo Nishimura, MD, Kazuno Negishi, MD, Murat Dogru, MD, Megumi Saiki, CO, Hiroyuki Arai, MD, Ikuko Toda, MD, Takefumi Yamaguchi, MD, Kazuo Tsubota, MD) - J Cataract Refract Surg. 2009; 35:1868–1872 Q 2009 ASCRS and ESCRS
- Diurnal Variation of Corneal Shape and Thickness – (Scott A. Read and Michael J. Collins) - Optom Vis Sci 2009;86:170–180)
- Comparison of central corneal thickness measurements by Pentacam®, noncontact specular microscope, and ultrasound pachymetry in normal and post-LASIK eyes – (Saleh Al-Ageel, MD, Abdulrahman M. Al-Muammar, MD, FRCS) - Department of Ophthalmology, College of Medicine, King Saud University, Riyadh, Saudi Arabia
- Minor Influence of Myopic Laser In Situ Keratomileusis on the Posterior Corneal Surface – (Alfonso Perez-Escudero, Carlos Dorronsoro, Lucie Sawides, Laura Remon, Jesus Merayo-Lloves, and Susana Marcos) - Investigative Ophthalmology & Visual Science, September 2009, Vol. 50, No. 9
- Anterior Segment Measurements Using Pentacam® and Orbscan II 1 to 5 Years After Refractive Surgery – (Sun Woong Kim, MD; Hae Jung Sun, MD; Jee Ho Chang, MD; Eung Kweon Kim, MD, PhD) - J Refract Surg. 2009;25:1091-1097
- Location of Steepest Corneal Area of Cone in Keratoconus Stratifi ed by Age Using Pentacam® - (Aylin Ertan, MD; Günhal Kamburoglu, MD; Joseph Colin, MD) - J Refract Surg. 2009;25:1012-1016
- Central Ablation Depth and Postoperative Refraction in Excimer Laser Myopic Correction Measured With Ultrasound, Scheimpflug, and Optical Coherence Pachymetry – (Maria Clara Arbelaez, MD; Camila Vidal, OD; Samuel Arba Mosquera, MSc) - J Refract Surg. 2009;25:699-708
- Agreement Between Pentacam® and Videokeratography in Corneal Power Assessment – (Giacomo Savini, MD; Piero Barboni, MD; Michele Carbonelli, MD; Kenneth J. Hoffer, MD, FACS) - J Refract Surg. 2009;25:534-538)
- Repeatability and Reproducibility of Corneal Curvature Measurements Using the Pentacam® and Keratron Topography Systems – (Takushi Kawamorita, CO, PhD; Nanami Nakayama, CO, MSc; Hiroshi Uozato, PhD From the Department of Orthoptics and Visual Science, Kitasato Universit) - J Refract Surg. 2009;25:539-544

- Central and peripheral corneal thickness measured with optical coherence tomography, Scheimpflug imaging, and ultrasound pachymetry in normal, keratoconus-suspect, and post–laser in situ keratomileusis eyes – (Claudia Maria Prospero Ponce, MD, Karolinne Maia Rocha, MD, PhD, Scott D. Smith, MD, MPH, Ronald R. Krueger, MD, MSE) - J Cataract Refract Surg. 2009; 35:1055-1062
- Comparison of Anterior Chamber Depth of Normal and Keratoconus Eyes Using Scheimpflug Photography – (Charles R. Edmonds, O.D., F.A.A.O., Shu-Fen Wung, Ph.D., A.C.N.P., F.A.A.N., Bart Pemberton, O.D., F.A.A.O., and Steven Surrett, B.S) - Eye & Contact Lens 2009;3:120-122)
- Comparison of Central Corneal Thickness Measurements with Pentacam®, Orbscan II, and Ultrasound Pachymeter – (Abbas-Ali Yekta, PhD Hassan Hashemi, MD Mehdi KhabazKhoob, MSc Asghar Dostdar, MSc Shiva Mehravaran, MD Javad Heravian, PhD Akbar Fotouhi, MD) - Iranian Journal of Ophthalmology 2009;21(2):51-57
- Measurement of Depth of Intacs Implanted Via Femtosecond Laser Using Pentacam® - (Günhal Kamburoglu, MD; Aylin Ertan, MD; Osman Saraçbasi, PhD) - J Refract Surg. 2009;25:377-382
- Repeatability of Corneal Thickness Measured Using an Oculus Pentacam® - (Marco A. Miranda, Hema Radhakrishnan, and Clare O'Donnell) - American Academy of Optometry; Optometry and Vision Science 2009; 86(3):266-272; 1040-5488/09/8603-0266/0
- Pentacam® and Orbscan II Measurements of Posterior Corneal Elevation Before and After Photorefractive Keratectomy – (Byoung Jin Ha, MD; Sun Woong Kim, MD; Sang Woo Kim, MD; Eung Kweon Kim, MD, PhD; Tae-im Kim) - J Refract Surg. 2009;25:290-295
- Intraobserver and interobserver repeatability of curvature and aberrometric measurements of the posterior corneal surface in normal eyes using Scheimpflug photography – (David P. Pin˜ ero, PhD, Cristina Saenz Gonza´lez, OD, Jorge L. Alio´, MD, PhD; Vissum-Instituto de Oftalmolo´gico de Alicante, Alicante, Spain) - J Cataract Refract Surg. 2009; 35:113–120
- Repeatability, reproducibility, and agreement characteristics of rotating Scheimpflug photography and scanning-slit corneal topography for corneal power measurement – (Takushi Kawamorita, CO, PhD, Hiroshi Uozato, PhD, Kazutaka Kamiya, MD, Leon Bax, PhD, Kenta Tsutsui, CO, Daisuke Aizawa, MD, Kimiya Shimizu, MD) - J Cataract Refract Surg. 2009; 35:127-133
- Repeatability and concordance of the Pentacam® system. Comparative study of corneal parameters measured with Pentacam® and Atlas – (B. Doménech, D. Mas, E. Ronda, J. Pérez, J. Espinosa, C. Illueca) - Optica Pura Y Aplicada 2009; 42(1):51-602008
- Diurnal Variation of Axial Length, Intraocular Pressure, and Anterior Eye Biometrics – (Scott A. Read, Michael J. Collins, and D. Robert Iskander) - Investigative Ophthalmology & Visual Science, 2008, 49:2911-2918 DOI:10.1167/ iovs.08-1833
- Corneal elevation and thickness in relation to the refractive status measured with the Pentacam® Scheimpflug system – (Omur O Ucakhan, MD, Pelin Gesoglu, MD, Muhip Ozkan, PhD, Ayfer Kanpolat, MD) - J Cataract Refract Surg. 2008; 34:1900–1905 Q 2008 ASCRS and ESCRS
- Corneal Biomechanical Metrics in Eyes With Refraction of -19.00 to +9.00 D in Healthy Brazilian Patients – (Bruno M. Fontes, MD; Renato Ambrósio, Jr, MD, PhD; Ruiz S. Alonso, MD; Daniela Jardim, MD; Guillermo C. Velarde, DSc; Walton Nosé, MD) - J Refract Surg. 2008; 24: 941-945
- Intrasubject Corneal Thickness Asymmetry – (Stephen S. Khachikian, MD; Michael W. Belin, MD; Joseph B. Ciolino, MD) - J Refract Surg. 2008;24:606-609

- Changes in posterior corneal elevation after laser in situ keratomileusis enhancement - (Diego Vicente, Thomas E. Clinch, MD, Paul C. Kang, MD; SETTING: Private practice, Chevy Chase, Maryland, USA) - J Cataract Refract Surg. 2008; 34:785–788. doi:10.1016/j.jcrs.2007.12.040
- Comparison between central corneal thickness measurements by Oculus Pentacam® and ultrasonic pachymetry – (Hani S. Al-Mezaine; Saleh A. Al-Amro; Dustan Kangave; Abdulkareem Sadaawy; Taher A. Wehaib; Saleh Al-Obeidan) - Int Ophthalmol 2008, 28:333–338. DOI 10.1007/s10792-007-9143-9
- Comparison of central corneal thickness measurements by Orbscan II and Pentacam® after corneal refractive surgery – (Matsuda J, Hieda O, Kinoshita S) - Jpn J Ophthalmol. 2008 Jul-Aug; 52(4):245-9. Epub 2008 Sep 5

2007

- Comparison of Central Corneal Thickness Measured With Orbscan and Pentacam® - (Nicola Rosa, MD; Michele Lanza, MD; Maria Borrelli, MD; Biagio Polito, MD; Maria Luisa Filosa, MD; Maddalena De Bernardo, MD) - J Refract Surg.. 2007;23:895-899
- Central Corneal Thickness Measurements in Unoperated Eyes and Eyes After PRK For Myopia Using Pentacam®, Orbscan II, and Ultrasonic Pachymetry – (Sun Woong Kim, MD; Yeo Jue Byun, MD; Eung Kweon Kim, MD, PhD; Tae-im Kim, MD; from the Department of Ophthalmology, Korea) - J Refract Surg. 2007;23:888-894
- Central corneal thickness measurement with Pentacam®, Orbscan II, and ultrasound devices before and after laser refractive surgery for myopia – (Hassan Hashemi, MD, Shiva Mehravaran, MD) - J Cataract Refract Surg. 2007; 33:1701–1707
- Evaluation of anterior segment parameters in Keratoconic eyes measured with the Pentacam® system – (Sinan Emre, MD, Selim Doganay, MD, Saim Yologlu, Ph) - J Cataract Refract Surg. 2007; 33:1708-1712
- Repeatability of corneal parameters with Pentacam® after laser in situ keratomileusis – (Rajeev Jain, MS; Grewal Dilraj, MBBS; Satinder Pal Singh Grewal, MD) - Indian J. Ophthalmology 2007, 55:341-7
- Corneal curvature and central corneal thickness in eyes with pseudoexfoliation syndrome – (Ibrahim F. Hepsen, MD; Ramazan Yagci, MD; Urgcan Keskin, MD) - Can J Opthalmol 2007; 42:667-680. doi:10.3129/can j ophthalmol.i07-145
- Graft central thickness measurement by rotating Scheimpflug camera and ultrasound pachymetry after penetrating keratoplasty – (de Sanctis U, Missolungi A, Mutani B, Grignolo FM) - Ophthalmology 2007; 114; 1461-1468. doi:10.1016/j.ophtha.2006.10.059
- Long-term stability of the posterior cornea after laser in situ keratomileusis – (Joseph B. Ciolino, MD, Stephen S. Khachikian, MD, Michael J. Cortese, OD, Michael W. Belin, MD) - J Cataract Refract Surg. 2007; 33:1366–1370
- Central corneal thickness measurements using Orbscan II, Visante, ultrasound, and Pentacam® pachymetry after laser in situ keratomileusis for myopia – (Thomas Ho, MRCOphth, Arthur C.K. Cheng, MCRS, FCOphth(HK), Srinivas K. Rao, FRCS, Silvania Lau, Chris K.S. Leung, MRCS, Dennis S.C. Lam, FRCS, FRCOphth) - J Cataract Refract Surg. 2007; 33:1177–1182 Q 2007

- Comparison between central corneal thickness measurements by Oculus Pentacam® and ultrasonic pachymetry – (Hani S. Al-Mezaine; Saleh A. Al-Amro; Dustan Kangave; Abdulkareem Sadaawy; Taher A. Wehaib; Saleh Al-Obeidan) - 2007 Springer Science+Business Media B.V. 2007
- Effect of Proparacaine on Central Corneal Thickness Values. An Evaluation Using Noncontact Specular Microscopy and Pentacam® – (Andrew K. C. Lam, PhD, FAAO and Davie Chen, BSc(Hons)) - Cornea Volume 26, Number 1, January 2007
- PIOL Simulation for High Res Imaging This software provides preoperative detection of post-operative phakic IOL positioning – (H. BURKHARD DICK, MD, MANA TEHRANI, MD; H. Burkhard Dick, MD) - J Cataract Refract Surg. Today europe I January/February 2007
- Reproducibility and repeatability of CCT measurement in keratoconus using the rotating Scheimpflug camera and ultrasound pachymetry – (de Sanctis U, Missolungi A, Mutani B, Richiardi L, Grignolo FM) - Am J Ophthalmol 2007;144:712–718
- No Forward Shifting of Posterior Corneal Surface in Eyes Undergoing LASIK – (Ryo Nishimura, MD, Kazuno Negishi, MD, Megumi Saiki, CO, Hiroyuki Arai, MD, Satomi Shimizu, MD, Ikuko Toda, MD, Kazuo Tsubota, MD Tokyo) - Ophthalmology 2007 by the American Academy of Ophthalmology doi:10.1016/j.ophtha.2006.09.014
- Pentacam® pachometry: comparison with non-contact specular microscopy on the central cornea and inter-session repeatability on the peripheral cornea – (Andrew KC Lam PD(Optom) MPhil PhD FAAO, Davie Chen BSc(Hons)) - Clin Exp Optom 2007; 90: 2: 108–114
- Comparison of Pentacam® Scheimpflug Camera with Ultrasound Pachymetry and Noncontact Specular Microscopy in Measuring Central Corneal Thickness – (Miyuki Fujioka, Makoto Nakamura, Yasuko Tatsumi, Azusa Kusuhara, Hidetaka Maeda, and Akira Negi.) - Current Eye Research 2007, 32:89–94
- Central and peripheral pachymetry measurements according to age using the Pentacam® rotating Scheimpflug camera (2007) – (Ramin Khoramnia, MD, Tanja M. Rabsilber, MD, Gerd U. Auffarth, MD) - J Cataract Refract Surg. 2007, 33: 830-836
- Evaluation of anterior segment parameters in Keratoconic eyes measured with the Pentacam® system – (Sinan Emre, MD, Selim Doganay, MD, Saim Yologlu, PhD) - J Cataract Refract Surg. 2007; 33:1708-1712 doi:10.1016/j.jcrs.2007.06.020
- Intrasession and intersession repeatability of the Pentacam® system on posterior corneal assessment in the normal human eye – (Davie Chen, Andrew K.C. Lam, PhD, FAAO) - J Cataract Refract Surg. 2007; 33:448–454. doi:10.1016/j.jcrs.2006.11.008
- Keratoconus: It Is Hard to Define, But – (Michael W. Belin, MD, and Stephen S. Khachikian, MD) - Elsevier INC. 2007

2006

- Corneal-thickness spatial profile and corneal-volume distribution: Tomographic indices to detect keratoconus – (Renato Ambrosio Jr, MD, PhD, Ruiz Simonato Alonso, MD, Allan Luz, MD, Luis Guillermo Coca Velarde, DSc) - J Cataract Refract Surg. 2006; 32:1851–1859
- Changes in the posterior cornea after laser in situ Keratomileusis and photorefractive keratectomy – (Joseph B. Ciolino, MD, Michael W. Belin, MD) - J Cataract Refract Surg. 2006; 32:1426–1431 doi:10.1016/j.jcrs.2006.03.037

- Corneal thickness measurements in normal and keratoconic eyes: Pentacam® comprehensive eye scanner versus noncontact specular microscopy and ultrasound Pachymetry – (Omur Ozlenen Ucakhan, MD, Muhip Ozkan, PhD, Ayfer Kanpolat, MD) - J Cataract Refract Surg. 2006; 32:970–977. doi:10.1016/j.jcrs.2006.02.037
- Comparison of Central Corneal Thickness Measurements by Rotating Scheimpflug Camera, Ultrasonic Pachymetry, and Scanning-Slit Corneal Topography – (Shiro Amano, MD Norihiko Honda, MD Yuki Amano, MD Satoru Yamagami, MD Takashi Miyai, MD Tomokazu Samejima, COT Miyuki Ogata, COT Kazunori Miyata, MD) - American Academy of Ophthalmology 2006. doi:10.1016/j.ophtha.2006.01.063
- Progressão da espessura corneana do ponto mais fino em direção ao limbo: estudo de uma população normal e de portadores de ceratocone para criação de valores de referência; Corneal thickness progression from the thinnest point to the limbus: study based on a normal and a keratoconus population to create reference values – (Allan Luz, Mário Ursulio, Daniel Castañeda, Renato Ambrósio Jr) - Arq Bras Oftalmol. 2006; 69(4):579-83
- Comparison of Three Methods of Measuring Corneal Thickness and Anterior Chamber Depth – (Wolf Buehl, MD, Danijela Stojanac, MD, Stefan Sacu, MD, Wolfgang Drexler, MD, Oliver Findl, MD) - American Journal of Ophthalmology 8 January 2006. doi: 10.1016/j.ajo.2005.08.048

2005

- Repeatability and Reproducibility of Central Corneal Thickness Measurement With Pentacam®, Orbscan, and Ultrasound – (Birgit Lackner, MD, Gerald Schmidinger, MD, Stefan Pieh, MD, Martin A. Funovics, MD and Christian Skorpik, MD) - Optometry and Vision Science, Vol. 82, No. 10, October 2005
- Central corneal thickness measurement with the Pentacam® Scheimpflug system, optical low-coherence reflectometry pachymeter, and ultrasound Pachymetry – (Yaniv Barkana, MD, Yariv Gerber, PhD, Uri Elbaz, MD, Shulamit Schwartz, MD, Gie Ken-Dror, MSc, Isaac Avni, MD, David Zadok, MD) - J Cataract Refract Surg. 2005; 31:1729–1735. doi: 10.1016/j.jcrs.2005.03.058
- Agreement and Repeatability of Central Thickness Measurement in Normal Corneas Using Ultrasound Pachymetry and the OCULUS Pentacam® - (O'Donnell, Clare PhD, MCOptom, FAAO; Maldonado-Codina, Carole PhD, MCOptom, FAAO) - 2005 Lippincott Williams & Wilkins, Inc.

26.2 Case reports:

- Corneal Ectasia After LASIK Despite Low Preoperative Risk: Tomographic and Biomechanical Findings in the Unoperated, Stable, Fellow Eye – (Renato Ambrósio, Jr, MD, PhD; Daniel G. Dawson, MD; Marcella Salomão, MD; Frederico P. Guerra, MD; Ana Laura C. Caiado, MD; Michael W. Belin, MD)
- Rotating Scheimpflug imaging system assists in diagnosis of posterior polymorphous corneal dystrophy in a 6 years old patient – (Victoria K.M. Law, Davie Chen)
- A Case of Weill-Merchesani Syndrome with Inversion of Chromosome 15 – (Jae Lim Chung, MD, Sun Woong Kim, MD, Ji Hyun Kim, MD, Tae-im Kim, MD, Hyung Keun Lee, MD, Eung Kweon Kim, MD) - Korean Journal of Ophthalmology 2007: 21(4):255-260
- Role of Scheimpflug Imaging in Traumatic Intralenticular Foreign Body – (Satinder Pal Singh Grewal, MD, Rajeev Jain, MD, Rajeev Gupta, MD, Dilraj Grewal, MBBS) – American Journal of Ophthalmology 676 October 2006

26.3 Cataract studies:

2016

- Comparison of Corneal Diameter and Anterior Chamber Depth Measurements using 4 Different Devices - (Mehdi Shajari, MD, Ulrike C. lehmann, BSc, Thomas Kohnen, MD, PhD, FEBO) - Cornea 2016,; 35:838-842
- Comparisons of the in-the-bag stabilities of single-piece and three-piece intraocular lenses for age-related cataract patients: a randomized controlled trial - (Xiaojian Zhong, Erping Long, Wan Chen, Wu Xiang, Zhaochuan Liu, Hui Chen, Jingjing Chen, Zhuoling Lin, Haotian Lin and Weirong Chen) - BMC Ophthalmology (2016) 16:100, DOI 10.1186/s12886-016-0283-4
- Dealings between Cataract and Retinal Reattachment Surgery in PVR - (Svenja Deuchler, Pankaj Singh, Michael Müller, Thomas Kohnen, Hanns Ackermann, Joerg Iwanczuk, Rachid Benjilali, and Frank Koch) - Journal of Ophthalmology, Volume 2016, Article ID 2384312, 9 pages, http://dx.doi.org/10.1155/2016/2384312
- Surgical approach affects intraocular lens decentration - (Pei-Yao Chang, Chi-Yang Lian, Jia-Kang Wang, Pei-Yuan Su, Jiun-Yi Wang, Shu-Wen Chang) - Formosan Medical Association, http://dx.doi.org/10.1016/j.jfma.2016.04.003
- Keratometry versus total corneal refractive power: Analysis of measurement repeatability with 5 different devices in normal eyes with low astigmatism - (Sylvia Fityo, Jens Bühren, MD, PhD, Mehdi Shajari, MD, Thomas Kohnen, MD, PhD, FEBO) - Journal of Cataract Refractive Surgery 2016; 42:569–576 Q 2016 ASCRS and ESCRS

2015

- An Analysis of the Factors Influencing the Residual Refractive Astigmatism After Cataract Surgery With Toric Intraocular Lenses - (Giacomo Savini and Kristian Næser) - Invest Ophthalmol Vis Sci., 2015;56:827–835. DOI:10.1167/iovs.14-15903
- Repeatability and Inter-device Agreement for Three Different Methods of Keratometry: Placido, Scheimpflug, and Color LED Corneal Topography - (Irene Ruiz Hidalgo, MSc, Jos J. Rozema, MSc, PhD, Sorcha Ní Dhubhghaill, MB, PhD, Nadia Zakaria, MB, BS, PhD, Carina Koppen, MD, PhD, Marie-José Tassignon, MD, PhD) - Journal of Refract Surgery. 2015;31(3):176-181

- New algorithm for intraocular lens power calculations after myopic laser in situ keratomileusis based on rotating Scheimpflug camera data - (Richard Potvin, OD, Warren Hill, MD) - Journal of Cataract Refractive Surgery 2015; 41:339–347 Q 2015 ASCRS and ESCRS
- Refractive cylinder outcomes after calculating toric intraocular lens cylinder power using total corneal refractive power - (James A Davison, Richard Potvin) - Clinical Ophthalmology 2015:9 1511–1517
- Precision of 5 different keratometry devices - (Jonas Vejvad Nørskov Laursen • Peter Jeppesen •Thomas Olsen) - Int Ophthalmol, Received: 24 January 2015 / Accepted: 23 March 2015
- Area densitometry using rotating Scheimpflug photography for posterior capsule opacification and surface light scattering analyses - (Keiichiro Minami, PhD, Masato Honbo, Yosai Mori, MD, Yasushi Kataoka, MD, Kazunori Miyata, MD, PhD) - Journal of Cataract Refractive Surgery 2015; 41:2444–2449 Q 2015 ASCRS and ESCRS
- Reproducibility of Scheimpflug Tomography Measurements Regarding Corneal front and Back Surface Power - (E. Stavridis, T. Eppig, N. Szentmary, B. Seitz, A. Langenbucher) - Klinische Monatsblätter Augenheilkunde, DOI http://dx.doi.org/10.1055/s-0035-1558092
- Assessing the corneal power change after refractive surgery using Scheimpflug imaging - (Anders Gyldenkerne, Anders Ivarsen and Jesper Ø. Hjortdal) - Ophthalmic & Physiological Optics ISSN 0275-5408, 2015

2014

- Anterior Surface–Based Keratometry Compared With Scheimpflug Tomography–Based Total Corneal Astigmatism - (Bastian Tonn, Oliver Klaus Klaproth, and Thomas Kohnen) - Invest Ophthalmol Vis Sci. 2015;56:291–298. DOI:10.1167/iovs.14-15659
- Long-term stability of keratometric astigmatism after limbal relaxing incisions - (Rongxuan Lim, BM BCh, Edmondo Borasio, MedC, BQOphth, FEBO, Luca Ilari, FRCOphth) - Journal of Cataract and Refract Surgery, 2014; 40:1676–1681 Q 2014 ASCRS and ESCRS
- Repeatability of lens densitometry using Scheimpflug imaging - (Xenia Weiner, MD, Martin Baumeister, MD, Thomas Kohnen, MD, PhD, FEBO, Jens Bühren, MD) - J Cataract Refract Surg 2014; 40:756–763 Q 2014 ASCRS and ESCRS

2013

- Impact of Crystalline Lens Opacification on Effective Phacoemulsification Time in Femtosecond Laser-Assisted Cataract Surgery – (Wolfgang J. Mayer, Oliver K. Klaproth, Fritz H. Hengerer, and Thomas Kohnen) - Am J Ophthalmol 2013; 2013 by Elsevier Inc. All rights reserved
- Anterior chamber depth, intraocular lens position, and refractive outcomes after cataract surgery – (Anna-Lotta Engren, Anders Behndig, MD, PhD) - J Cataract Refract Surg. 2013; 39:572–577 Q 2013 ASCRS and ESCRS
- Modified double-K method for intraocular lens power calculation after excimer laser corneal refractive surgery – (Megumi Saiki, MS, Kazuno Negishi, MD, Naoko Kato, MD, Rika Ogino, Hiroyuki Arai, MD, Ikuko Toda, MD, Murat Dogru, MD, Kazuo Tsubota, MD) - J Cataract Refract Surg. 2013; 39:556–562 Q 2013 ASCRS and ESCRS

- Scheimpflug analysis of corneal power changes after myopic excimer laser surgery – (Giacomo Savini, MD, Kenneth J. Hoffer, MD, Michele Carbonelli, MD, Piero Barboni, MD) - J Cataract Refract Surg. 2013; 39:605–610 Q 2013 ASCRS and ESCRS
- Comparison of methods to measure corneal power for intraocular lens power calculation using a rotating Scheimpflug camera – (Giacomo Savini, MD, Piero Barboni, MD, Michele Carbonelli, MD, Kenneth J. Hoffer, MD) - J Cataract Refract Surg. 2013; 39:598–604 Q 2013 ASCRS and ESCRS
- Scheimpflug Corneal Power Measurements for Intraocular Lens Power Calculation in Cataract Surgery – (Elie Saad, Maya C. Shammas, and H. John Shammas) - American Journal of Ophthalmology Septemner 2013

2012

- Corneal power estimation for intraocular lens power calculation after corneal laser refractive surgery in Chinese eyes – (Haiying Jin, MD, Gerd U. Auffarth, MD, Haike Guo, MD, Peiquan Zhao, MD) - J Cataract Refract Surg. 2012; 38:1749–1757 Q 2012 ASCRS and ESCRS
- Comparison of anterior chamber depth measurements by 3-dimensional optical coherence tomography, partial coherence interferometry biometry, Scheimpflug rotating camera imaging, and ultrasound biomicroscopy – (Shunsuke Nakakura, MD, PhD, Etsuko Mori, CO, Nozomi Nagatomi, CO, Hitoshi Tabuchi, MD, PhD, Yoshiaki Kiuchi, MD, PhD) - J Cataract Refract Surg. 2012; 38:1207–1213 Q 2012 ASCRS and ESCRS
- Comparability and repeatability of corneal astigmatism measurements using different measurement technologies – (Nienke Visser, MD, Tos T.J.M. Berendschot, PhD, Frenne Verbakel, BSc, John de Brabander, PhD, Rudy M.M.A. Nuijts, MD, PhD) - J Cataract Refract Surg. 2012; 38:1764–1770 Q 2012 ASCRS and ESCRS
- Comprehensive assessment of nuclear and cortical backscatter metrics derived from rotating Scheimpflug images – (Katja Ullrich, BBioMedSc, BM BS, Konrad Pesudovs, PhD) - J Cataract Refract Surg. 2012; 38:2100–2107 Q 2012 ASCRS and ESCRS

2011

- Evaluation of corneal endothelial cell loss and corneal thickness after cataract removal with light-adjustable intraocular lens implantation: 12-month follow-up – (Fritz H. Hengerer, MD, H. Burkhard Dick, MD, Simone Buchwald, Werner W. Hütz, MD, Ina Conrad-Hengerer, MD) - J Cataract Refract Surg. 2011; 37:2095–2100 Q 2011 ASCRS and ESCRS
- Comprehensive assessment of nuclear and cortical backscatter metrics derived from rotating Scheimpflug images – (Katja Ullrich, BBioMedSc, BM BS, Konrad Pesudovs, PhD) - J Cataract Refract Surg. 2012; 38:2100–2107 Q 2012 ASCRS and ESCRS
- Anterior segment imaging in pediatric ophthalmology – (Kamiar Mireskandari, MBChB, FRCSEd, FRCOphth, PhD, Nasrin N. Tehrani, MBChB, MSc, FRCSEd (Ophth), FRCSC, Cynthia VandenHoven, BAA, CRA, Asim Ali, MD, FRCSC) - J Cataract Refract Surg. 2011; 37:2201–2210 Q 2011 ASCRS and ESCRS
- Estimation of effective lens position using a method independent of preoperative keratometry readings – (Ian Dooley, MRCOphth, Sofia Charalampidou, MRCPI, MRCOphth, John Nolan, PhD, James Loughman, FAOI, PhD, Laura Molloy, BA, Stephen Beatty, FRCOphth, MD) - J Cataract Refract Surg. 2011; 37:506–512 Q 2011 ASCRS and ESCRS

- Anterior chamber depth in normal subjects by rotating scheimpflug imaging – (Matthew T. Feng, MD a, Michael W. Belin, MD, FRANZCO , Renato Ambrosio Jr., MD, PhD, Satinder P.S. Grewal, MD, Wang Yan, MD, PhD, Mohamed S. Shaheen, MD, PhD, Charles McGhee, MD, PhD, Naoyuki Maeda, MD, Tobias H. Neuhann, MD, H. Burkhard Dick, MD, PhD, Saleh A. Alageel, MD, FRCS, Andreas Steinmueller) - Saudi Journal of Ophthalmology (2011) 25, 255–259
- Comparison of Anterior Chamber Depth Measurements Conducted With Pentacam® HR and IOL-Master® - (Gábor Németh, MD, PhD; Ziad Hassan, MD; László Módis, Jr., MD, PhD; Eszter Szalai, MD; Kristof Katona, MD; Andras Berta, MD, PhD, DSci) - Ophthalmic Surgery, Lasers& Imaging Vol. 42, No. 2, 2011 145
- Automated keratometry in routine cataract surgery: Comparison of Scheimpflug and conventional values – (Richard J. Symes, BSc, MRCOphth, Paul G. Ursell, MD, FRCOphth) - J Cataract Refract Surg. 2011; 37:295–301 Q 2011 ASCRS and ESCRS

2010

- Evaluation of anterior segment parameter changes using the Pentacam® after uneventful phacoemulsification – (Selim Doganay,Penpegul Bozgul Firat, Sinan Emre; Saim Yologlu) - Acta Ophthalmol. 2010: 88: 601–606; [a] 2008
- Changes in intraocular pressure and anterior segment morphometry after uneventful phacoemulsification cataract surgery – (I Dooley, S Charalampidou, A Malik, J Loughman3, L Molloy and S Beatty) - Eye (2010) 24, 519–527; & 2010 Macmillan Publishers Limited All rights reserved 0950-222X/1
- Preoperative cataract grading by Scheimpflug imaging and effect on operative fluidics and phacoemulsification energy – (Donald R. Nixon, MD) - J Cataract Refract Surg., February 2010
- Intraocular lens power calculation after laser refractive surgery. Corrective algorithm for corneal power estimation – (Haiying Jin, MD, Mike P. Holzer, MD, Tanja Rabsilber, MD, Andreas F. Borkenstein, MD, Il-Joo Limberger, MD, Haike Guo, MD, Gerd U. Auffarth, MD) - J Cataract Refract Surg. 2010; 36:87–96 Q 2010 ASCRS and ESCRS
- Determining corneal power using Pentacam® after myopic photorefractive keratectomy – (Khalil Ghasemi Falavarjani MD, Masih Hashemi MD, Mahmoud Joshaghani MD, Pejvak Azadi MD, Mohammad J Ghaempanah MD and Gholam H Aghai MD) - Clinical and Experimental Ophthalmology 2010; 38: 341–345

2009

- Comparison of central corneal thickness and anterior chamber depth measurements using three imaging technologies in normal eyes and after phakic intraocular lens implantation – (Muriël Doors & Lars P. J. Cruysberg & Tos T. J. M. Berendschot & John de Brabander & Frenne Verbakel & Carroll A. B. Webers & Rudy M. M. A. Nuijts) - -Graefes Arch Clin Exp Ophthalmol (2009) 247:1139–1146; DOI 10.1007/s00417-009-1086-6
- Anterior chamber parameters measured by the Pentacam® CES after uneventful phacoemulsification in normotensive eyes – (OzlenenO Ucakhan, Muhip Ozkan and Ayfer Kanpolat) - Acta Ophthalmol. 2009: 87: 544–548
- Repeatability and validity of lens densitometry measured with Scheimpflug imaging – (Bradley J. Kirkwood, MA, Peter L. Hendicott, PhD, Scott A. Read, PhD, Konrad Pesudovs, PhD) - J Cataract Refract Surg. 2009; 35:1210–1215

- Clinical application of a Scheimpflug system for lens density measurements in phacoemulsification – (Jung-Sub Kim, MD, So-Hyang Chung, MD, PhD, Choun-Ki Joo, MD) - J Cataract Refract Surg. 2009; 35:1204-1209
- Anterior Chamber Depth Measurement in Pseudophakic Eyes: A Comparison of Pentacam® and Ultrasound – (Giacomo Savini, MD; Thomas Olsen, MD; Claudio Carbonara, MD; Sebastiano Pazzaglia, MD; Piero Barboni, MD; Michele Carbonelli, MD; Kenneth J. Hoffer, MD, FACS;) - J Refract Surg. 2009;26:341-347
- Use of the Pentacam® True Net Corneal Power for Intraocular Lens Calculation in Eyes After Refractive Corneal Surgery – (Sang Woo Kim, MD; Eung Kweon Kim, MD, PhD; Beom-Jin Cho, MD; Sun Woong Kim, MD; Ki Yung Song, MD; Tae-im Kim) - J Refract Surg. 2009;25:285-289
- Intraobserver and interobserver repeatability of curvature and aberrometric measurements of the posterior corneal surface in normal eyes using Scheimpflug photography – (David P. Pinero, PhD, Cristina Saenz Gonzalez, OD, Jorge L. Alio, MD, PhD) - J Cataract Refract Surg. 2009; 35:113–120
- Repeatability, reproducibility, and agreement characteristics of rotating Scheimpflug photography and scanning-slit corneal topography for corneal power measurement – (Takushi Kawamorita, CO, PhD, Hiroshi Uozato, PhD, Kazutaka Kamiya, MD, Leon Bax, PhD, Kenta Tsutsui, CO, Daisuke Aizawa, MD, Kimiya Shimizu, MD) - J Cataract Refract Surg. 2009; 35:127-133
- Repeatability and concordance of the Pentacam® system. Comparative study of corneal parameters measured with Pentacam® and Atlas – (B. Doménech, D. Mas, E. Ronda, J. Pérez, J. Espinosa, C) - Optica Pura Y Aplicada 2009; 42(1):51-60
- The Comparison of Central and Mean True-Net Power (Pentacam®) in Calculating IOL-Power After Refractive Surgery – (Jeong-Ho Yi, MD, Joo Youn Shin, MD, Byoung Jin Ha, MD, Sang Woo Kim, MD, PhD3, Beom Jin Cho, MD, Eung Kweon Kim, MD, Tae-im Kim, MD) - Korean Journal Ophthalmology 2009;23:1-5
- Accuracy of Corneal Astigmatism Estimation by Neglecting the Posterior Corneal Surface Measurement – (JAU-DER HO, CHING-YAO TSAI, AND SHIOW-WEN LIOU) - American Journal of Opthalmology 2009; 147(5): 788-795
- Correlation of Nuclear Cataract Lens Density using Scheimpflug Images with Lens Opacities Classification System III and Visual Function – (Dilraj S. Grewal, MD, Gagandeep S. Brar, MD, Satinder Pal Singh Grewal, MD) - American Academy of Ophthalmology 2009 ISSN 0161-6420/09 Published by Elsevier Inc.
- Quantification of glistenings in intraocular lenses using Scheimpflug photography – (Anders Behndig, MD, PhD, Eva Mo¨nestam, MD) - J Cataract Refract Surg. 2009; 35:14–17

2008

- Estimation of the effective lens position using a rotating Scheimpflug camera -(Jau-Der Ho, MD, PhD, Shiow-Wen Liou, MD, PhD, Ray Jui-Fang Tsai, MD, Ching-Yao Tsai, MD, PhD) - J Cataract Refract Surg. 2008; 34:2119–2127 Q 2008 ASCRS and ESCRS
- Corneal Power Measurements Using Scheimpflug Imaging in Eyes With Prior Corneal Refractive Surgery – (Jack T. Holladay, MD, MSEE, FACS; Warren E. Hill, MD, FACS; Andreas Steinmueller) - J Refract Surg. 2008

- Anterior Chamber Depth Measurement in Phakic and Pseudophakic Eyes – (Po-Fang Su, Andy Y. L*, Chao-Yu Hu, and Shu-Wen Chang) - Optometry and Vision Science, Vol. 85, No. 12, December 2008
- Correlation of lens density measured using Pentacam® Scheimpflug system with LOCS III grading score and visual acuity in age-related nuclear cataract – (Xueting Pei, Yongzhen Bao, Yi Chen and Xiaoxin Li) - Br. J. Ophthalmol. published online 27 Jun 2008. doi:10.1136/bjo.2007.136978
- Alterations in the anterior chamber angle after implantation of iris-fixated phakic intraocular lenses – (Takefumi Yamaguchi, MD, Kazuno Negishi, MD, Kenya Yuki, MD, Megumi Saiki, OD, Ryo Nishimura, MD, Nanae Kawaguchi, MD, Kazuo Tsubota) - J Cataract Refract Surg. 2008; 34:1300–1305
- Comparability and Intra-/Interobserver Reliability of Anterior Chamber Depth Measurements With the Pentacam® and IOLMaster – (Vijay Savant, FRCS(Ed), MRCOpth; Randhir Chavan, MRCOphth; Sreekumari Pushpoth, MRCOphth; B. Ilango, FRCOphth) - J Refract Surg. 2008;24:615-618
- Estimation of the effective lens position using a rotating Scheimpflug camera – (Jau-Der Ho, MD, PhD, Shiow-Wen Liou, MD, PhD, Ray Jui-Fang Tsai, MD, Ching-Yao Tsai, MD, PhD) - J Cataract Refract Surg. 2008; 34:2119–2127

2007

- Influence of accommodation on the anterior and posterior cornea – (Scott A. Read, PhD, Tobias Buehren, PhD, Michael J. Collins, PhD) - J Cataract Refract Surg. 2007; 33:1877–1885 Q 2007 ASCRS and ESCRS
- Scheimpflug imaging to determine intraocular lens power in vivo – (Stephen J. Turner, MA, MR-COphth, Edward J.K. Lee, MRCOphth, Victor Hu, MRCOphth, Emma J. Hollick, MD, MRCOphth) - J Cataract Refract Surg. 2007; 33:1041–1044
- PIOL Simulation for High Res Imaging This software provides preoperative detection of postoperative phakic IOL positioning – (H. Burghard Dick, MD, Mana Tehrani, MD; H. Burghard Dick, MD) - Cataract & Refractive Surgery Today Europe I January/February 2007
- Tilt and decentration of intraocular lenses in vivo from Purkinje and Scheimpflug imaging Validation Study – (Alberto de Castro, Patricia Rosales, Susana Marcos) - J Cataract Refract Surg. 2007

2006

- Estimation of true corneal power after keratorefractive surgery in eyes requiring cataract surgery: BESSt formula – (Edmondo Borasio, MedCBQ Ophth, FEBO, Julian Stevens, MRCP, FRCS, FRCOphth, Guy T. Smith, FRCOphth) - J Cataract Refract Surg. 2006; 32:2004–2014
- Phacoemulsification Associated Corneal Damage Evaluated by Corneal Volume – (Hisaharu Suzuki, MD, Hiroshi Takahashi, MD, PhD, Junko Hori, MD, PhD, Miki Hiraoka, MD, PhD, Tsutomu Igarashi, MD, PhD, Toshihiko Shiwa, MD, PhD) - American Journal of Ophthalmology 2006
- Anterior chamber measurements using Pentacam® Scheimpflug Camera – (Tanja M. Rabsilber, Ramin Khoramnia, Gerd U. Auffarth, MD) - J Cataract Refract Surg. 2006; 32:456-459
- Scheimpflug Biometry of the Anterior Segment After Implantation of Foldable Iris-fixated Lenses – (Mana Tehrani, MD; H. Burkhard Dick, MD) - J Refract Surg. 2006;22:243-246

- Anterior chamber depth measurements in phakic and pseudophakic eyes: Pentacam® versus ultrasound device – (Gabor Nemeth, MD, Attila Vajas, MD, Bence Kolozsvari, MD, Andras Berta, MD, PhD, DSci, Laszlo Modis Jr, MD, PhD) - J Cataract Refract Surg. 2006; 32:1331–1335
- In vivo measurement of opacified H60M intraocular lenses using Scheimpflug photography – (A H Ross, M V Mundasad, S M Neilson, E J Mayer, J M Sparrow, A D Dick, D M Tole) - Br. J. Ophthalmol. 2006; 90;1328-1329
- Comparison of Three Methods of Measuring Corneal Thickness and Anterior Chamber Depth – (Wolf Buehl, MD, Danijela Stojanac, MD, Stefan Sacu, MD, Wolfgang Drexler, MD, Oliver Findl, MD) - American Journal of Ophthalmology 8 January 2006

2005

- Validity and Repeatability of Anterior Chamber Depth Measurements with Pentacam® and Orbscan – (Birgit Lackner, MD, Gerald Schmidinger, MD, and Christian Skorpik, MD) - Optometry and Vision Science, Vol. 82, No. 9, September 2005

26.4 Case reports:

- The role of Scheimpflug imaging in the management of posterior scleritis – (Natalia Pawlowska, Jonathan Luck) - Eye and Brain 2010:2 43–46
- Posterior capsule rupture following closed globe injury: Scheimpflug imaging, Pathogenesis, and management – (D.S: Grewal, R. Jain, G:S. Brar, S.P.S. Grewal) - Eur J Ophthalmol 2008; 18
- Unilateral electric Cataract: Scheimpflug imaging and review of the literature – (Dilraj Singh Grewal, MBBS, Rajeev Jain, MS, Gagandeep Singh Brar, MS, Satinder Pal Singh Grewal, MD) - J Cataract Refract Surg. 2007; 33: 116-119
- Scheimpflug Imaging in Late Capsular Bag Distention Syndrome After Phacoemulsification – (Rajeev Jain, MS, Dilraj Grewal, MBBS, Rajeev Gupta, MS, Satinder Pal Singh Grewal, MD) - Am J Ophthalmol 2006; 142:1083–1085
- Role of Scheimpflug Imaging in Traumatic Intralenticular Foreign Body – (Satinder Pal Singh Grewal, MD, Rajeev Jain, MD, Rajeev Gupta, MD, Dilraj Grewal, MBBS) - American Journal of Ophthalmology 676 October 2006
- Nanophthalmos: Ultrasound biomicroscopy and Pentacam® assessment of angle structures before and after cataract surgery – (Sapna Sharan, DNB (Ophth), MNAMS, John R. Grigg, FRACO, FRACS, Ralph A. Higgins, FRACO, FRACS) - J Cataract Refract Surg 2006; 32:1052–1055
- Accommodative Intraocular Lens Tilting (2005) – (Jorge Cazal, MD, Cosme Lavin-Dapena, MD, Jesus Marín, OD, Carlos Vergés, MD, PhD) - From the Department of Ophthalmology, Institut Universitari Dexeus, Barcelona, Universidad Autónoma de Barcelona, Barcelona, Spain. Am J Ophthalmol 2005; 140:341–344

26.5 Glaucoma studies:

2013

- Assessment of the anterior chamber parameters after laser iridotomy in primary angle close suspect using Pentacam® and gonioscopy – (Alireza Esmaeili, Behzad Barazandeh, Sina Ahmadi, Alireza Haghi, Seyed Mahdi Ahmadi Hosseini, Fereshteh Abolbashari) - Int. J. Ophthalmol 2013;6(5):680-684

2011

- Comparing Corneal Variables in Healthy Subjects and Patients with Primary Open-Angle Glaucoma – (Federico Saenz-Frances, Julian Garcia-Feijo, Luis Janez, Lara Borrego-Sanz, Jose M. Martinez de la Casa, Ana Fernandez-Vidal, Carmen Mendez-Hernandez, Enrique Santos-Bueso, Juan Reche-Frutosand, Julian Garcia-Sanchez) - OphthalmologyCopyright © 2011 52,no. 6, 2011, 3683-3688
- Comparison of Scheimpflug imaging and spectral domain anterior segment optical coherence tomography for detection of narrow anterior chamber angles – (DS Grewal, GS Brar1, R Jain and SPS Grewal) - Eye (2011), 1–9; & 2011 Macmillan Publishers Limited All rights reserved 0950-222X/11

2010

- Quantitative evaluation of anterior chamber changes after iridotomy using Pentacam® anterior segment analyzer – (Cristina López-Caballero, Beatriz Puerto-Hernández, Francisco J. Muñoz-Negrete, Gema Rebolleda, Inés Contreras, Carmen Cabarga) - Eur J Ophthalmol 2010
- Anterior chamber measurements taken with Pentacam®: an objective tool in laser iridotomy – (Antoniazzi E, Pezzotta S, Delfino A, Bianchi PE) - European Journal of Ophthalmology,2010 May-Jun;20(3):517-22, 2010
- Prospective evaluation of changes in anterior segment morphology after laser iridotomy in Chinese eyes by rotating Scheimpflug camera imaging – (Shuning Li MD PhD, Hongtao Wang MD, Dapeng Mu MD PhD, Jing Fu MD, Xiaozhen Wang MD PhD, Jian Wang MD PhD and Ningli Wang MD) - Clinical and Experimental Ophthalmology 2010; 38: 10
- Measurement of anterior chamber volume with rotating scheimpflug camera and anterior segment optical coherence tomography – (FU Jing, LI Shu-ning, WANG Xiao-zhen, WU Ge-wei, MU Da-peng, WANG Jian and WANG Ning-li) - Chin Med J 2010;123(2):203-207

2009

- Detection of Occludable Angles with the Pentacam® and the Anterior Segment Optical Coherence Tomography – (Samin Hong, Jeong-Ho Yi, Sung Yong Kang, Gong Je Seong, and Chan Yun Kim) - Yonsei Med J 50(4): 525-528, 2009
- Anterior Chamber Depth Measurement in Pseudophakic Eyes: A Comparison of Pentacam® and Ultrasound – (Giacomo Savini, MD; Thomas Olsen, MD; Claudio Carbonara, MD; Sebastiano Pazzaglia, MD; Piero Barboni, MD; Michele Carbonelli, MD; Kenneth J. Hoffer, MD, FACS) - J Refract Surg. 2009;26:341-347
- Quantitative assessment of anterior chamber volume using slit-lamp OCT and Pentacam® - (Umut Asli Dinc, banu Oncel, Ebru Gorgun, Levent) - European Journal of Ophthalmology 2009; 19(3): 411-415 1120-6721/411-05

2008

- Anterior Chamber Measurements by Pentacam® and AS-OCT in Eyes With Normal Open Angles - (Jeong-Ho Yi, MD, Samin Hong, MD, Gong Je Seong, MD, PhD, Sung Yong Kang, MD, Kyoung Tak Ma, MD, Chan Yun Kim, MD, PhD) - Korean Journal of Ophthalmology 2008;22:242-245; ISSN : 1011-894

26.6 Case reports:

- Corneal Ectasia After LASIK Despite Low Preoperative Risk: Tomographic and Biomechanical Findings in the Unoperated, Stable, Fellow Eye – (Renato Ambrósio, Jr, MD, PhD; Daniel G. Dawson, MD; Marcella Salomão, MD; Frederico P. Guerra, MD; Ana Laura C. Caiado, MD; Michael W. Belin, MD) – J. Refractive Surg. Vol. 26, No. 11, 2010
- Rotating Scheimpflug imaging system assists in diagnosis of posterior polymorphous corneal dystrophy in a 6 years old patient – (Victoria K.M. Law, Davie Chen)
- The role of Scheimpflug imaging in the management of posterior scleriti – (Natalia Pawlowska Jonathan Luck) - Eye and Brain 2010:2 43–46
- Assessment of capsular block syndrome with Scheimpflug camera Pentacam® Scheimpflug system with LOCS III grading score and visual acuity in age-related nuclear cataract – (Yongzhen Bao, Yi Chen and Xiaoxin Li Br) - J. Ophthalmol. published online 27 Jun 2008
- Posterior capsule rupture following closed globe injury: Scheimpflug imaging, pathogenesis, and management – (D.S. Grewal, R. Jain, G.S. Brar, S.P.S. Grewal) - European Journal of Ophthalmology / Vol. 18 no. 2008
- Nanophthalmos: Ultrasound biomicroscopy and Pentacam® assessment of angle structures before and after cataract surgery – (Sapna Sharan, DNB (Ophth), MNAMS, John R. Grigg, FRACO, FRACS, Ralph A. Higgins, FRACO, FRACS) - J Cataract Refract Surg 2006; 32:1052–1055 Q 2006 ASCRS and ESCRS
- Scheimpflug Imaging in Late Capsular Bag Distention Syndrome After Phacoemulsification – (Rajeev Jain, MS, Dilraj Grewal, MBBS, Rajeev Gupta, MS, and Satinder, Pal Singh Grewal, MD) - American Journal of Ophthalmology December 2006
- Role of Scheimpflug Imaging in Traumatic Intralenticular Foreign Body – (Satinder Pal Singh Grewal, MD, Rajeev Jain, MD, Rajeev Gupta, MD, Dilraj Grewal, MBBS) - American Journal of Ophthalmology 676 October 2006
- Accommodative Intraocular Lens Tilting – (Jorge Cazal, MD, Cosme Lavin-Dapena, MD, Jesus Marín, OD, Carlos Vergés, MD, PhD) - American Journal of Ophthalmology August 2005

27 References

1. Tonn et al, Anterior Surface–Based Keratometry Compared With Scheimpflug Tomography–Based Total Corneal Astigmatism; Invest Ophthalmol Vis Sci. 2015;56:291–298. DOI:10.1167/ iovs.14-15659
2. Jack T. Holladay, MD, MSEE, FACS; Warren E. Hill, MD, FACS; Andreas Steinmueller, MSc: Corneal Power Measurements Using Scheimpflug Imaging in Eyes With Prior Corneal Refractive Surgery: The Journal Of Refractive Surgery, 25, 863-868, 2009
3. Grewal DS, Brar GS, Jain R, Grewal SP. Comparison of Scheimpflug imaging and spectral domain anterior segment optical coherence tomography for detection of narrow ACA. Eye (Lond). 2011 May;25(5):603-11
4. Jain R, Grewal D, Grewal SP. Quantitative analysis of anterior chamber following peripheral laser iridotomy using Pentacam® in eyes with primary angle closure. Eur J Ophthalmol. 2012 May 14:0
5. Ambrósio R Jr, Alonso RS, Luz A, Velarde LGC. Corneal-thickness spatial profile and corneal-volume distribution: Tomographic indices to detect keratoconus. J Cataract Refract Surg. 2006; 32: 1851- 1859
6. Mandell RB, Polse KA. keratoconus: spatial variation of corneal thickness as a diagnostic test. arch ophthalmol. 1969;82:182-188
7. (Belin MW, Ambrosio R. Scheimpflug imaging for keratoconus and ectatic disease. Indian J Ophthalmol 2013;61(8):401-6
8. Ambrosio R Jr, Valbon BF, Faria-Correia F, et al. Scheimpflug imaging for laser refractive surgery. Curr Opin Ophthalmol 2013;24(4):310-20
9. Ambrosio R Jr, Caiado AL, Guerra FP, et al. Novel pachymetric parameters based on corneal tomography for diagnosing keratoconus. J Refract Surg 2011;27(10): 753-8
10. Ambrosio R Jr, Nogueira LP, Caldas DL, et al. Evaluation of corneal shape and biomechanics before LASIK. Int Ophthalmol Clin 2011;51(2):11-38
11. Ambrosio R Jr, Dawson DG, Salomao M, et al. Corneal ectasia after LASIK despite low preoperative risk: tomographic and biomechanical findings in the unoperated stable, fellow eye. J Refract Surg 2010; 26(11):906-11
12. Ambrosio R Jr, Randleman JB. Screening for ectasia risk: what are we screening for and how should we screen for it? J Refract Surg 2013;29(4):230-2
13. Klyce SD. Chasing the suspect: keratoconus. Br J Ophthalmol 2009;93(7):845-7)
14. Ambrosio R Jr, Klyce SD, Wilson SE. Corneal topographic and pachymetric screening of keratorefractive patients. J Refract Surg 2003;19(1):24-9
15. Ambrosio R Jr, Nogueira LP, Caldas DL, et al. Evaluation of corneal shape and biomechanics before LASIK. Int Ophthalmol Clin 2011;51(2):11-38
16. Rabinowitz YS, Rasheed K, Yang H, Elashoff J. Accuracy of ultrasonic pachymetry and videokeratography in detecting keratoconus. J Cataract Refract Surg 1998;24(2):196-201
17. Randleman JB, Trattler WB, Stulting RD. Validation of the Ectasia Risk Score System for preoperative laser in situ keratomileusis screening. Am J Ophthalmol 2008;145(5): 813-18
18. Randleman JB, Woodward M, Lynn MJ, Stulting RD. Risk assessment for ectasia after corneal refractive surgery. Ophthalmology 2008;115(1):37-50

19. Ambrosio R Jr, Dawson DG, Salomao M, et al. Corneal ectasia after LASIK despite low preoperative risk: tomographic and biomechanical findings in the unoperated, stable, fellow eye. J Refract Surg 2010; 26(11):906-11

20. Ambrosio R Jr, Randleman JB. Screening for ectasia risk: what are we screening for and how should we screen for it? J Refract Surg 2013;29(4):230-2

21. Klein SR, Epstein RJ, Randleman JB, Stulting RD. Corneal ectasia after laser in situ keratomileusis in patients without apparent preoperative risk factors. Cornea 2006;25(4):388-403

22. Chan CC, Hodge C, Sutton G. External analysis of the Randleman Ectasia Risk Factor Score System: a review of 36 cases of post LASIK ectasia. Clin Experiment Ophthalmol 2010;38(4):335-40; 40

23. Binder PS, Trattler WB. Evaluation of a risk factor scoring system for corneal ectasia after LASIK in eyes with normal topography. J Refract Surg 2010;26(4): 241-50

24. Ambrosio R Jr, Randleman JB. Screening for ectasia risk: what are we screening for and how should we screen for it? J Refract Surg 2013;29(4):230-2

25. Ambrosio R Jr, Nogueira LP, Caldas DL, et al. Evaluation of corneal shape and biomechanics before LASIK. Int Ophthalmol Clin 2011;51(2):11-38

26. Ambrosio R Jr, Randleman JB. Screening for ectasia risk: what are we screening for and how should we screen for it? J Refract Surg 2013;29(4):230-2

27. Ambrosio R Jr, Nogueira LP, Caldas DL, et al. Evaluation of corneal shape and biomechanics before LASIK. Int Ophthalmol Clin 2011;51(2):11-38

28. Ambrosio R Jr, Ramos I, Faria-Correia F, Belin MW. Tomographic Screening for Ectasia Susceptibility - Analysis must go beyond corneal curvature and central thickness. J. Cataract Refract Surg Today Europe 2012;20-5

29. Ambrosio R Jr, Valbon BF, Faria-Correia F, et al. Scheimpflug imaging for laser refractive surgery. Curr Opin Ophthalmol 2013;24(4):310-20

30. Normative values for corneal densitometry analysis by Scheimpflug optical assessment. Ní Dhubhghaill, Rozema et al IOVS 2014

31. Hill WE, Steinmueller A: Corneal Power Measurements Using Scheimpflug Imaging in Eyes With Prior Corneal Refractive Surgery. J Refract Surg. 2009;25:862-868

32. Li Wang, MD, PhD, Douglas D. Koch, MD. Custom optimization of intraocular lens asphericity. J Cataract Refract Surg 2007; 33:1713–1720

33. Holladay JT. Quality of Vision: Essential Optics for the Cataract and Refractive Surgeon. Thorofare: Slack, 2007 pp 32-4

34. Holladay JT. Corneal topography using the Holladay Diagnostic Summary. J Cataract Refract Surg. 1997; 23: 209-21

35. Holladay JT, Hill WE, Steinmueller A: Corneal Power Measurements Using Scheimpflug Imaging in Eyes With Prior Corneal Refractive Surgery. J Refract Surg. 2009;25:862-868

36. Holladay JT. Accuracy of Scheimpflug Holladay equivalent keratometry readings after corneal refractive surgery. J Cat Ref Surg. 2010;36:182-3

37. Holladay JT. Automated keratometry in routine cataract surgery: Comparison of Scheimpflug and conventional values. Journal of Cataract & Refractive Surgery. 2011; 37:1738-9

38. Li Wang, MD, PhD, Douglas D. Koch, MD. Custom optimization of intraocular lens asphericity. J Cataract Refract Surg 2007; 33:1713–1720

39. Holladay JT. Exact Toric IOL Calculations Using Currently Available Lens Constants. Arch Ophthalmol. Holladay JT 2012;130(7): 946-7

40. Martinez CE, Klyce SD: Corneal topography in cataract surgery. Curr Opin Ophthalmol. 1996; 7:31-8

41. Wang L, Hill WE, Koch DD: Evaluation of intraocular lens power prediction methods using the American Society of Cataract and Refractive Surgeons Post-Keratorefractive Intraocular Lens Power Calculator. J Cataract Refract Surg. 2010;36:1466-73

42. Holladay JT, Piers PA, Koranyi G, van der Mooren M, Norrby NE: A new intraocular lens design to reduce SA of pseudophakic eyes. J Refract Surg. 2002; 18:683-91

43. Marcos S, Barbero S, Llorente L, Merayo-Lloves J: Optical response to LASIK surgery for myopia from total and corneal aberration measurements. Invest Ophthalmol Vis Sci. 2001; 42:3349-56

44. Mayer WJ, Klaproth OK, Hengerer FH, Kohnen T. Impact of crystalline lens opacification on effective phacoemulsification time in femtosecond laser-assisted cataract surgery. Am J Ophthalmol 2014;157:426–432.e1

45. Ho JD, Tsai CY, Liou SW. Accuracy of corneal astigmatism estimation by neglecting the posterior corneal surface measurement. Am J Ophthalmol 2009;147:788-95

46. Koch DD, Ali SF, Weikert MP, et al. Contribution of posterior corneal astigmatism to total corneal astigmatism. J Cataract Refract Surg 2012;38:2080-7

47. Savini G, Versaci F, Vestri G, et al. The influence of posterior corneal astigmatism on total corneal astigmatism in eyes with high moderate-to-high astigmatism. J Cataract Refract Surg 2014;40:1645-1653

48. Savini G, Naeser K. An analysis of the factor influencing the residual refractive astigmatism after cataract surgery with toric intraocular lenses. Investig Ophthalmol Vis Sci 2015;56:827-835

49. Fam HB, Lim KL. Meridional analysis for calculating the expected spherocylindrical refraction in eyes with toric intraocular lenses. J Cataract Refract Surg 2007;33:2072-6

50. Savini G, Hoffer KJ, Carbonelli M, et al. The influence of axial length and corneal power on the astigmatic power of toric intraocular lenses. J Cataract Refract Surg 2013;39:1900-3

51. Gulani AC. Corneoplastique™: Art of vision surgery. Indian J Ophthalmol 2014;62:3-11

52. Gulani AC. Using excimer laser PRK--not PTK--for corneal scars: Straight to 20/20 vision. Advanced Ocular Care. 2012(Sept/Oct);1-3

53. Gulani AC. Corneoplastique. Video Journal of Ophthalmology. 2007;22(3)

54. Gulani AC. Corneoplastique system repairs cornea before or after laser refractive surgery. Ocular Surgery News. 2007 (Nov);25(21):124-5

55. Gulani AC. "Excimer laser PRK and corneal scars: Refractive surgery to the rescue." In: Textbook Mastering Advance Surface Ablation Techniques. New Dehli, India: JP Publishers;2007:246-8

56. Gulani AC. "Irregular Astigmatism Management in Unstable Cornea." In: Textbook of Irregular Astigmatism. Thorofare, NJ: SLACK Incorporated;2007:251-61

57. Gulani AC. ART of LASIK surgery: Raising the bar on outcomes and safety. In: Afshari N, Copeland R, eds. Textbook of Cornea& Refractive Surgery. 1st ed. J.P. Publishers; 2012

28 List of illustrations

29 Tables directory

30 List of abbreviations

- A axis
- ACA anterior chamber angle
- ACD anterior chamber depth
- ACV anterior chamber volume
- ATRA against the rule astigmatism
- BFE best fit ellipse
- BFS best fit sphere
- BFTE best fit toric ellipse
- BFTEF best fit toric ellipse fixed
- BSCVA best spectacle corrected visual acuity
- CI coincidence interval
- CTSP corneal thickness spatial profile
- cyl cylinder
- D diopter/s
- EKR/EKR65 equivalent keratometer readings/equivalent keratometer readings 65
- EPT effective phacoemulsification time
- HRT Heidelberg-Retina-Tomograph
- IOL/s intraocular lens/es
- IOP intraocular pressure
- INTACS® ICRS intrastromal corneal ring segment, most named as INTACS®
- KA keratometric astigmatism
- mmHG unit for intraocular pressure
- OCT optical coherence tomography
- OD right eye
- OS left eye
- pIOL phakic intraocular lens
- PIT percentage increase thickness

- PKP penetrating keratoplasty
- PMD pellucid marginal degeneration
- PNS Pentacam® nucleus staging
- PRK photorefractive keratectomy
- PTK phototherapeutic keratectomy
- QS Quality Specification
- R radius
- RGPCL rigid gas permeable contact lens
- RK radial keratotomy
- RNFL retinal nerve fiber layer
- RP relative pachymetry
- SA spherical aberration
- SD standard deviation
- sph sphere
- TCA total corneal astigmatism
- TCRP Total Cornea Refraktive Power
- TP thinnest point
- UCVA uncorrected visual acuity
- WTRA with the rule astigmatism
- µm micron

31 Authors and contact addresses

Prof. Renato Ambrósio Jr
Director of Cornea and Refractive Surgery
Instituto de Olhos
Renato Ambrósio & Refracta - RIO
Rua Conde de Bonfim 211/712
20520-050 Tijuca, Rio de Janeiro, Brazil
Email: renatoambrosiojr@terra.com.br
www.iolhosrenatoambrosio.com.br

Prof. Michael W. Belin, MD
The University of Arizona
Department of Ophthalmology
and Vision Science
655 N. Alvernon Way, Suite 108
Tucson, Arizona 85711, USA
Email: mwbelin@aol.com

Ina Conrad-Hengerer, MD
Privatpraxis für Augenheilkunde
Eichenstr. 3
65468 Trebur, Germany
Phone: +49-(0)6147-502180
Fax: +49-(0)6147-502181
Email: email@augenarzt-trebur.de

Sorcha S. Ní Dhubhghaill, MB, PhD
Department of Ophthalmology
Antwerp University Hospital
Wilrijkstraat 10
2650 Edegem, Belgium
Email: Sorcha.NiDhubhghaill@uza.be

Alain-Nicolas Gilg, MD
Lyon-Europe Vision Center
14 Rue Rabelais
69003 Lyon, France
Email: docteurangilg@club-internet.fr

Dilraj S. Grewal, MD
Duke Eye Center
Duke University
2351 Erwin Road
Durham, North Carolina 27705, USA
Phone: +1-617-584-2334
Fax: +1-919-681-6474
Email: dilraj@gmail.com

Arun C. Gulani, MD
GULANI VISION INSTITUTE
8075 Gate Parkway (W)
Suite 102 & 103
Jacksonville, Florida 32216, USA
Phone: 904-296-7393
Fax: 904-296-0393
Email: gulanivision@gulani.com
www.gulanivision.com

Jack T. Holladay, MD, MSEE, FACS
Holladay Consulting, Inc.
P. O. Box 717
Bellaire, Texas 77402 - 0717, USA
Fax: +1-713 669 9153
Email: holladay@docholladay.com

Jörg Iwanczuk, Graduate Engineer
OCULUS Optikgeräte GmbH
Münchholzhäuser Str. 29
35582 Wetzlar, Germany
Phone: +49-(0)641-2005-0
Fax: +49-(0)641-2005-295
Email: j.iwanczuk@oculus.de
www.oculus.de

Prof. Thomas Kohnen, MD, FEBO
Professor and Chair
Department of Ophthalmology
Goethe-University
Theodor-Stern-Kai 7
60590 Frankfurt am Main, Germany
Phone: +49 (0)69 6301 3945
Fax: +49 (0)69 6301 3893
Email: kohnen@em.uni-frankfurt.de

Prof. Naoyuki Maeda, MD, PhD
Department of Ophthalmology
Osaka University Graduate School of Medicine
Room E7, Yamadaoka 2-2
Suita, Osaka 565-0879, Japan
Phone: +81-(6)6879-3456
Fax: +81-(6)6879-3458
Email: nmaeda@ophthalmol.med.osaka-u.ac.jp

Tobias H. Neuhann, MD
Clinical Director
AaM Augenklinik am Marienplatz
Marienplatz 18/19
80331 Munich, Germany
Phone: +49-(0)89-230 8890
Fax: +49-(0)89-230 88910
Email: sekretariat@a-a-m.de
www.augenklinik-marienplatz.de

Jos J. Rozema, MSc, PhD
Department of Ophthalmology
Antwerp University Hospital
Wilrijkstraat 10
2650 Edegem, Belgium
Email: Jos.Rozema@uza.be

Giacomo Savini, MD
Studio Oculistico d'Azeglio
Via d'Azeglio, 5
40123 Bologna, Italy
Email: giacomo.savini@alice.it

Eduardo Viteri, MD
Humana Vision, Centro Oftalmologico
Panama 616 y Roca
4759 Guayaquil, Ecuador
Email: eviteri@ecuadorlaser.com

The following pages remain free and offer space for personal notes

Interpretation Guide Pentacam® / Pentacam® HR / Pentacam® AXL

45/0417/EN/LA
P/SD/004/EN

WWW.OCULUS.DE

OCULUS Optikgeräte GmbH
Postfach • 35549 Wetzlar • GERMANY
Tel. +49 641 2005-0 • Fax +49 641 2005-295
E-Mail: export@oculus.de • www.oculus.de

- OCULUS USA, info@oculususa.com
- OCULUS Asia, info@oculus.hk
- OCULUS Czechia, oculus@oculus.cz
- OCULUS Iberia, info@oculus.es
- OCULUS Poland, biuro@oculus.pl
- OCULUS Slovakia, office@oculus.sk
- OCULUS Turkey, info@oculus-turkey.com.tr